Development of Novel Microcarriers for Adipose Derived Stem Cell Material Directed Differentiation and Expansion

A thesis submitted for the degree of

Doctor of Philosophy

(Ph.D)

Claire Gibson

September 2012
Cardiff School of Biosciences

Cardiff University

DECLARATION

This work has not been submitted in substance for any other degree or award at this or any other university or place of learning, nor is being submitted concurrently in candidature for any degree or other award.

Signed …………………………......... (candidate)   Date ………………

STATEMENT 1

This thesis is being submitted in partial fulfillment of the requirements for the degree of PhD.

Signed ………………….....................(candidate)   Date ………………

STATEMENT 2

This thesis is the result of my own independent work/investigation, except where otherwise stated.Other sources are acknowledged by explicit references. The views expressed are my own.

Signed ……….............…………......... (candidate)   Date ………………

STATEMENT 3

I hereby give consent for my thesis, if accepted, to be available for photocopying and for inter-library loan, and for the title and summary to be made available to outside organisations.

Signed ……........……………….......... (candidate)   Date ………….….…

STATEMENT 4: PREVIOUSLY APPROVED BAR ON ACCESS

I hereby give consent for my thesis, if accepted, to be available for photocopying and for inter-library loans **after expiry of a bar on access previously approved by the Academic Standards & Quality Committee.**

Signed ………………….................... (candidate)   Date …………………

Acknowledgments

Finally, I would like to thank my Mum who has given me unequivocal support throughout, as always, for which my mere expression of thanks does not suffice.

Abstract

Regenerative medicine and tissue engineering are being revolutionised by developments in the field of stem cell science. Mesenchymal Stem Cells (MSCs) are emerging as a desirable tool in regenerative medicine and cell therapy due to their wide ranging differentiation potential, large expansion capacity, and their lack of immune rejection following transplantation. Early *in vivo* studies have demonstrated therapeutic effects of hMSCs; however to clinically exploit the potential of hMSCs, the adherent cell type must be expanded to therapeutically relevant lot sizes (10^9 to 10^{12} cells). Hence now there is a need to develop protocols for stable, controlled *in vitro* expansion, isolation and preservation of a homogenous population of functionally viable cells. Specifically a practical, clinically safe and scalable system which adheres to current GMP guidelines is required to develop reproducible and cost effective therapeutic products.

Here we describe the design, manufacture and characterisation of biofunctionalised hydrogel microcarriers containing ECM derived adhesion peptides and a range of compressive moduli for adipose derived stem cell expansion. Microfluidic devices were employed to produce monodisperse spherical particles which were polymerised *in situ*. In addition, these microcarriers have tunable characteristics which make them a particularly useful tool for the systematic investigation of cellular responses. Microcarriers modified to contain fibronectin and laminin derived peptides supported ADSC attachment and growth in a concentration dependent manner. ADSCs cultured on peptide modified microcarriers were capable of differentiating into osteocytes, chondrocytes and adipocytes, indicating cells cultured on microcarriers maintained multipotency. Substrate compressibility was found to effect ADSC differentiation, corroborating previous literature reports. Bioreactor culture demonstrated successful ADSC expansion with fold increases in cell number far higher than have previously been reported in the literature. High cell seeding densities produced large quantities of viable cells. However, decreasing initial cell seeding density, increased the total fold expansion and reduced cell doubling rates.

Table of contents

TABLE OF FIGURES

Abbreviations

ACAN	Aggrecan
ADSC	Adipocyte Derived Stem Cell
BM-MSC	Bone Marrow Derived Mesenchymal Stem Cell
CFU-Fs	Colony Forming Unit-Fibroblasts
CHO	Chinese Hamster Ovary
CV	Coefficient of Variance
DMEM	Dulbecco's Modified Eagle Medium
ECM	Extracellular Matrix
ESC	Embryonic Stem Cell
ESEM	Environmental Scanning Electron Microscopy
ESI	Electrospray Mass spectrometry (
FABP4	Fatty Acid Binding Protein 4
FACS	Flow Cytometric analysis
FBS	Foetal Bovine Serum
FDA	Food and Drug Administration
GMP	Good Manufacturing Process
GvHD	Graft Versus Host Disease
iPSC	Induced Pluripotent Stem Cell
Matrix-Assisted Laser Desorption/Ionization Time of Flight Time of Flight	MALDI ToF ToF
MI	Myocardial Infarction
MMP	Matrix Metalloproteinases
MSC	Mesenchymal Stem Cell
NHS	N-hydroxysuccinimidyl
PBR	Packed Bed Bioreactor
PDMS	Polydimethylsiloxane
PEG	Polyethylene glycol
PEGDMA	Polyethylene glycol Dimethacrylate
PEGDA	Polyethylene glycol Diacrylate
PFA	Perfluoroalkoxy Polymer

PLGA	Poly(lactic-co-glycolic acid)
PLLA	Poly-L-Lactic Acid.
PTFE	Polytetrafluoroethylene
PVA	Poly (Vinyl Alcohol)
RGC32	Response Gene to Complement 32
RGD	Arginine-Glycine-Aspartic Acid
ROCK	Rho Kinase Inhibitor
RPM	Revolutions Per Minutes
RT-PCR	Real-time polymerase chain reaction
SFM	Serum Free Media
SVF	Stroma Vascular Fraction
TGF-β	Transforming Growth Factor Beta
TRITC	Tetramethylrhodamine-5-(and 6)-isothiocyanate
UV	Ultraviolet
W/O	Water in Oil

1.0   Introduction

1.1 Regenerative medicine and stem cells

Regenerative medicine is a rapidly progressing scientific and medical discipline which aims to develop therapeutics to replace, restore or maintain damaged tissues or organs in the body, in order to recover normal function (1, 2). It is hoped that evolving technologies will generate therapeutic remedies for disorders where current chemical treatments are inadequate. Cell therapy and tissue engineering constitute the wider field of regenerative medicine, with a primary goal of delivering safe, effective and reliable therapies. Stem cells within the body provide endogenous mechanisms for repair and regeneration (3), and regenerative medicine hopes to utilise these stem cells as a key tool to repair or replace damaged tissues. Stem cells have two definitive properties; they are capable of self-renewal, and can differentiate, generating lineage specific progeny.

Candidates for cell therapies in regenerative medicine include Embryonic Stem Cells (ESCs), induced Pluripotent Stem Cells (iPSCs) and adult stem cells, such as Multipotent Stromal Cells (Mesenchymal Stem Cells or MSCs). Human Embryonic Stem cell lines are derived from the inner cell mass of pre-implanatation embryos at the blastocyst stage (4), and have a potentially unlimited capacity for self-renewal whilst remaining karyotypically and phenotypically stable (5). In addition, ESCs are pluripotent and are capable of differentiating into derivatives of all three germ layers, ectoderm, endoderm and mesoderm, both *in vitro* and *in vivo* (4). This potential of ESCs to generate an unlimited supply of 220 cell types, make them excellent candidates for use in regenerative medicine and tissue replacement (6). ESCs are currently being developed to treat a wide variety of diseases including Parkinson's disease (7), several types of cancer (8) and blindness (9). In addition, clinical trials in both the UK and US have tested hESC based cellular therapies to treat spinal cord injury and macular degeneration (10). The ability of ESCs to propagate in *in vitro* culture indefinitely under controlled conditions, also make ESCs a valuable research tool. ESCs are currently being utilised in toxicology testing and to study human development and investigate genetic disease (11). However, there are legal and ethical concerns associated with ESC based therapies, in particular the initial isolation, which requires the destruction of a fertilised embryo (12). Further drawbacks include teratoma formation (an encapsulated tumour derived from all three germ layers) and elicited immune rejection after allogeneic ESCs transplantation (13). Problems concerning histocompatibility may be overcome by therapeutic cloning, also known as Somatic

Cell Nuclear Transfer (SCNT), whereby a nucleus from an oocyte is substituted with a nucleus from an adult somatic cell taken from the patient requiring a transplant. The resulting egg is stimulated to form a blastocyst, where the inner cell mass can be used to generate ESC lines that are genetically identical to the patient (14). Other strategies employed include novel immunosuppressants, stem cells banks and reprogramming patients' own somatic cells with defined factors to generate iPSCs (15).

iPSCs are pluripotent stem cells that are artificially derived from a non-pluripotent cell by inducing overexpression of specific genes using variable sets of transcription factors (16). iPSCs share similar, but not identical characteristics to ESCs, displaying comparable pluripotency, as demonstrated by embryoid body and teratoma formation assays, in addition to similar expression of genes, proteins and chromatin methylation patterns (17). iPSCs have been differentiated into multiple functional cell types, including cardiomyocytes (18) hematopoeitic cells and neurons (19, 20). Hence, iPSCs hold great potential as renewable sources of autologous cells for regenerative medicine. However, the method of iPSC generation can result in significant risks that could limit their potential use in humans. One example is if viruses are used to alter gene expression within cells, this could potentially trigger the expression of unwanted oncogenes (21). Further developments have introduced a technique to remove oncogenes after pluripotency induction, increasing the potential for iPSC use (21), however both methods require integrating exogenous sequences into the target cell genome which is undesirable. A method has been developed to introduce the necessary proteins *via* poly-arginine anchors without loss in pluripotent potential to create protein-induced pluripotent stem cells (piPSC) (22). iPSCs, like ESCs, also pose a risk of possible teratoma formation (23), and although it was hoped that as iPSCs are generated form a patient's own somatic cells this would circumvent any immunogenic responses, *in vivo* experiments have shown an immune response after transplantation (24).

MSCs are present in a number of postnatal organs and connective tissue, and hold great potential for the treatment of various degenerative diseases and immune disorders because of their differentiation and immunoregulatory capacity, and because they do not suffer from many of the problems of ESCs and iPSCs detailed above (25).

1.2   Mesenchymal stem cells

MSCs were first isolated, cultured and differentiated through the osteogenic lineage from the stromal compartment of rat marrow by Friedenstein and Petrakova in 1966 (26). Later studies have found MSCs are rare and quiescent populations, which reside within specialised niches in numerous fully specialised tissues (27). MSCs are capable of self-renewal and possess multipotent potential with the ability to differentiate into multiple mature cell types of mesodermal lineage including cartilage, bone, fat and muscle under defined conditions *in vitro*. It was postulated that the differentiation potential of adult stem cells is constricted to that of the tissue of origin and mesodermal lineages (28). However, recent studies have confirmed the plasticity of MSCs by demonstrating their capacity to trans-differentiate into cells of all three germ layers (mesodermal, endodermal and ectodermal) both *in vitro* and *in vivo* (27, 29-33). These findings could dramatically increase the potential uses of MSCs in regenerative medicine. Most commonly isolated from the bone marrow (BM), BM-MSCs are the most widely studied MSC and possess a spindle-shaped, fibroblast-like morphology, and are thought to function as a stromal support system for haematopoietic stem cells, in addition to participating in BM tissue homeostasis and in the turnover of skeletal cell types (32).

Evidence suggests cultured MSCs consist of a heterogeneous population of cells, containing subsets of stem cells in addition to more lineage committed (progenitor) cells (34). There are inconsistencies in the literature regarding both the biological properties and the correct nomenclature to describe such a heterogeneous population of cells. Like other stem cell types, MSCs can be characterised immunologically by a specific panel of markers, however there is controversy over which accurate, unique and definitive cellular markers to use. In response to this, the International Society for Cellular Therapy has published guidelines that suggest plastic adherent cells, isolated from any adult tissue should be designated multipotent mesenchymal stromal cells (35). The term Mesenchymal stem cell should be reserved for cultured cells that meet a specific set of criteria. Firstly, MSCs should be isolated using a plastic adherent technique. Secondly, MSCs should be expanded using standard *in vitro* culture methods and express the cell surface markers CD73, CD90, CD105 but lack CD11b, CD17, CD19, CD79a, CD45 and HLA-DR expression. Lastly MSCs should remain multipotent *in vitro*, and classically be able to undergo tri-lineage differentiation into adipocytes, chondrocytes and osteocytes (35).

1.3 ADSCs

Adult bone marrow is now a standard site for MSC isolation, however more recently MSCs have been isolated from nearly all adult tissues, including synonovium, dermis, periosteum, deciduous teeth and in solid organs (e.g., liver, spleen, lung) (36). Human subcutaneous adipose tissue is gaining increasing interest as a promising source for MSCs (denoted as adipocyte derived stem cells (ADSCs)). Worldwide obesity is a growing pandemic, and has resulted in increased incidence of subcutaneous fat deposits, which are easily accessible using the elective cosmetic surgical procedure liposuction (37, 38). In the United states, approximately 400,000 liposuction procedures are performed annually, and each procedure can generate between 100mL to over 3L of lipoaspirate tissue (39). Liposuction surgery yields large quantities of aspirate material and is relatively safer and better tolerated than bone marrow aspiration (40). This is routinely considered clinical waste and discarded, however fat tissue comprises adipocytes and a stroma vascular fraction (SVF), and within the latter resides a relatively abundant source of ADSCs and progenitor cells. Isolated relatively recently, (2002) studies have isolated $0.5\text{-}2.0 \times 10^6$ SVF cells/gram of adipose aspirate and it is estimated as many as 3% are stem and progenitor cells (41). This is more frequent than the traditional source of MSCs from bone marrow aspirates, which typically yields a SVF fraction of 6×10^6 cells, within which 0.001-0.002% of cells are BM-MSCs (37, 41-44). Furthermore, ADSCs can be plated at a lower seeding density (3,000cells/cm^2) when compared to BM-MSCs (>50,000cells/cm^2). There are defined *in vitro* differentiation protocols that comply with regulations whereby ADSCs can differentiate down multiple cell lineages reproducibly (45).

There are several terms used to describe the multipotent population of cells isolated form adipose tissue. These include "adipose-derived adult stem (ADAS) cells," "adipose derived adult stromal cells," "adipose-derived stromal cells (ADSC)," "adipose stromal cells (ASC)," "adipose mesenchymal stem cells (AdMSC)," "preadipocytes," "processed lipoaspirate (PLA) cells," and "adipose-derived stromal/stem cells (ASCs)". As the reported isolation procedures and biological and phenotypic characteristics are similar, it is presumed that these terms describe the same cell population. This prompted the International Fat Applied Technology Society (IFATS) to eliminate the discrepancy in reporting findings and for the field to use a common term adipocyte derived stromal/stem cells. This definition concurs with the terms used to define MSCs whereby the population isolated from adipose tissue must be

plastic adherent, be expanded by passage *in vitro* and have a tri-lineage differentiation potential (46, 47).

BM-MSCs and ADSC share several similarities, they both have a multipotent differentiation potential, share similar morphology, behaviour and cell surface markers and they share an >90% identical immunophenotype (32, 41). Contrastingly there are differences in surface protein expression between the two cell types. Notably CD34 is present on ADSCs (early passage) but absent on BM-MSCs (32, 48). There are several conflicting reports in the literature regarding specific cell surface markers. For instance, evidence has demonstrated that the classic BM-MSC cell surface marker, the Stro-1 antigen, is both present and absent in human ADSCs (41, 49, 50). The differences could possibly be attributed to different antibody sources and antigen detection methods e.g. immunocytochemistry versus flow cytometry.

1.4   Clinical uses of MSCs

MSCs have become a desirable tool in regenerative medicine and cell therapy due to their wide-ranging differentiation potential, large expansion capacity and lack of immune rejection following transplantation. In addition ADSCs can be isolated in clinically relevant amounts from multiple adult tissues. MSCs have demonstrated an immunosuppressive action and reduced immunogenic properties in *in vivo* studies which make them attractive candidates for allogeneic MSC therapies, by which a single donation of cells can be expanded and applied to multiple patients (51, 52). Possible clinical applications include the repair and regeneration of damaged tissue and the treatment of chronic inflammatory conditions. Currently (July 2012) over 227 clinical trials are ongoing, testing the efficacy and safety of MSCs in numerous conditions including cardiovascular disease, brain and spinal cord injury, cartilage and bone injury and diabetes (clinicaltrials.gov). In order to utilise MSCs for clinical therapies, they must be isolated at high cell quantities using a minimally invasive procedure with little risk to the patient. In addition they must be expanded in culture, and still be able to be differentiated into a wide range of lineages (53).

Initially it was postulated that possible MSC based therapies would be harnessed from their multipotent differentiation ability, in particular from mature differentiated osteoblasts, to treat fractures and osteogenesis imperfecta (54). However, clinical trials observed a therapeutic effect of infused MSCs despite a lack of homing and engraftment

into the targeted host tissue long term (55). Despite a lack of attachment and differentiation, inflammation and apoptosis were reduced in several disease models, including myocardial infarction and kidney disease (56-59). *In vitro* experiments suggest the observed immunomodulatory effects are attributable to MSC trophic modulators, such as secretion of multiple bioactive molecules (e.g. cytokines) and pro-angiogenic and anti-apoptotic factors (52, 60, 61). Evidence suggests the immunoregulatory potential is due to the suppression of many T, B, K and dendritic cell functions. It is thought infused MSCs also provide protective micro-environmental cues and stimulate tissue-resident progenitor populations to repair (62). This has driven many clinical trials to examine the therapeutic benefits of MSCs to treat and prevent diseases such as graft-versus-host disease, Crohn's disease and certain haematological malignancies, based solely on their immunoregulatory properties (63).

Consequently, administration of MSC therapy has transitioned from local delivery to systemic administration. Infusions are less invasive and are more convenient, particularly when treatments require multiple dosing procedures (54). Typically, relatively high doses of MSCs are infused at 150-300 million cells per treatment in clinical trials. However, evidence suggests that by using this technique less than 1% of the infused MSCs reach the target tissue. Instead cells often become trapped in capillaries inside the liver, lung and spleen due to their relatively large size and because they express multiple cell surface adhesion receptors (64-67). Benefits have been observed in various clinical studies where MSCs have been systemically infused, including different preclinical models of acute lung injury, myocardial infarction, diabetes and multiple sclerosis, as well as renal and hepatic failure (52, 68). Prochymal[TM] is an allogeneic human BM-MSC based stem cell product being developed for clinical use by Osiris Therapeutics, and is currently the only stem cell therapeutic to have FDA approval (69). Prochymal[TM] is being developed for multiple indications and is currently being evaluated in 14 Phase 3 clinical trials to treat several conditions, including Crohn's disease and acute graft versus host disease (GvHD) (70). Prochymal[TM] has been used to treat Chronic Obstructive Pulmonary Disease (COPD). Preliminary reports after 6 months post treatment displayed reduced C reactive protein and hence reduced systemic inflammation, however pulmonary function was not significantly improved (71). In addition, Prochymal[TM] is currently being developed to treat degenerative conditions including repairing heart tissue following myocardial infarction (69). Single MSC infusions have been used in trials in both rats and humans

who have suffered a myocardial infarction (MI). Results showed a reduction in scarring and increased cardiac output in phase I clinical trials (72, 73). A trial using Prochymal[TM] has demonstrated the potential of MSCs in allogeneic therapies. Patients treated with a single cell dose, 10 days post-acute MI experienced a four-fold reduction in arrymthias and premature ventricular contractions. Furthermore, patients generally displayed improved overall health in relation to the placebo control (74). The precise mechanism of MSC action is unknown, though *in vivo* experiments attempting to treat myocardial infarction in animals have shown systemically infused MSCs can differentiate into tissue specific cell types including cardiomyocytes (75).

Approximately 40% of patients who undergo bone marrow and hematopoietic stem cell transplantation develop Graft vs Host Disease (GvHD), a severe complication of immune rejection of stem cells. GvHd is typically treated with steroids, however this isn't always effective and patients often become 'steroid-resistant'. Advances have been made in using MSCs to treat GvHD. Successful results were observed in Phase I and II trials with patients displaying a lack of severe adverse side effects. Despite promising initial results, two multicentre phase III trials conducted in 2009 were unable to achieve their primary endpoints, with data showing no significant differences to placebo controls (76, 77).

These pre-clinical and clinical trials have demonstrated the potential of using MSCs for therapeutic benefit. The results from phase I and II clinical trials have been promising however the results are preliminary and treatment efficacy has not been conclusively established (78). The fate of MSCs after injection and the mechanisms by which they exert therapeutic effects, in particular how they modulate the immune system, are mostly unidentified (79). Conflicting clinical data should be resolved in order to develop routine clinical therapies by improving the understanding surrounding MSC biology and function, and their fate after systemic infusion (65). Outstanding difficulties that need to be overcome in order to develop MSC cell therapies include producing standardised protocols for MSC isolation and developing efficient expansion methods to generate homogenous undifferentiated MSCs *in vitro* (80). Research is currently ongoing to determine the role of endogenous stem cells in many adult tissues and organs and how various stem cell niches act to control these populations (81). Development of *in vivo* cell trackers and progress in biomaterials *in vitro* will aid this research (82, 83).

1.5   MSCs for Tissue Engineering

For regenerative medicine and tissue engineering purposes, local delivery into damaged tissue sites is preferred to systemic infusion. To ensure the MSCs are retained in the target damaged tissue they can be combined (differentiated or undifferentiated) with either natural or synthetic biomaterial scaffolds prior to *in vivo* implantation (84). Tissue engineering using cell laden constructs have been proved effective in the treatment of cartilage and long-bone repair (85). Using a delivery vehicle, cells can be controlled and manipulated at the site of damage, reducing side effects to other organs and tissues (86). Improvements in scaffolds in terms of enhancing MSC compatibility and grafting into the host tissue will develop the technology for reliable and effective clinical therapy (69). In addition, more work is needed to identify how these stem cells respond to host-cell interactions after implantation, for example how such cells respond to local differentiation cues *in vivo,* and how they evade rejection as seen with many autologous/allogeneic treatments (as discussed in Section 1.4) (87).
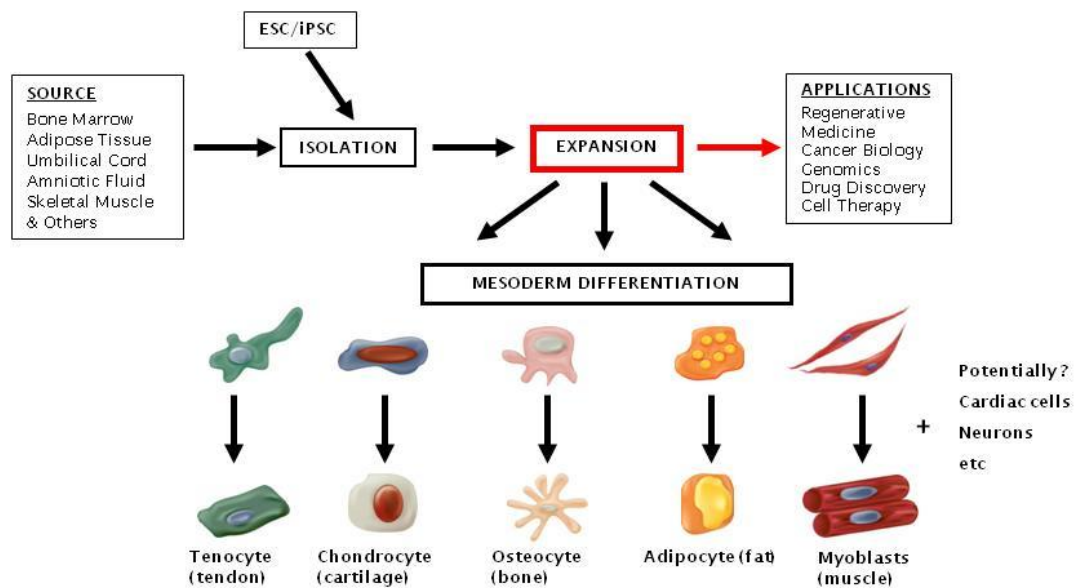
Figure 1: Isolation, expansion and mesodermal differentiation of stem cells.

Stem cells can be isolated from a variety of sources and it is a considerable challenge to expand these cells into therapeutically relevant lot sizes, whilst maintaining mesodermal differentiation potential. (Modified from Invitrogen.com)

1.6   Methods to expand MSCs

Early *in vivo* studies have demonstrated therapeutic effects of hMSCs; however to clinically exploit the potential of hMSCs, the adherent cell type must be expanded to therapeutically relevant lot sizes (88). For example, a typical single clinical treatment dose (intravenous administration) can potentially require 3 x 10^8 MSCs. Multiple autogenic treatments, or the potential to use MSCs for allogenic therapies will increase this several fold. Alternatively, to generate cellularised tissue engineered scaffolds, a range of cell seeding densities from 10^6 to 10^7 cells per cm^2 is required (89). Hence, there is now a need to develop protocols for stable controlled *in vitro* expansion, isolation and preservation of a homogenous population of functionally viable cells (89). MSCs are now considered as advanced therapy medicinal products (ATMPs) by the European Medicines Agency (EMA) by regulation No. [EC] 1394/2007 of the European Commission and must be produced in compliance with Good Manufacturing Practices (GMP) to ensure reproducibility, efficacy and safety of the therapeutic product. The defined GMP standards ensure that cells are produced under highest standards of sterility, quality control and documentation following a standard operating procedure. Regulatory authorities mandate cell production according to GMP-grade system with appropriate and rigorous process validation and quality controls. Quality controls must include bacteriological tests, phenotypic control, viability, safety and efficacy of the final product. Hence, a practical, safe and scalable system which adheres to current GMP guidelines is required to develop therapeutic products that are both reproducible and cost-effective. Unfortunately, as the current cell culture technologies are both expensive and limited, few GMP compliant MSC based therapies are currently available. Several GMP compliant MSC specific media and tissue culture flasks have been developed and are commercially available. In addition to the materials used, several automated robots capable of seeding, maintaining and harvesting MSCs from multi-layer tissue culture flasks in a GMP compliant manner (93).

Optimally, the *in vitro* culture conditions should be performed in a closed, sterile container as prevention of contamination is paramount for a clinical treatment and to protect clinical personnel from exposure to bloodborne pathogens (90). In addition to the culture vessel, MSC culture must be developed to eliminate animal products and serum from expansion methods to prevent complications from prion and viral transmission or other xenogeneic infections (46). To develop a routine clinical therapy, protocols will need to be developed to optimize how to store ADSCs, including which

containers and labels to use, the optimal shelf life and how to deliver the MSCs to the point of care destination (46). This is of paramount importance as extended culture of human ADSCs *in vitro* demonstrated the ability to form tumours when transplanted to immunodeficient mice (91). In the future the safety and terminal fate of injected ADSCs long term will also need to be examined.

1.6.1 Tissue culture plastic/2D planar formats

Conventionally, anchorage-dependant cells are cultured in a 2D planar format on tissue culture treated plastic in the form of plates or flasks. Theoretically, therapies requiring 100-400 billion MSCs will require a culture area of 3-5million cm^2 (88). Using 2D planar tissue culture plastic is reliable and well defined, however the potential to use this format for scale-up is restricted as it is labour intensive, prone to contamination, costly and cell expansion is greatly limited by available surface area (92). To increase the potential for cell expansion using flask based processes, multilayer stacked plate systems were developed over 30 years ago for large scale cell culture. Currently, adherent stem cells (and other therapeutic primary cells) for allogeneic therapies are expanded in tissue culture treated 10 layer vessels for closed system processing in compliance with GMP regulations (93). These systems have been commercially developed, for example parallel plate flasks from Nunc (cell factories) and Corning (cell stacks).

To maximise the quantity of expanded cells in planar vessels, the total surface area per unit and the number of layers in 2D vessels must be increased. Standard 10 layer vessels have been successfully scaled up to 120 layers to generate a total surface area of approximately ~60,000 cm^2 (Hyperstack). However, the increase in stacks within a multi-layer vessel decreases the possible yield of viable cells that can be recovered. In order to avoid contamination from manual handling, automated robotic instrumentation for multi-layer vessels have been developed. Using automation, 120-layer vessels can be manipulated and this is a potential avenue to scale up cell production and to generate millions of cells per run (dependant on cell type).

As well as the total surface area for cell growth, another major bottleneck of a 2D scaled system is the cell density at harvest. Variables that can affect harvested cell densities are media composition, cell donor, cell type and confluency at the time of passage. These variables also fluctuate between cell types, which generate different cell densities at confluency (due to differences in the surface area of individual cells). For

example, ESCs are small and grow in tight colonies, however they can be unstable and prone to spontaneous differentiation. In future, as further robust embryonic cell lines are developed it is possible that 1 trillion ESCs could be achieved per lot (88). However, generating similar quantities of large, flat fibroblastic adult primary cells such as MSCs in 2D systems would be difficult to achieve without substantial automation and parallel processing.

Traditional 2D culture systems are limited as they require large volumes of culture media, incubator space, expense and are labour intensive (92). Due to limited surface area for cell expansion, cell passaging is frequently required, leading to extensive manual handling and increased cultivation times which can increase the possibility of undesired genetic changes within genetically unstable cells such as MSCs (94). Multilayer vessels inherently have inefficient gas–liquid oxygen transfer, intrinsic concentration gradients, and difficulties with monitoring and control. In addition, they are also restricted to one log of expansion. Industrial developments have attempted to optimise planar systems to increase the possible surface area efficiently, and to add bioreactor control which can automate culture variables such as (dissolved) O_2, CO_2 and pH in addition to using robotics to control several other processes. A comparison of different bioreactors including parallel plate vessels have been summarised in Figure 2. Commercially available products include the RepliCell (Aastrom) (95) which is a fully automated, closed, aseptic expansion system which can increase multiple bone marrow cell types in 14 days.

1.6.2 Packed Bed cultures

Adherent and non-adherent cells can be cultured on immobilized substrates, such as beads, porous structures, fibres and hollow fibers within Packed Bed Bioreactor (PBR) culture systems. The substrates can be composed of various materials including glass beads and ceramic, polyester, and polyurethane materials. In addition, scaffolds can be used in a smooth, porous, woven, or nonwoven configuration and are packed into two main configurations; i) with the medium reservoir integral to the packed bed or ii) external to it (96-98).

Traditionally PBRs have been used for the large scale culture of antibody and protein producing cells. The desired cell products are secreted into the medium and are continuously collected without disturbing or removing attached cells. Recently, PBRs

have become favourable candidate systems for the efficient expansion of adherent dependent therapeutic cells, such as MSCs and hESCs in commercial research (99-101).

Using PBR perfusion based systems, high cell densities can be achieved per millilitre of packed bed volume. The system can also be closed, preventing potential contamination and the essential culture parameters such as (pH, dO_2, temp, perfusion, agitation) can be controlled in real time, an essential tool in cultures that last weeks to months (98). Substrates can also allow 3D culture of cells, an emerging factor known to effect stem cell behaviour (102). Lack of diffused oxygen, the accumulation of catabolites and inefficient CO_2 clearance can be detrimental to cell proliferation and multipotency. In addition, PBRs provide a low shear stress environment, relative to stirred suspension culture systems, such as aggregate and microcarrier cultures (discussed in section 1.7.2).

Cells cultured on porous beads or woven or non-woven fibres are able to reach densities of 100 million cells/mL, (typically the total volume of a PBR system is between 10mL and 40mL) depending on the cell and carrier type and culture conditions (88). PBR systems typically contain a surface area $119x10^3/m^2$, an advantage over multilayered planar flask systems which is relatively lower at $\sim0.5x10^3/m^2$ (98). The quantity of harvested cells can vary depending on the cell type, scaffold type and culture conditions.

Several different PBRs have been developed as optimisation is required for each cell type to maximise the quantity and quality of harvested cells. Factors to be optimised can be separated into initial seeding efficiency, maximum expansion limit and harvesting. Factors that can potentially affect initial cell seeding efficiency include, scaffold properties (size, shape, charge, chemistry, porosity and structure), total media volume and media flow, cell attachment potential and packed bed dimensions.

To maximise expansion during the culture phase, important parameters can be controlled in real time using automated processes (103). A potential limiting factor in PBRs is efficient transfer of nutrients (glucose and lactose) and oxygen throughout the entire packed bed culture volume, both in the radial and axial dimensions. This is essential to ensuring homogenous cell density, an important factor when scaling up the total volume. This can be aided by impellers which increases media transfer throughout the vessel, however this can also cause the cells to experience shear stress, which is known to impact cell behaviour and expansion (discussed in section 1.7.2).

Lastly, adherent cell removal from the scaffolds can be a challenging aspect of PBRs culture. Cell harvesting must generate a high yield of healthy, undamaged cells for therapeutic use. PBRs are attractive candidates for primary adult cell scale up, due to the large surface area and variability of the scaffolds and bioreactor's control over key culture parameters. Currently, only small packed-bed bioreactors are commercially available for cell production (104).

1.6.3 Suspension cultures

Suspension culture is a method whereby stem cells are cultured as aggregates. The technique does not require microcarrier scaffolds or extracellular matrix (105). The method requires single cell seeding to maintain high cell viability. The system often requires stabilising inhibitors and growth factors, such as ROCK inhibitors (as discussed in Section 1.11.3) (106). Controlling aggregate size is difficult, and large clumps require dissociation usually with manual passaging every few days (107). This can be labour intensive, increase the probability for contamination, and represents a significant challenge for high cell density cultures. In addition, maintaining fine control over stem cell function and pluri/multi-potency as volumes increase remains a challenge (108).

Both hESCs and iPSCs have been successfully cultured in aggregates (106, 109). Furthermore, MSCs have also been cultured at relatively low cell densities in aggregates; however results indicated a reduced doubling rate (110). In addition, like microcarrier cultures, aggregates in suspension are subject to shear stresses, which can result in unstable cell growth and unwanted spontaneous cell differentiation (111). More research into this system is required to ensure product consistency and efficacy.

1.7 Microcarriers

Microcarriers are small spherical particles or beads originally described in 1967 by Van Wezel (112) for the culture and expansion of anchorage-dependant cells and production of viral vaccines and pharmaceuticals. Microcarriers have a high surface-area to volume ratio and are therefore frequently used for growing high-density cell cultures in a suspension culture system. With the development of several commercially available microcarriers and the improvement of bioreactors, they have become popular in large-scale industrial cell culture.

Bioreactor Type	Bioreactor Design	Materials	Key Features
Parallel plates bioreactor		•Multilayer vessels •Tissue Culture plastic •Up to 120 layers , equivalent to a cell culture area of ~60,000 cm2	• High productivities can be achieved • Medium-intensive culture system • Accumulation of toxic metabolic side-products is minimized, but continuous removal of secreted factors may be detrimental • Effects of hydrodynamic shear stress are unknown

Packed and fluidised bed bioreactor		•Immobilised substrates
		  •Microcarriers
		  •Fibre and hollow fibres (either smooth, porous or woven)
		•Materials
		  •Glass beads
		  •Ceramic
		  •Polyester
		  •Polyurethane materials
			• Provides 3D scaffolding for cell attachment and growth
			• Spatial concentration gradients (in the fixed bed configuration)
			• Cell–cell or cell–matrix interactions are possible, providing a better mimic of the *in vivo* intricate structure
			• Possible shear stress effects (in the fluidised bed configuration)
			• Low volumes and difficulties in scaling-up, when compared with other systems
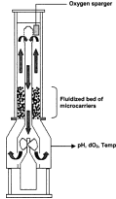
Spinner flask bioreactors		• Compatible with microcarriers • Requires mechanical agitation using different types of impeller • Can tightly regulate culture parameters such as gas exchange nutrient feeding and pH using probes and online monitoring.	• Simple design. Homogeneous conditions are achieved • In addition to suspension culture (as cell aggregates or single cells), also allows adherent growth when microcarriers are used • Bioreactor operation and sampling are easily performed • Hydrodynamic shear stress due to mechanical agitation can be harmful to cells • Monitoring and control solutions are widely available • Microcarrier bridging and/or cell agglomeration may occur
Wave Bioreactors		•Compatible with microcarriers •Rocking motion agitates cell microcarrier suspension . •Removes need for an impeller. Potentially reducing shear stress damage to cells	• Disposable system and easily scalable • Sampling, monitoring and control are not as simple as with other systems • Contamination issues are minimized and sterilization is not needed, rendering it suitable for GMP operations • High-cost solution

Figure 2: Summary of the main characteristics of different bioreactors used for mesenchymal stem cell culture.

1.7.1 Microcarrier properties

Microcarrier properties have been shown to significantly affect cell attachment, growth rates and cell multi- or pluripotency and there are several different types of microcarriers that are commercially available with various bulk material properties (113, 114). Microcarriers can be made from cross-linked dextran matrices (Cytodex 1, GE Healthcare) (112, 115), or polystyrene (HyQSphere, HyClone and Hillex, SoloHill Engineering) (116). In addition they can contain surface chemistry modifications to include whole animal protein (typically ECM components) such as covalently bound collagen (117) or gelatin (118, 119), (Cytodex 3, GE Healthcare and HyQsphere, Hyclone). Such protein coatings provide an *in vivo*-like element to the cell culture platform, a factor shown to improve cell adhesion and expansion (120). A comparison of different microcarrier properties is shown in Figure 2.

Traditionally, microcarriers rely largely on charge potential for cell attachment (115), where cells are electrostatically attracted to the microcarrier surface (121). Microcarriers often contain a net charge (mainly positive and occasionally negative), by

incorporating cross-linked diethylaminoethyl (DEAE) anion exchange groups. Other common microcarrier materials include glass, (122) cellulose, (123, 124) gelatin, (118, 125) and polyacrylamide (126). Most microcarriers have smooth surfaces, however in order to increase surface area for cell adhesion, macroporous microcarriers containing cross linked cotton cellulose have been developed such as the Cytopore range (GE).

Further advances in microcarrier composition include the incorporation of magnetic particles that can aid cell separation from beads and *in vivo* monitoring (127). Hexagonal Microcarrier's μHex product (Nunc, Thermo Scientific) has flat surfaces, replicating conventional planar surfaces, whilst maintaining a high surface area: volume ratio synonymous with microcarrier technologies for spherical particles (92). Maximum cell attachment and expansion in microcarrier culture systems is limited to the carrier diameter. The optimum microcarrier diameter has previously been determined to be between 100–400 μm), with a density typically between 1.02 and 1.10 g/ml) (128). Microcarriers are typically designed to have a density that allows them to be maintained in suspension (in culture medium) with gentle stirring.

Biopharmaceutical uses of microcarriers in large scale bioreactors is applicable to large scale production of therapeutic adherent cells. Typical harvests are 1×10^6 cells/mL for MSCs and 1×10^6 to 3×10^6/mL for ESCs (88). Using large scale (>1,000L) bioreactor systems for stem cell expansion could potentially generate lot sizes of approximately 1 trillion cells.

Microcarrier Type or Brand	Porosity	Core chemistry	Surface Chemistry	Diameter (µm)	cm²/g	Density (g/cm3)	Manufacturer
Cytodex 1	Microporous	Cross-linked dextran	Charged throughout the matrix	131-220	4,400	1.03	GE Healthcare
Cytodex 3	Microporous	Cross-linked dextran	Acid-denatured porcine gelatin	131-220	2,700	1.04	GE Healthcare
Cytopore 1	Mcroporous; average pore diameter 30µm	Cross-linked cotton cellulose	Hydrophillic DEAE exhanger (postive charge 1.1 meq/g)	Average 230 (range not reported)	11,000	1.03	GE Healthcare
Global Eukaryotic Microcarrier (GEM)	Porous	Alginate with magnetic particles cross-linked	Multiple	75-150	342	NA	Global Cell Solutions Inc
Cultispher G	Macroporous	gelatin cross-linked	Porcine gelatin	130-380	NA	1.02-1.04	Percell
Cultispher S	Macroporous	gelatin Cross-linked	Porcine gelatin	130-380	NA	1.02-1.04	Percell SoloHill
Collagen, Gelatin	Nonporous	polystyrene Modified	Type I porcine collagen (gelatin)	90-150/125-212	480/360	1.02/1.04	Engineering SoloHill
Hillex II	Microporous	polystyrene Cross-linked	Cationic trimethyl ammonium	160-200	515	1.11	Engineering SoloHill
Plastic Plus	Nonporous	polystyrene Cross-linked	Cationic	90-150/125-212	480/360	1.02/1.04	Engineering SoloHill
FACT III	Nonporous	polystyrene	Cationic type I porcine collagen (gelatin)	212	480/360	1.02/1.04	Engineering
Nunc 2D MicroHex	NA	Polystyrene	NunclonΔ surface	125 L x 25 D	760	1.05	Thermo Fisher Scientific SoloHill
Pronectin F	Microporous	Polystyrene	Pronectin F poly RGD peptide repeat	125-212	480	1.02	Engineering

Figure 2: Table of commercially available microcarriers and their respective properties.

1.7.2   Spinner flask bioreactors for cell expansion on microcarriers

There are four types of bioreactors compatible with microcarrier based stem cell expansion; these include PBRs, Roller bottles, Spinner flasks and the Wave bioreactor (GE). In order to maximise the microcarrier surface area for cell attachment and growth, the particles must remain fully suspended in culture medium. In bioreactors, such as spinner flasks this is achieved using mechanical agitation. This also has the effect of homogenising the culture media, allowing nutrient transfer and diffusion of oxygen, whilst most importantly allowing CO_2 release (129). Using spinner flask bioreactors parameters such as, gas exchange, nutrient feeding and pH can be tightly regulated using probes and online monitoring (130). A disadvantage of this technique is the agitation required can damage the attached cells, either by direct mechanical damage or by shear stress caused by continuous fluid flow (131). Cell laden microcarriers incur damage mainly due to particle-impeller and particle-particle collisions. This damaging effect increases with increasing particle size, concentration and agitation intensity. Under stirred culture conditions, cells are exposed to hydrodynamic shear stress. Cells cultured either in suspension, in aggregates or on microcarriers may become damaged when the turbulent eddy size has the same order of magnitude as the diameter of a single cell, aggregate, or microcarrier (132). With increasing agitation intensity, the eddy size decreases, hence cells adhered to microcarriers or in aggregates can be affected at much lower agitation rates compared to single cells (133). Factors that increase hydrodynamic stress include increasing impeller diameter and rpm, in addition to impeller geometry and location. Within bioreactors, probes and other internal vessel components can disrupt radial flow patterns and increase shear stress. When subjected to continuous shear stress, spontaneous undesirable differentiation of MSCs has been shown to occur and can be exacerbated under serum-free conditions (134, 135). Studies have shown that MSCs cultured on microcarriers expanded in spinner flasks, upregulated the expression of cell markers for early osteocytes and chondrocytes (135-137). This indicates that shear stress experienced by cells in a microcarrier-based, stirred bioreactor has a potential priming effect on MSC differentiation. Several studies have confirmed this, reporting greater shear stress can induce upregulation of osteogenesis related genes (137). However, further microcarrier based spinner flask expansion studies using BM-MSCs and ADSCs cultured in xeno-free medium demonstrated a multi-lineage potential, suggesting the mesodermal progenitor properties remained intact (138). More recently, an alternative bioreactor has been designed (GE) which removes the need for an impeller. Microcarriers are cultured in a

single use bag termed a Wave bioreactor which applies a rocking motion to agitate the cell microcarrier suspension, potentially reducing the damaging effects of shear stress (139). The impact of agitation rates and mixing dynamics vary greatly between different style bioreactors and microcarrier properties and therefore individual optimisation is required to reduce shear stress and its potential effects. In addition to microcarrier properties, both cell culture medium and bioreactor system have been shown to affect cell proliferation, phenotype and differentiation potential (140). This has been observed in primary cells (human fibroblasts and bovine embryonic kidney cells). However, few studies have investigated the full effects of agitated culture of hMSCs.

1.7.3 Harvesting cells from microcarriers

Similarly to PBR systems, generating large cell yields relies on the ability to dissociate the therapeutic cells efficiently and completely from the scaffolds, whilst maintaining the cells' integrity. Traditional enzymatic dissociation methods using proteases (i.e. collagenase, Accutase, dispase and Trypsin) are the most common means of cell-microcarrier separation (141). Typically this yields 60-70% cell recovery for smooth microcarriers and ~50% for macroporous microcarriers depending on the microcarrier properties. This poses a substantial drawback to using the currently available microcarriers for therapeutic cell expansion. In addition, significant optimisation and validation is required to guarantee that microcarriers and particulates can be fully separated from the therapeutic cell population, as any carryover will present a serious safety risk during intravenous administration (88). This risk can be reduced by using magnetically charged microcarriers, or by using microcarriers with biodegradable and thermosensitive elements (142).

1.7.4 Microcarrier based expansion of primary cells

In addition to providing a support for cell culture, microcarriers have also been used for tissue engineering purposes by providing a scaffold for delivering therapeutic cells to repair damaged or degenerated tissue to restore function (143). To use microcarriers for musculoskeletal or dermatological purposes, biodegradable materials such as FDA approved hydrogels and natural polysaccharides have been shown by Wang *et al.* (2008) to support cell adhesion of anchorage dependant cells, and facilitate proliferation and differentiation of hMSCs and progenitor cells (144, 145). Biodegradable microcarriers have been developed, the typical materials used include

gelatin (CultiSpher family) (146), collagen (CellagenTM)(147), poly-lactic-co-glycolic acid (PLGA) (148), poly-L-lactic acid (PLLA) (149), and hydroxyapatite (150). Primary cell–laden microcarriers have been used successfully in *in vivo* experiments to treat various diseases in animal models including liver insufficiency (151), cartilage repair (146, 152), skin repair (153), and Parkinson's disease (154). Clinical trials have demonstrated positive results for using gelatin based microcarriers laden with human retinal pigment epithelial cells for the treatment of Parkinson's disease (155).

Cytodex 3 has been successfully used as a support for the expansion and transplantation of primary hepatocytes, resulting in extended *in vivo* hepatocyte viability and function (151). Furthermore the transplanted hepatocytes in liver-damaged rats provided a restorative effect giving metabolic support and increasing survival rates (156). This has since been supported in other rat models of acute liver failure and further developed into a bio-artificial liver system facilitating metabolic support (157, 158). To enhance wound healing and skin repair, Cytodex 3 has also been used to culture primary keratinocytes and develop a multilayered and keratinised epithelium in a full thickness wound healing model (153). However Cytodex 3 microcarriers are not biodegradable *in vivo* and hence can induce an inflammatory reaction. Consequently in 2002 the research group Stark *et al.* generated biodegradable PLGA microcarriers which were surface modified to contain a layer of gelatin and recombinant human epidermal growth factor (159). At 14 days post-transplantation, a new stratified epithelium was detected in the full-thickness wound healing model using this novel PLGA microcarrier. Human nasal chondrocytes have been expanded on CultiSpher-G (macroporous gelatin-based) microcarriers to generate cartilage. After implantation into nude mice, collagen expression was higher in the chondrocytes-laden microcarriers than in cells cultured in 2D T flasks (146). Furthermore, chondrocytes have also been expanded on gelatin and PLGA microcarriers (148). PLGA microcarriers have also been used in mouse models by Kang *et al.* (2005) to demonstrate articular cartilage repair (160). Previously the use of microcarriers was confined to generation of therapeutic proteins, however the use of microcarriers to deliver therapeutic cells to the site of damage or diseased tissues (2001) has demonstrated the feasibility of utilising microcarriers in regenerative medicine.

1.7.5   Microcarrier based expansion of MSCs

There has been a growing trend in the use of microcarriers for stem cell expansion (161-163). MSC based clinical therapies require large MSC quantities (as

discussed in Section 1.6), as typical intravenous treatment dose uses 5×10^6 cells/kg body weight. Therefore a reproducible, scalable method to yield un-differentiated homogeneous MSC populations is required. Several strategies are available to deliver cells expanded on microcarriers, e.g. harvested cells can be injected into the body, transferred to a scaffold for tissue engineering purposes; or the microcarrier-cell construct can be injected directly to repair damaged or diseased tissues such as, brain, bone, cartilage, liver or skin. Previously, growth and expansion studies of embryonic stem cells (ESC) on microcarriers have shown that both human and murine ESCs maintain their pluripotency with Cytodex^{TM} and trimethyl ammonium-coated polystyrene carriers (164). However, until relatively recently few studies have indicated the success of a microcarrier based system for MSC expansion.

Pioneering work by Wu *et al.* in 2003, demonstrated human MSCs attaching, proliferating and differentiating on macroporous microcarriers in spinner flasks (165). Expansion over 7 days gave a 10-fold increase in viable cells. Also lactate production from glucose consumption was lower in spinner culture (indicating better cell health) than in static culture. Most importantly, MSCs cultured on microcarriers were still multipotent after 12 days in culture. Other studies performed by Marc *et al.* in 2011 compared the culture of porcine derived BM-MSCs on three different commercially available Cytodex (1,2 and 3) microcarrier types (166). Cytodex 1 showed the highest level of attachment, the cells remained multipotent and also demonstrated cell migration from one microcarrier to another in 'bead to bead transfer'. Other experiments performed by Schop *et al.* (2008) have shown that using goat derived MSCs cultured on microcarriers, the addition of 30% fresh medium containing virgin microcarriers every 3 days allowed a more homogenous cell distribution of cells across the microcarriers due to bead to bead transfer (113). In addition, cell proliferation increased whilst the production of lactate from glucose decreased. The transfer of cells from colonised beads to fresh beads facilitates an extendable culture surface, potentially lengthening *in vitro* culture times. However cell multipotency and 'stemness' have not been fully characterised on microcarrier expanded MSCs.

Injectable microcarriers may act as tissue engineering scaffolds allowing for the precise placement of cells within a site of injury, in addition to enhancing the function of injected cells. Adipose derived stem cells have been successfully expanded and differentiated *ex vivo* into adipocytes and osteoblasts in 2011 by Santos *et al.* on Cultispher-G microcarriers (138). Similarly Yang *et al.* in 2007 compared apoptosis of

BM-MSCs directly injected into subcutaneous tissue to BM-MSC laden Cultispher-G microcarriers. It was found in short term conditions that apoptosis was significantly reduced in cell-microcarrier constructs. Long term effects demonstrated *in vivo* that there was an induction of *de novo* trabecular bone formation (167).

Proof of principle studies have demonstrated the successful expansion of MSCs on microcarrier supports in spinner flask bioreactors, whilst maintaining important multipotent characteristics. Furthermore, bioreactor techniques have been established including proliferation of cells on microcarriers *via* bead to bead transfer (113). However, microcarrier properties need to be optimised to generate a clinically useful expanded MSC population as several experiments have demonstrated the genomic and behavioural changes of these cells in response to culture substrates (168).

1.7.6 Issues with microgravity

Bioreactors such as roller bottles or spinner flask can induce a microgravity environment, (the bioreactor subjects the suspended cells to a continual state of free fall, hence, simulating microgravity). This microgravity environment can alter the differentiation of cultured MSCs on plastic microcarriers, inhibiting osteoblastic lineages and inducing adipogenic differentiation (169). This has been attributed to RhoA and cytoskeletal disruption (170). This models the reduction in bone mass experienced by humans after a prolonged time in space, and also suggests that a bioreactor system whereby cultured MSCs on microcarriers experience microgravity, cannot sustain the differentiation potential of MSCs within the appropriate level of control.

1.8 Biomaterials

Cell adhesion is substrate dependant (171, 172) and there are optimum surfaces for cell growth (173, 174), which vary between cell types (61, 173, 175). A key aim in biomaterials research is to provide cells with adhesive substrata that convey cues similar to those received *in vivo* (176). In mimicking the native environment in which the cells develop, differentiate and function, the development of microcarrier surfaces for animal cell culture has advanced to include characteristics from the extracellular matrix (ECM). These may be mechanical, chemical and/or topographical stimuli (177-179).

In vivo, cells growing within soft tissues reside within an ECM, a hydrogel scaffold comprised of cross-linked proteins and polysaccharides. The ECM provides mechanical and chemical cues which influence cell behaviour and differentiation. To generate homogenous populations of stem cells for cell therapies and pharmaceuticals it is important to determine the factors within the stem cell niche which tightly regulate stem cell self-renewal and differentiation. Furthermore, to develop therapeutic applications of MSCs, instructive biomaterials are required that can provide key regulatory signals and exert control over MSC behaviour and phenotype. Directed biomaterials will need to be designed to expand homogenous multi-potent and differentiated stem cells populations *ex vivo*.

Most scaffolds are generated from polymers, (both natural and synthetic), metals or ceramics. Metals and ceramics are restricted to models of very hard tissues such as bone. However, polymers can be manipulated to mimic the physical properties of the ECM of all tissues from the mechanically weak cornea to harder tissues such as cartilage and can be fabricated into porous, fibrous or solid scaffolds (180). Polymers were first suggested for use in biomedical applications in 1960 (181), and can be made from natural materials, e.g. collagen, gelatin, hyaluronan, fibrin and alginate, or from synthetic chemicals such as Poly(ethylene oxide), Poly(acrylic acid), Poly(vinyl alcohol) and biodegradable poly lactic glycolic acid (PLGA).

1.9   Natural Polymers

Collagen comprises 30% of total body protein, is highly conserved and forms a thermally and ionically reversible hydrogel under certain conditions. There are several different collagen isoforms, which have been widely investigated and have been shown to promote ESC and MSC attachment, growth and differentiation (182, 183). In addition, gelatin (denatured collagen) has been widely used in scaffolds and microcarriers (184). MSCs cultured in collagen-based matrices can degrade and re-assemble the underlying matrix structure using matrix metalloproteinases (MMPs) (185). In addition, the cultured cells were able to differentiate into spherical chondrocytes and synthesise several cartilage specific proteins (146). Collagen-based hydrogels have comparatively large pores allowing for efficient diffusion of nutrients and waste and have weak mechanical properties which can be improved with chemical crosslinking reagents, e.g. glutaraldehyde (186, 187).

Fibrin is a key mediator in blood clotting and normal wound healing processes and hence has been used as a biomaterial (alone and in combination with other materials) to differentiate stem cells (180). In 2005 Lee *et al.* demonstrated that both ADSCs and BM-MSCs differentiate into several mesodermal lineages on 2D fibrin scaffolds and within 3D fibrin-agarose scaffolds. Furthermore BM-MSCs performed chondrogenesis and osteogenesis more effectively than 2D culture (188).

Silk protein has high mechanical strength and is elastic with high tensile strength due to strong hydrogen bonding when compared to other biomaterials such as collagen (180). Silk proteins make good candidate materials to model bone, cartilage and ligament tissue as they have slow degradation kinetics *in vivo* (189). In 2006 Kaplan *et al.* compared hMSC differentiation to chondrocytes on silk biomaterials and found chondrogenesis was more effective and extensive on silk scaffolds when compared to collagen (190).

Matrigel, marketed by BD Biosciences, is a soluble protein blend of basement membrane proteins isolated from Engelbreth-Holm-Swarm (EHS) mouse sarcoma cells. It is gelatinous and contains several ECM components including laminin, collagen IV, and heparin sulphate proteoglycans and entactin, as well as several unknown components (191). Matrigel has been successfully used as a model system providing a 3D environment to culture a variety of cell types to study cell morphology, biochemical function, cell migration and invasion, and gene expression (192). Matrigel has also been used to maintain an undifferentiated stem cell state, for example hESCs have been cultured in mouse fibroblast conditioned medium in a feeder-free system (193). Furthermore, Matrigel has been used to study differentiation. For example, ESC-derived neural precursors cells cultured on Matrigel were capable of differentiating into neurons (194). However, several factors limit the use of Matrigel in large scale or high throughput experiments. Firstly, Matrigel is expensive relative to traditional cell culture methods or other biomaterials. Secondly, Matrigel is a thermally responsive hydrogel and begins gelation above 4°C, which can generate technical challenges in handling and can form matrices with heterogeneous properties. In addition, due to its source Matrigel can pose a risk of possible pathogen transmission and immunogenicity (195). Batch-to-batch inconsistencies and the inability to experimentally vary both the composition and compliance of Matrigel have led to researchers seeking synthetic ECM equivalents which can generate a 3D environment with *in vivo*-like properties.

In addition to proteins, polysaccharides are essential in maintaining the structure of the ECM. Common polysaccharides utilised to culture stem cells include agarose, alginate, and chitosan. Agarose is derived from seaweed, and forms a thermally responsive, biodegradable, porous, hydrophilic hydrogel (180). However as a biomaterial substrate it lacks adhesion cues, and therefore has limited utility in cell culture processes. In addition, humans lack the necessary enzymes to degrade agarose hydrogels, hence it is unsuitable for injectable MSC delivery. Agarose gels have been exploited to analyse hMSC chondrogenesis under compression loading by Bader *et al.* in 2006 (196). For example, BM-MSCs seeded in agarose constructs were shown to change cell morphology under chondrogenic conditions into a spherical shape and under hydrostatic pressure undergo chondrogenesis.

Alginate is an anionic polysaccharide which forms cross-linked networks *via* ionic interactions to yield flexible gels mimicking soft tissues such as brain and liver (197). It is widely used as a biomaterial as it evades immune and inflammatory responses. Alginate scaffolds have been shown to support attachment of ADSCs and BM-MSCs and in addition support chondrogenic differentiation (198). Alginate hydrogels contain interconnected pores which can generate a 3D microenvironment for cell culture. In addition alginate gels have been used to make porous microspheres, in which many cell types have been encapsulated and supported (199). GEM, a commercially available microcarrier contains a porous highly negatively charged alginate core, with optional extracellular matrix coating. The microcarrier also contains magnetic particles for ease of manipulation (200). Cell recovery from alginate microcapsules is simple as the matrix can be dispersed using divalent cation chelators such as citrate. This property makes alginate hydrogel processing more flexible and increases its potential uses in regenerative medicine.

Chitosan is a biodegradable linear polysaccharide which can vary according to the degree of deacetylation. Chitosan-based biomaterials are both biocompatible and nontoxic and display cationic behaviour. In addition they are versatile in their ability to form hydrogels, films, fibres, 3D porous structures and microcarriers. They are therefore useful for developing wound dressings, space filling implants and scaffolds for stem cell applications (201). Chitosan can be modified *via* covalent bonding due to its primary amino groups and blended with other polymers to add strength. In addition, it has tunable mechanical properties, for example high molecular weight chitosans produce relatively tough scaffolds used for modelling bone (202). In its protonated

state, it is also capable of ionic interactions and thus can be used to enhance adhesion of stem cells. Chitosan has been used to generate smooth microcarriers to culture both human and mouse fibroblasts (201). Chitosan is composed of glucosamine and N-acetylglucosamine, which shares a structural similarity to glycosaminoglycan (GAG) and its analogs, a major component of ECM found in cartilage. Therefore chitosan coated PLLA microcarriers have been used by Gao *et al.* in 2008 to study chondrogenesis, where chondrocytes were able to attach and maintain their phenotype *in vitro*, creating a potential cell delivery vehicle for cartilage repair (203). In 2009 Kim *et al.* generated porous chitosan microcarriers by electrospraying techniques (discussed in Section 1.12.2) and demonstrated that hMSCs were able to attach and proliferate within the pores of the chitosan beads and be maintained in spinner flask culture for up to 21 days (204).

Natural polymers most closely resemble the tissues they are meant to replace and they are nearly always biocompatible and biodegradable. However, biologically derived materials also have several disadvantages, they require isolation, purification and processing which can be expensive and exacting (205). They may elicit undesirable immune responses and pose an increased risk of endotoxin contamination (206). In addition, they demonstrate restricted versatility (207); though natural hydrogels based on ECM components such as alginate (198), hyaluronic acid and collagen (187) have been well studied and used successfully for stem cell culture, natural scaffolds lack the capacity for tailoring the mechanical and degradation properties required to study a range of tissue environments.

1.10   Synthetic polymer scaffolds for cell adhesion

A wide variety of biomaterials based on synthetic polymers have been developed for cell culture applications, due to their ease of handling, processing and purification (83). Synthetic hydrogels can be generated from a variety of polymers using different gelation techniques, resulting in gels with a wide range of mechanical properties, chemical compositions and overall shape (83). Additionally, controlling molecular weight and cross-link density parameters permits greater control of material properties (205). Hydrogels are hydrophilic polymeric networks that can absorb water without dissolving, and can be made from natural or synthetic materials (207). They are attractive materials for the production of tissue engineering scaffolds because they possess characteristics similar to the ECM in many tissues including chemical and

structural similarities. They provide an aqueous environment for cells; they are highly porous to allow for nutrient transport, readily modifiable and are generally biocompatible (208). Hydrogels are typically processed under mild conditions. Due to their compatibility with *in vivo* tissues, hydrogels have provided the primary scaffold material for several varied applications including drug and growth factor delivery, artificial tissue replacements in tissue engineering processes amongst many others (209).

Polyethylene glycol dimethacrylate (PEGDMA) hydrogels have proven to be excellent biocompatible substrates (210). PEGDMA is hydrophilic, easily manipulated, highly wettable and resistant to non-specific protein adsorption (211). It is now widely used in tissue engineering as a preferred cell culture substrate (212-214), and can be processed simply, forming hydrogels *via* chemically initiated or UV-initiated free radical photo-polymerization (215). The resulting hydrogel has a high water content (216), and possesses mechanical properties similar to those of soft tissues, such as a high elastic modulus (resulting in greater compressibility) making it ideally suited to study MSC adhesion and controlled differentiation (215). Synthetic hydrogels generated from polymers such as poly(ethylene glycol) are bioinert systems, and can provide a scaffold to anchorage dependant cells, but lack directed cues causing adhered cells to alter their cellular functions, often leading to apoptosis (217, 218). Recently, the modification of biomaterials has been expanded to include functionalised polymers with ECM-derived bioactive factors, which has been widely shown to increase cell viability and direct cell function (205, 206). Biomaterials can provide not only a structural and mechanical support but can also interact with cells and alter their biological functions. Various biological signals, such as ECM proteins, have been incorporated into biomaterials, either as a surface modification or tethered throughout the bulk of the matrix to alter cell adhesion spreading, proliferation and matrix production (217).

1.11 Influence of bioactive-functionalised materials on cell growth

Integrating proteins isolated from the ECM such as laminin, collagen and fibronectin onto artificial polymer surfaces can be problematic (214, 219). Isolation, purification and immunogenicity can be costly and generate undesirable responses (as discussed in Section 1.9). Such proteins contain several different cell recognition and adhesion motifs which are responsible for binding cell surface integrin receptors (220, 221). ECM deposition onto materials with variable surface properties such as charge,

wettability (222) and topography can influence protein orientation and conformation (223, 224), potentially sterically hindering cell-protein interaction (225). A more controllable solution is to present cell recognition motifs as small, immobilised peptides. Originally demonstrated by Hern and Hubbell, incorporating ECM-derived peptide sequences into PEGDMA hydrogels creates a synthetic material with cell-adhesive and/or proteolytically cleavable properties (226). They can be used to functionalise materials in a defined, concentration dependant manner (227). Incorporating defined, synthetic peptides can therefore be used to target and select for a particular cell type (228, 229). Linear peptides can be susceptible to enzymatic degradation and have a relatively short half-life, cyclic peptides however exhibit excellent long term stability (228).

The most commonly used bioactive peptide for the functionalisation of surfaces is the Arg-Gly-Asp (RGD) sequence (229). RGD is a conserved peptide sequence found in several core proteins of the ECM, including collagen, fibronectin and laminin. Peptides containing this core sequence have been shown to bind 12 of the known 24 integrins (230) and have a vital role in cell adhesion, in addition to influencing many other cellular functions including embryogenesis and cell differentiation (231). Previously, a range of peptides has been used to functionalise various biomaterials that are derived from conserved ECM peptide sequences. For example, a commonly used peptide derived from fibronectin is arginine–glutamic acid–aspartic acid–valine (REDV), and peptides derived from laminin are tyrosine–isoleucine–glycine–serine–arginine (YIGSR) and isoleucine–lysine–valine–alanine–valine (IKVAV) (207).

Peptide sequence	ECM/Molecular source	Function	Ref.
RGD	Fibronectin, vitronectin, laminin, collagen , osteopontin and thrombospondin	Promotes hMSC adhesion, spreading, migration and proliferation Regulates hMSC differentiation	(233-235)
IKVAV, YIGSR	Laminin	Enhances hMSC adhesion and viability	(236, 237)
KIPKASSVPTELSAISTLYL	Bone morphogenetic protein-2 (BMP-2)	Promotes MSC differentiation and mineralization	(238)
GPQGIWGQ, LGPA	Collagen type I (MMP substrate)	Cell -mediated proteolytic degradation	(239, 240)
QPQGLAK	Collagen type II (MMP-13 substrate)	Cell -mediated proteolytic degradation	(241)
VRN, YKNR	Fibrinogen (plasmin substrate)	Cell -mediated proteolytic degradation	(242, 243)
$Y(GPO)_7$	Collagen type I	Collagen retention Promotes hMSC differentiation	(244)
$(GPO)_4GFOGER(GPO)_4GCG$	Collagen type I	Collagen -integrin β1 interactions Promotes hMSC differentiation	unpublished data
KLER	Decorin	Collagen type II retention and organization Promotes hMSC differentiation	(245)
AKA_3KA	Elastin	Enhances gel elasticity	(246)
K-βAla-FAKLAARLYRKA	Anti-thrombin III	Heparin binding	(242, 243)
E_6	Osteonectin	Hydroxyapatite binding	(247)

Figure 3: Bioactive peptides for improved MSC-biomaterial interactions

Other agents that mediate cell adhesion include growth factors and adhesion molecules. It is possible to incorporate growth factors or growth factor derived peptides into hydrogels by chemically tethering them to the polymer backbone as demonstrated using ECM components (207). Such hydrogel modifications provide an opportunity to regulate the function of interacting cells. In 2001, West *et al.* cultured smooth muscle cells in PEG hydrogels containing the tethered peptides RGDV and transforming growth factor β (TGFβ) active fragment, and found enhanced cellular functions, in particular increased ECM production (232). TGFβ has a significant role in regulating ECM production, by presenting the growth factor in this manner it was able to interact with cellular receptors constitutively without being internalized (233).

1.11.1 Hydrogel polymerisation methods

Hydrogels are cross-linked, hydrophilic swollen polymer networks which can retain large quantities of water (215). Hydrogels can be used for biomedical applications to encapsulate cells and bioactive peptide or protein therapeutics (199, 234). Hydrogels based on the synthetic oligomer PEG can be crosslinked either chemically or physically. Chemical crosslinking gelation results in ionic or covalent bonds between polymer chains (235). This method of gelation can result in hydrogels with greater mechanical stability, however, chemicals and conditions, (temperature, pH, initiators, catalysts or UV) required for polymerisation are often cytotoxic and result in undesirable reactions

and can generate a hydrogel which is not biocompatible, limiting its uses (83). Physical crosslinking of hydrogels occurs under relatively mild conditions by either ionic interactions, hydrogen bonding or hydrophobic interactions or by molecular entanglement and/or weak secondary forces such as Van der Waals interactions. However they are mechanically weaker than chemically crosslinked hydrogels. Covalently-crosslinked PEGDMA hydrogels are commonly used as scaffolds for tissue engineering and regenerative medicine applications, where tunable mechanical strength and stability are required. Hence chemical crosslinking is often favoured.

PEG dimethacrylate can be polymerised using radical mediated chain growth mechanism in the presence of appropriate radical generating initiators and conditions (236). This is the most commonly used method of generating PEG based hydrogels for tissue engineering purposes. This method can generate stable hydrogels under physiologically relevant conditions and within a relatively short time period (minutes). In redox initiated polymerisation, radicals are formed by a pair of redox active chemical initiators, typically a persulfate with N,N,N',N' -tetramethyl ethylenediamine (TEMED) (236). However, recent advancements (2009) utilising PEG based hydrogels for stem cells encapsulation have used UV photo-polymerisation which gives faster crosslinking and spatial and temporal control over gel formation (as radical production can be restricted to a focused light source) (237). In addition several UV photo-initiators have been widely studied in cell encapsulation demonstrating biocompatibility (238). Photopolymerisable PEG hydrogels have been extensively studied including by Liu *et al.* (2009) for the biomaterial culture of both ESCs and MSCs and have proved to be a useful platform in the study of stem cell differentiation (83, 239). A drawback of radical initiated chain growth polymerisation is that macro-monomer crosslinking can be low. Changes in UV exposure time or pH can increase macromer crosslinking; however this can be incompatible if attempting to encapsulate cells during polymerisation.

Incorporation of bioactive peptides into PEG polymers to direct cellular function requires new polymerisation techniques (229). There are several established techniques to tether bioactive peptide to PEG hydrogels. The most common approach covalently links target peptides to a monoacrylated PEG monomer through an *N*-hydroxysuccinimidyl group (226). This is an extensively studied method of peptide

incorporation and is similar to traditional techniques of coupling proteins to PEG. This system requires a pre-synthesis reaction off resin using expensive reagents, which is time consuming and produces a variable product yield (240). In addition it involves an unstable NHS ester intermediate.

An alternative technique, termed 'click chemistry', utilizes free thiol groups on cysteine containing peptides to tether bioactive sequences into unsaturated alkene or acrylate groups during photo-polymerisation (241). Step growth thiol-acrylate polymerisation occurs in the presence of a photoinitator, generating peptide functionalized PEG hydrogels (242). The system comprises mixed-mode polymerisation, the reaction mechanism consists of two competing reactions; that of the acrylate homopolymerization and the thiol acrylate step growth reaction (Figure 4) (243). Described by Anseth *et al.* in 2008, this method provides a robust, cost-efficient, and cytocompatible reaction scheme for the incorporation of peptide sequences into PEG hydrogels for 3D cell culture and the direction of cellular function (244, 245). The reaction produces a high yield with fast kinetics that can occur in mild, solventless conditions or in water. This has been shown to be a very successful modification of PEG hydrogels with approximately 95% incorporation of a target bioactive peptide (240).
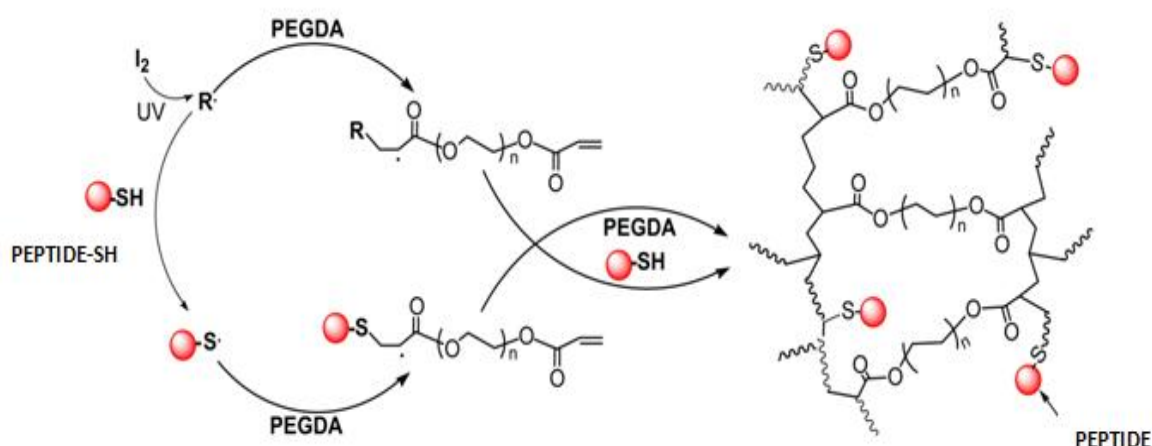
Figure 4: Preparation of cell-adhesive PEG hydrogels by thiol-acrylate photo-polymerisation

Thiol-acrylate photo-polymerisation of PEGDA with monothiol-containing cell adhesive peptide (PEPTIDE-SH) (Adapted from (246)).

1.11.2 Mechanical cues

MSCs reside within a niche where they are surrounded by ECM which presents an array of complex biophysical and biochemical signals. During normal periods of regeneration adult stem cells are thought to egress and travel away from their niche to other tissues where they can engraft and differentiate (247). During migration, cells will experience a diverse variety of tissue or matrix microenvironments. MSCs are known to differentiate into a wide range of cell types from neurons to osteoblasts, each of which typically reside in very different physical microenvironments. One physical cue is the surrounding elasticity or stiffness of the ECM, which can influence cell morphology and function (248). When a cell exerts a force that deforms the surrounding ECM it feels a level of resistance, this can be measured by the elastic constant, E, of the matrix or microenvironment. The compressibility of the culture substrate can drive differentiation or maintain stem cell phenotype in adult stem cells (249).

MSCs interpret their surrounding substrate elasticity and transduce information into changes in morphology and differentiation potential (249). To 'feel or sense' the matrix and respond, cells must first pull against the matrix. Following this, an intracellular mechano transducer(s) must generate a signal proportional to the force required to deform the matrix (250). The actin cytoskeleton is linked to focal adhesion groups at the cell surface, which provide the site for attachment to the ECM *via* cell surface receptors termed integrins and allow force to be transmitted from the extracellular elastic matrix to the cytoskeleton inside the cell (251). At focal adhesion sites, a number of proteins form an intracellular complex at the plasma membrane, which is known to interact with well characterised signalling molecules, and are the sites for mechano-transduction (252). Studies by Chen *et al.* in 2004 have shown proteins that contribute to actin cytoskeletal motors, (such as non-muscle myosin II isoforms), act as mediators modulating contractile forces in the cytoskeleton. These are implicated in providing tension in cortical actin structures, which can sense matrix elasticity and result in differentiation (253). Blocking of myosin in MSCs using inhibitors blocks differentiation of all lineages on both stiff and compliant substrates. Rac and Rho have significant roles in MSC anchorage, contraction and motility, interacting with both growth factors and integrins (254). Indirectly inhibiting ROCK, a Rho Kinase inhibitor, can deactivate myosin and selectively block compressibility directed differentiation of MSCs to osteoblasts on rigid substrates, but not on compliant substrates (255).

It is known that by varying matrix stiffness, both the intracellular cytoskeleton and focal adhesion structure are affected in both naïve MSCs and differentiated cell types. It is difficult to identify and isolate how small changes to substrate stiffness directly influences cell behaviour from the effects of other physical parameters of culture substrates such as topography. However, matrix stiffness at the tissue-level has been shown to have very strong influences on naïve MSCs in *in vitro* cultures, including lineage specification and commitment (255). Furthermore, tensional homeostasis effects, a mechano-regulatory network that integrates physical and biochemical cues between the cells and the tissue microenvironment, can be seen throughout the cell (including morphology, transcript profiles, cytoskeletal organization and contraction and changes to gene regulatory pathways) (256).

In vivo, MSCs not only adhere, but contract and crawl within both soft (e.g. brain) and hard tissues (e.g. the surface of crosslinked collagen 'osteoids' in remodelling bone) (255). Several research groups have attempted to analyse the effects of matrix stiffness on cell behaviour using a range of synthetic hydrogels. For example, Engler *et al.* in 2006 developed an *in vitro* model composed of collagen type I coated acrylamide gels which were tuned to create a wide range of substrate stiffnesses. The research group demonstrated that multipotent MSCs will commit to a specific lineage when cultured on gel substrates with stiffnesses comparable to their counterpart tissues *in vitro*. For example, MSCs differentiate into neurons when cultured on physiologically relavant soft substrates (0.1-1kPa), into myocytes when cultured on slightly stiffer substrates (8-17kPa), and into osteoblasts when cultured on relatively hard surfaces such as collagenous bone (25-40kPa (255). In 2009 Stevens *et al.* demonstrated that culturing ESCs on 'soft' hydrogel substrates establishes a cellular context to promote stem cell self-renewal. ESCs have been shown to upregulate early mesendoderm markers on increasingly stiff polydimethylsiloxane substrates, resulting in increased levels of osteogenic differentiation (257).

Further work must be done to evaluate the synergistic effects of soluble signals such as growth factors, topography and matrix compressibility on cells cultured on biomaterials *in vitro*. To alter the mechanical properties of an artificial cell culture substrate, the following material parameters must be considered: molecular composition, water content, elasticity and structure (256). These can affect both the intermolecular and intramolecular forces and stress distributions. *In vivo* tissues and cells display viscoelastic behaviour, yet several models fail to represent this property

and more work is required to determine the effects of different elastic substrates on cell renewal and differentiation. Traditionally, analysis of MSC function is examined on cells cultured on plastic or glass, which both have a relatively rigid stiffness, 1GPa and 70GPa respectively. Whereas *in vivo* cells typically experience an environment approximately 100,000 fold less stiff (less than 100 kPa).

1.11.3 Topographical and geometrical control over stem cell fate

Cells exist within a spatial context within the *in vivo* stem cell niche. The niche micro-architecture is known to generate concentration gradients of bioactive factors, can modulate cell-matrix and cell-cell adhesion and can establish proximity between compartments such as vasculature and the basal membrane (258). Many instances exist *in vivo* including the formation of crypt to villus patterns in the gut, which is able to direct stem cell differentiation (259).

Since cells recognise their environment on a micro or nano-scale, several fabrication techniques have been developed to generate artificial microenvironments with different topologies and geometries to understand reductively the influence of these factors on stem cell fate (260). Initial techniques studied the behaviour of single cells adhered to surfaces micropatterned with and without adhesion ligands (261). Initial studies revealed primary cells cultured on larger substrates (1500μm^2) proliferated, whereas smaller substrates (500μm^2) induced apoptosis (262). ADSCs demonstrated altered cytoskeletal tension when cultured on substrates with varying geometries, this also influenced subsequent differentiation (255, 263).

Biomaterial scaffolds can be further developed to include topographical cues, for example changes in patterns and orientations of biochemical or biophysical features. Commonly, within hydrogels pore size and interconnectivity can be controlled, which can enable influence over cell proximity and adhesion (264). It can be difficult to isolate the effects of topography from chemical cues and hence cell substrate contact area and cell shape. These have been decoupled by creating scaffolds containing fibronectin adhesive regions with uniform size but varying shape (260). In 2010 Kilian *et al.* showed that by culturing MSCs on small, discrete islands with varying geometry in the presence of competing angiogenic and osteogenic differentiation signals, a relationship between differentiation and the spatial arrangement of the MSC developed, which was found to correspond to cytoskeletal stress mediated by RhoA GTPase signalling (260). In particular, cells cultured on convex islands formed a rounded shape inducing

adipogenesis. Contrastingly, on more angular shapes, the MSC shape was observed to be more spread with increased cytoskeletal tension inducing osteogenesis (260).

The curvature of spherical particles, such as microcarriers, has been shown by Dobler *et al.* in 2009 to have an effect on cell behaviour (265). The curvature or micro-topography of microcarriers can be controlled by altering the particle diameter. Research has shown microspheres containing a diameter of less than 100 μm have limited cell adhesion to their surface. In 2011, Kong *et al.* investigated the effects of curvature on BM-MSCs cultured on RGD modified alginate microspheres with varying diameters (in the microscale). A decrease in cell proliferation and osteogenic differentiation was observed as microsphere diameters decreased from 3cm to 0.5cm independent of RGD concentration (266). This was attributed to increasing shear stress experienced by cells cultured on the surface of microcarriers during spinner flask culture (as discussed in Section 1.7.2). Kilian *et al.* (2010) have examined the effects of convex substrates on MSC differentiation in static culture, and found cytoskeletal changes; in addition to altered lineage commitment in response to differentiation induction medium (260).

A study using melanoma cells on varying convex and concave adhesive islands demonstrated that adherent cells respond to convex features by promoting the assembly of lamellipodia, and concave features resulted in the assembly of stress filaments (267). The use of small molecule inhibitors of actomyosin contractility demonstrated that the cytoskeleton controls cell polarity according to geometric cues in the surrounding extracellular environment. In another study it was proposed that surface curvature could mechanically inhibit the formation bundled microfilaments involved in cell locomotion (268). The effect of curvature has also been theoretically modelled, which concurred with experimental data showing higher contractile force inhibition as curvature increases (265). It has previously been proposed that neurite outgrowth is modulated by substrate curvature (269). In addition, the effect of substrate curvature has also been observed at the tissue level, whereby tissues grew preferentially on substrates with higher curvatures (270).

Typically the effect of curvature on cell behaviour has been analysed on concave shapes, however cells grown on spherical microcarriers would experience a convex substrate. Very little research has been conducted in this area, due to a lack of convenient reproducible methods to create curved substrates of this type (270, 271). In

order to examine the effects of convex substrates on cell behaviour (as experienced on microcarriers), a system would be needed that could generate spherical particles of uniform size and properties. Incorporating synthetic peptides into PEGDMA hydrogels has become a frequently used technique to generate functionalised biomaterials to study cell behaviour. However, to date, this technique has been limited by the methods of solid PEGDMA polymer generation. For example, typically PEGDMA hydrogels are cast into cylindrical moulds using photolithography, whereby cells can either be encapsulated within the hydrogel matrix or cultured in the surface of the gel slab. The opportunity to utilise a proprietary microfluidic technique (provided by the industrial sponsor in this project Q Chip, and discussed in more detail in section 3.2) to generate PEGDMA biofunctionalised microspheres presents an method to utilise this material in a new way, as microcarrier system. Furthermore, it allow generates a tool to potentially expand stem cell populations. As such, Q Chip took the opportunity to apply for two UK patents based on the outcomes of this research. In the first application, the generation of a spherical charge neutral PEGDMA microcarrier containing adhesion peptides using microfluidics was protected. Additionally, the use of said microcarriers to expand stem cell populations was also claimed. The latter patent application can be found at the end of this thesis.

1.12   Preparation methods of hydrogel microspheres

Polymeric hydrogel microspheres have been used for a wide range of biomedical and biotechnology applications including encapsulation of enzymes, drugs and cells (272). Delivering protein based vaccines *via* spherical polymeric particles has been demonstrated to enhance the response of the immune system (273). In addition, cell encapsulation has been used in clinical applications, for example insulin producing islet cells have been encapsulated to treat diabetes (199). This method of cell delivery allows immune isolation, potentially removing the need for pharmaceutical/chemical immunosuppression. Alginate is the most commonly used matrix when generating microspheres for biomedical applications as these can be produced relatively easily under gentle conditions. However synthetic polymers such as PEG and poly (vinyl alcohol) (PVA) once covalently cross-linked offer many advantages including superior chemical and mechanical stability (274).   Despite this, there are limited examples of the use of synthetic hydrogels for biomedical purposes and encapsulation. A key limiting factor has been that the production of microspheres from synthetic hydrogels typically

requires harsh conditions such as high temperatures, non-physiological pH or organic solvents, which are incompatible with labile enzymes, protein therapeutics, or cells (as discussed in Section 1.11.1 (275)). UV photo-polymerisation has been widely used for biomedical applications and cell encapsulation as it occurs quickly at physiological temperature and pH and allows spatial and temporal control over gelation (276). The most common techniques to generate polymeric microspheres include emulsion polymerization and suspension polymerization. However these methods often require tedious removal of surfactants or stabilisers required to stabilise the discrete polymer droplets prior to and during polymerisation. In addition hydrogel properties, particularly swelling behaviour is influenced by their dimensions and interface and using these common manufacturing methods (above), it is impossible to generate hydrophilic microspheres with uniform size and shape.

1.12.1 Emulsion method

Fabrication of hydrogel microspheres requires a two-step process, droplet generation and an appropriate gelation reaction (277). Droplet formation methods include emulsion methods, air jet (278), jet-cutter (279) and vibration jet break up (280). Of these the emulsion method is compatible with UV photo-polymerisation. To generate microspheres using hydrophilic polymers the most widely used method is suspension polymerisation using water-in-oil (w/o) emulsions. This method requires two immiscible phases, an aqueous polymer phase which is dispersed in a continuous organic phase (which can contain oil-soluble surfactants) (281). Within the aqueous phase, synthetic monomers containing photopolymerisable groups are suspended as droplets in an immiscible fluid, intensively stirred or sonicated and are subsequently exposed to a UV source for crosslinking. The resulting emulsified droplets in the continuous phase can be solidified by the addition of water soluble cross-linker, using heat for physical crosslinking. To ensure the formation of stable droplets and to prevent coagulation after mixing, surfactants or emulsifiers can be added (282). To separate the resulting solidified microspheres from the organic phase, which can contain oils, chemicals or surfactants, the microspheres are washed using either a solvent, detergent or water (283). This has been demonstrated recently by Olabisi *et al.* (2010) using an aqueous phase containing PEG diacrylate macromer, photoinitiator and fibroblasts, which was emulsified in mineral oil using a vortex and photopolymerised (284). Mechanical emulsion techniques generate droplets, and subsequently microspheres, with a large size distribution, a major drawback as it is wasteful. Furthermore, key

obstacles with this technique are unreacted monomer and organic solvents, which can become incorporated in the final microspheres and can be undesirable for some applications. The combined drawbacks of the technique mean that the use in biomedical applications is limited. Microsieve technology has been generated to overcome the emulsion problem of polydispersity. By dispersing a fluid into another immiscible fluid through a sieve with pores or a uniform size, droplets that are monodisperse and reproducible are generated which can be polymerised (285). However, this technique still requires a toxic bulk solvent phase.

1.12.2 Electrospray

An alternative method known as submerged electrospray can be used to create a controlled emulsion. Also known as electrostatic atomisation or electrohydrodynamic atomisation, this technique uses a high voltage to break surface tension of the fluid meniscus resulting in the atomization of the liquid into fine droplets (286). Typically electrospray occurs in air or vacuum, however it has also been demonstrated in insulating liquids, known as a 'submerged electrospray'. In 2012 Martens *et al*. applied submerged electrospray for droplet generation by electrospraying poly (vinyl alcohol) PVA hydrogel macromer solution into oil. Resulting droplets were UV-photopolymerised *in situ* (277). The researchers showed cytocompatibility by demonstrating successful encapsulation of fibroblasts with high viability. Previously, the electrospray technique was used to generate spherical alginate particles (in air) with a tight size distribution. However the submerged electrospray technique demonstrated a large polydisperse range of microspheres, comparable to that of mechanical stirred emulsion methods (287).

1.12.3 Microfluidics

Microfluidics describes the manipulation or processing of small volumes of fluid (10^{-9} to 10^{-18} litres) through artificial fluid conducting channels with dimensions of tens to hundreds of micrometres. The technology of microfluidics was first applied to analysis, offering several advantages over conventional techniques, principally the ability to greatly reduce required samples and reagent volumes. In addition to being inexpensive, microfluidic systems are capable of carrying out separations and detections with high resolution and sensitivity and short analysis times (288).

Microfluidics has seen a surge in technology development of the last decade mainly due to the many potential applications available. At present the basis of any microfluidic system is a method of introducing reagents and samples, a chip, containing a series of microchannels (which can be made by several methods and from various materials), a method for moving fluids around the system, and various other devices for manipulating the behaviour of the 'on chip' fluid. When used for analytical purposes this technology is often referred to as 'Lab on a Chip' (288). Microfluidic devices have previously been used as novel biocompatible droplet generation systems, with applications including the bioencapsulation of therapeutic protein-expressing cells (289).

Polydispersity is a key factor in manufacturing microcarriers, as cell confluence should preferably be reached at the same time point on each carrier. In addition, the surface curvature of the particle can alter cellular morphology and behaviour (as discussed in section 1.11.3). In response to this, the use of microfluidics is ideally suited to the production of microcarriers. Monodisperse linear emulsions can easily be produced in a sealed sterile microenvironment, utilizing the phenomenon of segmented flow (reviewed in (290). In microfluidic devices, droplets of various sizes and size distributions can be generated by varying geometrical sizes and shapes within microchannels and junctions (291). The most commonly used configuration for droplet formation is a T-junction owing to its ability to form uniform droplets relatively easily (292). Droplet formation occurs at the junction where the dispersed phase (containing polymer) enters the microchannel which already contains the continuous phase (immiscible with the dispersed phase) where they are segmented into discrete droplets forming a linear emulsion. Various parameters can control the rate and size of droplet formation including the relative flow rate, viscosity, the interfacial tension, in addition to channel geometry (293). The size of the droplets can be increased by increasing the flow rate of the dispersed phase or by decreasing the flow rate of the continuous phase (294). Using microfluidics, the diameter of the produced hydrogel microspheres can be accurately controlled, with size distributions of <2% coefficient of variance and well-defined structure and morphology. The chemical composition of the dispersed phase determines the method of polymerisation of liquid droplets to solid microspheres. Several methods of initiation can be used within a microreactor including thermal initiation (295), UV-initiation (296), chemical reaction (297), or ionic cross-linking (298). Using microfluidics to produce microcarriers provides a low-waste, high-

throughput, inexpensive method for microsphere generation. As demonstrated in 2009, monodisperse microcarriers made from PEGDMA hydrogels can be photo-polymerized *in situ,* eliminating harsh solvents and lengthy post-processing steps (299). Microfluidic reactors offer several advantages over more conventionally used polymerisation techniques; by producing monodisperse microspheres with a narrow size distribution and uniform shape. In addition, the size of the microspheres can be easily controlled by adjusting the flow rate and/or interfacial tension of the liquid inputs. The method can be readily scaled up to increase the production of microspheres and the method can be adjusted to generate microspheres from a variety of materials, including hydrogels.

1.13 Project Aims

The overall aim of this project was to develop a microfluidic method to generate synthetic monodisperse microcarriers containing a range of ECM-derived cues. If successful, a further aim was to expand ADSCs in spinner flasks bioreactors, whilst maintaining their differentiation potential. This process took part in several stages:

Aim 1: To develop a novel microfluidics-based production platform to generate synthetic monodisperse microcarriers. Further, it was intended to incorporate recent progress in synthetic biomaterials to generate a microcarrier with an advanced surface for cell attachment and growth. Several microcarrier types were generated with varying chemical, mechanical and topographical properties. A microfluidic method for the synthesis of highly monodisperse PEGDMA hydrogel microspheres with a range of diameters was developed, utilising continuous *in situ* photo-polymerization. Two methods were investigated in an attempt to incorporate a number of cell adhesive peptides into the hydrogel matrix. The well-characterised fibronectin derived cell-adhesive peptide cyclic (RGDfC), and two laminin based peptides, IKVAV and YIGSR were assessed as to their ability to support ADSC growth. The affect of modifying the microcarrier composition (the polymer content) on the substrates compressive moduli was investigated.

Aim 2: To understand the effect of microcarrier composition, in particular chemical and physical cues on ADSC attachment and differentiation. Initial experiments assessed cell attachment to a planar hydrogel surface using a number of cell adhesive peptides. Cell proliferation on peptide modified microcarriers (at a range of peptide concentrations) was assessed over 7 days, and the effect of microcarrier compressibility

on cell differentiation was investigated to measure the effects on adhesion and adipogenic, osteogenic and chondrogenic differentiation.

Aim 3: To expand multipotent populations of ADSCs on novel microcarriers within spinner flask bioreactors. To maximise ADSC expansion the effect of seeding density relative to microcarrier number was investigated. To investigate if the spinner flask culture primed ADSCs for differentiation, RT-PCR and was employed. In addition ADSCs were driven to differentiate into adipocytes, chondrocytes and osteocytes and observed by histochemical staining.

2.0   Materials and Methods

2.1   Materials

Unless otherwise stated, all chemicals were purchased from Sigma, UK.

2.2   Microcarrier production and analysis

2.2.1   Microfluidic Manifold Assembly

The microfluidic device used in all experiments (MicroPlant[TM]) consists of a circular stainless steel manifold into which high performance liquid chromatography (HPLC) fluid connectors (Anachem, Befordshire, UK) were introduced equatorially. Vertical through holes were sealed with nitrile rubber O-rings, (Sealmasters, Cardiff, UK), allowing fluid to flow to the top surface of a virgin polytetrafluoroethylene (PTFE) disc (100mm diameter x 3mm) located on the manifold. A circular polyfluoroalkoxy (PFA) polymer film gasket (250μm thickness; Polyflon, Staffordshire, UK) was placed in between the PTFE chip and a borosilicate glass disc cover (100mm diameter x 5mm; H Baumbach, Suffolk, UK). A stainless steel clamping piece was bolted using screws (RS Components Ltd., Northants, UK) to the fluidic manifold, allowing the entire laminated assembly to be compression sealed. (Unless otherwise stated all MicroPlant components were produced by Cotton and Brooks, Caerphilly, Wales). Fluids were introduced into a microfluidic circuit *via* 1/16 inch and 1/8 inch (inner diameter) Teflon-FEP tubing (Anachem, Befordshire, UK) using syringe drivers (KD Scientific – Linton Instrumentation, Norfolk, UK).

2.2.2   Fabrication and Design of Microfluidic Chips

Microfluidic channels were machined into polytetrafluoroethylene (PTFE) discs (Polyflon, UK) using a Computer Numerical Controlled milling machine (Roland, Swansea, UK).   An example of a milled chip is shown in Chapter 3 Figure 11. Microfluidic circuit diagrams used to mill each chip are shown in Chapter 3. A range of microfluidic circuits were produced with varying channel dimensions, typically in the range of $150\mu m^2 - 1000\mu m^2$. The width of fluidic input channels were 500μm, opening out to 700μm in the sphere forming channel.

Briefly, channels were designed using computer software (AutoCAD 2009) into lines/layers which relate to machined channels on chip, with coloured layers assigned to different tool sizes. Blank PTFE chips were initially skimmed on both sides to create a

flat surface and to aid sealing. Channels were milled to desired layout/orientation set on computer software with a square drill; fluid entry holes were milled with a circular microdrill. All chips were produced in collaboration with the engineering department within Q Chip.

2.2.3 Preparation of polymer solutions

Hydrogel solutions were prepared using a 10-22% (wt.%) solution of PEGDMA (Sartomer, Warrington, PA, USA) in H_2O with 0.025 wt.% of either photoinitiator 2,2'-azobis(2-amedinopropane) dihydrochloride (Vazo 56 WSP) (DuPont, US) or 4-(2-hydroxyethoxy)phenyl-(2-hydroxy-2-propyl)ketone (Irgacure 2959) (BASF, Yorkshire).

Peptide sequence (3 letter)	Acronym	Supplier
cyclic Cys-Arg-Ala-Asp-D-Phe-Cys	RADfC	Cambridge Bioscience, UK
cyclic Arg-Gly-Asp-D-Phe-Cys	RGDfC	Cambridge Bioscience, UK
Cys-Ser-Arg-Ala-Arg-Lys-Gln-Ala-Ala-Ser-Ile-Lys-Val-Ala-Val-Ser-Ala-Asp-Arg	IKVAV	Sigma Aldrich, UK
Cys-Asp-Pro-Gly-Tyr-Ile-Gly-Ser-Arg	YIGSR	Sigma Aldrich, UK

Figure 5: List of cystiene-containing peptides used for the study.

All peptides were incorporated at 0.1 mM, 0.35mM, 1mM or 2mM. Acryloyl-PEG-peptide, was incorporated at 1wt%. All resulting solutions were vortexed until homogeneous and transferred to a 1mL polycarbonate syringe (BD Biosciences, Oxford, UK).

2.2.4 Incorporation of fluorescent markers into microcarriers

To test the feasibility of incorporating traceable ligands into the microcarrier matrix, fluorescently conjugated antibodies (goat anti-mouse Alexa 405,488,568 (Invitrogen,UK)) or semiconductor quantum dots (Qdot 625 (Invitrogen, UK)) were incorporated into the polymer solution at 1µg/mL (antibodies) or 8nM (Qdots). Incorporation was confirmed by widefield fluorescence microscopy. To determine whether populations of microcarriers could be distinguished, equal number of microcarriers with incorporated Alexa 405,488 and 568 antibodies were mixed, and visualised by widefield fluorescence microscopy.

2.2.5 *In situ* Microfluidic Synthesis of Monodisperse Microspheres

Two immiscible fluids were supplied into microchannels using syringe drivers (KD Scientific, Linton Instrumentation, Norfolk, UK). A continuous-phase, high-oleic, sunflower oil (carrier fluid), (Statfold seed oils, UK), was injected vertically into the microchannel and a functional-phase comprising PEGDMA prepolymer and photoinitiator was supplied from a secondary through-hole producing a linear emulsion at a vertical T-junction. Segmented polymer droplets were irradiated with an ultraviolet source, (365nm UV light at an intensity of ~18 mW/cm^2), and solidified into microspheres. To prevent attachment of gel microspheres during UV polymerization, flow rates were altered to increase microsphere spacing. The MicroPlant device was placed under a steel UV light guide holder (Cotton and Brooks, Caerphilly, Wales), approximately 5.3cm above the surface of the chip. A UV light source (OmniCure Series 2000 UV illumination system 100W), (Jenton International Ltd., Hampshire, UK), fitted with a liquid light guide was used to irradiate the monomer/initiator mixtures. Polymer droplets were exposed to 365nm UV light at an intensity of ~18 mW/cm^2. The incident light intensity (%) was manually controlled at the internal aperture of the UV light source. Under the experimental condition, 95% UV intensity, PEGDMA microspheres could be rapidly solidified in a short exposure time *in situ* (≈175s). Following polymerization, the hydrogel microspheres were collected in glass vials.

2.2.6 Use of surfactants to remove excess oil from microspheres

Microspheres were collected directly from the MicroPlant for 60 mins, to which 30mL of 1% Tween 20 (in double distilled cell culture water) was added, inverted several times and centrifuged using a Fisher Scientific AcenSpin^{TM} centrifuge (144 x *g* for 3 mins), and the supernatant was removed. This process was repeated a minimum of 10 times or until all oil had been removed from the microspheres after visual inspection. Subsequently, 30mL of ddH$_2$O was added, inverted several times, incubated for 30 mins at RT, and centrifuged using a Fisher Scientific AcenSpin^{TM} centrifuge (144 x *g* for 3 mins), before removing all liquid. This step was repeated three times and the samples were stored in excess water and tested within 24 hours.

2.3 Analytical Measurements

Microsphere radii were measured using a light microscope (Leica Microsystems, Heidelberg GmbH) with attached Moticam-2000 camera. Sphere diameters were measured using associated software Motic Images Plus 2.0, (Motic, Suffolk, UK). Microspheres were measured from a representative sample of each microsphere type. The coefficient of variance (CV) was calculated as shown in Equation 2.1.

$$CV = \frac{standard\ deviation}{mean\ diameter}\ x\ 100$$

2.4 Manufacture of flat gels

Hydrogel discs were prepared using chip 100962A (Figure 21). The hydrogel chip contained a fluid entry and exit point and a large cavity (500μm depth). Hydrogel solutions were prepared as described in section 2.1.3 and pumped manually into the cavity. The solution was polymerised by exposure to 365nm UV light at an intensity of ~18 mW/cm2 for 180 seconds. The resulting hydrogel was cut into small discs (8 mm diameter x 500μm), washed three times in PBS and incubated in PBS overnight to equilibrate. The thickness of each sample was measured using a digital calliper prior to experimentation.

2.5 Microscopy analysis

For whole well visualisation of 96-well plates, a custom built platform was derived comprising of a 2D Olympus stage (Olympus Keymed, Southend-on-Sea, UK) mounted on to a 1.3-megapixel CMOS camera driven by photoimpression software (Arcsoft, California USA). Microcarrier numbers were counted using the cell counter plugin within the Fiji image processing package (www.fiji.sc).

Brightfield and phase images were taken on a Leica DMIL inverted microscope (4x,10x,20x,40x objectives) (Leica Microsystems, Heidelberg GmbH) with an attached Moticam-2000 camera driven by Motic image capture software, (Motic, Suffolk, UK).

Widefield fluorescence microscopy was performed using an inverted IX-71 frame and objectives (4x,10x,20x,40x,100x)(Olympus Keymed, Southend-on-Sea, UK). 3D stage, illumination and image capture automation was controlled through simplePCI software (Hamamatsu Photonics, Japan) driving an XYZ stage and filter wheel (Prior Scientific, Cambridge, UK) and an Orca-AG camera (Hamamatsu Photonics, Japan).

Fluorescence light source was an Exfo X-Cite120 (Lumen Dynamics, Ontario, Canada). Excitation, emission and dichroic filters were obtained from Chroma Technology (Chroma Technology Corporation, USA) and were optimised for the fluorophores in use.

Confocal analysis was performed using Leica SP2 and TCS SPE confocal microsopes. For microcarrier/cell analysis and assessment of peptide incorporation, a Leica TCS SP2 AOBS spectral confocal laser scanning microscope with 405,488 and 543 laser lines (Leica Microsystems, Heidelberg GmbH) controlled *via* a PC running Leica Confocal Software (LCS) was used. In all experiments, the laser power was minimized in order to avoid photobleaching and laser power was maintained at 40% intensity, using a 10x dry objective lens and 2x optical zoom, incorporating both fluorescence and bright field transmission scanners. Z-Stacks of optical sections were taken through the entire volume of the sphere at 5μm intervals (unless otherwise stated) using appropriate excitation and emission settings. Z-Stacks were processed and analysed using LCS and presented as 3-D reconstructions that defined the mid-plane of the stack at the highest cross sectional diameter of the microsphere. For microcarrier/cell analysis, images were taken using a Leica TCS SPE confocal microscope with 488,532 and 635 laser lines (Leica Microsystems, Heidelberg GmbH). Microcarrier images were visualised using a HC PL Fluotar 10x (NA=0.3) objective with an appropriate zoom to capture the entire microcarrier within a 1024x1024 pixel scan (typically 2x for a single microcarrier). Z-section resolution was defined through the Leica software as 'optimal' (2.5 microns) and resulted in around 170-200 sections per microcarrier. Individual z-sections were reconstructed within the Fiji image processing package (www.fiji.sc), utilising the 'Z-project' plugin to create a brightest point merge. Depth projections were recoloured using the 'Temporal-colour code' plugin.

2.6   Microcarrier characterisation

2.6.1   Characterisation of Peptide incorporation using Acryloyl-PEG-NHS

The fibronectin fragment peptides, Gly-Arg-Gly-Asp-Ser (GRGDS), Gly-Arg-Asp-Gly-Ser (GRDGS) and diamine-RGDS-6-aminohexanoate linker (LC)–biotin, were designed and custom synthesised (Peptide synthetics, Hampshire, UK). To determine

the efficiency of the conjugation reaction, samples were analysed using a variety of methods including Electrospray Mass Spectrometry and MALDI ToF ToF analysis.

2.6.2 Electrospray Mass Spectrometry Analysis of Acryloyl-PEG-NHS Conjugates.

Electrospray mass spectrometry (ESI) was performed on a Thermo Finnigan navigator Thermo Quest LC/MS, single-quadrapole mass spectrometer using the positive ion mode, running under Thermo Separation's Xcalibur software. ESI mass spectra were recorded on a single quadrupole mass spectrometer fitted with an electrospray ion source, the first detector was used for mass detection. Acryloyl-PEG-NHS, at a concentration of $1mg/cm^3$, dissolved in eluent Acetronitile/Water (1:1, v/v), 0.3% Formic Acid, and injected *via* flow injection into the ESI source at a flow rate of 10µl/min. All solvents used were HPLC grade. The mass spectrometer was calibrated in the positive ion mode using Polyethylene Glycol (PEG) (MW 1K). At least three charge states were used to determine the reported weights. Data were acquired in the scan mode from *m/z* 400 to 1500 in 5s at a 0.1 step size. Voltages were set at +30V for the capillary and adjusted for the sampling cone. The source was heated at 120°C.

2.6.3 Synthesis and purification of Acryloyl–PEG–Peptide

The acrylated peptide was synthesized through aminolysis of the N-hydroxy succinimide ester of acrylic acid (Acryloyl-PEG-NHS) (Jenkem, USA). N-hydroxysuccinimidyl-activated esters were used to couple the N-terminal primary amine of the peptide to an acrylate moiety, indirectly using a 3,500MW PEG spacer. (Figure 22). Three alternative methods were employed to produce the PEG-peptide conjugate.

Method 1: Synthesis of an acrylated peptide Acryloyl–PEG–GRGDS was performed following the modified method of Hern and Hubbell (1998) (300). A 3,500MW PEG (spacer) chain between the peptide and the acrylate moiety was produced by reacting the peptide with Acryloyl-PEG-N hydroxysuccinimide. The peptide was dissolved to a final aqueous concentration of 1mg/mL in 50mM of sodium bicarbonate buffer, pH 8.2. Specifically, two milligrams (1.23mmol) of peptide was dissolved in 2mL of 50 mm sodium bicarbonate solution. The 3,500MW Acryloyl–PEG–NHS was dissolved separately such that the final molar ratio of Acryloyl-PEG-NHS to peptide was 1:1 Acryloyl–PEG–NHS (9.11 mg, 1.23 mmol) was dissolved in 400uL of 50mM sodium bicarbonate solution and the resulting solution was added

drop-wise to the peptide solution, whilst under continuous stirring. The solution was shaken on an orbital shaker for 2h, at room temperature. Dialysis (MWCO 2,000 Da) was used to remove unreacted peptide and N-hydroxyl succinimide against deionized water for 72h with periodic bath changes. The solution containing the pure product was vacuum dried. A low reactant ratio of 1:1 was chosen to minimise the production of Acryloyl-PEG-OH, the product of the competing hydrolysis reaction, since this by-product was not removed from the Acryloyl-PEG-peptide.

Method 2: Two parameters, the molar ratio of peptide to the succinimide ester and the pH conditions, were varied to maximize conversion of the peptide to the desired product and minimise side reactions. Reactions were conducted at molar ratios of 1, 1.5, and 2 of the peptide to a succinimidyl ester at pH conditions 7.5, 8, 8.5 and 9. Briefly, the peptide was resuspended in water and aliquoted into an array format. Acryloyl–PEG–NHS were dissolved separately in trizma-based basic buffers to produce 4 samples of pH 7.5, 8, 8.5 and 9 according to manufacturer's instructions. Stoichiometric equivalents of Acryloyl–PEG–NHS samples were added to peptide aliquots immediately, in excess buffer to ensure the correct pH for each individual reaction. Reactions were conducted in duplicate and divided such that half the samples were stored at 25 or 37 degrees. Purification of samples was performed using dialysis at a MW cut off of 1,000Da.

Method 3: GRGDS peptide was dissolved in anhydrous dimethyl formamide (DMF) containing 4M excess of triethylamine (TEA). Acryloyl-PEG-NHS was also dissolved in anhydrous DMF and, immediately after, mixed with 1.1M excess of peptide. After incubating for 3h at RT, Acryloyl-PEG-GRGDS was precipitated twice in cold anhydrous ether and dried under vacuum overnight at room temperature (301). The peptide coupling reaction and molecular mass of the product was monitored by matrix-assisted laser desorption/ionization time-of-flight spectrometry (MALDI ToF ToF).

2.6.4 MALDI ToF ToF Analysis of Acryloyl-PEG-Peptide conjugates
1st Analysis

The MALDI ToF ToF 4800 mass spectrometer (Applied Biosystems) was used for analysis of peptide conjugates. One milligram of Acryloyl-PEG-NHS dissolved in 50mL of 50% Acetonitrile and Trifluoroacetic acid (ACN/TFA), followed by a further 1:100 dilution. 0.5μL sample of Acryloyl-PEG-peptide (~3 x 10^{-11}moles) was spotted on

a 384 well Opti-TOF plate (P/N 1016491, Applied Biosystems) and the air dried spot was overlaid with either 0.5 μL of 10 mg/ml α-cyano-4-hydroxycinnamic acid or sinapinic acid (donated by Cardiff Biotechnology Services) dissolved in 50% acetonitrile, 0.1% trifluoroacetic acid.

2nd Analysis

Acryloyl-PEG-peptide conjugate was resuspended in 10mL H$_2$O, diluted 1:100 with ACN/TFA and 0.5μl was pipetted onto the target. As samples were incompatible with α-cyano-4-hydroxycinnamic acid matrix due to high level of Tris salts, dialysis was performed. Briefly, 50μl of each taken and dialysed against water using mini-dialysis kits (MWCO 1000kDa) (Thermo Scientific Ltd., High Wycombe, UK) for 6hrs and dried in a SpeedVac, (Thermo Scientific, Ltd., High Wycombe, UK), resuspended in 2mL ACN/TFA and spotted 1μL onto the plate.

3rd Analysis

Acryloyl-PEG-peptide was dissolved in 1mL of a mixed methanol/water (50:50) solvent without cationizing agent. Twenty microlitres of sample was removed, dried in a SpeedVac and resuspended in a 1/50 dilution of methanol/water. 0.5μL was hand spotted onto the Opti-TOF plate. The MALDI matrix consisted of dihydrobenzoic acid (DHB), (donated by Cardiff Biotechnology Services), which was hand spotted onto the plate over a target and air dried. In each case, mass spectra were collected in positive ion reflector mode with an Nd-YAG laser at 355mn on a MALDI ToF ToF 4800 mass spectrometer. The final spectrum was the average of 800 laser shots. Masses were calibrated using CalMix 5 (Applied Biosystems, UK).

2.6.5 Visualising surface bound peptide incorporation

The surface concentration of bound peptide was determined by confocal microscopy. Acrylate-poly(ethylene glycol)-biotinylated peptide (Acryloyl-PEG-diamine–RGDS-LC-biotin) served as model ligand and was covalently linked to the microsphere polymer backbone during microfluidics assisted UV photo-polymerisation. To assess the presence of PEG-biotin on the particles´ surface, particles were incubated with a fluorescent streptavidin conjugate from Anaspec (Cambridge Biosciences, Cambridge, UK) and visualized by confocal laser scanning microscopy (CLSM). To account for false-positive results due to adsorption of the fluorescent

marker, biotin free PEGDM microspheres were treated the same way and compared to biotinylated peptide containing microspheres.

Microsphere suspension (500μL) were produced and washed (as above), placed in RNeasy MinElute Spin Column (Qiagen, West Sussex, UK) and centrifuged to remove excess fluid. Thirty microlitres of diluted streptavidin (1/50 in H_2O) was added to spin columns and spun immediately at 8,000 x g for 1min to remove fluid. To wash excess streptavidin off the microspheres, 600μL of distilled H_2O was added to the spin column, centrifuged at 8,000 x g, the elutant discarded and repeated 5 times. The microspheres where kept in 500uL of H_2O to ensure they remained hydrated and removed any excess strepavidin by passive diffusion.

The distribution and localisation of the conjugated peptide distribution was visualised by measuring the fluorescent signal from FITC conjugated Streptavidin bound biotinylated-peptide on the surface of the microspheres. The labelled microspheres were placed on a microscope slide with minimal fluid, and cross-sectional images were taken of several microspheres at different depths using an SP2 confocal laser scanning microscope.

2.6.6 Ninhydrin assay

The ninhydrin assay was used to verify the presence of amine groups within peptide modified microcarriers. Microcarrier samples were weighed, dried in a vacuum centrifuge at $25^{o}C$ overnight and re-weighed. The dehydrated spheres were digested in 6N HCl at $100^{o}C$ for 3 hours before being dried in a vacuum centrifuge at $25^{o}C$ for 6 hours. The resulting digested amino acids were dissolved in equal parts 0.1M sodium citrate buffer and ninhydrin solution and heated at $75^{o}C$ for 15 mins. The absorbance of the final solution was measured at 570 nm (Fluostar optima, BMG optima, Germany). A standard curve was prepared using a solution of a known concentration of Glycine.

2.6.7 Environmental Scanning Electron Microscopy of microcarriers

The structure of the hydrogel scaffolds were examined with an FEI (Holland), XL30, Field Emission Gun (FEG), Environmental Scanning Electron Microscope (ESEM) in "wet" mode. ESEM settings were accelerating voltage 20kV, spot size 4, working distance ~9mm. A Peltier stage was used to cool the spheres to ~5°C and the vapour pressure adjusted to yield slightly less than 100% humidity in the chamber.

A gaseous secondary electron detector (GSD) was used to image microspheres (*n*=6) in their hydrated state (suspended in sterilised water, 25μL, cell culture grade, Sigma, UK) (302).

2.6.8 Mechanical characterisation

Mechanical testing was performed in unconfined uniaxial compression using a Bose ELF 3200 testing system with a 250g load cell (Bose Corporation ElectroForce Systems Group, Minnesota, USA). Prior to mechanical testing, the hydrogel discs (Section 2.2.8) were swelled overnight in H_2O to ensure complete hydration. Compression (mm) and load (N) were recorded using Wintest software at a cross speed of 10 mm/s and a strain level of 60%. The compressive modulus was obtained as the tangent slope of the stress–strain curve. Three specimens were tested for each sample type. Samples were strained to 60% and the compressive Young's modulus was obtained from the slope of the stress-strain curve.

$$Compressive\ Modulus\ (Ec) = \left(\frac{\sigma}{\varepsilon}\right) = \frac{(\Delta mgL)}{(A\Delta L)}$$

Where σ is the stress applied, ε is the corresponding strain, Δ m is the change in load applied, g is the force of gravity, L is the length of the scaffold sample, A is the cross-sectional area of the scaffold, and ΔL is the change in length during compression.

2.6.9 Equilibrium water content

The equilibrium water content (EWC) of scaffolds was calculated according to:

$$EWC = \frac{(W_h - W_d)}{W_h}\ x\ 100\%$$

The hydrated mass (W_h) was measured after immersing the scaffolds in water for 3 days (*n*=6) with residual surface water removed by blotting. The dehydrated mass (W_d) was measured after drying the samples in a vacuum centrifuge overnight.

2.6.10 Microcarrier counting

Microcarriers were produced using microfluidics as detailed in Section 2.2.5. As the polymer (dispersed phase) enters the MicroPlant at a constant rate (mL/h), the microspheres were segmented and exited the MicroPlant at a constant rate. Based on the

polymer flow rate and average microsphere diameter, the frequency of microsphere production can be calculated using the following equations:

$$Volume\ of\ a\ sphere(ml) = \frac{\frac{4}{3}\pi\ x\ radius\ (mm)^3}{1000}$$

$$Frequency\ of\ microsphere\ production\ per\ second\ (Hz)$$
$$= \frac{Flow\ rate\ (ml\ per\ second)}{Volume\ of\ a\ sphere\ (ml)}$$

Accordingly, the average microsphere diameter was 461µm, with a polymer flow rate of 0.65mL/hr. This provided a frequency of 3.52 Hz, and therefore, within one 60 mins batch 12,671 microspheres can be generated. By resuspending microspheres in a defined volume (5mL) and aliquoting 250µL per into each well of a 24-well plate, an average yield of 506 beads per well should be achieved. However, manually dispensing microcarriers *via* pipetting can result in an uneven microcarrier distribution, therefore for viability assays, microscope images of individual wells within a multi-well plate were taken and microcarriers were counted using the Cell counter plugin within the FIJI image processing package (www.fiji.sc).

2.7 Cell culture methods

Routine cell culture work was carried out under a laminar flow (class II) hood. Cells were maintained at $37^{\circ}C$ in a hydrated atmosphere of 5% CO_2 and air in appropriate medium. Human alveolar epithelial cells (A549) cells (European Collection of Cell Cultures) were maintained in Dulbecco's modified Eagle medium containing 4500mg/L glucose and 110mg/L pyruvate supplemented with 10% heat inactivated foetal bovine serum (FBS). Penicillin (10,000 units per mL) and streptomycin (10,000 µg per mL) were also added to the medium. All medium was stored at $4^{\circ}C$ until use.

2.7.1 Sub-culturing of A549 cells

The cell line A549 was routinely passaged at 60-80% confluence, using 0.02% Trypsin/0.05% EDTA in PBS. Typically a cell seeding density of 750 x 10^3 in a T75 flask required sub-culturing every four days. Culture medium was removed and cells

rinsed twice with pre-warmed PBS (10mL). Attached cells were removed by adding Trypsin/EDTA (5mL) to a T75 culture flask. Cells were incubated for 5 mins at 37^oC to allow detachment of cells into a single-cell suspension. After incubation, enzymatic action was terminated through the addition of serum-containing medium (10mL). Total cell suspension was centrifuged at 900 x g for 5 mins. The supernatant was removed and the cell pellet resuspended in 1mL of complete medium by gentle pipetting to remove any cell clumps, before splitting approximately 1:8 into new T-75 flasks before in a final volume 15mL.

2.7.2   Culture of ADSCs

StemPro® Human-Derived Stem Cells (ADSC) obtained from Invitrogen (Invitrogen, UK) were cultured in DMEM (low glucose) containing Glutamax supplemented with 10% Mesenchymal stem cell qualified FBS, 75 µg/mL Gentamicin and 37.5 ng/mL Amphotericin. ADSC were seeded at 5,000 cells/cm^2 and incubated at $37°C$, 5% CO_2. The medium was changed approximately 24 hours post seeding and subsequently every three. Cells were harvested once they reached ~70% confluence (approx. 5 days), using Accutase (Invitrogen). Culture medium was removed and cells washed once with pre-warmed PBS. Attached cells were removed by adding Accutase and incubated for 5 mins at 37^oC to allow detachment of cells into a single-cell suspension. After incubation, enzymatic action was terminated through the addition of serum-containing medium. Total cell suspensions were centrifuged at 220 x g for 5 mins. The supernatant was removed and the cell pellet resuspended in 1mL of complete medium by gentle pipetting to generate a single cell suspension. ADSCs were cryopreserved at Passage 2, and all experiments were conducted at Passage 4.

2.7.3   Freezing and thawing cells

To preserve stocks of cells, harvested cells were diluted to ~1 x 10^6 cells/mL in Synth-a Freeze cooled to 4^oC, containing 10% DMSO (Invitrogen, UK). Cell suspensions (1mL) were aliquoted into cryovials and then frozen to -80^oC in a container filled with isopropanol that was designed to cool at a rate of less than 1^oC per min. Once frozen (overnight), cell vials were transferred into liquid nitrogen and stored until required. Recovery of stored cells was achieved by first removing a vial of cells stored in liquid nitrogen. These were then warmed rapidly by placing in a 37^oC water bath until all ice crystals were thawed. The warmed cell suspension was then diluted (1:2) in

culture medium (1mL) pre-warmed to 37°C. Total cell contents were seeded at 5,000 cells/cm^2 and incubated at 37°C, 5% CO_2.

2.7.4 Counting total and viable cell numbers of cell cultured on tissue culture plastic

After enzyme disaggregation, cell suspensions were quantified, in terms of total and viable intact cell numbers, using a haemocytometer in conjunction with phase contrast microscopy. The percentage of viable cells was determined using the dye exclusion method ((303); Section 2.7.5). To carry out a total cell count, cells were trypsinised, pelleted by centrifugation (220 x *g* for 5 mins) and resuspended into medium, ensuring a unicellular suspension. The haemocytometer and coverslip were cleansed (70% ethanol) and the coverslip placed squarely on top of the haemocytometer; lightly moistened at the polished surface of the slide before pressing the coverslip into position. Cells were redistributed throughout the medium by gentle agitation, before a sample (10μL) was loaded into the haemocytometer and counted.

2.7.5 Trypan blue dye exclusion

The percentage of viable cells was calculated using the dye exclusion method, whereby trypan blue (membrane lipid insoluble) becomes visible upon permeating cells that have damaged plasma membranes. An aliquot (10μL) of cell suspension was mixed with trypan blue solution (10μL), loaded into the haemocytometer, and the unstained (viable) versus stained (non-viable) cells counted. The percentage of viable cells was determined according to the following equation:

$$Percentage\ of\ viable\ cells = \frac{number\ of\ unstained\ cells}{total\ cell\ count} X\ 100$$

2.8 Differentiation of hADSCs

2.8.1 Adipogenesis

For adipogenic differentiation ADSCs were seeded at 1×10^4 cells/mL and incubated at 37°C, 5% CO_2 for 24 hours in complete medium. The medium was then switched to complete StemPro adipogenic differentiation (Invitrogen) for an additional 14 days with medium changes every 3–4 days, coincident with other analysis.

2.8.2 Osteogenesis

For osteogenesis studies, ADSCs were plated at 5 x 10^3 cells/cm^2 complete medium which was then switched to complete StemPro osteogenic differentiation (Invitrogen) and cultured for 14 days with medium changes every 3–4 days, coincident with other analysis.

2.8.3 Chondrogenesis

For chondrogenic differentiation studies, ADSCs were resuspended in complete medium to a concentration of 8×10^6 cells/mL. In a 12-well tissue-culture dish, 10µl of cell suspension was spotted per well and incubated for two hours at 37°C, 5% CO$_2$ and 90% humidity to form a pellet. After 2 hours StemPro chondrogenic differentiation medium was added gently to the wells. Differentiation media was replaced every three to four days. Chondrogenesis was analysed after 14 days.

2.9 Microcarrier seeding experiments

Immediately prior to cell seeding, all fluid from the prepared microspheres was removed *via* a micropipette. The microspheres were resuspended in 5mL of cell culture medium and gently pipetted to form a homogenous suspension. The suspension was aliquoted (250µL) into non-cell adhesive, ultra-low attachment 24-well plates to prevent normal cell attachment to tissue culture polystyrene (Corning, UK). Plates containing microspheres were placed in the incubator at 37°C, 5% CO_2 for a minimum of 4 hour prior to seeding to allow equilibration.

2.9.1 Optimisation of initial cell attachment

The following conditions were varied during the seeding experiments in order to determine the optimum culture conditions that favoured monolayer sphere attachment/growth of A549 cells:

2.9.1.1 Seeding Density

A549 cells were seeded onto microcarriers at 100,000, 50,000 and 25,000 cells per well.

2.9.1.2 Agitation

Samples were either static or agitated intermittently for the first 4 hours after cell seeding. Samples were agitated intermittently at different time intervals (every 20, 40 or 60 mins at 40 rpm for 2 mins), on a shaking mini-rocker in a humidified incubator at 37^oC and 5% CO_2.

2.9.1.3 Total Volume of medium

The total volume of media tested was 3mL and 500μL.

2.10 Seeding and differentiation of ADSC on microcarriers

Microcarriers were placed in ultra-low attachment tissue culture plates (Corning, UK). Microcarriers in either 6 well or 24 wells were seeded with 40,000 or 10,000 cells respectively and cultured in complete medium for 7 days. The medium was then switched to either StemPro adipogenic, osteogenic or chondrogenic medium, (Invitrogen). Control cultures were maintained with complete media. All cell-laden microcarriers were maintained for 7 days for RT-PCR analysis or 14 days for histochemical analysis in a humidified incubator at 37^oC and 5% CO_2 with medium changes every 3–4 days. Whole wells were imaged to observe differentiated cell laden microcarriers distribution using an Oxford Optronix GelCount device (Oxford, UK).

2.11 Analysis of ADSC attachment to hydrogels

2.11.1 DAPI nuclear staining to observe ADSC attachment to flat gels

Hydrogel discs prepared were seeded with 50,000 human ADSCs in ULA plates and incubated in DMEM with 10% MSC qualified fetal bovine serum medium for 24 h at 37^oC at 5% humidity. After 48 hours specimens were fixed for 20 mins in 3.7% paraformaldehyde (PFA) in PBS. After washing with PBS, the discs were immersed in 4',6' diamidino-2-phenylindole dihydrochloride (DAPI) solution (1:10000) and optionally Concanavalin A (both Sigma) (1:100) for 10 mins. The disks were washed three times in PBS inverted into an imaging chamber containing PBS and observed using widefield fluorescence microscopy.

2.12   Analysis of cell-laden microcarriers

2.12.1 SEM analysis

Microcarriers were analysed using scanning electron microscopy (SEM) to assess ADSC distribution and morphology. To prepare SEM samples, scaffolds were mounted on 0.5" carbon-coated aluminium specimen stubs (Agar Scientific) and gold-palladium (90:10) coated with a sputter-coater in a Biorad (K) vapor deposition unit, at 15 mA for 60 s. SEM (Zeiss SMT S360 Scanning Electron Microscope) was operated at a working distance of 15 mm and an accelerating voltage of 20 kV.

2.12.2 Cell growth measured by PrestoBlue viability assay

The proliferation of ADSCs on microcarriers was measured using the Prestoblue viability assay (Invitrogen, UK). ADSCs (10,000) were seeded onto approximately 100 microcarriers containing different cysteine containing peptides in ultra-low attachment 96 well plates (total volume 90μL). Alternatively, 90μL microcarrier samples were removed from spinner flasks placed into ultra-low attachment 96 well plates. Ten microliters of Prestoblue reagent was added to each well, mixed and incubated for 24 hours at $37^{o}C$ in a CO_2 incubator. The supermatent (90μL) was removed and transferred to a black walled, clear bottomed 96 well plate. The fluorescence of each sample was measured using a Fluostar Optima microplate reader (BMG Labtech Gmbh, Ortenberg, Germany) by fluorescence detection at excitation and emission wavelength of 540–570 and 580–610nm, respectively.

2.12.3   Immunocytochemistry

F-actin was detected in ADSCs cultured on microcarriers after 7 days either in static or spinner flask culture (samples transferred to a 12 well plate prior to analysis) using TRITC conjugated phalloidin (Sigma, UK). After removing ~85% of the media, the cell-laden microcarriers were washed twice with PBS by (by exchanging ~85% of the supernatant) and fixed for 20 mins in 3.7% paraformaldehyde in PBS. After aspirating the paraformaldehyde (PFA), 30mM Glycine was added and incubated for 5 mins at RT. The microcarriers were then immersed in 0.1% Triton X-100 for 5 mins, followed by a further washing step in PBS and blocked with 3% bovine serum albumin (BSA) for 30 mins at RT. After this procedure, in parallel the cell constructs were stained with either, anti-tubulin (1:1000)(Labvision corporation, California USA) or

phalloidin-TRITC (1:500) for 1 hour or 10 mins respectively at RT. The microcarriers were then washed in PBS a further 3 times for 5 mins each. Anti-tubulin samples were treated with Alexa 488-labeled anti-mouse secondary antibody (1:400) (Invitrogen, UK) at RT for 1 hour and washed in PBS a further 3 times for 5 mins each. Cells were counterstained with DAPI (1:10000) to visualise nuclei, the constructs were then washed in PBS a further 3 times for 5 mins each. The cell constructs were washed and viewed using an SP2 laser scanning confocal microscope.

2.12.4 LIVE/DEAD® viability/cytotoxicity kit

The viability/cytotoxicity kit (Sigma, UK Product number 04511) supplied prepared solutions of Calcein-AM and Propidium Iodide (PI). The assay solution was prepared according to manufacturers' instructions by combining Calcein-AM solution (10µL) and Propidium Iodide (PI) solutions (5µL) with PBS (5mL). As serum contains esterases, which can interfere with the analytical method, culture medium was removed from the wells and microcarriers were gently washed three times in PBS (1mL). To prevent any excess shear force removing bound cells, washing steps only removed ~85% of the supernatant (*via* gentle pipetting). In the final washing step PBS was replaced with 300µL of assay solution. The samples were incubated at $37^{o}C$ for 15 mins. Calcein generated from Calcein-AM by esterases in a viable cell emitted strong green fluorescence (excitation: 490nm, emission: 515nm). PI solutions emitted a strong red fluorescence (excitation: 535nm, emission: 617nm)). Both Calcein and PI-DNA could be excited at 490nm, and therefore, simultaneous monitoring of viable and dead cells was possible using fluorescence microscopy. With 570nm excitation, only dead cells could be observed.

2.12.5 RNA extraction and RT-PCR analysis of gene expression

Total RNA was extracted from cells directly from the microcarrier unless otherwise stated using an RNeasy Mini Kit (Qiagen, Crawley, UK) following the supplier's instructions. Cell-laden microcarriers were harvested at different time points according to the experimental design. ADSCs cultured on microcarriers with a range of compressive moduli were harvested at day 5, and 14 days after being placed in differentiation induction media. In addition cells were harvested from spinner flasks at either day 7 or Day 14. The samples at all time points were lysed in supplied lysis buffer. The lysate was homogenized with QIAshredder spin column (Qiagen, Crawley,

UK). The homogenised lysate together with 700µl of 70% ethanol was then transferred to RNeasy spin column for purification. Samples were treated with DNase to remove genomic contaminants. RNA was extracted according to the kit instructions. Total RNA concentration and quality was assessed using a NanoDrop 1000 spectrophotometer (NanoDrop Technologies, Labtech, Ringmer, UK). RNA samples were reverse-transcribed to cDNA using Promega cDNA synthesis kit (BioRad, UK) following the supplier's instructions. The real-time RT-PCR reactions were conducted and monitored with a Mastercycler® ep Realplex (Eppendorf, Cambridge, UK). TaqMan® Gene Expression assay kits (Applied Biosystems, UK) were used for transcript levels of genes (Figure 6). One µl of cDNA from each sample was mixed with 0.5µl of the assays-on-demand kit, 8.5 µl of RNase/DNase free water, and 10 µl of $2\times$ TaqMan® Universal PCR Master Mix (Applied Biosystems, UK). Final data were analysed by Mastercycler® ep realplex software (Eppendorf, Cambridge, UK). The Ct value for each sample was defined as the cycle number at which the fluorescence intensity reached a certain threshold where amplification of each target gene was within the linear region of the reaction amplification curves. Relative expression level for each target gene was normalized by the Ct value of TaqMan® endogenous gene B2M using an identical procedure ($2^{-\Delta\Delta}$Ct formula) (304). Each biological replicate was run in triplicate on and no Reverse transcriptase and no template controls (NTC) were run in parallel for each primer/probe set to ensure no contamination. Each sample was analysed in triplicate. B2M primers were used as an internal control. The samples were then subjected to an initial 50°C for 2 mins to optimise UDG enzyme activity and cycling conditions of: 95°C (10 mins), 50 cycles of 95°C (15 s) and 60°C (1 mins).

Gene name	Gene Symbol	Gene Aliases	Locus position
Aggrecan	ACAN	AGC1, AGCAN, CSPG1, CSPGCP, MSK16, SEDK	NM_001135.3
5'-nucleotidase, ecto (CD73)	NT5E	CD73, E5NT, NT, NT5, NTE, RP11-321N4.1, eN, eNT	NM_002526.3
Beta-2-microglobulin	B2M	CDABP0092	NM_004048.2
Fatty acid binding protein 4, adipocyte	FABP4	A-FABP, AFABP, ALBP, aP2	NM_001442.2
Regulator of cell cycle	RGCC	C13orf15, KIAA0564, MGC87338, RGC-32, RGC32, bA157L14.2	NM_014059.2

Figure 6: List of TaqMan® Gene Expression assay kits used for RT-PCR

Analysis of gene expression was performed using the Mastercycler® ep Realplex software (Eppendorf, Cambridge, UK). Content of cDNA samples was normalized and expression of each specific gene was calculated using the formulae $2^{-(\Delta Ct)}$ and was compared to the value obtained for MSC at J0.

Chondrogenic pellets were incubated with 1mL of collagenase type II at 2mg/ml in PBS for 1 hour in a humidified incubator at $37^{o}C$, 5% CO_2. Subsequently, the entire volume containing disassociated pellets (without microcarriers) was transferred to microcentrifuge tubes, vortexed and centrifuged at 300 x g for 5 mins at room temperature. The supernatant was removed *via* pipette and replaced by lysis buffer.

Softer microcarriers such as those generated from 12% PEGDMA are not compatible with Qiagen supplied lysis buffer. Hence cells are enzymatically removed from 12% microcarriers using Trypsin, transferred to microcentrifuge tubes and centrifuged at 300 x g for 5 mins, the supernatant was removed and replaced by lysis buffer.

2.12.6 Analysis of cell phenotype by flow cytometry

Flow cytometry analysis was performed in order to characterise the multipotency ADSCs prior to microcarrier seeding. At least 50,000 cells were harvested *via* Accutase (to preserve cell surface markers), counted and resuspended in Block solution (5% Goat serum in PBS) for 15 mins at RT to yield 0.5 x 10^6 cells/mL. Suspensions were incubated with primary antibodies (diluted 1:200) against human: CD34, CD44, CD45, CD90, CD105 (all AbCam, Cambridge, UK) and CD29-FITC

(Chemicon, UK) at 4°C for 30 mins. Cells were collected *via* centrifugation (200 x g for 5 mins) and then washed 3 times with PBS. Non-specific background staining was determined by staining cells with corresponding isotype control antibodies mouse IGG2A, mouse IGG1 and rabbit IGG in parallel. Bound primary antibodies were then detected by incubating cells with corresponding Alexa 488 conjugated anti-mouse or anti-rabbit secondary antibody (diluted 1:100) and incubated at 4°C for further 30 min. Cells were pelleted *via* centrifugation (200 x g for 5 mins) and then washed 3 times with PBS to remove unbound antibodies. Stained cells were then analysed using a BD FACS Canto instrument equipped with FACS Diva software (BD Biosciences, UK). A minimum of 10,000 cells were counted in each sample. All experimental data were analysed offline using FlowJo software (Tree Star, Inc., USA), and the mean fluorescent intensity for each sample was used to determine the relative expression of each of the CD markers.

2.13 Histological analysis and immunostaining studies

2.13.1 Adipogenesis

Adipocytes on tissue culture plastic or adipogenic-microcarrier constructs were washed with PBS and fixed in 3.7% PFA for 1 hour at RT. The cells were then rinsed with distilled H$_2$O and incubated in 60% isopropanol for 5 mins. Samples were stained with double-filtered Oil Red O stain for 5 mins. To prepare the staining solution, a saturated isopropanol-Oil Red O solution was mixed with dH$_2$O (ratio of 3:2). Excess stain was removed and washed several times with distilled H$_2$O. Alternatively adipogenic samples were fixed in 3.7% paraformaldehyde for 20 mins and washed with PBS to remove residual formaldehyde. Paraformaldehyde-fixed samples were incubated in LipidTOX™ Red neutral lipid stain (1:2000) for 30 mins at room temperature. In the final 10 mins, Reddot-1 nuclear stain (Biotium inc, California, USA) was added (1:200). Samples were washed three times in PBS and fluorescent cells were imaged using confocal microscopy.

2.13.2 Osteogenesis

Control cells and osteocytes were washed with PBS and ice cold 70% ethanol for 1 hour at RT. The ethanol was removed and washed twice for 10 mins each with distilled water and stained with Alizarin red solution and incubated for 30 mins. Excess

stain was washed with distilled H_2O. Images of stained cells were taken using a brightfield microscope.

2.13.3 Chondrogenesis

Differentiation of ADSCs into chondrocytes was achieved using two distinct methods. The first method followed the gold standard of MSC chondrogenic differentiation using tissue culture plastic, whereby ADSCs are cultured at a high density as pellets, also known as micromass culture (outlined in section 2.8.3). Alternatively, ADSCs cultured on microcarriers were transferred to chondrogenic induction media (as outlined in section 2.10) whereby cells mass migrated from monolayer culture on the surface of the spheres to high density pellets (mostly associated to multiple microcarriers) spontaneously.

To assess chondrogenic pellets maintained in chondrogenic medium using histological stains (generated from either method 2.8.3 or 2.10), the samples were fixed with 3.7% paraformaldehyde for 15 mins and washed three times with PBS and stained with 1% (w/v) alcian blue in HCl (pH 1.0) for 30 mins at RT. Excess stain was removed using 0.1N HCl.

To assess ECM production, microcarrier associated chondrogenic pellets (generated using method 2.10) were fixed in 10% neutral buffered Formalin overnight at 4^oC and washed in PBS. The pellets were the dehydrated using cold (4^oC) industrial methylated spirit (IMS) at 70% 90% 100% (v/v%) for 30 mins each, followed by two incubations of 100% RT IMS for 30 mins each. The samples were placed in xylene for 30 mins and then embedded in paraffin wax for 30 mins using a Leica EG1150H Embedding Centre, the blocks were then placed on a Leica EG1140C cold plate to allow the wax to harden rapidly. Sections were cut at a thickness of 5μm using a Leica RM2235 rotary microtome, floated on warm water and mounted on Polysine microscope slides. The sections were dried overnight at 45^oC. The slides were stained with Toluidine Blue to visualise glycosaminoglycan (GAG) content or heamatoxylin & eosin (H&E) for structural analysis. The images were photographed using a brightfield microscope. Immunohistochemistry was used to detect collagen type I and II, in chondrogenic cell-microcarriers. Sections were deparaffinised in xylene and permeabilised using 0.01% Tween for 5 mins each. Sections were washed in Tris-acetate 6.5 pH for 2 mins and pre-digested for 2 hours at 37^oC in 0.25 U/mL of chondroitinase A/B/C and hyaluronidase (2U/mL). The sections were subsequently

washed in PBS for 5 mins and blocked with 5% normal goat serum in PBS for 20 mins at RT. Sections were incubated overnight at 4°C in collagen type I and II primary antibodies in parallel at 11µg/mL and 10µg/mL respectively. The sections were then washed with PBS 3 times at 5 mins intervals. The slides were then incubated in the relevant FITC conjugated anti-mouse or anti-rabbit secondary antibodies (1:100 dilutions in PBS) (Invitrogen, UK) for 1 hour at RT. After washing with PBS 3 times at 5 mins intervals, the slides were mounted in Vectashield containing DAPI (Vector, UK). The images were observed using a widefield fluorescent microscope.

2.14   Cleaning spinner flask glassware

To remove organic matter, cell debris and protein from the spinner flasks, the insides were brushed using distilled water, sigmaclean and a large pipe cleaner and then rinsed. Flasks were filled with 1M NaOH solution at RT for 2 hours before being rinsed with distilled water. The spinner flask was then filled with 1M phosphoric acid, rinsed with distilled water and dried in a 90°C oven for 1 hour. Spinner flasks were then treated with Sigmacote to siliconise the glassware (and reduce cell binding to the glass surface), air dried and rinsed several times with distilled water. The flasks were then dried at 90°C for 30 mins before being sterilised in an autoclave at 121°C for 15 mins. Clean sterile flasks were subsequently dried in a 90°C oven for 1 hour prior to use.

2.15   ADSC expansion in spinner flasks

Approximately 12,300 microcarriers containing 1mM cRGDfC were generated in one microfluidic 60 minute run, washed to remove all oil and placed in spinner flasks containing 30mL of DMEM (low glucose) (containing Glutamax supplemented with 10% Mesenchymal stem cell qualified FBS, 75 µg/mL Gentamicin and 37.5 ng/mL Amphotericin), and incubated at 37°C, 5% CO_2 for 8 hours to equilibrate the microcarriers.

2.15.1 Seeding experiment 1

500,000 ADSCs were seeded into the spinner flasks and cultured under intermittent stirring (18-21rpm 1 min every 45 mins) for 7 days. After 24 hours the medium was increased to 100mL. Partial media changes (50%) were performed every three days. Samples were removed daily for microscopic and viability analysis. After 7 days the microcarriers were removed and either transferred to ultra low attachment

wells containing differentiation media or processed for RNA extraction. Microcarriers containing differentiated cells were analysed using lineage specific histochemical stains.

2.15.2 Seeding experiment 2

Approximately 215,000, 114,000, 38,000 or 12,000 ADSCs (counted using the dye exclusion method described in section 2.7.4) were seeded into spinner flasks and cultured under intermittent stirring (60rpm 1 min every 45 mins) for 14 days. After 24 hours the medium was increased to 100mL. Partial media changes (50%) were performed every two days. Samples were removed daily for microscopic and viability analysis. After 7 days the microcarriers were removed, washed twice in PBS and either transferred to ultra low attachment wells containing differentiation media or processed for RNA extraction. Microcarriers containing differentiated cells were analysed using lineage specific histochemical stains.

After 14 days all cells were enzymatically removed from the microcarriers (as described in Section 2.16). The number of viable cells was counted (as described in Section 2.17), and the specific growth rate and the doubling time of the MSCs can be calculated, using the following equations:

$$Specific\ growth\ rate = \frac{\ln(Xf) - ln(Xi)}{\Delta t}$$

Where Xf = final cell density, Xi = initial cell density.

$$td = \frac{ln2}{\mu}$$

Where t_d represents the generation time (h) and μ is the specific growth rate (h_{-1}).

2.16 Enzymatic detachment of cells from microcarriers

The culture medium was partially removed (~85%) and microcarriers rinsed twice with pre-warmed PBS. Attached cells were removed by adding TrypLE express (500µL) to each well. Cells were incubated for 5 mins at 37^oC to allow detachment of cells into a single-cell suspension. After incubation, enzymatic action was terminated through the addition of serum-containing medium (3mL). The total supernatant was removed and centrifuged at 220 x g for 5 mins. The cell pellet was resuspended in 1mL

of complete medium by gentle pipetting to dissociate any cell clumps. Cell viability was determined using the exclusion dye method (Section 2.4.6).

2.17 Measurement of anti Il-8 using ELISA

A 96-well plate (Corning) was coated with a goat anti-human IgG-Fc polyclonal antibody (100 µL/well, 10 µg/mL; Bethyl Laboratories) in 0.1 M sodium hydrogen carbonate buffer. After overnight incubation at room temperature, the plate was washed three times with phosphate-buffered saline (PBS) containing 0.05% (v/v) Tween 20 (PBS-T). Unbound active sites were blocked with 300 µL of 1% (v/v) bovine serum albumin (BSA)/PBS per well for 1 h. The plate was washed with PBS-T and reference samples of human IGG or supernatant samples were taken from CHO cell laden microcarrier cultures were added to the plate. The plate was incubated for 2 h at room temperature. After being washed in PBS-T washing solution, the plates were incubated at room temperature for 1 h with 100 µL of horseradish peroxidase-conjugated goat anti-human IgG-Fc polyclonal antibody solution (1 µg/ mL; Bethyl Laboratories) in 1% (v/v) BSA/PBS. Following washing of the plates in PBS-T washing solution three times, 100 µL of 2,2'-azino-bis(3-ethylbenzothiazoline-6-sulphonic acid) or ABTS (Thermo Scientific Ltd., High Wycombe, UK). The samples were transferred to a new plate and absorbance was measured at 405 nm using a microplate reader (Fluostar optima, BMG optima, Germany).

3.0 Generating a microfluidic platform for the synthesis of microspheres with tunable properties

3.1 Introduction

In vivo, cells integrate physical and biochemical cues from the surrounding environment and ECM. This is a complex process whereby each cell receives a unique combination of external stimuli, which synergistically defines a variety of cellular processes including cell morphology, cytoskeletal organization, differentiation and gene regulatory pathways (256). Classified into three broad areas; cells recognise and receive input from mechanical, chemical and topographical stimuli (177-179).

The versatility in PEG chemistry and the biocompatibility of synthetic PEGDMA hydrogels have prompted the development of hydrogel systems for directing cellular functions and regenerative medicine applications (305). PEGDMA hydrogels can be readily processed using UV photo-polymerisation and are of particular interest as they provide a bio-inert platform which can be used to systematically investigate the effects of mechanical and chemical factors on cellular processes (240). PEG hydrogels can be modified to incorporate covalent coupling of functional groups, such as bio-adhesive peptides, and to generate relatively stable gel structures with tunable mechanical properties such as swelling ratio, permeability and elasticity (306).

The primary objective of this chapter was to establish a novel microfluidics-based platform for the production of synthetic microcarriers. A microfluidic method for the synthesis of highly monodisperse PEGDMA hydrogel microspheres was developed herein using continuous droplet formation and *in situ* UV photo-polymerisation. The production method developed can be tuned to generate PEGDMA microspheres with a wide range of target diameters, and hence surface topographies, each with an extremely narrow size distribution (299).

A key factor in the development of normal cellular structure and function is the signal(s) received though chemical interactions at the cell surface. *In vivo*, interactions between integrin receptors on the surface of mammalian cells and ligands present within the extracellular matrix (ECM) regulate a diverse range of cellular functions, including adhesion, growth, differentiation, and motility (307). PEGDMA has previously been co-polymerised with functional motifs, such as ECM-derived cell adhesive peptides, to interact with cells and to render the otherwise inert PEG hydrogels bioactive (308). Modification of PEG hydrogels to include specific peptide sequences can be achieved through several different methods. This chapter describes the incorporation of ECM-derived peptides into PEGDMA microspheres using two methods: a) By covalently

linking peptides to a monoacrylated PEG monomer through an *N*-hydroxysuccinimidyl group (309) b) By directly reacting cysteine-containing peptide sequences into hydrogels through Michael-type addition (240).

When developing biomaterials, scaffolds should provide mechanical support for cells as well as transmit mechanical stimuli (310). To probe the mechanical properties that can influence cell fate, a variety of PEGDMA hydrogel microspheres with a wide range of mechanical properties, including compressive modulus and mesh size, were generated and characterised. Surface topography was assessed using environmental scanning electron microscopy (ESEM).

The objective was to design and optimise a robust microfluidic method to synthesise monodisperse microspheres reproducibly, capable of presenting ECM-like stimuli to adhered cells. The optimisation of polymer content generated a range of microcarriers with different sizes, synthetic peptide modifications and compressive moduli. Presenting these factors in a spatially defined and controlled manner, the bioinert PEGDMA hydrogel microspheres developed herein provide a platform whereby chemical, mechanical and topographical parameters can be individually assessed based on cell responses.

3.2   Emulsion formation in Microfluidic devices

Microfabricated devices consist of microchannels arranged in specific, user-defined geometries to exploit specific microfluidic phenomena. Such arrangements are termed fluidic circuits. The most commonly used microfabrication method to generate fluidic circuits is soft lithography of polydimethylsiloxane (PDMS) due, in part, to its relatively low cost and standardized technique. Typically, such devices are permanently sealed, with external connections through which fluids are introduced.

For this study, a novel microfluidics-based device, termed MicroPlant^{TM}, was used. The system developed by Q Chip (Cardiff, UK), was designed to enable rapid evaluation of microfluidic circuits and junctions. To produce fluidic circuits in PDMS is laborious and requires a minimum of 8 hours (311). The system developed by Q Chip employs a single milling operation to produce microchannels, which is much quicker and easier, (typically circuits can be produced within 60 minutes). Therefore, using the MicroPlant^{TM} allowed ideas to be rapidly converted to testable circuits. In addition, design iterations to the fluidic circuit were quick and easy to investigate.

Unlike traditionally fabricated microfluidic devices, MicroPlants™ are not permanently sealed. This allows the device to be assembled and disassembled rapidly. In addition, any blockage of channels (which can occur rapidly after commencement of an experiment) can be easily rectified. This is particularly useful in cases of accidental experimental failure (e.g., channel blockage due to unwanted polymer cross-linking), allowing rapid recovery during testing and optimisation of conditions, which would be impossible in permanently sealed devices.

Microfluidic circuits are machined into hydrophobic and rigid polytetrafluoroethylene (PTFE) discs 'chips'. Fluidic circuits consist of microchannels, which are rectangular in cross-section. A computer Numerical Controlled (CNC) milling machine is used to create the microchannels in the PTFE surface. Microchannels, by definition, must be less than 1mm in at least one dimension, and can be made any size, to a minimum of 100μm, which represents the limit of the micromilling method.

The finished PTFE chip containing the desired milled microfluidic circuit is placed onto a 316 stainless steel fluid distribution manifold, into which high performance liquid chromatography fluid connectors are introduced vertically. To provide a top surface to the fluidic channel, a hydrophobic gasket (PFA film, 250μm thick) is placed onto the surface of the chip. In addition, a transparent borosilicate disc is placed over the chip (and gasket), thus allowing observation of fluid flows in microchannels. Disposable sterile syringes containing the required fluids are connected to the base of the microfluidic device *via* narrow bore tubing. Fluids (pumped using syringe drivers) enter the fluid distribution manifold *via* vertical through-holes (sealed with nitrile rubber O-rings) and flow to the top of a chip into the microchannels through entry holes. Finally, a stainless steel clamping piece is bolted to the fluidic manifold, allowing the entire laminated assembly to be compression sealed. The device is illustrated schematically in Figure 9.

To form droplets (and therefore a linear emulsion) in a microfluidic circuit, the inherent physical properties of immiscible liquids are exploited. In a microfluidic circuit, a linear microemulsion can be formed when immiscible fluids flow together into a microfluidic junction. The simplest of these is the T-junction, illustrated in Figure 7A. Fluid flowing in one channel is sheared by a second immiscible phase, flowing into the cross-channel (312). Co-flowing streams can be used to generate emulsions, these can

take the form of cross-junctions and flow focusing junctions (Figure 7B and C (313)). Conventionally, when forming an emulsion the fluid which forms droplets is termed the disperse phase (Fluid α in Figure 7), and the immiscible fluid is termed the continuous phase (Fluid β in Figure 7).
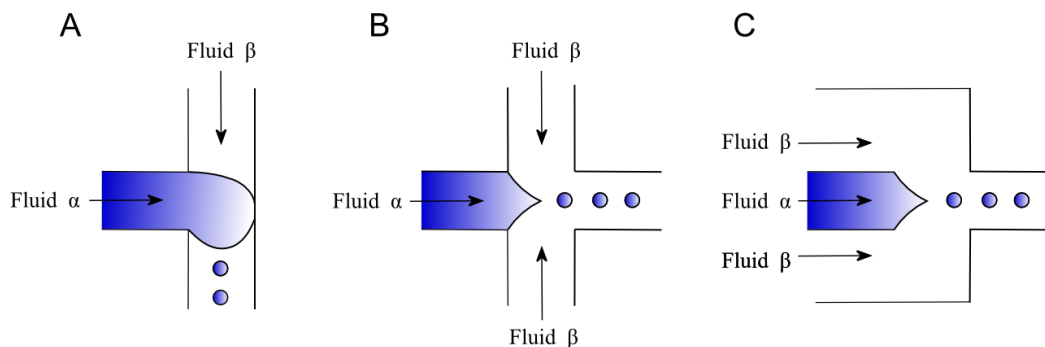
Figure 7 Schematic representation of microfluidic junctions.

Emulsion formation at (A) T-junction, (B) Cross-junction or (C) Flow focusing junction

Channel properties, such as contact angle, surface energy and hydrophobicity, influence the ability of a given liquid to form droplets. Aqueous PEGDMA solutions are repelled from the hydrophobic PTFE chip surface used in the MicroPlant[TM]. A fluid which is immiscible with an aqueous PEGDMA solution is required to form a linear emulsion. The nature of a linear emulsion is dependent on the surface tensions (and interfacial tension) of the component fluids, as well as the energies of the microchannel surfaces. The particular characteristics of a linear emulsion, e.g. droplet size, size variance, and droplet production frequency are strongly dependent upon fluid flow rate and microchannel architecture. As the interfacial surface tension is constant for a given pair of fluids at a given temperature, variations in relative flow rates are used to produce different flow patterns.

At slow fluid flow rates, plug formation occurs, rather than spherical droplet formation (Figure 8B). A plug is defined as a droplet large enough to fill the cross-sectional of a channel (in addition to a thin layer of continuous phase, preventing it from contacting the channel walls) with its length in the direction of fluid flow greater than its width (314). Upon passing into a channel with a greater cross-sectional area, liquid plugs form spheres due to the surface tension forces.

By increasing the continuous fluid flow rate, droplet formation is favoured (Figure 8A). The dispersed phase is forced to break into droplets by the increased pressure and viscous forces exerted by the continuous phase. However, if the continuous phase flow rate is increased further, the disperse phase is pulled into a stable neck formation with droplets pinched off near the tip (Figure 8C). In this flow pattern, although droplets are very small, (much smaller than the channel diameter), satellite droplets are often produced leading to a large observed droplet polydispersity (315). In all experiments, flow rates were empirically determined to bring about stable segmentation, as opposed to plug or unstable droplet formation.

Previously the MicroPlant has been employed to generated polymeric microspheres for small peptide therapeutics and PCR reagents. In addition, it has been used to encapsulate dopamine expressing cells.
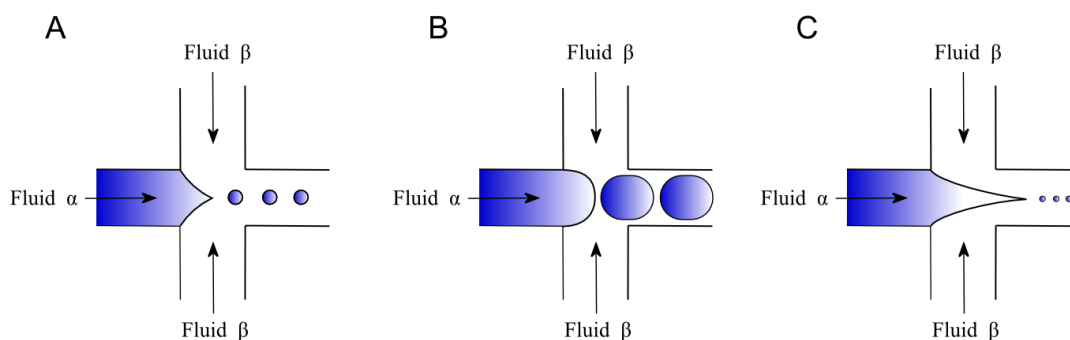
Figure 8 Flow patterns produced in a microfluidic cross-junction.

(A) Droplet formation, (B) Plug formation and (C) stable neck formation.
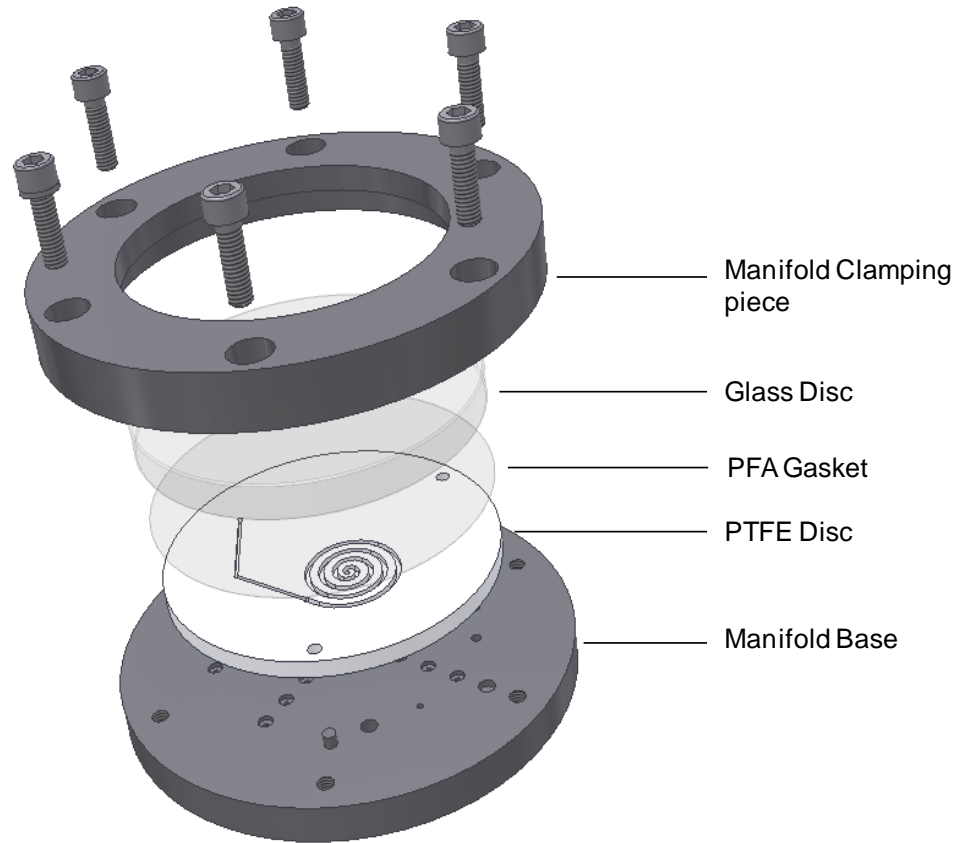
Figure 9 The microfluidic evaluation platform (MicroPlant^{TM}) used in microfluidic experiments.

Expanded schematic showing the components of the microfluidic device. The MicroPlant assembly consists of a circular 316 stainless steel base containing several fluid entry points..

3.3 Results

3.4 Generation of Monodisperse PEGDMA Microspheres in a MicroPlant.

The MicroPlant, (depicted in Figure 9) was used to synthesise PEGDMA hydrogel microspheres (both unmodified and peptide-containing). A continuous phase (high-oleic acid sunflower oil; Statfold seed oils, UK) was brought into contact with a dispersed phase, (an aqueous solution of PEGDMA macromer, photoinitator (and peptide conjugate where applicable)), at a T-junction. These immiscible phases formed a linear emulsion at the microfluidic junction by a process called segmented flow. The dispersed phase droplet size could be controlled by varying the relative flow rates of the two immiscible fluids. By increasing the flow rate of the continuous phase, segmentation can occur more rapidly, producing droplets more frequently. If the discontinuous polymer rate remains the same at the inlet, increasing the continuous phase will have an inversely proportional effect on microsphere size. In order to produce discrete droplets of approximately 500μm diameter, PTFE chip design, and fluid flow rates were tested and optimised. UV-induced photo-polymerisation was used to irreversibly crosslink the PEGDMA containing dispersed phase droplets, producing solid PEGDMA hydrogel microspheres.

3.5 PTFE Chip design

In an effort to produce UV photopolymerised PEGDMA microcarriers of approximately 500μm diameter, PTFE chips containing several different microchannel designs and junctions were fabricated and tested.

3.5.1 Chip 100073A

Initially, a smaller evaluation MicroPlant (a miniaturised version of the MicroPlant described in section 3.1), was employed to trial dispersed phase segmentation and determine the ultimate method that would be used to produce the spheres. Using chip 100073A (labeled according to an internal referencing system), the polymer was segmented at a flow-focusing junction by two equivalent inputs of immiscible continuous phase (Figure 10) (288). The polymer droplets generated continued into the microchannel spiral (the 'UV curing zone'), designed to increase the time the droplets were retained within the chip, increasing UV exposure and hence

photo-polymerisation time. Chip 100073A provided valuable information regarding *in situ* curing rates and optimum channel sizes to produce microspheres of 500µm diameter. However, improvement was required on two points. Firstly, the top mounted UV light source illuminated the entire surface of the chip, including the whole microchannel circuit, crosslinking the polymer at the fluidic junction prior to segmentation. Future designs would require the polymer entry point to be shielded from UV light. Secondly, the microchannel, and hence, 'on-chip' retention time was too short to allow complete photo-polymerisation of polymer droplets. Again, subsequent designs featured longer channels for increased residual exposure. Experimental data gathered from the evaluation MicroPlant, elucidated suitable channel dimensions and these remained consistent in all channel designs hereafter. The fluidic input channels were of cross-sectional dimension 500µm^2, opening out to 700µm^2 into a spiral UV-curing zone.
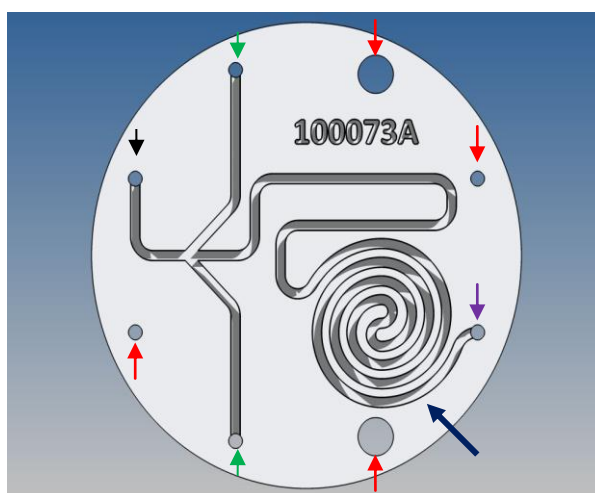
Figure 10 PTFE chip 10073A.

An evaluation chip, the polymer is segmented at a flow-focussing junction by two immiscible carrier flows. Carrier fluid entry points are indicated by green arrows. Functional fluid (polymer) entry holes are indicated by black arrows. Red arrows indicate points anchored to the manifold. Fluid exit holes are indicated by a purple arrow. A dark blue arrow indicates the spiral UV curing zone, designed to increase UV retention time.
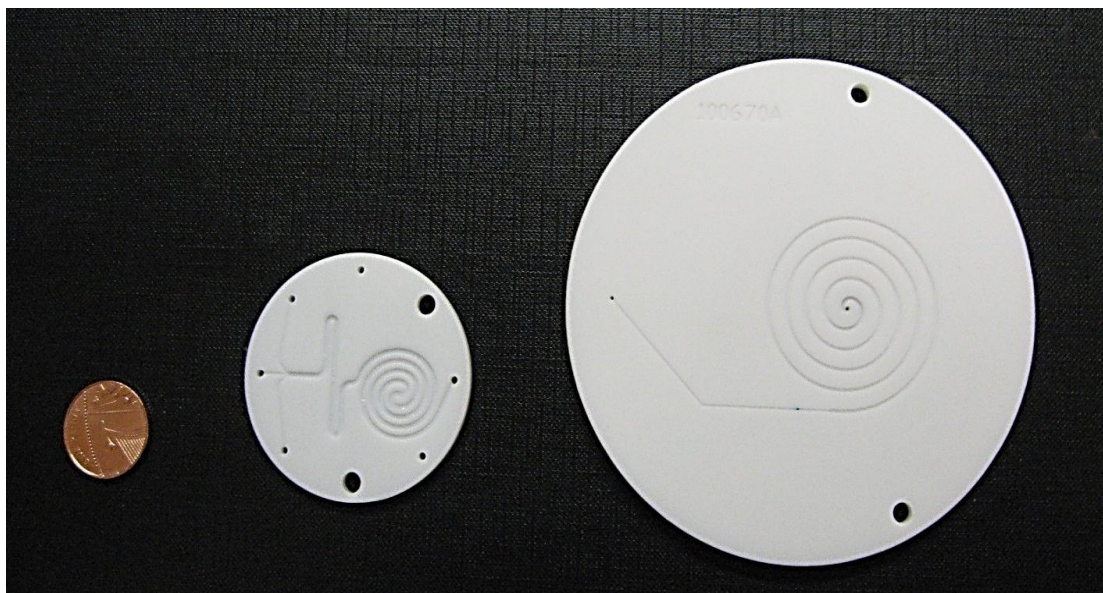
Figure 11 Size comparisons of evaluation and full size PTFE chip designs.

Diameters: 1 penny = 12mm, evaluation MicroPlant chip = 50mm, and MicroPlant chip = 100mm.

3.5.2   Chip 100660A

In order to allow the microchannel to be lengthened and increase on-chip retention time, all subsequent chips were designed for use on the larger MicroPlant, which holds significantly larger chips than those on the evaluation MicroPlant (for a comparison of chip sizes see Figure 11). The junction used to segment the dispersed phase was changed from a flow-focusing junction to a T junction in Chip no. 100660A (Figure 12) by introducing the dispersed phase into the microchannel using a vertical though-hole (as described in section 3.2) (Figure 13). The polymer solution was segmented immediately as it entered the channel, and using a mask, the entry hole was shielded from UV exposure. Post-polymerisation, extra fluid channels were added, providing the potential to add further reagents to the microspheres post-curing. However, it was observed that this chip was suboptimal as the UV curing zone contained a tight exit from the spiral, which caused microspheres to slow down. This allowed partially photo-polymerised polymer droplets to contact one another forming large hydrogel aggregates (as shown in Figure 14), or alternatively deposit partially crosslinked polymer residue on the microchannel walls, both of which resulted in the channel becoming blocked.
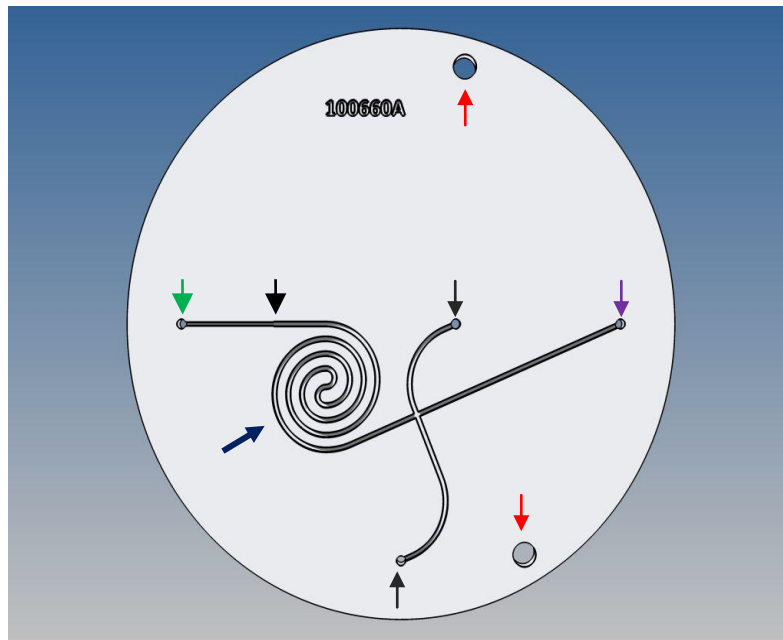
Figure 12 PTFE chip 100660A

A full sized chip, the flow-focussing junction has been replaced by a vertical junction to prevent polymerization prior to segmentation. Carrier fluid entry points are indicated by green arrows. Functional fluid (polymer) entry holes are indicated by black arrows. Red arrows indicate points anchored to the manifold. Fluid exit holes are indicated by a purple arrow. A dark blue arrow indicates the spiral UV curing zone, designed to increase UV retention time.
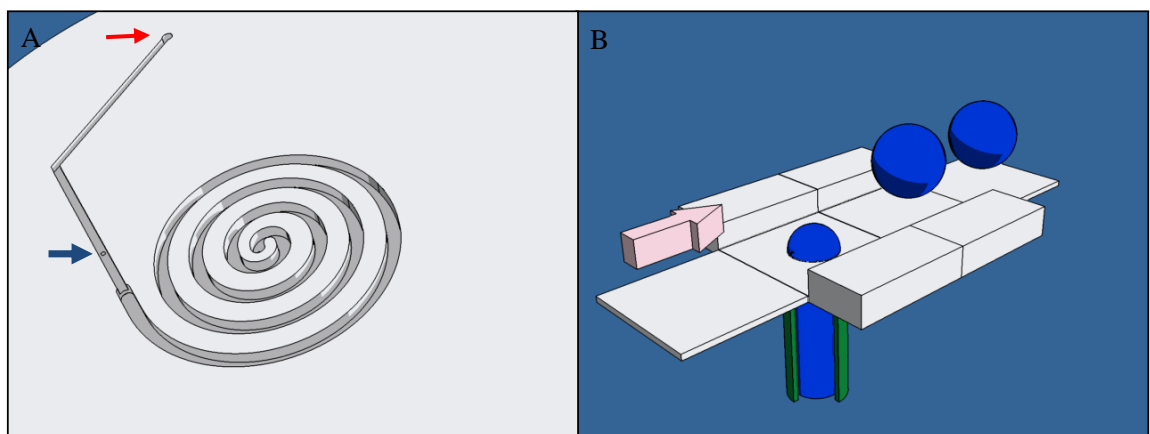
Figure 13 Cartoon schematic of a microchannel and droplet formation at a T-Junction.

A) The PTFE microchannel consisted of a continuous phase input (red arrow) followed by disperse phase inlet at a T-junction (blue arrow). The fluidic input channels were of cross-sectional dimension 500μm^2, opening out to 700μm^2 into a spiral UV-curing zone. B) The continuous phase represented by a pink arrow was brought into contact perpendicularly with the PEGDMA solution (shown here in blue), at a fluidic T-junction to produce a segmented flow stream.
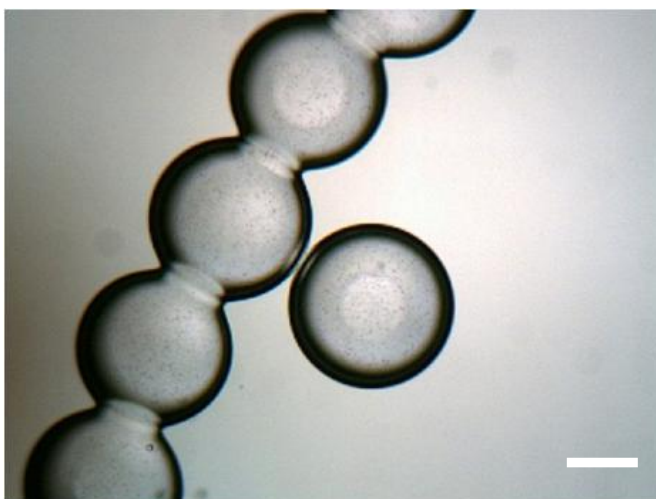
Figure 14 Covalently cross linked microspheres

The microspheres in this image have contacted one another prior to complete polymerisation. The result is the microspheres attach to form a solidified 'string' of beads.

3.5.3   Chip 100670A

Chip 100670A (Figure 15) was engineered to contain the same T junction as chip 100660A, however the length of the curing zone was further increased. The microchannel was designed to allow the spheres to exit the surface of the chip from the center of the spiral to overcome the tight turn used in 100660A. Previously, the microspheres had to travel through a small piece of PTFE tubing, (approximately 3cm in length) before falling into a collection vessel. This caused back pressure in the channel as the spheres tended to stall before the exiting the chip. To increase the efficiency with which the polymerised microspheres exited the MicroPlant, a section of the steel manifold (below the exit junction on the PTFE chip) was milled out. However, the exit hole was preceded by a tight turn in the microchannel spiral, which also resulted in the channel becoming blocked.
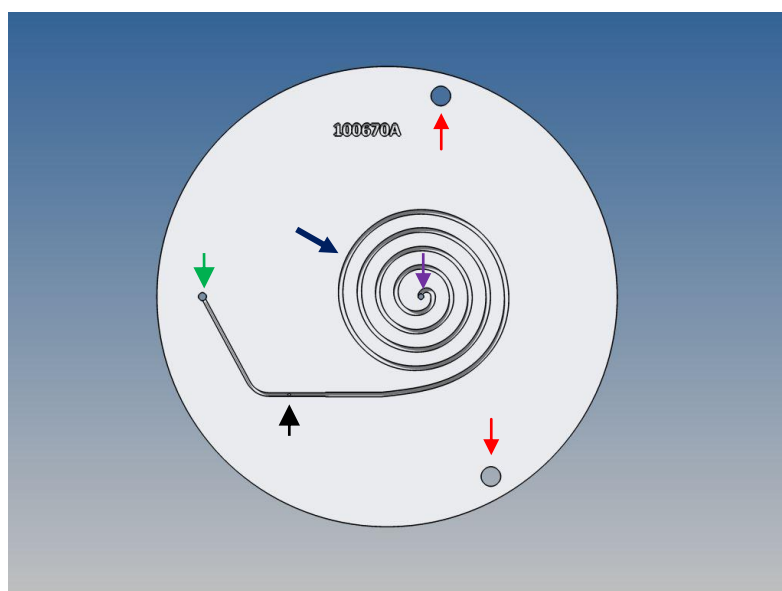
Figure 15 PTFE chip 100670A

The curing zone has been enlarged for longer UV exposure. Carrier fluid entry points are indicated by green arrows. Functional fluid (polymer) entry holes are indicated by black arrows. Red arrows indicate points anchored to the manifold. Fluid exit holes are indicated by a purple arrow. A dark blue arrow indicates the spiral UV curing zone, designed to increase UV retention time.

3.5.4 Design and Manufacture of a UV light-guide holder

To produce microspheres with reproducible, monodisperse characteristics including chemical crosslinking, uniform UV exposure was required during *in situ* photo-polymerisation. Previously, the positioning of both the MicroPlant and UV light-guide was implemented using a clamp stand. The distance, angle and position of the UV light-guide relative to the surface of the PTFE microchannels introduced several variables into microsphere production. Most importantly, it was difficult to reproduce both the distance of the UV light source in relation to the chip, and to illuminate the entire curing zone equally. Hence, amendments to the steel manifold were designed and implemented with the assistance from engineers at Q Chip. Firstly, the manifold base was adapted to include a permanent stage. Three metal supports of 15cm length were inserted into the manifold base to form a tripod stand.
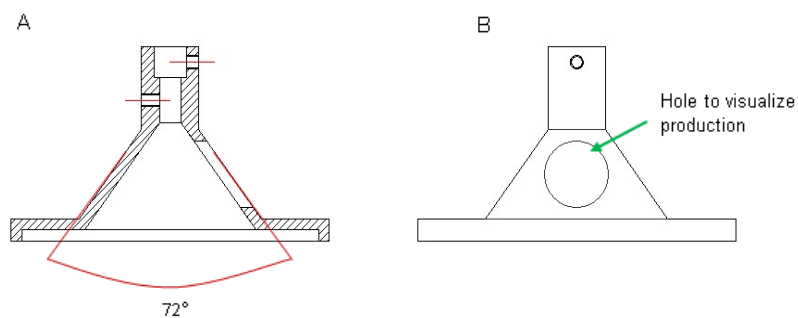
Figure 16 AutoCad-2008 generated blueprint of UV light-guide holder, designed to fit a 316 manifold.

(A) Cross sectional view: The UV light-guide is held in place by a stepped section with two nylon screw entry holes to hold the light-guide in place. The cone portion has been designed to have a curvature of 72°, matching the angle of incidence of the UV light source. (B) An overview, the 'hat' contains a hole in the steel cone to allow visualization of microspheres in situ.

Secondly, a UV light-guide holder was designed to provide an optimal illumination height for polymer curing. As shown in Figure 16, the UV light-guide could be placed into the custom designed steel unit and held in place by nylon screws. The light-guide holder was designed to fit on top of the assembled MicroPlant. This enabled control over the distance between the UV source and the chip, and uniform chip illumination. This also ensured the entire surface of the chip was illuminated, and created an enclosed system, thus providing a shield between the UV light and the user during microcarrier production. The light-guide holder was designed to have an incidence angle at 72° degrees matching the angle of incidence of the UV light source. To aid in quality control during microsphere production, a hole was milled into the holder to allow the visualization of microsphere production. The final MicroPlant assembly is shown in Figure 17.
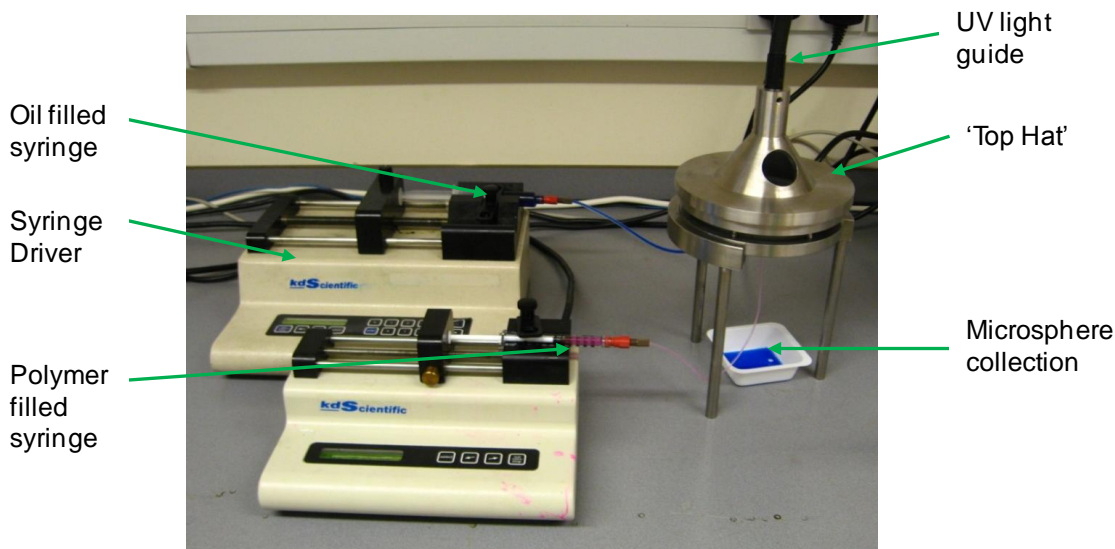
Figure 17 Photograph of the final assembled MicroPlant after modifications

Experimental assembly comprising two syringe drivers pumping fluid into the MicroPlant though narrow bore capillary tubing.

3.5.5   Chip 100718A

The final chip layout, 100718A (Figure 15), was designed and produced after the UV light-guide holder was engineered (Section 3.5). Consequently, the UV curing zone was centralised on the chip to achieve even and maximum exposure to the UV source. From experimental data, the time taken for complete photo-polymerisation to occur was determined to be 180 seconds and the total length of the microchannel was shortened accordingly. In addition, the tight turn prior to the exit hole found in chip 100670A was removed to increase the stability and ease of microsphere exit from the microchannel. The size distribution of the microspheres, along with their coefficient of variance were calculated from measured values from product microspheres (

Figure 20). Using chip 100718A, monodisperse microspheres with a diameter of approximately 461µm were manufactured reproducibly. The evolution of microchannel designs are summarised in Figure 19.
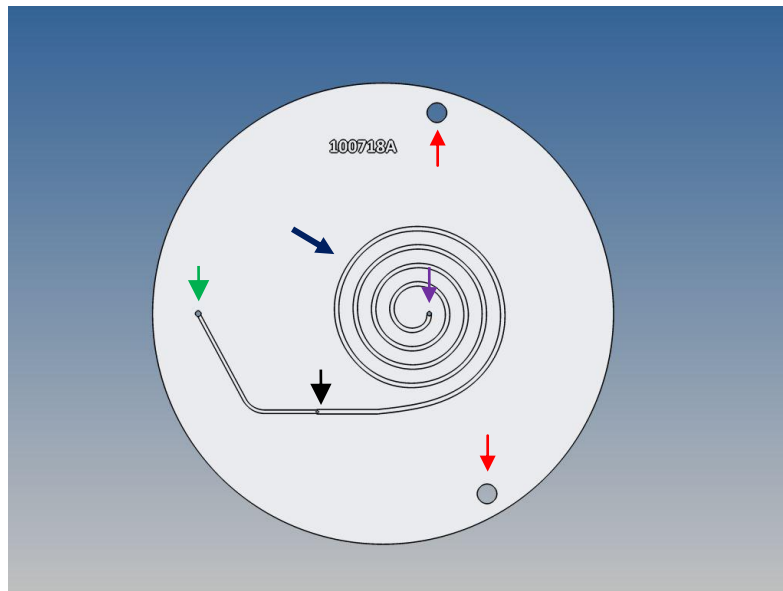
Figure 18 PTFE chip 100718A

The final chip design, the curing zone was centralised and the sharp bend near the exit has been removed. Carrier fluid entry points are indicated by green arrows. Functional fluid (polymer) entry holes are indicated by black arrows. Red arrows indicate points anchored to the manifold. Fluid exit holes are indicated by a purple arrow. A dark blue arrow indicates the spiral UV curing zone, designed to increase UV retention time.

3.5.6   Chips 101019A and 101020A

To produce alternatively sized microspheres Chips 101019A and 101020A were designed and tested. The microchannel layout remained identical to 100718A, however the dimensions of the channel and the entry and exit holes were increased and decreased accordingly, and resulted in microcarriers with an average diameter of 261.3μm and 950.7μm. Frequency distribution graphs of the resulting microspheres are shown in

Figure 20.

101019A	101020A
300μm Continuous phase entry hole	700μm Continuous phase entry hole
100μm Dispersed phase through hole	350μm Dispersed phase through hole
300μm channel opening to 500um	1000μm channel opening to 1300μm
700μm exit hole	1300μm exit hole

Chip design	Example of resulting microspheres	Key alterations to chip design
	No microspheres produced	• Evaluation MicroPlant (50mm chips) • Polymer cured prior to segmentation (at green asterisk) due to top mounted UV illumination source • UV curing spiral (indicated by blue arrow) too short (and hence 'on chip' retention time) for complete polymerisation
		• Larger MicroPlant (100mm chips) employed to allow a larger UV curing spiral and longer 'on chip' retention times. • The segmentation junction (black arrow) was changed to a T Junction and shielded using a mask. • Spiral design contained a tight turn causing microcarriers to contact one another co-polymerising prior to exiting the chip.
		• The exit hole (indicated by the purple arrow) was moved to the centre of the spiral. • The length of the curing zone was increased to allow complete polymerisation prior to exiting the chip • A tight turn at the end of the spiral resulted in spheres blocking the channel and co-polymerising
		• The tight turn prior to he exit hole was removed to allow for fully polymerised discrete microcarrier to be consistently produced. • UV curing zone centralised to allow for even UV exposure.
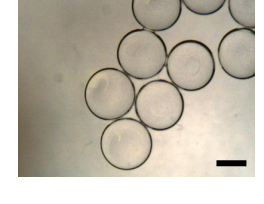
Figure 19 Evolution of microchannel design.

Multiple channel designs were generated, milled and tested. Carrier fluid entry points are indicated by green arrows. Functional fluid (polymer) entry holes are indicated by black arrows. Red arrows indicate points anchored to the manifold. Fluid exit holes are indicated by a purple arrow. A dark blue arrow indicates the spiral UV curing zone, designed to increase UV retention time. (Scale bar 300µm)
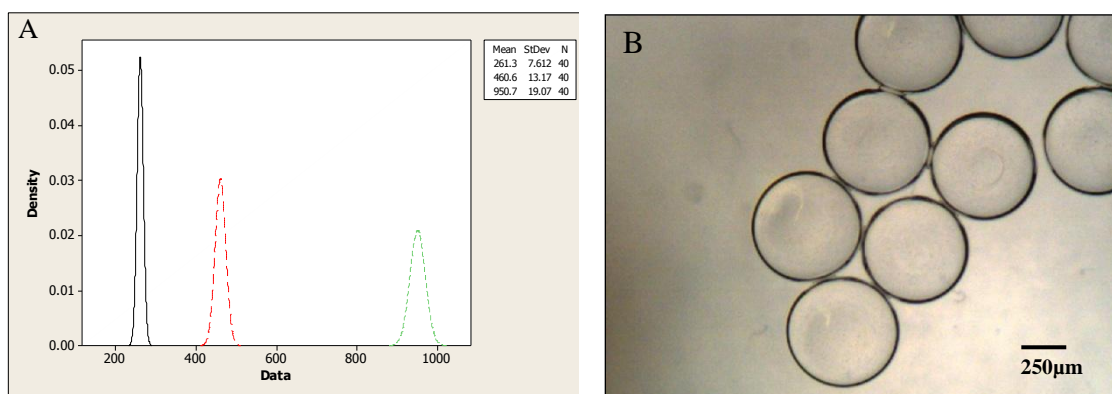
Figure 20 Size distribution of generated microcarriers

(A)Frequency distribution graph displaying the mean microsphere diameter of microfluidic generated microspheres was 261.3µm, 460.6µm and 950.7µm with a CV of 2.91%, 2.86% and 2.00% respectively (n = 40). (B) Compound light microscope image of solid PEGDMA microspheres demonstrating uniform size and shape.

3.5.7   Chip 100962A

To study hydrogel compressibility and to assess cell attachment after various peptide modifications, flat PEGDMA hydrogels discs with a depth of 500µm were required. Chip 100962A was generated to contain a large uniform chamber with a depth of 500µm, containing fluid entry and exit holes (Figure 21). Polymer solutions were manually syringe driven into the chip cavity and exposed to UV for 180 seconds. The MicroPlant was then disassembled and the flat gel slab removed and using a circular cutter, (diameter 8mm) hydrogel discs were generated.
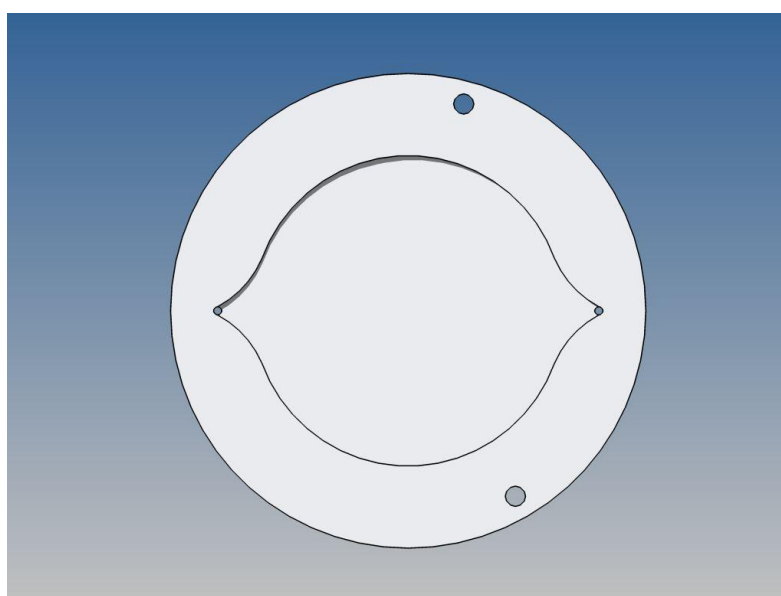
Figure 21 PTFE Chip 100962A

A large uniform chamber allows the production of flat PEGDMA gels of 500μm depth.

3.6 Optimised Flow rates Table and MicroPlant Assembly

To produce stable segmented flow within the microchannels, the flow rates of the polymer and continuous phases required optimisation and fine-tuning. A main obstacle to successful microsphere production was caused by partially polymerised microspheres contacting each other in the microchannel during long 'on-chip' retention times, particularly in the UV curing zone. Ideally the microspheres should remain separate until they have exited the MicroPlant. If contact occurred prior to complete photo-polymerisation, the microcarriers could become crosslinked to one another resulting in semi-polymerised multimers of beads, which typically block flow within the channel (Figure 14). To prevent this, the continuous phase fluid flow-rate was increased to enlarge the spacing between polymer droplets, helping to maintain discrete structures until fully solidified.

3.7 Incorporation of cell adhesive peptides using an Acryloyl-PEG-NHS linker.

Calculating the efficiency of the conjugation reaction was essential to determine the final concentration of peptide incorporated into the microsphere. The well characterised fibronectin-derived peptide sequence, GRGDS was selected for incorporation into PEGDMA microspheres. Previous research has demonstrated that GRGDS enhances cell binding and proliferation of multiple cell types to PEG hydrogels (316, 317). To incorporate the adhesive peptide GRGDS into PEGDMA hydrogel microspheres, peptides were first conjugated to a monoacrylated PEG macromer with a carboxylic end group activated by N-hydroxysuccinimide (NHS) to give acryloyl-PEG-NHS. GRGDS was conjugated to PEG *via* the reaction between *N*-hydroxysuccinimide and primary amines within the peptide, forming acryloyl-PEG-GRGDS (as shown in Figure 22). The success of this conjugation was assessed by Electrospray mass spectrometry and MALDI ToF ToF mass spectrometry.
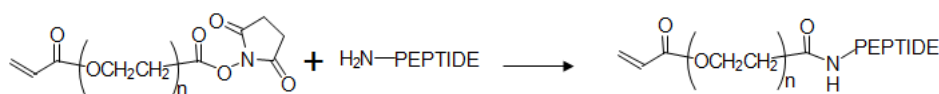
Figure 22 Incorporation of cell adhesive peptides using an Acryloyl-PEG-NHS linker.

3.8   Electrospray Mass Spectroscopy of Acryl-PEG-peptide Conjugates

The molecular weight of the acryloyl-PEG-NHS was measured before and after the conjugation reaction. The molecular mass of the precursor molecule, Acryloyl-PEG-NHS was $3711 gmol^{-1}$. After cleavage of the NHS moiety and incorporation of GRGDS peptide ($490.06 gmol^{-1}$), the expected molecular weight of the polymer-peptide conjugate was $4084 gmol^{-1}$ (Figure 23).

Electrospray Mass spectrometry (ESI) was employed to assess the yield of acryloyl-PEG-GRGDS produced from the above conjugation reaction. Initially the compatibility of ESI to analyse Acryloyl-PEG-NHS was assessed. The resulting spectra generated an array of signals (Figure 23), but did not provide defined peaks. The technique demonstrated the poly-dispersity of the repeating PEG units, which contains an average molecular mass of 3400. A lack of separate peaks confirmed that ESI was not suitable to analyse the conjugation reaction as it is not possible to track a single mass/charge ratio shift effectively.
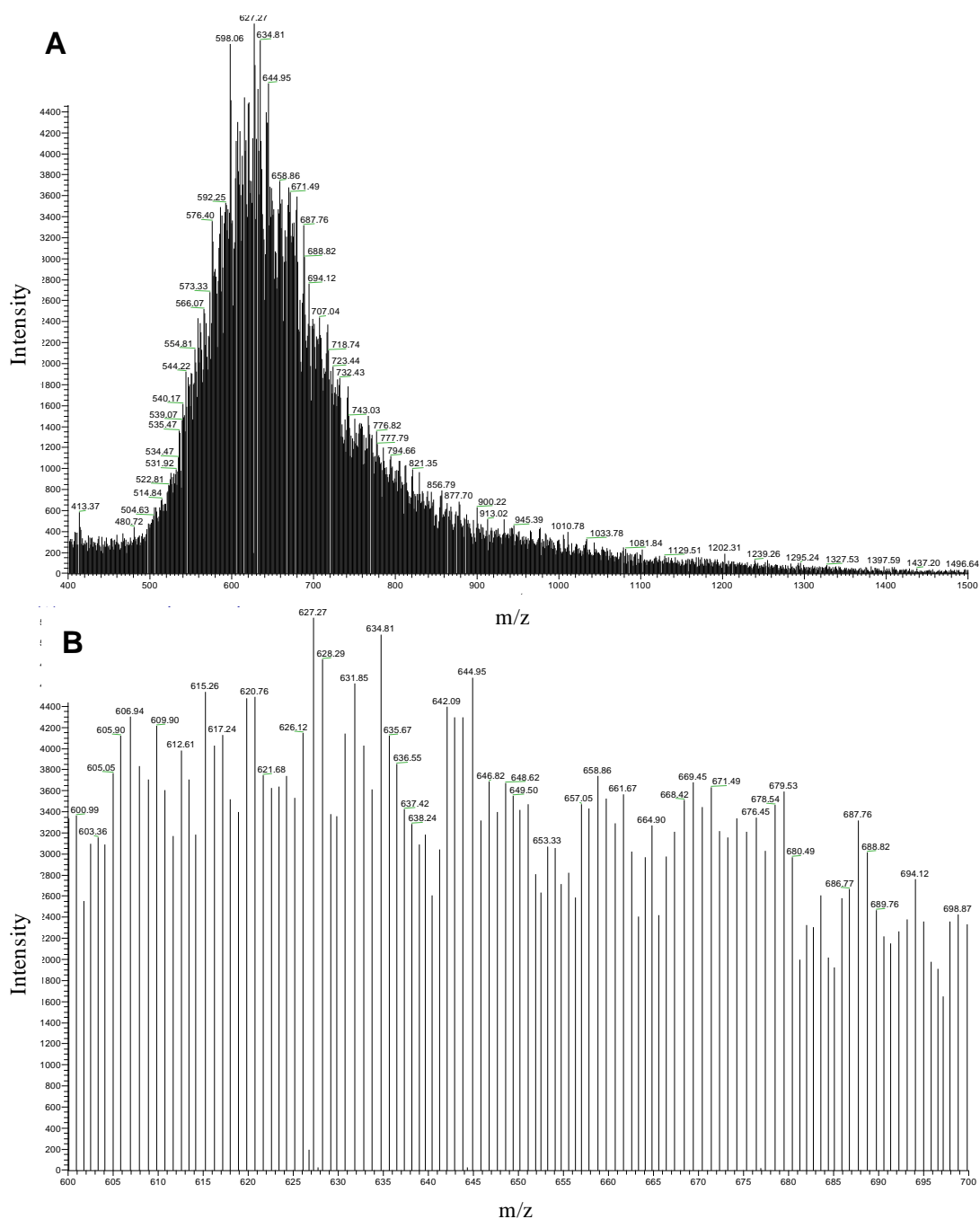
Figure 23 Spectrum of Acryl-PEG-NHS generated using Mass Spectrometry

A) Full scan showing a cluster of peaks with a large range of mass/charge ratios (m/z). (B) Sub section of full scan of Acryl-PEG-NHS around the mean.

3.9   MALDI ToF ToF Analysis of GRGDS Peptide Conjugate.

To analyse the conjugate Acryloyl-PEG-GRGDS, MALDI ToF ToF was performed. As shown in Figure 26, the detected mass of the reaction product was shifted by approximately 382±3Da (relative to starting material), corresponding to the molecular mass of the peptide gained after successful conjugation. Both the starting material and product MALDI ToF ToF mass spectra showed complex multiplets with a repeating Mw difference of 44Da, which corresponded to repeating ethylene glycol units. Several optimisation steps were required to successfully form and detect Acryloyl-PEG-GRGDS, detailed below.

First attempts at MALDI ToF ToF analysis aimed to determine whether a clear spectrum could be obtained from the PEG sample. Using sinapic acid as a matrix, this could not be achieved. However the sample was compatible with the α-cyano-4-hydroxycinnamic acid matrix (Figure 24A). The maximum peak at 3720.98gmol^{-1} corresponds to the average size of the acryloyl-PEG-NHS macromer.

The conjugated samples were analysed following a method outlined by Hern and Hubbell (300). In Figure 24C, the green spectrum represents the control sample, Acryloyl-PEG-NHS. Overlaid onto this spectrum is the conjugate sample, prepared by reacting the control sample with GRGDS peptide in a 1:1 ratio (Section 2.6.4 Method 1). The spectrum showed the conjugate contained a slight shift in mass/charge ratio. However, the shift was not consistent with the calculated shift in mass/charge ratio expected after the addition of peptide (4408.87Da). Figure 24B shows that despite dialysis, a large amount of unreacted peptide remained in the sample, shown by a large red peak at the left hand side of the spectrum.
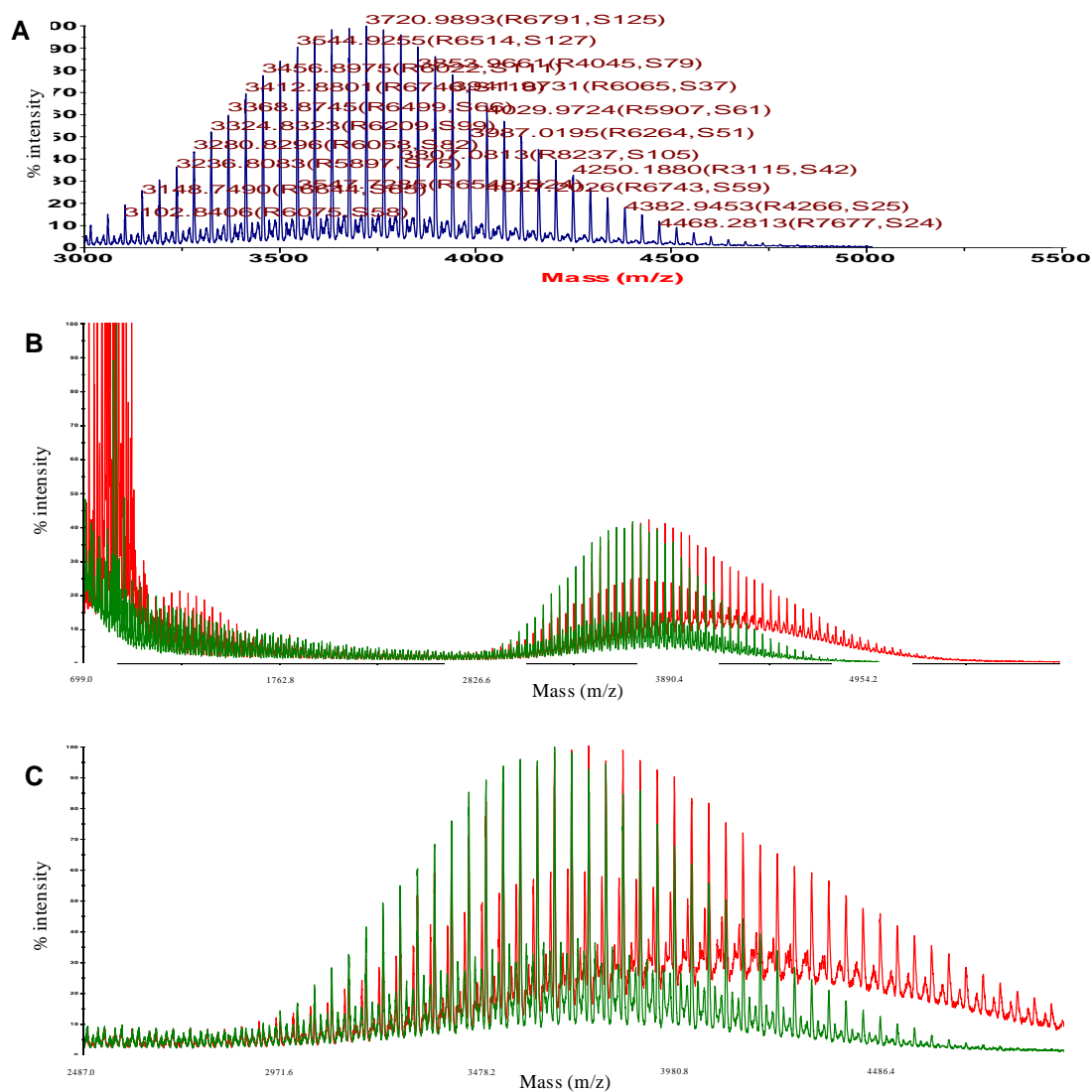
Figure 24 MALDI ToF ToF Spectra of Acryloyl-PEG-(3500)-NHS

(A) Demonstrating a classic polydisperse PEG spectra. All peaks indicate the intensity of each sample mass and are labeled with their mass/charge ratio and signal intensity. MALDI ToF ToF spectrum of Acryloyl-PEG-NHS (green), overlaid with the 'conjugate' sample (red). (B) The spectra shows a large red peak at a low mass/charge ratio. This is partly attributed to the presence of unreacted peptide in the sample. (C) A subsection of the spectra displayed in Figure 20B demonstrating the closely overlapping peaks which indicates a lack of peptide conjugation.

It was hypothesised that the rate of reaction would increase under higher pH conditions. A series of controlled reactions varying both the stochiometric ratio of peptide to Acryloyl-PEG-NHS, and the pH of reaction was performed (Section 2.6.4 Method 2). An array of basic pH conditions was employed, however, the TRIS buffer used was incompatible with the α-cyano-4-hydroxycinnamic acid matrix causing an intractable yellow by-product to form and degrading the treated matrix. Subsequently, the signal intensity was low due to poor loading of the sample onto the plate reader. Higher concentrations of Acryloyl-PEG-peptide resulted in a gel being formed upon drying which proved incompatible with the MALDI ToF ToF technique, as the laser required a flat surface to take an accurate mass measurement. The samples were further dialysed at a 1KDa MWCO to remove excess TRIS salts. However this shown to be insufficient to remove the entire TRIS base, which was still present in relatively high quantities at higher pH conditions. Consequently, only data for reactions performed at pH 7.5 were recorded. The data gathered at pH 7.5 are shown in Figure 25. The spectra for both the control and experimental samples (at pH 7.5) (both 1:1 and 1:1.5 ratios) were found to be identical. However, the spectrum produced at a PEG to peptide ratio of 1:2, showed additional peaks. The conjugate showed two overlapping peaks, one that corresponded to the MW of the control, Acryloyl-PEG-NHS, and one that corresponded to the calculated molecular mass shift expected for the conjugate Acryloyl-PEG-GRGDS. However, this technique failed to provide a quantitative measure of conjugation; therefore it was not possible to determine what percentage of the sample contained the successfully conjugated peptide.

The final experiment, outlined by Bencherif *et al.* 2009, and as used here, included dihydrobenzoic acid (DHB) as the matrix (301). This provided a conjugate spectrum that had a clear mass shift in relation to the control sample. The molecular mass of the precursor molecule, Acryloyl-PEG-NHS is 3711gmol-1. The reaction occurs *via* substitution of the NHS moiety, which is replaced by a peptide GRDGS of 490.07 gmol-1 resulting in a molecular mass shift of 4084 ($\pm$13gmol⁻1) (Figure 26). Overlapping graphs of the control and experimental samples showed a clear shift in the entirety of the spectrum corresponding to and centered around the molecular mass of the conjugate, this was unseen in previous experiments (Figure 24, Figure 25).
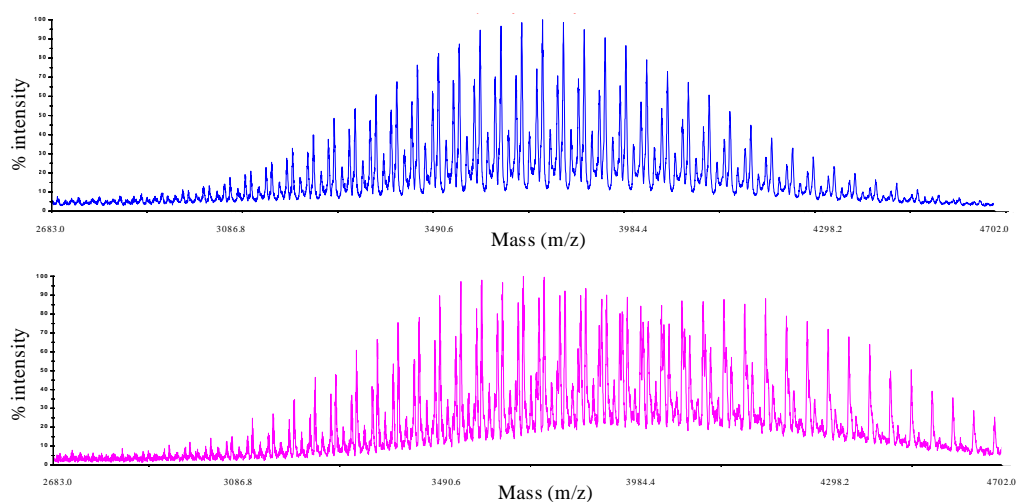
Figure 25 MALDI ToF ToF spectra for samples reacted at pH 7.5.

(A) The spectra shows a characteristic pattern equivalent to the range of masses found in Acryl-PEG-NHS. The highest peak intensity matches the average molecular mass of Acryloyl-PEG-NHS stated of approximately 3711. (B) Acryloyl-PEG-GRGDS conjugate (Section 2.6.4 Method 2). Close inspection reveals two conjugate peaks, one that corresponds to the MW of Acryl-PEG-NHS, and the other to the MW of the conjugate.
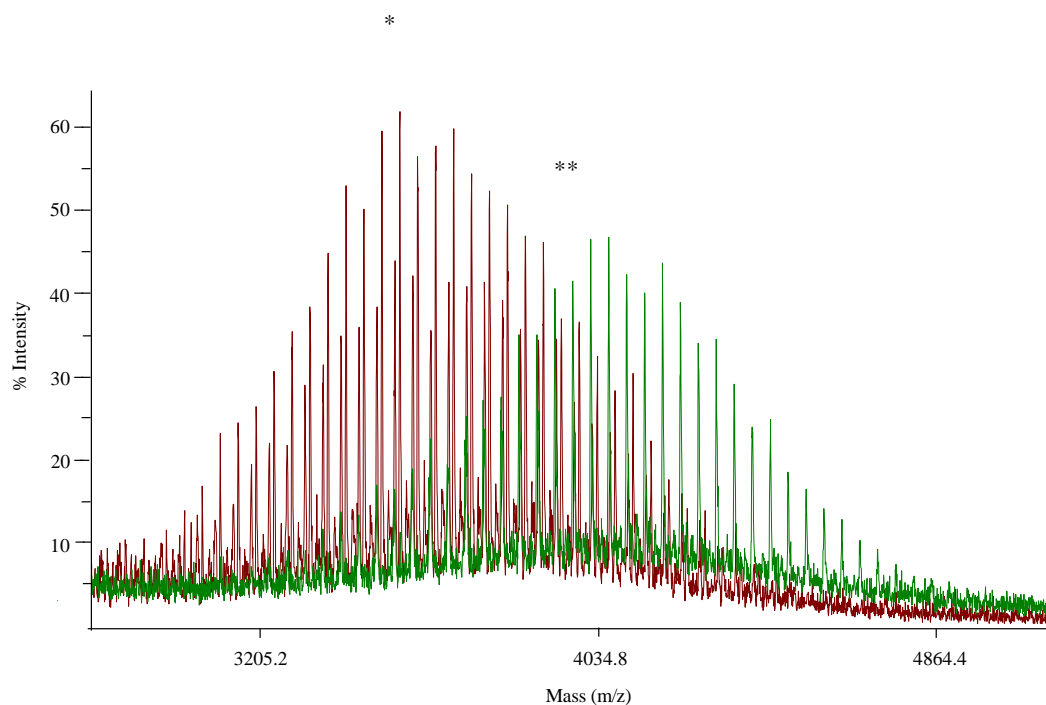
Figure 26 Comparison of Acryloyl-PEG-NHS and Acryloyl-PEG-GRGDS MALDI-ToF spectra.

Acryloyl-PEG-NHS spectrum (average MW 3711gmol-1(*)) prior to conjugation is shown in red. Acryloyl-PEG-GRGDS (average MW 4084gmol-1(**)) spectrum has shifted post-conjugation, shown in green, indicating successful conjugation of GRGDS.

3.10   Confocal Analysis of Peptide Distribution

Confocal microscopy was employed to visualise the presence of biotinylated peptide residues on the surface of PEGDMA hydrogel microspheres. PEGDMA microspheres were bulk modified to contain a biotinylated peptide (throughout the sphere volume) using acryloyl-PEG-RGDS-6-aminohexanoate linker (LC) − biotin, (formed through the conjugation of diamine-RGDS-6-aminohexanoate linker (LC) − biotin with acryloyl-PEG-NHS) (custom synthesised by Peptide Synthetics UK). After extensive washing steps, the resulting microspheres were treated with fluorescently labeled (HyLyte Fluor) Streptavidin and the level of incorporation was assessed using confocal microcopy.

Streptavidin is capable of diffusing non-specifically into PEGDMA hydrogel microspheres, hindering analysis by generating false positive results in control and peptide modified microspheres. Therefore, the staining method was optimised to minimise the exposure of streptavidin to the microspheres (detailed in Section 2.6.5. After streptavidin treatment, the microspheres were washed extensively to remove unbound streptavidin. Biotin was conjugated to the matrix throughout the microsphere. However, due to the method in which microspheres were exposed to streptavidin, positive staining (indicating the presence of biotinylated peptide) was detected at the microsphere surface only. Figure 27B depicts the presence of biotinylated peptide at the microsphere surface following streptavidin treatment and was compared to PEGDMA microspheres without peptide modification. Cross-sectional images (Figure 27) demonstrated that at the same laser intensity, biotinylated microspheres exhibited higher fluorescence when compared to peptide-free control microspheres. This was further demonstrated by fluorescence intensity plots (Figure 27C and D)
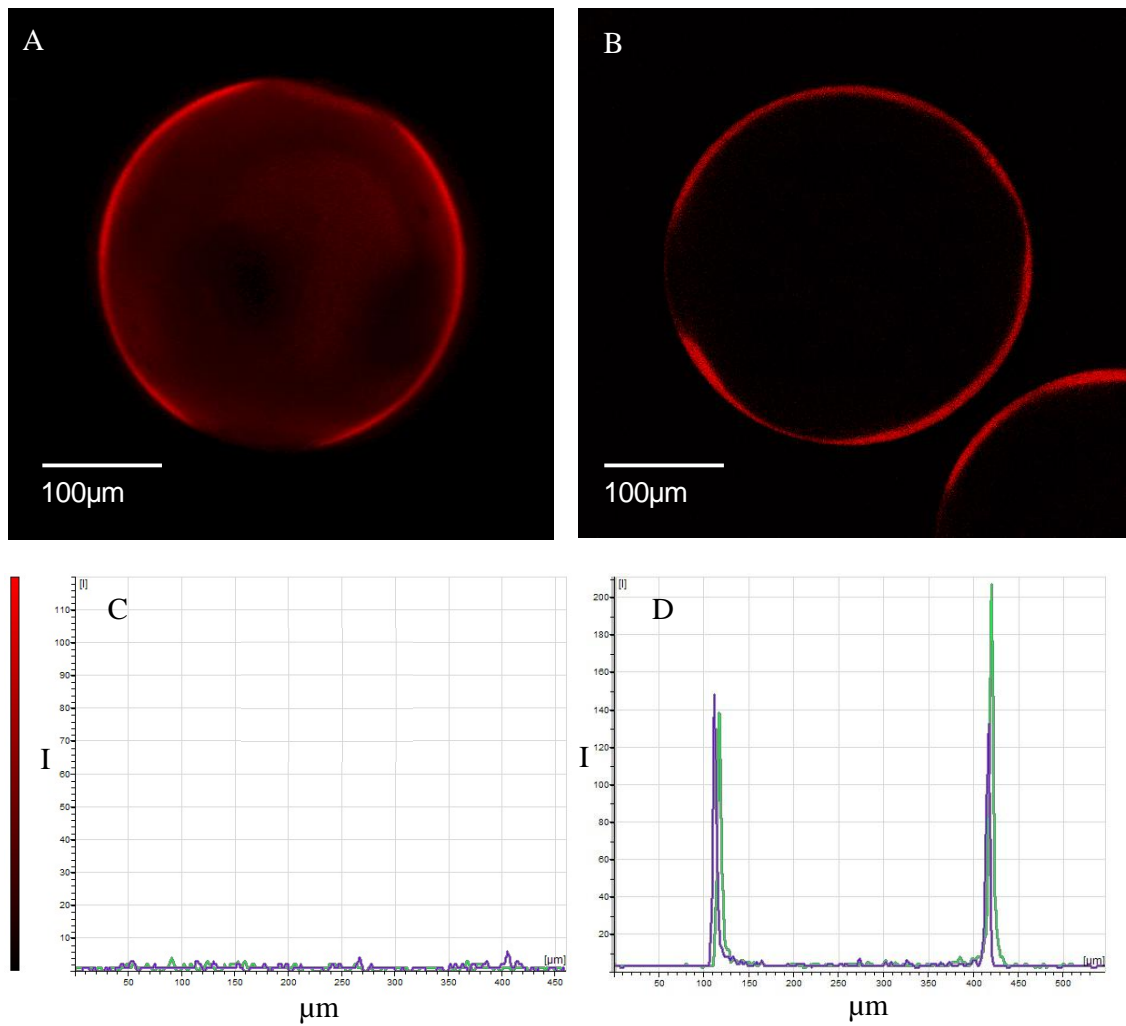
Figure 27 Confocal microscopy images of streptavidin-treated PEGDMA microspheres.

(A) Compiled image, (100 Z-stacks), showing streptavidin fluorescence of PEGDMA microsphere containing Acryloyl-PEG-LC-biotin. (B) Cross-sectional image of a biotinylated-peptide containing microsphere. No fluorescence was visualized in biotin-free microspheres (not shown). Fluorescence intensity plots of PEGDMA hydrogel microspheres. (C) Two biotin-free PEGDMA microspheres demonstrating the nominal fluorescent signal detected in cross-sectional (Z stack) images. (D) Two PEGDMA microspheres containing biotinylated-peptides demonstrating a high fluorescent signal isolated to the microsphere circumferences (the peak separation was equal to the diameter of a single bead).

.

3.11 Incorporation of peptides using thiol-acrylate "click" chemistry

Incorporation of peptides using intermediate PEG linkers requires a pre-conjugation reaction. This necessitates time consuming and costly characterisation as it is essential to determine the concentration of peptide which is subsequently conjugated into the microspheres. In 2008, Salinas *et al.* showed successful incorporation of cysteine-containing peptides into PEGDMA hydrogels *via* click chemistry using photo-polymerisation (Shown in Figure 4) (240). Utilising thiol-acrylate mixed mode photo-polymerisations, peptides can be incorporated using a robust cytocompatible method. Previously, the fibronectin analogue GRGDS, which is capable of binding the αVβ3 integrin, has been incorporated into the microspheres by NHS coupling chemistry. To generate microspheres with similar chemical characteristics as those used in preliminary cell attachment studies, the peptide cyclic RGDfC was employed as it also binds the integrin αVβ3. Two further laminin–based peptides were tested, CSRARKQAASIKVAVSADR, containing the IKVAV motif and CDPGYIGSR containing the YIGSR motif. To determine whether cell attachment was peptide specific, PEGDMA microspheres containing the nonsense peptide cyclic RADfC, and unmodified PEGDMA microspheres were generated and tested in parallel (Chapter 4).

3.11.1 Ninhydrin assay

The Ninhydrin assay was used to assess the efficiency of peptide incorporation using thiol-acrylate photo-polymerisation. Peptide modified microspheres underwent aminolysis, and the free amino acids were detected using the Ninhydrin reagent. All peptides demonstrated a concentration-dependent increase in peptide content per mass of microspheres, as measured by absorbance (Figure 28).
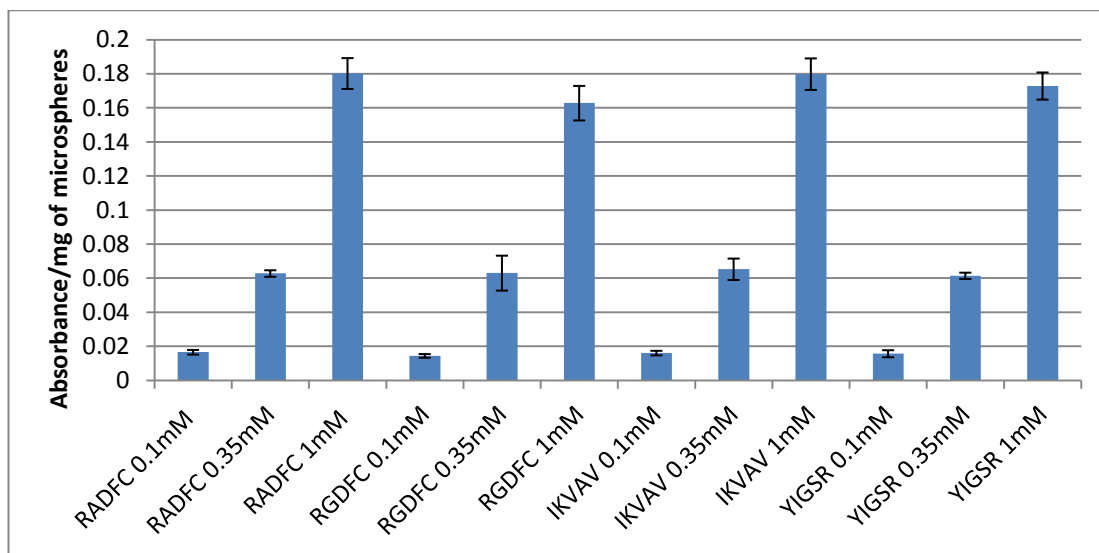
Figure 28 Ninhydrin assay to demonstrate relative peptide incorporation *via* click chemistry.

Relative peptide concentration was measured using a Ninhydrin assay which was normalized to a mass of dried microspheres.

3.12 Morphology and Surface Topography of Microspheres

Environmental scanning electron microscopy (ESEM) experiments were performed to study the morphology of PEGDMA hydrogel microspheres. Unmodified and peptide-modified (cRGDfC) samples were imaged at ~99% humidity to prevent shrinkage / surface deformation. The consistent surface-smoothness and surface-uniformity of PEGMDA hydrogels synthesised using microfluidics was apparent (Figure 29). Samples containing the cRGDfC peptide conjugate showed no meaningful difference in surface properties, when compared with unmodified microspheres on the macro-scale.
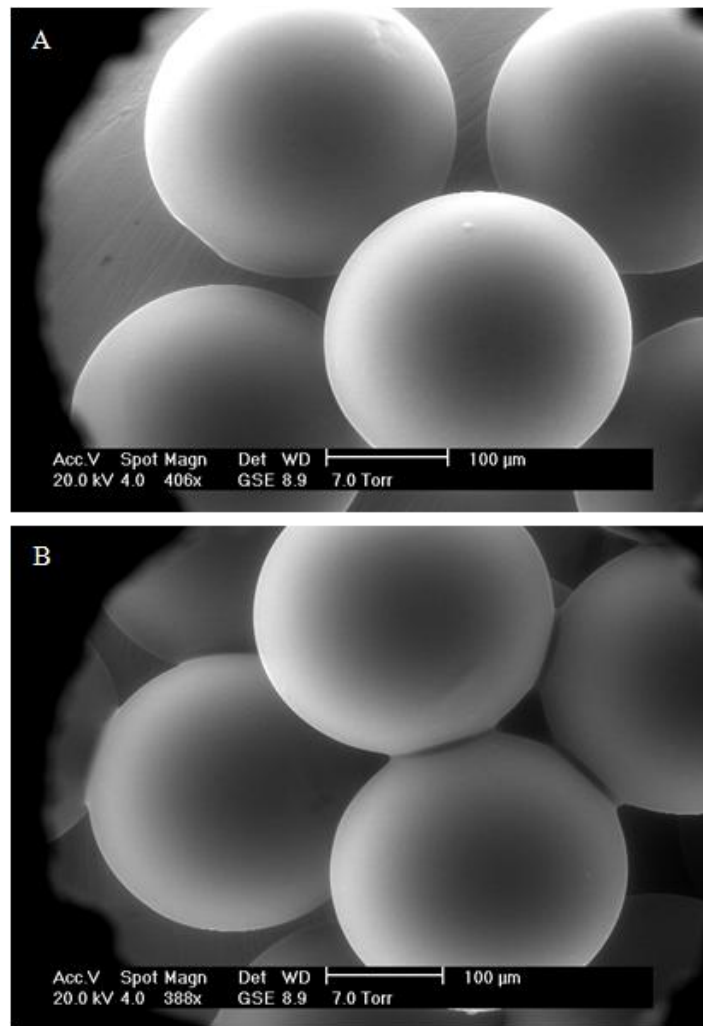
Figure 29 Environmental microscopy image of monodisperse PEGDMA microspheres

(A) Peptide-free microspheres. (B) cRGDfC-containing microspheres. There were no appreciable differences in surface characteristics between peptide-free and peptide-containing microspheres. ESEM conditions: wet mode, 7.0 Torr of H_2O vapor, and gaseous secondary electron (GSE) image.

3.13   Compression analysis of PEG hydrogels

To determine the mechanical properties of the microfluidic produced microspheres compression testing was employed. To simplify calculations and handling, PEGDMA discs were generated which were comprised of the same chemical composition as microspheres (as described in Section 3.5.7). Several hydrogels discs containing a range of PEGDMA concentrations, 14, 16, 18, 20 and 22 w/v%, were prepared and allowed to swell overnight in PBS, before being mechanically tested using uniaxial unconfined compression (Bose Electroforce EF3200). The compressive modulus was calculated as the linear portion of the stress-strain curve (shown in Figure 30). As expected, increases in hydrogel modulus were associated with increased PEGDMA concentration, and the compressive moduli ranged from 69.0 ± 13.3 to 273.9 ± 15.7 kPa for 14 w/v% and 22 w/v% respectively.

Hydrogels containing 10 and 12 w/v% were also generated; however, 10 w/v% hydrogels were mechanically too weak to be moved after polymerisation without breaking. In addition, 12 w/v% hydrogel discs were functional as cell culture substrates, though they were too weak to be compression tested and disintegrated after force was applied and before effective measurements could be taken within our experimental setup. However, the compressive moduli was extrapolated from the linear relationship between PEGDMA concentration and compressibility, and calculated to be 8.14kPa.

Incorporating thiol-containing peptides inhibits complete crosslinking of the PEGDMA hydrogel by taking up methacrylate end groups. To determine the effects of peptide incorporation on the mechanical properties of the modified hydrogels, 1mM cysteine was incorporated, (the highest concentration of peptide added into the microspheres) and the resulting hydrogels were compression tested in parallel with PEGDMA hydrogels. The stress strain curves showed no difference in compressive properties (Figure 30).
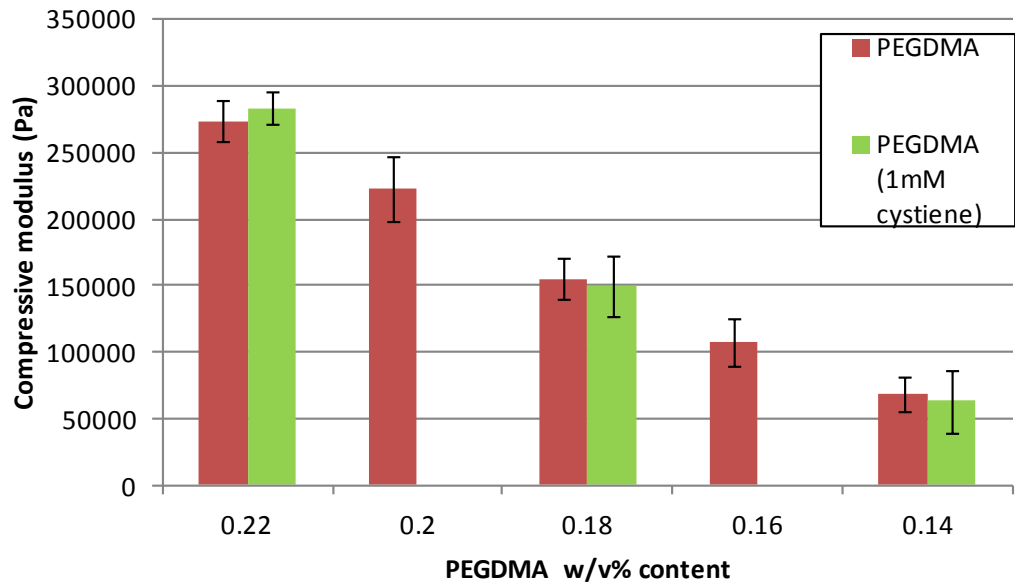
Figure 30 Compression analysis of PEGDMA hydrogels

Change in compressive moduli resulting from a change in PEGDMA concentration. Hydrated hydrogel discs were tested using uniaxial compression (*n*=3). Compressive moduli were taken from the linear portion of a stress strain graph. No changes were observed on hydrogel compressibility when 1mM cysteine was incorporated.
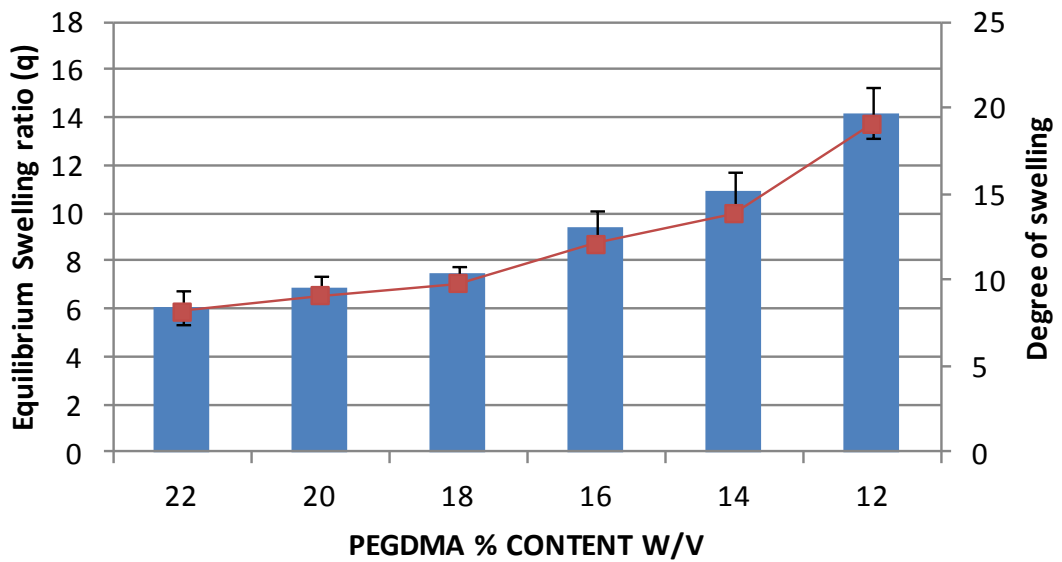
Figure 31 Swelling ratio analysis of PEGDMA hydrogels.

Changes in equilibrium swelling ratio and degree of swelling as a result of changing PEGDMA concentration (*n*=3).

3.14 Swelling ratio analysis

The degree of equilibrium swelling of a polymeric hydrogel is known to be inversely proportional to its mechanical strength (or G'). The amount of water a gel can take-up is represented by the swelling ratio, (Q). To determine the effects of PEGDMA concentration on the degree of equilibrium swelling, hydrogel discs were swollen in excess PBS for 3 days, weighed, dehydrated and then re-weighed. From the results in Figure 31, the degree of swelling is an inverse function of PEGDMA concentration, with equilibrium swelling ratios ranging from 14.2 to 6 for 14 w/v% and 22 w/v% hydrogels respectively.

3.15 Discussion

PEG based hydrogels containing synthetic ECM analogs have been proven to be suitable for cell culture (318-321) due, in large part to their inherent biocompatibility and the fact that they provide a blank slate upon which key functionalities of native ECM can be conferred (300, 322). To date, PEG hydrogels have been widely explored as substrates for cell culture to compare the effects of varying mechanical and chemical stimuli (306, 323, 324). To facilitate cell adhesion, Hern and Hubbell reported the use of monoacrylated RGD peptides with and without a PEG spacer, copolymerized with PEGDA (300). This method has been extensively studied and has been shown to stimulate cell adhesion, spreading and growth on the otherwise non-adhesive PEG hydrogel surface (308, 325-329). Altering the mechanical properties of the polymerised hydrogel has been demonstrated to change the level to which cells can bind and to alter the phenotype of adhered cells (210). This chapter describes a novel application for bio-adhesive PEGDMA hydrogels in the production of neutrally-charged microcarriers.

Recently, a variety of microspheres has been developed for biomedical applications, such as drug delivery (330), cell microcarriers (331), and tissue-engineering scaffolds (332-334). Microfluidics is an established technology for the production of hydrogel microspheres (299, 335). A key feature of microfluidic generated microspheres is high inter/intra-batch uniformity, in addition to strict control over microsphere size. According to

Figure 20 and size distributions and coefficients were variance (CV) of were 261.3µm, 460.6µm, 950.7µm and 2.91%, 2.86% and 2.00% respectively, demonstrating the resulting microspheres were highly monodisperse. The US National Institute of Standards and Technology (NIST) defines "monodispersity" as a narrow size distribution having a CV < 5% (336, 337).

Yeh *et al.* have previously demonstrated the synthesis of non-biocompatible hydrogel microspheres (due to a cytotoxic continuous phase), based on ethylene glycol dimethacrylate, using a polydimethylsiloxane microfluidic device (338). Using UV-initiated cross-linking, solid microspheres were produced *on-chip*. However, the product microspheres were non-uniform and polydisperse (~10% C.V), due to unstable segmented flow conditions. Yeh *et al*. also demonstrated that the properties of hydrogel microspheres could be subtly changed by varying the fluid flow conditions and architecture of the microfluidic device (338). Further, changes in microsphere size and composition can vary the cross-link density of the hydrogel, altering the material's mechanical properties. In the present study, the intended purpose of the PEGDMA microspheres is to support cell cultures, hence, their size distribution should be narrow such that cell confluency is attained at a uniform rate.

Generation of PEGDMA hydrogel microspheres using *on-chip* photo-polymerisation has recently been demonstrated by Choi *et al*. (2009), using hexadecane as a continuous phase to produce PEGDMA droplets at a flow-focussing junction (299). As we intend to use our microspheres as cell adhesive substrates, hexadecane was avoided as it is cytotoxic. Instead, high oleic acid sunflower oil (previously shown to be non-cytotoxic) (335) was used as the continuous phase. In addition, the harsh solvents used in spray-drying and double-emulsion techniques for microsphere generation could be avoided by using the UV-assisted polymerization method described here. This is advantageous as the deleterious effects of solvents upon adhered cells could be precluded. Complete polymerization is required to prevent coagulation of microspheres, an undesirable property for microcarriers. The MicroPlant system allowed variable UV exposure *in situ* by altering the PEGDMA droplet flow rate and therefore retention time in the microchannel.

Microspheres produced using the microfluidic method outlined in this chapter have consistent topographies with uniformity across their surface. Surface homogeneity is an important factor in designing microcarriers to ensure adherent cells experience identical surface binding conditions. This is particularly important as changes in surface texture have been shown to influence the adhesiveness of materials and affect cell morphology (210). There were no observed changes in surface properties (by ESEM) between control and peptide containing microspheres, suggesting peptide incorporation has no effect on surface topography. Inter/intra-batch surface uniformity allows systematic investigation into the effects of incorporating ECM analogues and varying

compressibility (i.e. chemical and mechanical cues) on adherent cell morphology and behaviour.

Microcarriers also provide a curved surface for cell attachment and growth, which is a simple yet often overlooked feature. Research has shown microspheres containing a diameter of less than 100 μm have limited cell adhesion to their surface. In 2011, Kong *et al.* investigated the effects of curvature on BM-MSCs cultured on RGD modified alginate microspheres. A decrease in cell proliferation and osteogenic differentiation was observed as microsphere diameters decreased from 3cm to 0.5cm independent of RGD concentration. This was attributed to increasing shear stress experienced during bioreactor culture. Kilian *et al.* (2010) have examined the effects of convex substrates on MSC differentiation in static culture, and found cytoskeletal changes; in addition to altered lineage commitment in response to differentiation induction media. Varying the size of the microcarriers would provide an opportunity to assess cellular responses to micro-topography. As proof of principle, a range of microspheres was generated containing average diameters of 278μm. 483μm and 986μm.

Several groups have demonstrated the use of Acryloyl-PEG-NHS to attach a variety of synthetic ECM analogs, such as laminin, (325), elastin, (325) collagen derived sequences (339) and growth factors (340). MALDI ToF ToF was employed to analyse the extent of conjugation of the fibronectin peptide fragment, GRGDS to Acryloyl-PEG-NHS. The MALDI ToF ToF technique generated semi-quantitative data for this peptide-polymer construct. After determining successful conjugation of GRGDS to the PEG-NHS monomer, the conjugate was incorporated into PEGDMA hydrogels using microfluidic assisted photo-polymerisation. This provided a cell-adhesive element to the normally bio-inert material. This technique can be applied to other ECM derived peptides (with a suitable nucleophilic terminus) and incorporated into PEGDMA microspheres.

It is predicted that cells bind to the surface of the hydrogel microcarrier by interacting with incorporated peptides, hence, the distribution of these peptides across the surface is of critical importance. In previous work, Hern and Hubbell (300) estimate that peptides located within 10nm of the hydrogel surface are 'available', i.e. 'able to bind to cell surface integrins' (341). Consequently, a proof-of-concept experiment was performed to detect the accessibility and location of peptides on the surface of our

PEGMDA microcarriers. The biotinylated peptide (RGDS-LC-Biotin) was used to provide a binding motif for a fluorescent streptavidin reporter. A spacer group (PEG Mw 3500gmol^{-1}) (previously optimized by Shin *et al*.) was incorporated in the hydrogel in accordance with previous literature. After treatment with Streptavidin-HiLyte Fluor 647 solution, CLSM allowed the model peptide to be visualized and fluorescence was detected at the outermost circumference of the microcarrier. Confocal analysis demonstrated photo-polymerising monoacrylated GRGDS into PEGDMA hydrogel microcarriers allowed the RGD ligand to be presented at the hydrogel surface.

Incorporation of peptides using an intermediate monoacrylated PEG-NHS monomer requires a pre-conjugation reaction. Characterisation of peptide conjugation was both time consuming and costly. After determining the optimum reaction conditions and characterisation method, the results were very difficult to reproduce. After consulting with peptide conjugation specialists, who also could not produce the results described herein using the same starting materials, it was decided that we would employ a simpler "click" chemistry method which bypassed the use of an acrylate linkage. Researchers have demonstrated cysteine-containing peptides can be incorporated into PEGDMA hydrogels *via* click chemistry using thiol-acrylate photo-polymerisation (240). This method has been shown to be robust and reproducible (245). Anseth and co-workers have demonstrated, using acrylate-thiol chemistry, high quantities (>95%) of thiol-containing RGD peptide incorporation into PEG hydrogels (342). In this study peptide incorporation in microspheres was successfully demonstrated; however an exact concentration of peptide per microsphere has not been determined, as the exact quantity of starting microspheres prior to analysis is not known. Due to the large quantity of expensive peptide required to generate the microspheres for this experiment, it could not be repeated. However, an increase in peptide content proportional to starting peptide concentration was shown, and an increase in cell attachment to hydrogels in a (starting) peptide concentration dependent manner was also evident. Although this gives confidence of successful peptide incorporation, future work would characterize the incorporation of peptide into microspheres.

Photo-polymerisable PEGDMA hydrogels have a number of characteristics that are desirable for tissue engineering scaffolds. The mechanical properties of these hydrogels, namely compressive modulus and ultimate tensile strength, can be tailored over a fairly broad range to resemble a variety of soft tissues. The mechanical

properties of the hydrogels can be controlled by varying the molecular weight or concentration of the polymer. Compressive modulus increases with increasing polymer concentration or decreasing polymer molecular weight (343). The mesh size and swelling ratio can be similarly controlled (306). Cells are routinely cultured on plastic or glass, (1GPa and 70GPa respectively), however the compressibility of soft tissues is several orders of magnitude 'softer' (approximately 100kPa). Engler *et al.* demonstrated the effects of culturing MSCs on hydrogels with a range of compressive moduli between 0.1-40kPa. MSCs committed to a specific lineage, i.e. neurons, when cultured on substrates with elastic properties similar to their counterpart tissues *in vivo*. To probe the mechanical properties that can influence cell fate, a variety of PEGDMA hydrogel microspheres with a wide range of mechanical properties, including compressive modulus and mesh size, were generated and characterised. This was accomplished by changing the concentration of the starting PEGDMA macromer, therefore altering the crosslink density. The hydrogels generated contained a compressive modulus range from 8 kPa to 273 kPa, for 12 to 22 w/v% PEGDMA respectively.

Incorporation of peptide ligands though acrylate linkage affects the overall hydrogel structure. To determine the effects of substrate compressibility on cell adhesion and behaviour, it is important that the mechanical and biochemical properties i.e. polymer and peptide ligand concentrations can be varied independently. Previous studies have shown incorporation of cysteine-containing peptides into PEGDMA hydrogels at a ratio 1:4 thiols:acrylate showed no significant difference in mechanical properties, including elastic modulus. To confirm this result PEGDMA hydrogels containing 1mM cysteine were analysed. No changes in mechanical properties were observed.

3.16 Conclusion

The microfluidic technique described in this chapter has been demonstrated as a simple but efficient tool to generate highly monodisperse PEGDMA hydrogel microspheres. Using continuous droplet formation and *in situ* photo-polymerisation, we have synthesized microcarriers with average diameters of 278µm, 483µm and 986µm and extremely narrow size distribution. The successful incorporation of the ECM peptide analogues using two separate techniques introduced a cell adhesive element to otherwise bioinert PEGDMA microcarriers. This technique could also be applied to incorporate a wide range of functional peptides. In addition, microspheres were

generated with a broad range of mechanical properties including compressive moduli. The microfluidic methodology described here has produced a flexible tool to generate tuneable, synthetic microcarriers. The microspheres developed in this chapter will be assessed for a variety of cell culture applications.

4.0 Investigation into ADSC attachment to microcarriers with tunable chemical, mechanical and topographical properties

4.1 Introduction

Recent advances in the field of biomaterials have shown that presenting cues derived from the ECM can improve cell growth, intracellular signalling and differentiation (217). Previously, a wealth of research has eluded to possible biomaterial compositions that could potentially control MSC fate (189, 271, 306). Various parameters have been considered, including chemical compositions, biomechanical properties and surface topographies. However, published reports on the precise cellular responses to various biomaterials, (such as MSC response to bio-adhesive peptides) are often conflicting (308, 344, 345). This is largely due to the subtle differences in scaffold properties used to probe the effects of ECM derived cues on cell growth and behaviour. PEGDMA hydrogels are uncharged and lack any cues that allow the directed binding and attachment of cells, providing a "blank" bioinert microcarrier. They are tunable, and can be used to systematically investigate the physical and chemical factors on cellular processes (241).

PEGDMA hydrogels have been widely used to assess the effects of compressibility and bio-adhesive peptide on MSC fate (241, 261, 308). However, typically the studies were performed on cells encapsulated within photopolymerised PEG hydrogels, and focussed on assessing one parameter individually. For example, Jongpaiboonkit *et al.* (2009) developed a hydrogel array system for analysing MSC adhesion, viability and migration to IKVAV and RGD based peptides encapsulated within degradable and non-degradable PEG hydrogels (346). This method generates a 3D culture system, however cell-cell contacts are lost and topography cannot be assessed (345). Cells cultured on microcarriers in monolayer culture experience a different microenvironment, and therefore we hypothesised MSC responses to changes in these parameters may be different to those previously reported in the literature.

The overall aim of this project was to develop a synthetic microcarrier capable of providing a solid growth support for MSC expansion within a bioreactor. In Chapter 3 we developed a microcarrier system containing tunable ECM-derived peptide sequences, mechanical properties and topographies. Few studies have investigated the effects of ECM derived peptides on ADSC attachment. However, it has been reported that ADSCs adhere and spread more extensively on IKVAV modified polycaprolactone surfaces, as compared to RGD or YIGSR modified surfaces (347). In this chapter we optimised ADSC attachment to novel microcarriers by examining various peptide ligands at a range of concentrations. This system permitted us to investigate the effects

of peptide ligand and compressive modulus on ADSC growth and cell fate, particularly examining adipogenesis, osteogenesis and chondrogenesis.

4.2 Microcarrier attachment optimisation

4.2.1 Comparison of cell seeding densities on the rate of initial cell attachment

To determine the optimum cell inoculum per microcarrier, a range of cell seeding densities were tested. Microcarrier density was kept constant at 360 microcarriers per well (24 well plate) giving an evenly distributed monolayer of microcarriers (460µm diameter). It was postulated that higher cell inoculum per microcarrier would increase the probability of a binding event and increase the initial growth rate kinetics. Therefore three cell seeding densities were investigated, 100,000, 50,000 and 25,000 cells per well.

The effects of cell seeding density on cell attachment rates are shown in Figure 32. The results show that by increasing the cell inoculum in relation to microcarrier concentration increased the amount of cell binding. However, the results revealed an upper limit on this effect. Large cell aggregates formed with increasing cell concentrations, with very few cells bound individually to the microcarrier.

Microcarriers seeded with 25,000 cells showed a relatively high amount of cell adhesion, with few cells unattached in the medium. By increasing the cell concentration the level of cell attachment increased proportionally. This demonstrates initial cell attachment is dependent on the cell to microcarrier ratio.

| 25,000 cells | 50,000 cells | 100,000 cells |
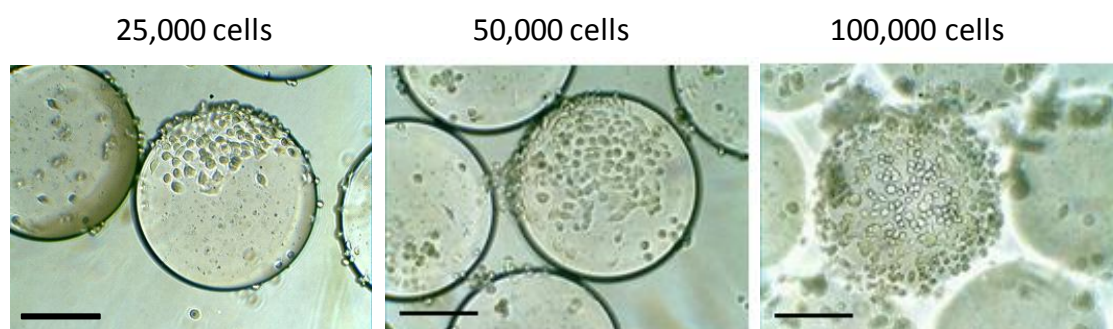
Figure 32 Effect of the initial cell seeding density on A549 adhesion to PEGDMA microcarriers.

A549 cells were seeded into wells containing 360 of PEGDMA microcarriers suspended in cell culture medium and agitated at different rates. Cell attachment and growth was imaged 24 hours post seeding. Scale bars 240µm.

4.2.2   The effect of total culture volume on the initial rate of cell adhesion to microcarriers

As the microcarriers are neutrally charged initial binding events are reliant on the probability that a collision will occur. To increase the probability of cell-microcarrier contact the volume was incrementally reduced to increase the proximity between cells and microcarriers. A qualitative increase in cell attachment was observed in the wells (24 well plate) containing 500µL of total medium when compared to cells cultures in 3mL of medium. This was observed to be consistent across various parameters including different intermittent agitation levels and microcarrier compositions (Figure 33). This observation was not made for samples which were continuously agitated, where no cell adhesion was observed at either 0.5mL and 3mL starting volumes.

4.2.3   The effect of agitation rates on cell adhesion to microcarriers

To improve the probability of initial cell attachment, avoid cell clumping and increase nutrient transfer throughout the medium the culture was agitated at various intervals. To assess the effect of agitation on the initial rate of cell attachment the cultures were kept static, or were subjected to intermittent or continuous agitation.

From Figure 33 it was observed that static conditions permitted cell binding to microcarriers. However, the amount of cell attachment appeared less than those microcarriers which had undergone intermittent agitation (stirred for 2 minutes at 40rpm every 30 or 60 minutes). No qualitative differences were observed between those agitated every 30 or 60 minutes. This affect appears to be mirrored in a repeat experiment, shown in Figure 33. Continuous agitation was shown to prevent any attachment of cells to microcarriers.
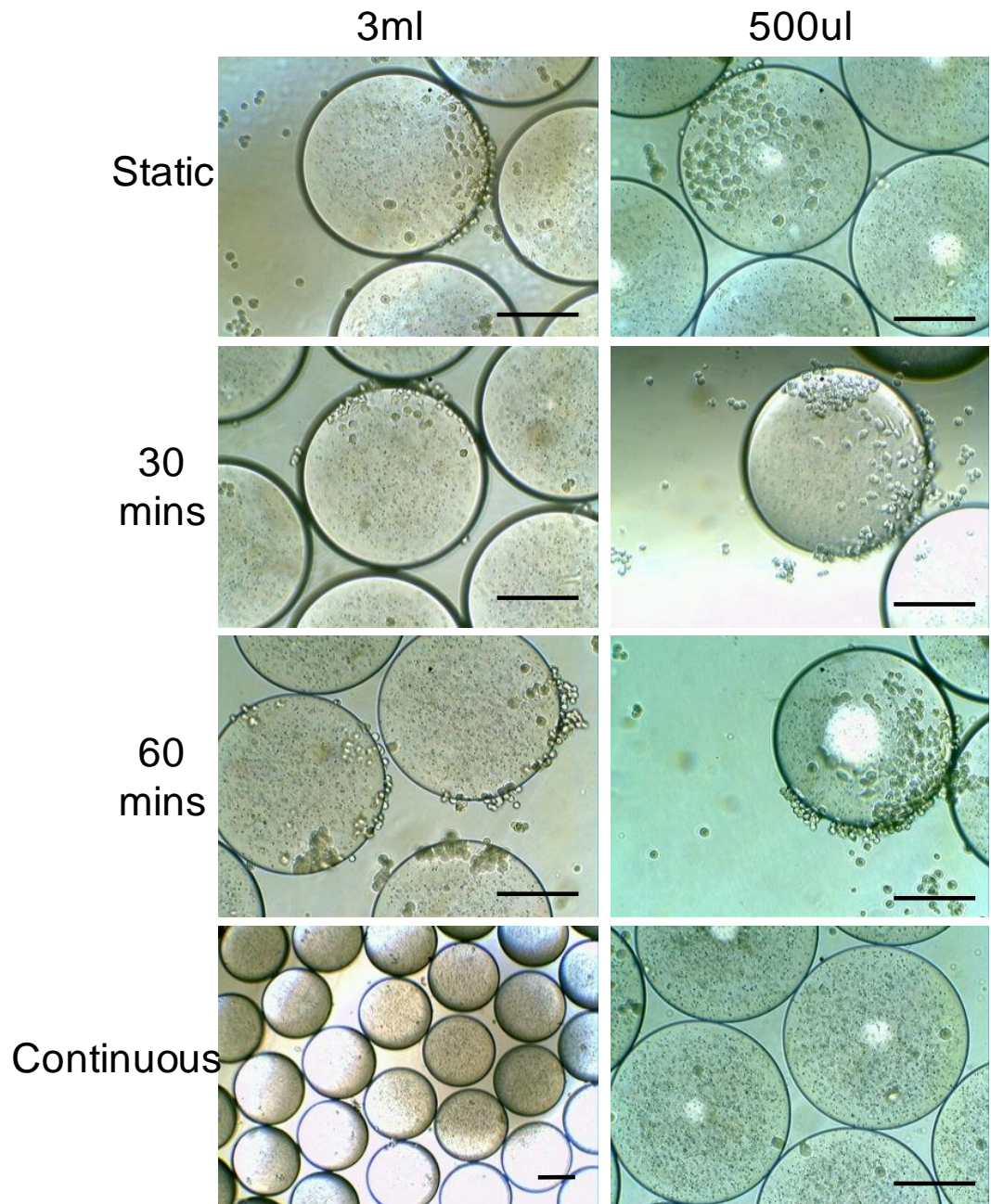
Figure 33 Effect of the culture medium volume and agitation rates on cell adhesion to PEGDMA microcarriers.

A549 cells were seeding into wells containing 460 of PEGDMA microcarriers suspended in cell culture medium and agitated at different rates. Cell attachment and growth was imaged 24 hours post seeding. Scale bars 240μm.

4.3   Comparison of photoinitiators

For effective cell-microcarrier attachment, numerous types of photoinitiator have previously been employed to polymerise PEGDMA hydrogels. However, the cytocompatibility of the resulting hydrogels can vary between several cell lines (348). To determine the biocompatibility of the microcarriers generated in Chapter 3, several cell types were seeded onto the microcarriers and attachment was monitored. Initially VAZO 56 WSP (VAZO) was utilised as a photoinitiator to generate the microcarriers, as it is readily soluble in polymer solutions generated by H_2O and PEGDMA, and should not be incorporated into the final gel structure of the microsphere. However, attachment to the microcarriers was variable, even where the cell type and conditions remained constant. This was initially thought to be due to initial attachment conditions, i.e. culture agitation, total media volume, cell and microcarrier seeding densities. Cells did bind to the microcarriers containing cell adhesive peptides, but were easily prone to dissociation upon mechanical agitation (i.e. pipetting), indicating the attachment was weak and unstable. As described in Chapter 3, the Ninhydrin assay was employed to determine the concentration of incorporated peptides by measuring free amino groups. Positive readings were generated for PEGDMA control microspheres which had not been modified with a peptide (Figure 34). As amino groups are not present in any of the components required to produce PEGDMA microspheres except the VAZO photoinitiator, it was postulated that despite extensive washing steps, VAZO remained in the hydrogel microspheres, producing a cytotoxic effect, thus rendering the microcarriers non-biocompatible. ADSCs adhered to microcarriers with inter and intra batch variability. For example, different batches of microcarriers containing the same chemistry were prepared in parallel. However, ADSCs formed confluent monolayers on some microcarriers and not others. Hence the photoinitiator Irgacure 2959 was employed, which has previously been demonstrated to be cytocompatible in acrylate based hydrogels with a variety of mammalian cell types including hMSCs (348). Irgacure 2959 generated microcarriers gave reproducible cell attachment and growth, in addition the cell-laden microcarriers were stable and remained intact after reasonable mechanical agitation, allowing immunostaining to visualise cells.
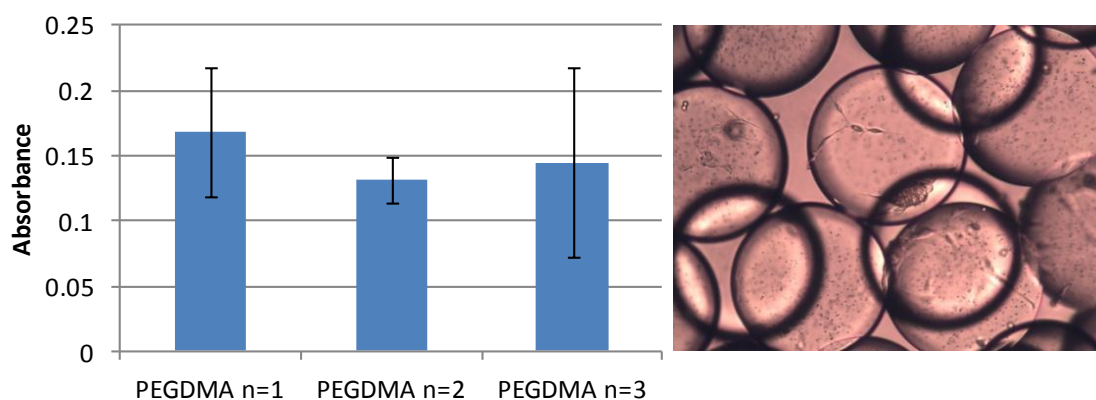
Figure 34 Ninhydrin assay showing varying presence of VAZO photoinitator in microspheres.

A Ninhydrin assay demonstrated the presence of primary amino acids within PEGDMA microspheres, with inter and intra batch variability. ADSC adhesion to RGD-modified microcarriers was variable, and often cells would attach to some microcarriers and not others within the same sample.

4.4   Assessment of bio-adhesive peptides for ADSC attachment

The novel microcarriers are intended for ADSC expansion. To optimise ADSC adhesion, three different bio-adhesive peptides were incorporated into the microcarriers and cell attachment was assessed. This included fibronectin derived cyclic RGDfC (cRGDfC), and two laminin-based peptides; (i) CSRARKQAASIKVAVSADR, which contains the IKVAV motif and (ii) CDPGYIGSR, containing the active cell-binding site YIGSR. To determine if cell attachment was peptide specific, PEGDMA microspheres containing the nonsense peptide cyclic RADfC, and unmodified PEGDMA microspheres were generated and tested in parallel.

4.4.1   Comparison of different peptides incorporated into flat hydrogels on ADSC attachment

To determine the suitability of the chosen peptides for ADSC attachment, several different 'flat' gels were generated to examine cell attachment to a planar surface. A peptide concentration of 0.35mM was employed in concordance with those typically reported in hydrogels culture (349). Hydrogels prepared according to Chapter 3 Section 3.11.1) were placed in non-adhesive wells, seeded with ADSCs and left to attach over 7 days and assessed using DAPI staining (Figure 35).

Unmodified PEGDMA hydrogels have intrinsic bio-inert properties and are well known to be non-cell adhesive. However, cell adhesion was observed on PEGDMA

gels; though this was limited to a relatively small area of the gel. Flat gels containing the nonsense peptide cRADfC also showed cell adhesion to a small fraction of the gel, however the cell morphology appeared to have either long thin extensions or to be very condensed, i.e. not demonstrating the typical ADSC fibroblastic morphology. A high level of cell attachment was observed on cRGDfC gels; however the cells appeared to grow in clusters, with a dense centre flanked by spindle like cells growing out from the centre, resembling cell colonies. Cell colonies form when seeding low density cultures of highly-proliferative, fibroblast-like spindle-shaped cells and are termed colony forming unit-fibroblasts (CFU-Fs). These are typically used to isolate MSCs from heterogeneous populations of cells. IKVAV modified hydrogels showed on average a very high level of attachment however attachment was inconsistent. In line with previous research YIGSR hydrogels demonstrated little to no cell attachment, and any attached cells appeared very rounded with minimal spreading (347).
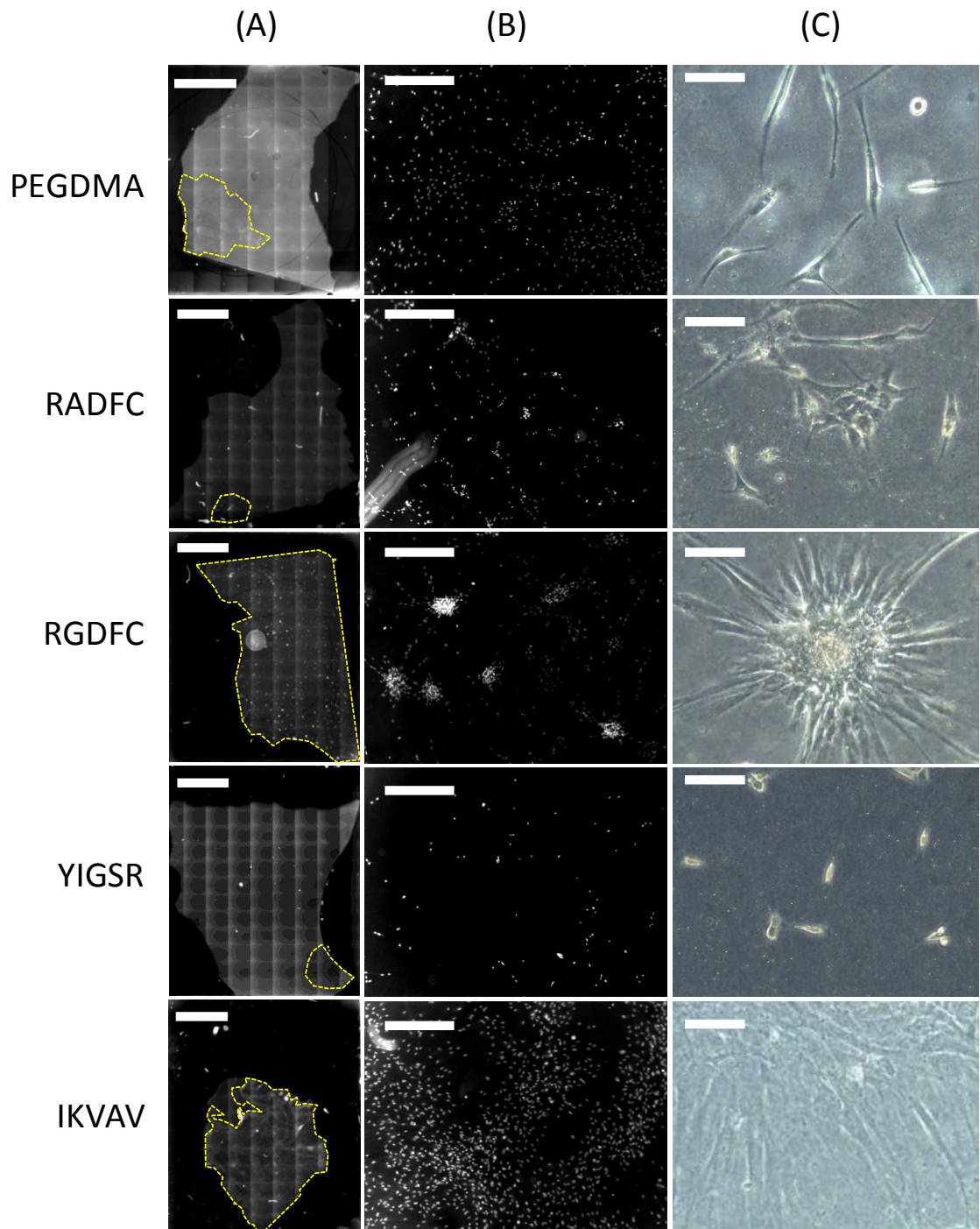
Figure 35Attachment of ADSCs onto flat gels containing different adhesion peptides

(A) Widefield fluorescence imaging of whole gel structure. (Scalebar=5mm), areas containing ADSC adhesion are highlighted in yellow. (B) Single widefield fluorescence image of DAPI stained nuclei on the flat gels (Scalebar=0.5mm) (C) Brightfield image of representative cell formations on flat gels. (Scalebar=100μm)
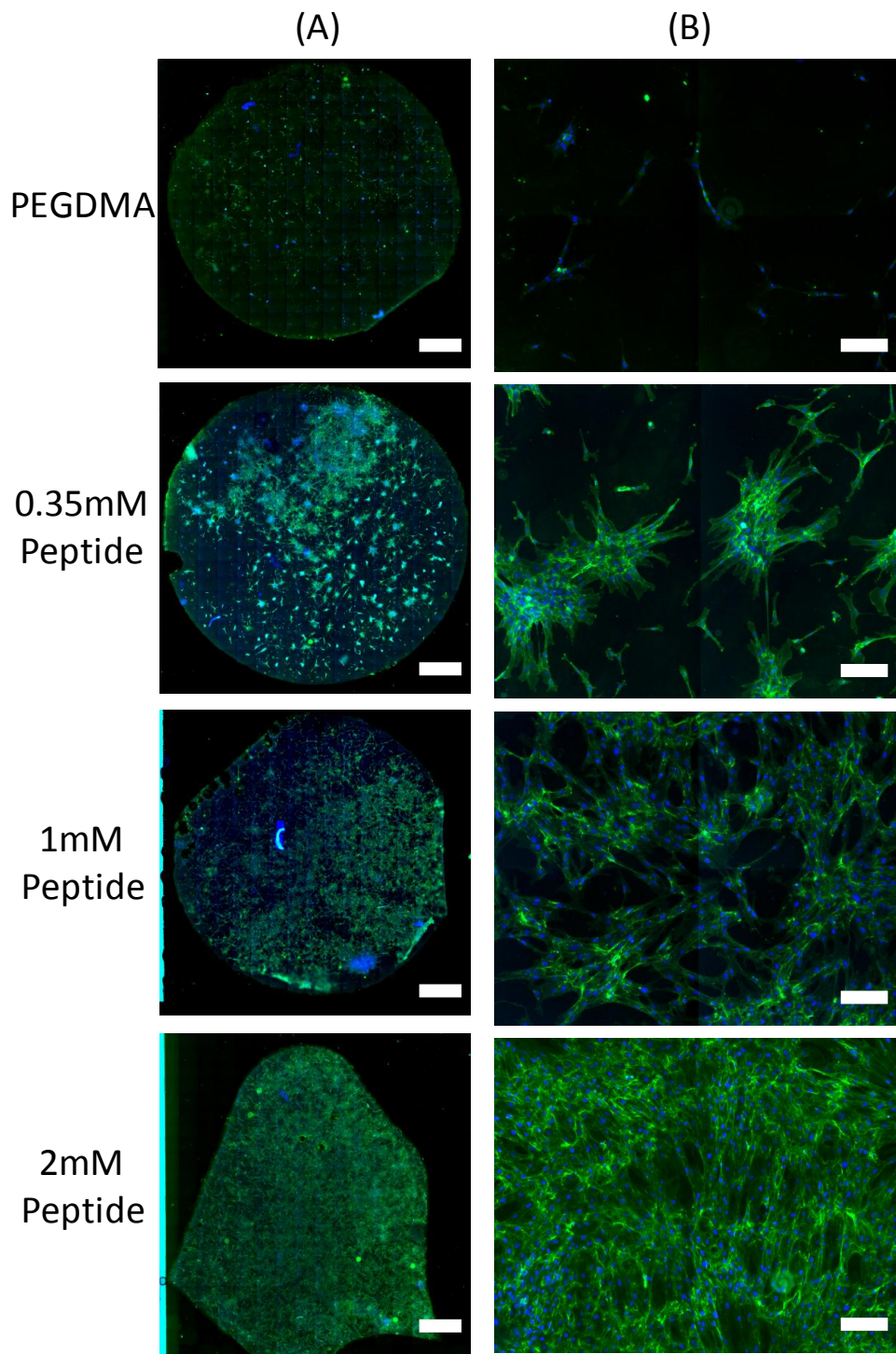
Figure 36 Visualisation of ADSC attachment onto fully hydrated flat gels at different RGD peptide concentrations.

ADSC attachment was assessed by visualising the whole gel system. Cells are stained with Concanavalin A (cells surface) and DAPI (nucleus). Images were taken at 10x and stitched into a montage by ImageJ. Scalebar=2mm

B) Four fields of view from the montage demonstrating organisation of cell growth. At 0.35mM cell attachment and growth occurs in small colonies, which progressively expands with increasing peptide concentration(1mM) and eventually covers the whole gel at 2mM. Scalebar=200μm.

As 0.35mM cRGDfC supported the formation of ADSC colonies, indicative of low cell attachment, the effect of increasing peptide concentration was further explored. The following concentrations of peptide were tested, 0.35mM, 1mM, and 2mM. Flat gel production was modified to produce uniform discs, to keep the surface area available for cell attachment consistent between samples. Peptide modified hydrogel discs were seeded with ADSCs and after 48 hours fixed and stained with DAPI and the cell surface glycoprotein marker concanavalin A to demonstrate cell morphology (Figure 36). Unmodified PEGDMA hydrogels were included as a control and demonstrated little cell attachment. In addition, little spreading was observed using the cell membrane marker. ADSCs cultured on 0.35mM cRGDfC hydrogel discs formed dense colonies as demonstrated previously. Cell attachment to 1mM cRGDfC hydrogels showed no distinct colony formation, but a more evenly distributed monolayer of cells which resembled the typical morphology of ADSCs observed on tissue culture plastic. Hydrogels with 2mM peptide concentration showed confluent monolayers of cells covering the entire surface of the hydrogels.

Qualitatively, it was shown that attachment was highest at 2mM concentration, however due to cost implications it was decided that the 1mM concentration should be used to modify PEG in future experiments. This decision was based on our desire to test a wide range of properties, cell types and differentiation states. Increasing the peptide concentration would be a limiting factor in the microcarrier compositions that could be assessed.

4.4.2 cRGDfC supports ADSC attachment to microcarriers

Substrate curvature, adhesive peptide and peptide concentration may impact upon cell attachment, cell motility and division. Therefore, it was hypothesised ADSCs may attach differently to microcarriers compared to flat gels, despite having the same chemical composition. Therefore to determine the optimum peptide sequence and concentration to facilitate ADSC attachment to microcarriers both laminin derived peptides, cRGDfC and the nonsense peptide cRADfC were incorporated into microcarriers at 3 different peptide concentrations, 0.1mM, 0.35mM and 1mM. Representative phase contrast and SEM images taken 7 days after ADSC seeding are shown in Figure 37 and

Figure 38.
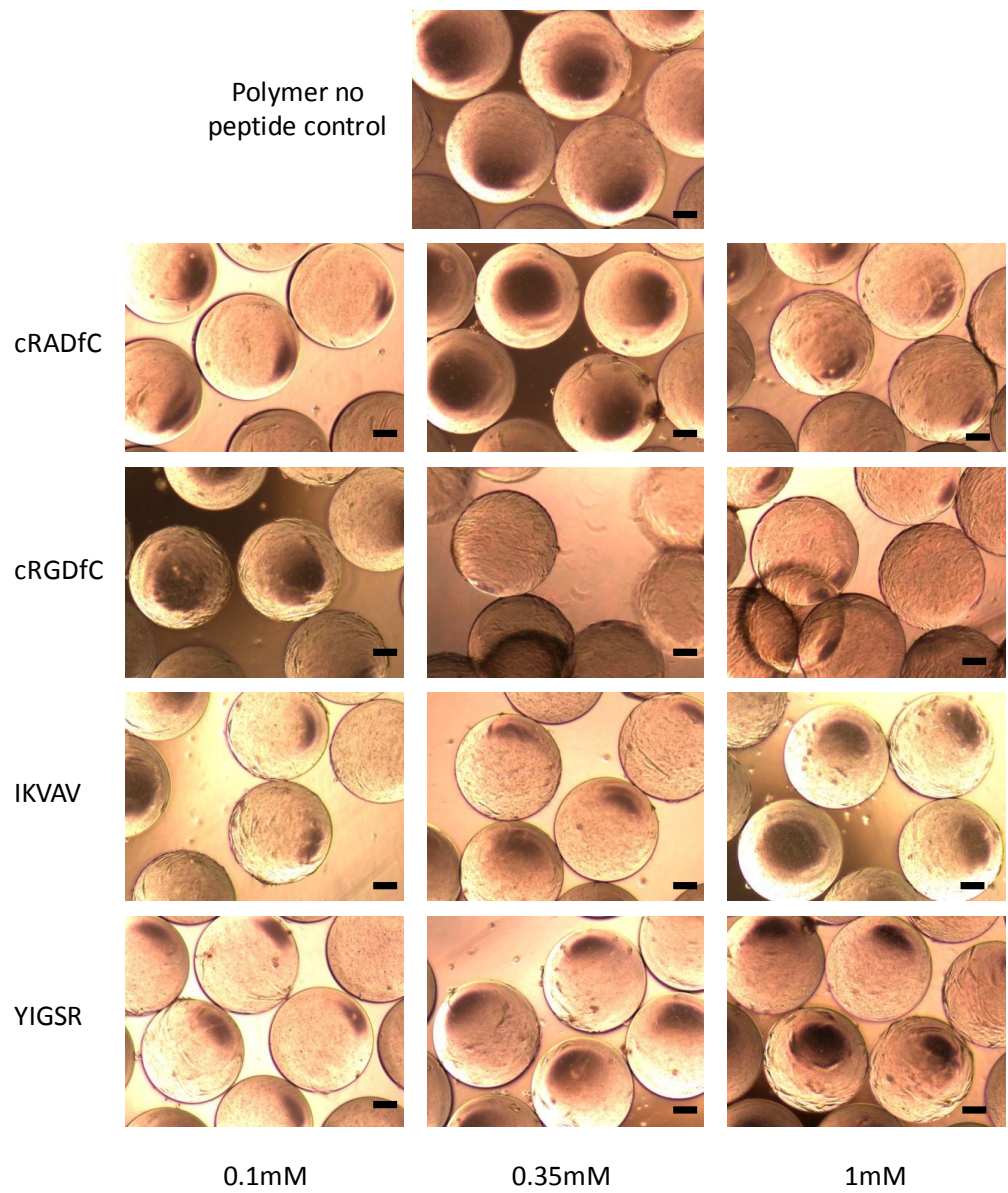
Figure 37 Brightfield images of ADSC attachment to peptide-modified microcarriers

ADSC attachment to microcarriers containing a range of peptides at either 0.1mM 0.35Mm or 1mM after 7 days in static culture. (Scale bar 100µm)
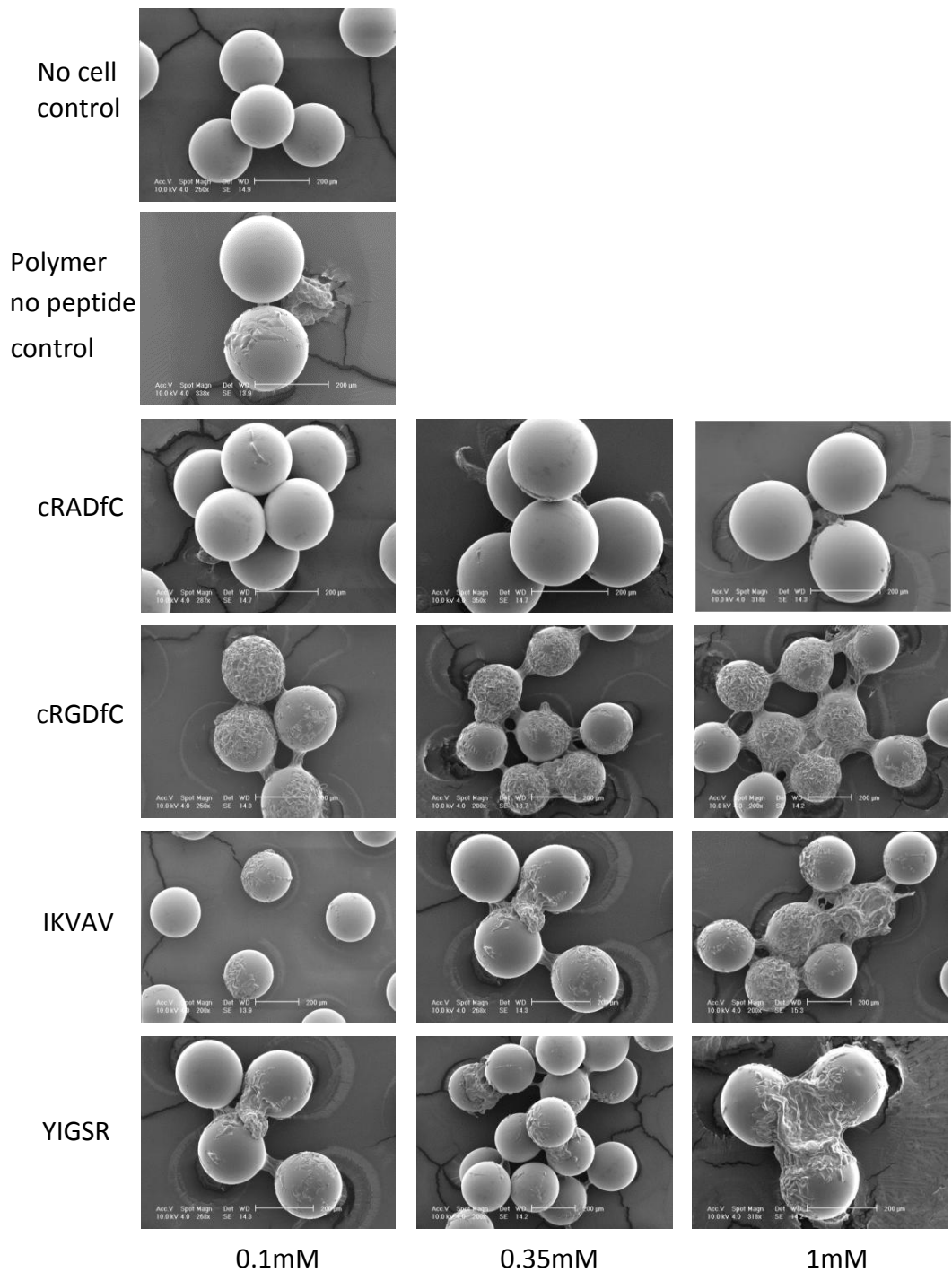
Figure 38 Scanning electron microscopy images of ADSC attachment to peptide-modified microcarriers

ADSC attachment to microcarriers containing a range of peptides at either 0.1mM 0.35Mm or 1mM after 7 days in static culture.

Phase contrast images show that initial cell attachment to PEGDMA and cRADfC containing microcarriers (at any concentration) was minimal. Cell adhesion to cRGDfC showed cell attachment at 0.1mM, however this increased with higher peptide concentrations. At 0.35mM, cells appeared to attach to microcarriers with a fibroblastic flat morphology. The colonies that had been observed on the 0.35mM cRGDfC modified flat gels were not evident on the microcarriers. IKVAV showed peptide concentration dependant attachment, however at 1mM the attachment appeared less than cRGDfC at the same concentration. As observed with 'flat gels', YIGSR showed limited attachment and the adhered cells appeared raised on the microcarriers' surface, with few cell-cell contacts. However, attachment was higher than would have been predicted from the flat gel experiments (seen in Figure 35).

As ADSCs are flat and fibroblastic it is difficult to assess the level of attachment using phase contrast imaging, hence the ADSC-laden microcarriers were assessed using ESEM. However, the images obtained using these techniques were limited as they lacked resolution and surface detail, hence SEM was employed to analyse the images (

Figure 38). This technique requires the specimen to be visualised under a vacuum, which causes hydrogel microcarriers to shrink. This resulted in the overlying attached cells becoming wrinkled. In addition the cell surface appears smooth, which is an artefact of the technique, in future critical point drying would enable more surface detail to be preserved. However it is still possible to visualise the similar pattern of attachment as observed using phase contrast imaging. The cells attached to the microcarriers in a peptide concentration manner, and at 1mM a large quantity of ADSCs cells were attached to the cRGDfC microcarriers.

4.5   ADSC proliferation on peptide modified microcarriers

As peptide concentration can effect cell proliferation and migration, cell attachment and growth over 7 days was analysed using a cell viability assay in static culture (Figure 35). Cell viability data were normalised to the number of microcarriers per well.

There was a minimal amount of attachment initially to both microcarriers modified with cRADfC (at all three concentrations) and PEGDMA control microcarriers. Reiterating the results seen by microscopy, cRGDfC modified microcarriers appeared to have the highest amount of ADSC attachment. Viability data

for cRGDfC containing microcarriers displayed a general trend peaking at Day 5 and gradually decreasing by day 7 suggesting near-confluence. From the SEM and phase contrast images it appeared on Day 7 that the microcarriers had indeed become confluent, possibly restricting further cell growth. IKVAV modified microcarriers showed an increase in cell adhesion, directly resulting from an increase in peptide concentration. At 0.1mM (IKVAV concentration) ADSC attachment on Day 1 was slightly higher than attachment to 0.1mM cRADfC microcarriers and PEGDMA controls. However, attachment was lower than to cRGDfC 0.1mM (on Day 1). At an IKVAV concentration of 0.35mM, ADSC viability declined after initial attachment on day 2, but then steadily increased over 7 days. At 1mM, cell attachment and growth was inconsistent over 7 days as can be seen by large error bars, this is most likely due to inconsistent binding to the microcarriers, as observed on 'flat gels' in section 4.3.1. YIGSR modified microcarriers showed an increase in initial attachment on Day 1 in a peptide concentration dependant manner but gradually decreased over 7 days. From the 'flat gels' experiments this is likely due to an inability to spread and migrate.
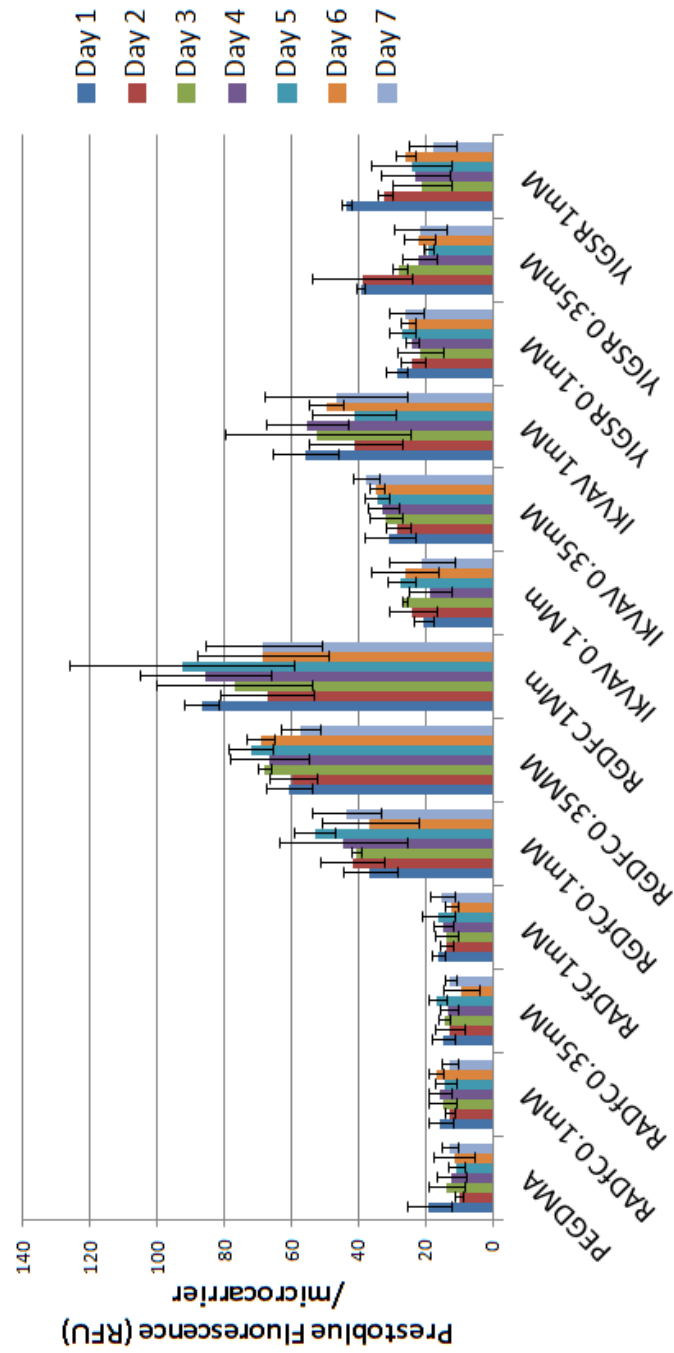
Figure 39 Prestoblue viability assay on ADSCs attachment and proliferation to peptide-modified microcarriers

ADSC attachment to peptide modified microcarriers (at a range of concentrations) was assessed daily using the Prestoblue viability assay and normalised to microcarrier number.

4.6 Observation of ADSC cytoskeleton when cultured on 1mM cRGDfC microcarriers

To further probe the influence of the adhesive peptide cRGDfC (at 1mM concentration) upon ADSC attachment and spreading, the cytoskeleton organisation was examined after 7 days. The actin cytoskeleton was visualised using TRITC conjugated phalloidin, which selectively stains F-actin. In addition microtubule structures were highlighted using anti-tubulin antibodies, and nuclei were stained using DAPI. Representative confocal images of actin and microtubule staining of ADSC laden microcarriers are shown in Figure 40.

Undifferentiated MSCs have a fibroblastic shape and demonstrate mostly long, thin parallel stress fibres, extending in the direction of the cell. However, Mao *et al.* demonstrated when stimulated to differentiate into either osteoblasts or chondrocytes, cytoskeletal changes occur concurrently with cell shape (350). After osteogenesis the cytoskeleton contains robust stress-fibres with more random patterning with a greater amount of actin filament crisscrossing and larger stress fibre bundles. Chondrogenic differentiation results in a more spread cytoskeleton with additional actin protrusions. Studies by Kilian *et al.* in 2012 have demonstrated when cRGDfC is presented as a monolayer for MSC attachment, cells display a higher degree of spreading, more stress fibres, and more focal adhesion structures (as compared to cells on monolayers presenting the linear form of RGD peptides). In addition, MSCs cultured on cRGDfC modified surfaces demonstrated enhanced actomyosin dependant osteogenesis (351).

After 7 days ADSC spreading was visualised on the high RGD density carriers as shown in Figure 40D. Analysis of the phalloidin stained F-actin cytoskeleton displayed well defined parallel stress fibres which were mostly stretched along the long axis of the cells. A network of stress fibres connected by microfilament vertices in the cytoplasm was also visualised. In addition anti-tubulin antibodies showed an organised microtubule network extending throughout the cytoplasm to the cell periphery.
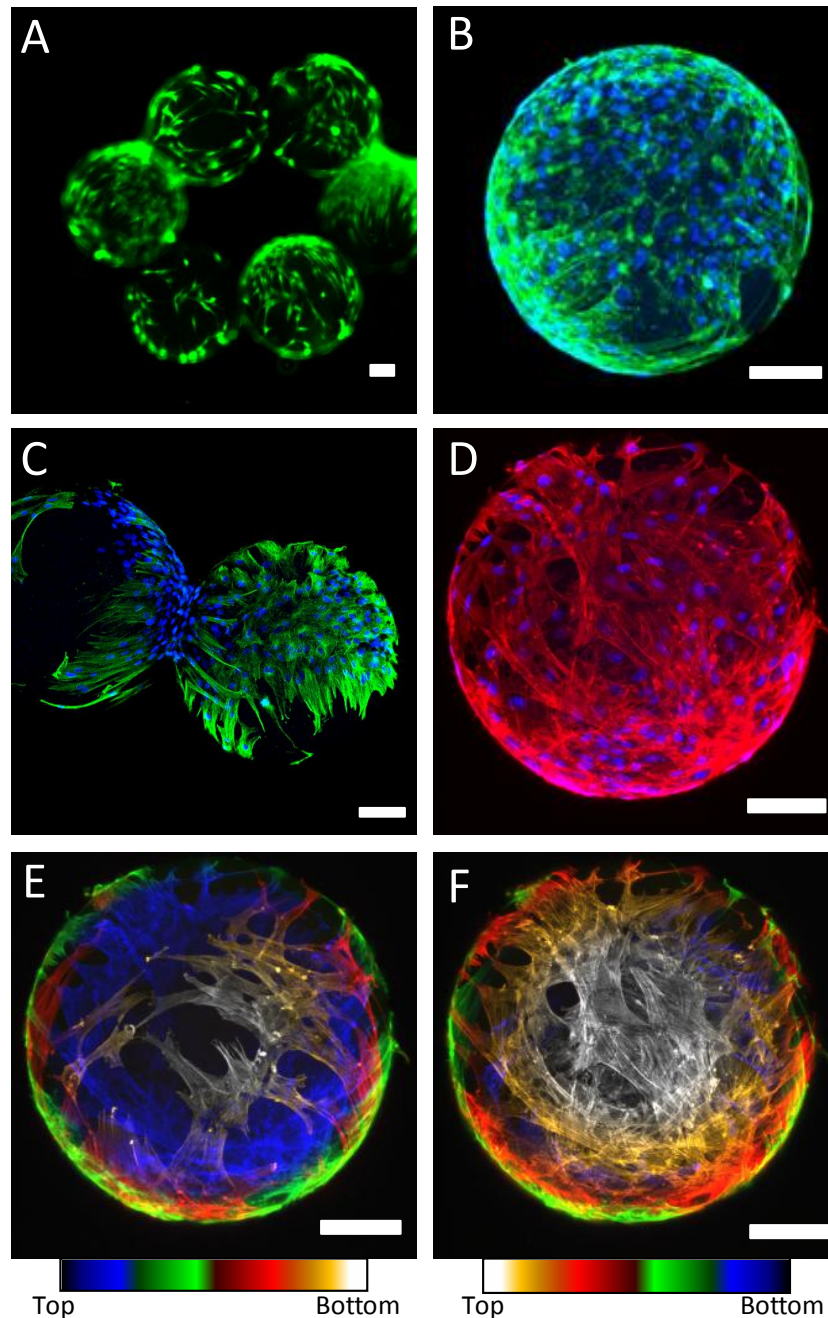
Figure 40 Analysis of ADSC morphology on the microcarrier.

(A) Widefield image of Live/Dead cell assay. (B) Maximum intensity projection of cell surface (concanavalin A)(green) and DNA (DAPI)(blue). (C) Maximum intensity projection of microtubules (anti-tubulin) (green) and DNA (DAPI)(blue). (D) Maximum intensity projection of actin cytoskeleton (phalloidin)(red) and DNA (DAPI)(blue). (E) Depth coded maximum intensity projection highlighting the top surface of the bead. (F) Depth coded maximum intensity projection highlighting the bottom surface of the same bead. All scale bars are 100µm.

4.7 Analysis of ADSC viability in microcarrier culture using a LIVE/DEAD assay

To assess the viability of the culture the LIVE/DEAD assay (Sigma, UK) was employed. This technique uses two chemical indicators which once inside the cell fluoresce according to cell viability. Calcein-AM stains live cells green and Propodium iodide stains dead cells red. The fluorescence was detected using widefield fluorescence microscopy.

The detected fluorescence revealed large populations of live cells bound to microcarriers, showing the culture was viable. Microcarriers containing the cyclic (RGDfC) peptide showed a large live cell population bound to the surface. In addition cell aggregates can be seen as associated to the microcarrier surface and also joining to adjacent microcarriers. The viability of the culture was observed to be very high (Figure 40A) with no visible dead cells.

4.8 ADSCs can attach to microcarriers with a wide range of compressive moduli.

To assess the effects of microcarrier compressibility on ADSC attachment and multipotency, microcarriers with a compressive modulus of 8kPa, 155kPa and 273kPa were generated, containing cRGDfC at a concentration of 1mM. As demonstrated in Chapter 3 section 3.13, altering the polymer content alters the mechanical strength of the PEGDMA hydrogel. Figure 41 depicts representative microcarriers at each compressibility. Softer 8kPa microcarriers appear to be damaged, with parts of the microcarrier missing, which occurred during routine preparation, most likely as a result of pipetting. In addition, it was observed that the bubble content increased as the polymer content increased, reducing the optical transparency of the microcarriers.

ADSCs were cultured on the microcarriers in static ultra-low attachment plates and images were taken at Day 3 and Day 7. ADSCs successfully attached and grew on all three microcarrier types. The level of attachment to 273kPa beads appeared similar the other microcarriers. However, in addition on Day 3 bridging between the microcarriers occurred and numerous cells appeared to make multiple contacts between neighbouring microcarriers which increased over the time course. Migration from one bead to another had previously been observed in our culture system, however long

standing contacts between microcarriers as seen in Figure 42, has previously (to the best of our knowledge) not been reported in the literature.
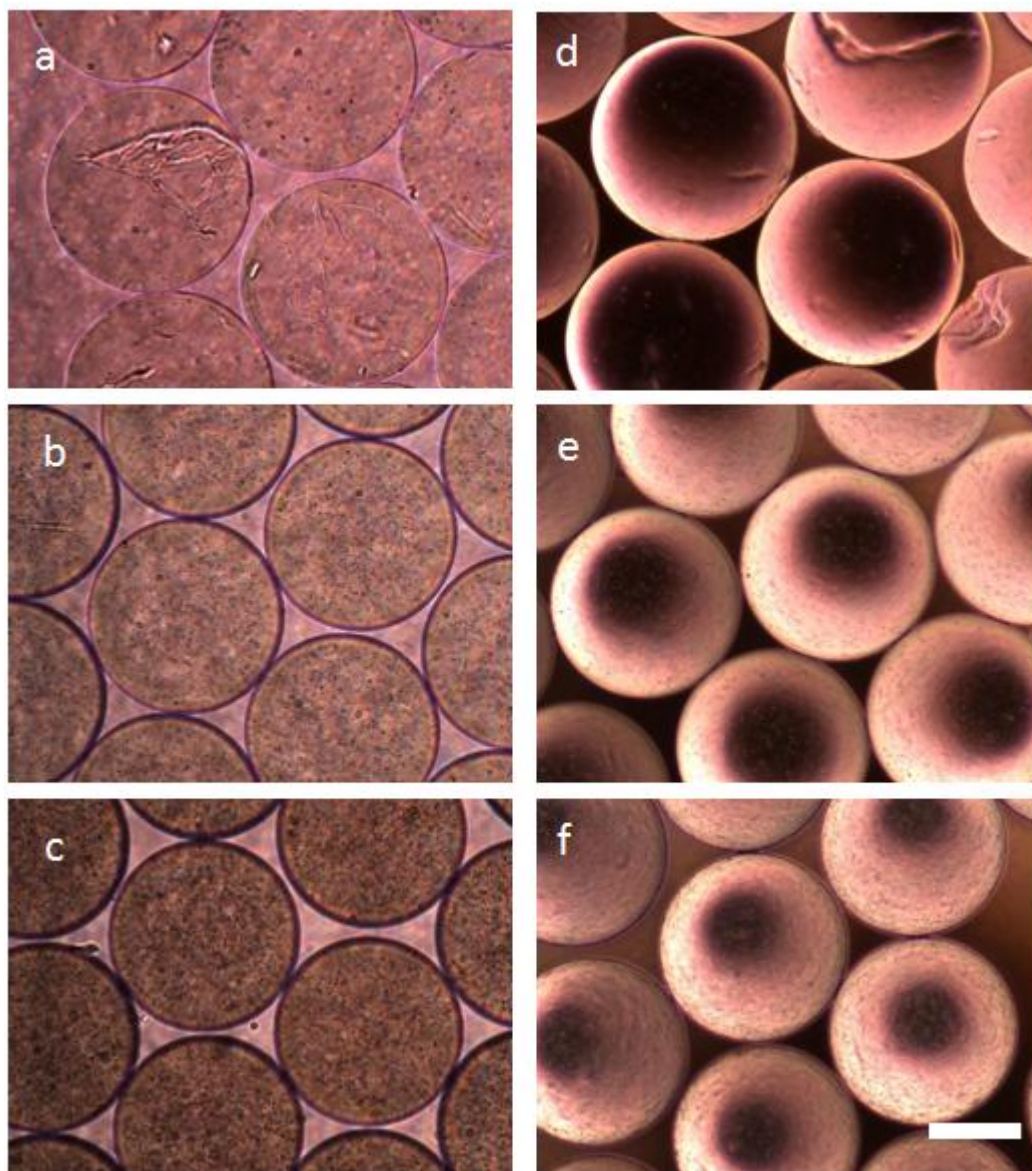
Figure 41 Brightfield and phase contrast images Microcarriers containing varying PEGDMA concentrations (w/v%)

Microcarriers generated using microfluidics containing a range of PEGDMA concentrations (a,d) 12% (8kPa) (b,e) 18% (155kPa) (c,f) 22% (273kPa). At 12% (w/v%) PEGDMA microcarriers were easily damaged during routine pipetting. As PEGMDA content increases, the optical transparency of the microcarriers is reduced.
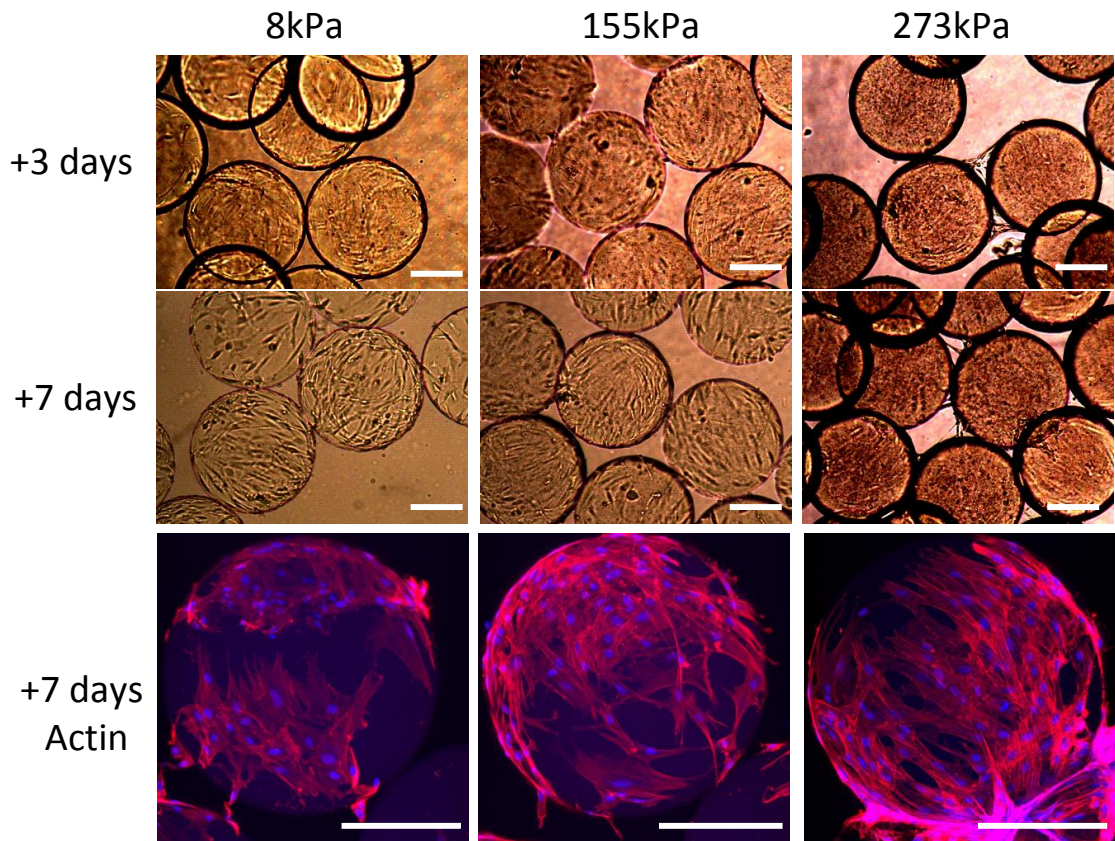
Figure 42 ADSC growth on microcarriers of different compressive moduli.

Attachment and growth of ADSCs occurs at all mechanical compressibilities tested, but with subtle differences within cultures. Most noticeable is the formation of bead bridges formed within 273kPa cultures at both 3 and 7 days as cells become attached to more than one bead

To determine the effect of microcarrier compressibility on cytoskeleton formation, a factor known to be related to differentiation capability, TRITC-Phalloidin staining of F-actin was employed. As actin microfilaments underlie the cell membrane and span the entire cytoplasm, it was postulated that alterations in actin cytoskeleton arrangement could occur as a direct result of changes in substrate mechanical strength. Diffuse actin staining was observed on soft substrates such as 8kPa microcarriers which can be seen in Figure 42. Also, stress fibres became progressively more organised and defined on stiffer substrates as seen on both 155kPa and 273kPa microcarriers.
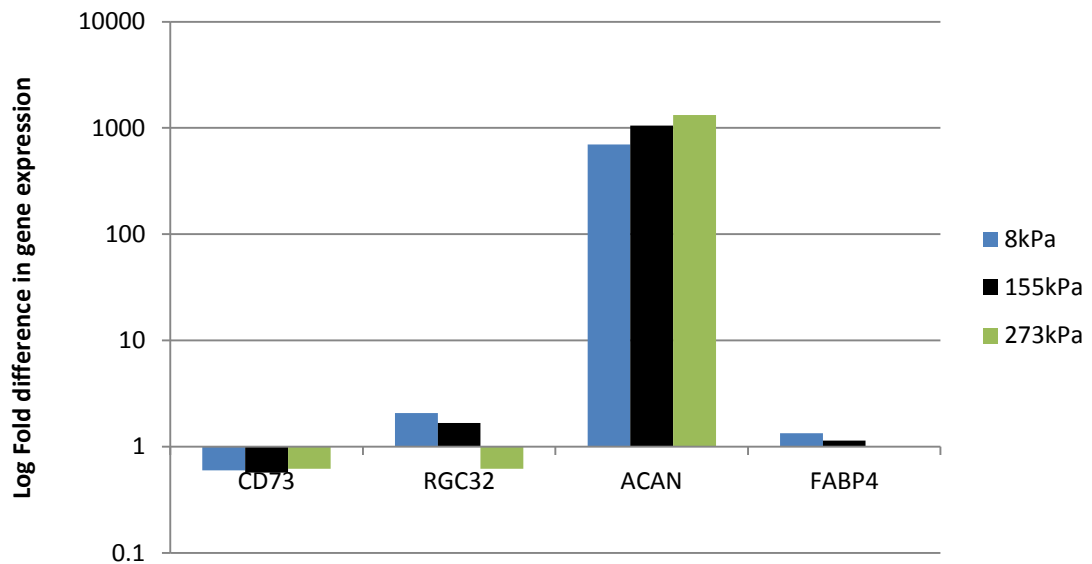
Figure 43 RT PCR analysis of ADSCs grown on microcarriers of different compressive moduli.

ADSCs cultured on microcarriers with a range of compressive moduli were harvested after 5 days to assess the levels of lineage specific gene expression.

Following the 5 days on microcarriers with the compressive moduli of either 8, 155 or 273 kPa in culture ADSCs, quantitative RT-PCR analysis was used to detect the expression of mRNA transcripts associated with lineage specific differentiation (Figure 43). To determine if microcarrier culture had an effect of priming ADSC differentiation to particular lineage, RT-PCR analyses were performed for CD73, a marker for multipotency and three early differentiation genes: RGC32, FABP4, and Aggrecan (ACAN), which are early cell markers for osteogenesis, adipogenesis, and chondrogenesis, respectively and normalised to multipotent controls cultured in flasks. Cell-laden microcarriers cultured all three microcarrier types demonstrated CD73 expression remained largely unchanged in the cultures (with a fold decrease of approximately 0.6), indicating multipotency remained. An increase in the osteogenic marker RGC32 showed an upregulation (2.07-fold increase) in expression on 8kPa microspheres. A downregulation in gene expression was observed on 273kPa microcarriers. The expression of the chondrogenic-specific gene, aggrecan was upregulated in all three cultures. The upregulation was most pronounced in 273kPa microcarriers (a 1323.37 fold increase), which also showed microcarrier contacts over 5 days (Figure 42). At 155kPa and 8kPa there was no contacts formed between the microcarriers decreased in fold increase in 1052 and 699 respectively. As described in Section 4.13, chondrogenesis on novel microcarriers generated herein, is typically associated with spontaneous cell aggregation on the microcarrier surface forming a

pellet like structure. As can be seen with phase contrast images (Figure 38), this was not observed on any microcarriers expanded in culture. Low levels of adipose-specific genes, Fatty Acid Binding Protein (FABP4) were detected, with a slight upregulation in three of the cultures. However, this was not substantial, as adipogenic induction in ADSC-laden microcarriers in static culture generated 45,000 fold increase in FABP4 gene expression. Furthermore, phalloidin staining demonstrated spread cells well defined actin structures, which is not typical of adipocytes, which have a round morphology. This indicates the cell population was heterogeneous.

4.9   ADSC properties on tissue culture plastic

ADSCs are capable of differentiating into three different cell types (adipocytes, chondrocytes and osteocytes), showing a classic tri-lineage potential. Typically ADSCs exhibit a fibroblastic phenotype when cultured in monolayers. To assess the multipotency of ADSCs using standard culturing techniques (tissue culture plastic), ADSCs were cultured in specialised induction media (Figure 44). After 14 days of adipogenic induction, ADSCs adopted a differentiated phenotype with accumulated lipid droplets within cells, typical of an adipocyte phenotype. Positive staining was observed using both Oil-red-O (a lipid specific stain). Under osteogenic induction conditions, mineralised calcium deposits were observed (*via* alizarin red staining) on a network-like monolayer. ADSCs cultured under chondrogenic conditions, i.e. high density 3D pellet culture, developed a rounded phenotype and cultures were positive for alcian blue staining.

Flow cytometry analysis was performed to characterise ADSC cell surface markers (Figure 45). The ADSC surface markers CD29, CD44, CD90 and CD105 were expressed to high levels. In contrast, the expressions of hematopoietic markers (CD45) was expressed at low levels <2% compared to isotype controls.
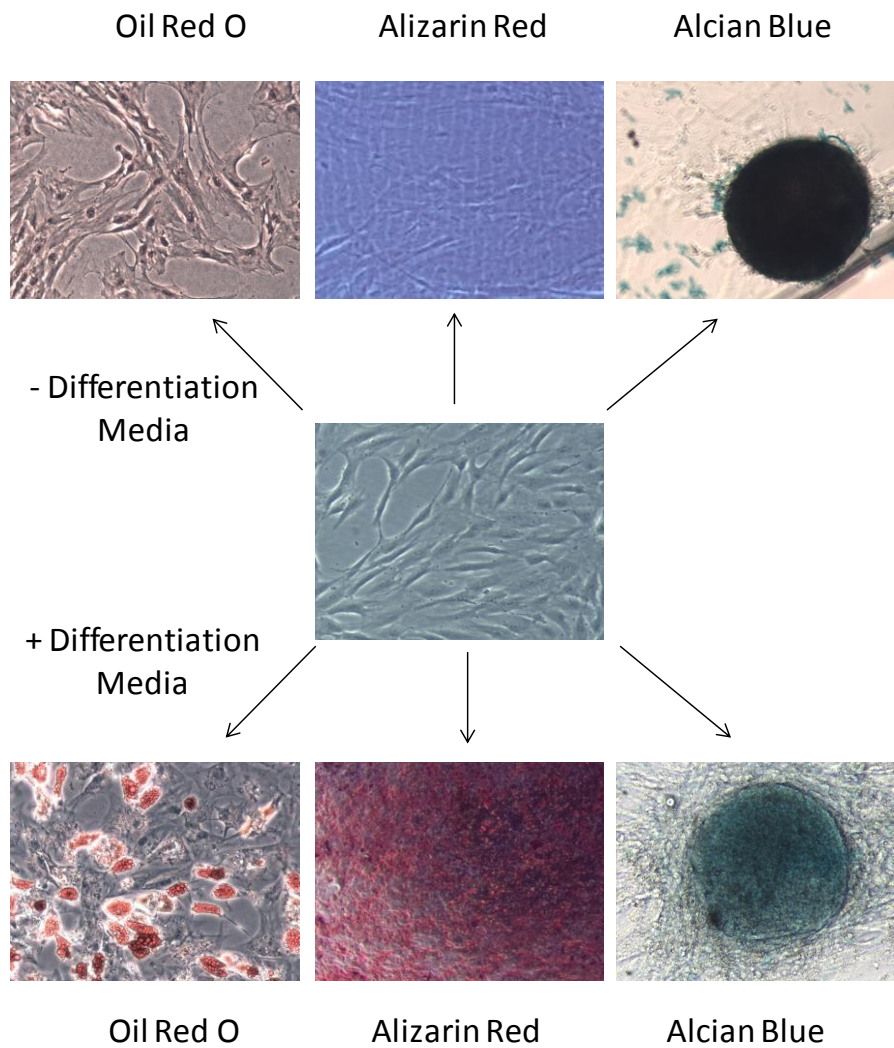
Figure 44 Differentiation of ADSCs cultured on conventional tissue culture plastic.

ADSCs cultured on tissue culture plastic were transferred to differentiation induction medium for 14 days. Adipogenesis was observed using the lipid stain Oil-red-O to detect the accumulation of lipid droplets. Osteogenesis was analysed using Alizarin red S histochemical stain which detects calcium secretions. Chondrogenesis in pellet culture was detected using Alcian blue, a histochemical stain for sulphated matrix production. All samples were tested alongside a control which was cultured in parallel in the absence of differentiation induction media.
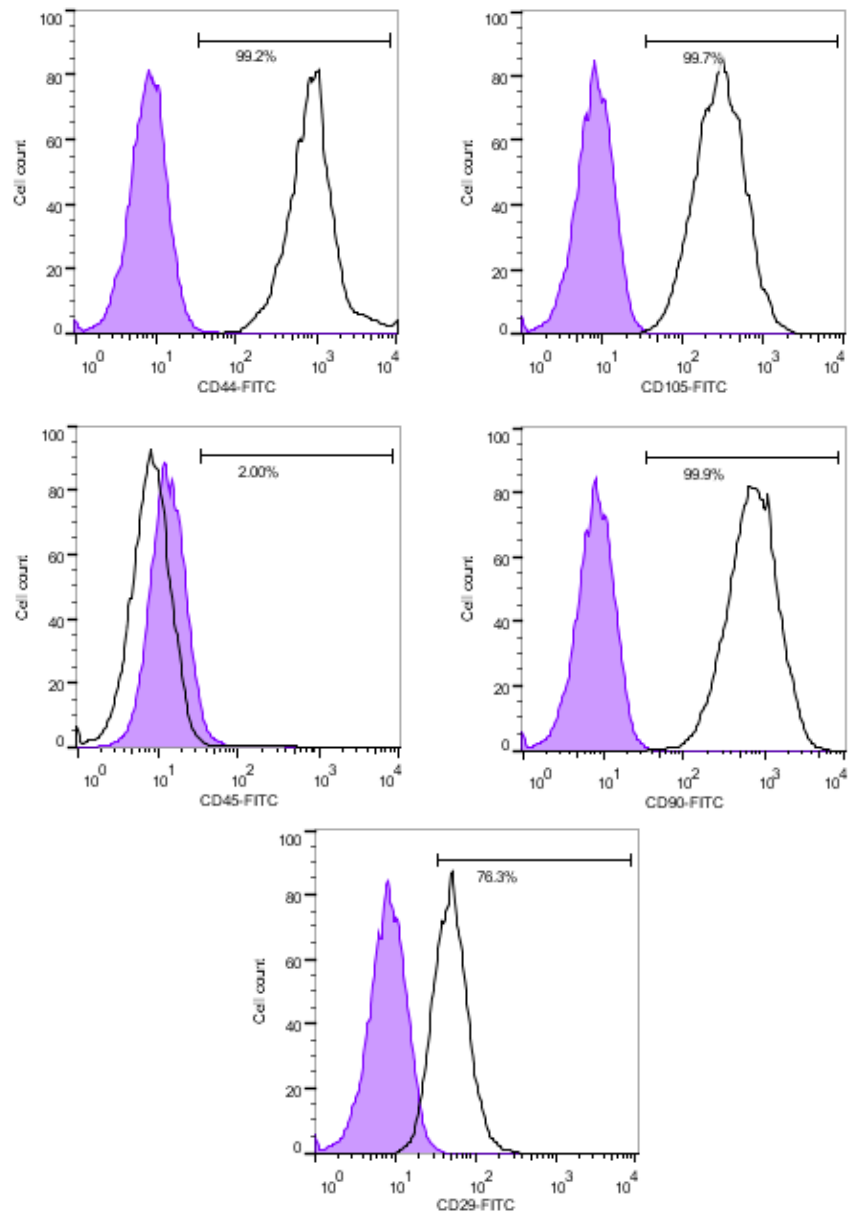
Figure 45 Flow cytometric analysis of typical surface markers expressed in ADSCs

ADSCs were stained with positive the surface markers: CD90; CD105; CD44, CD29 and negative for the hematopoietic marker CD45. The shaded peak areas show signals from isotype controls (background fluorescence), and the white peak areas represent signals from surface marker antibodies on ADSCs. FITC-conjugated secondary antibodies were used to detect CD labeling.

4.10 ADSCs maintain their multipotency on microcarriers with a varied compressive modulus

To determine the ability of the adhered ADSCs to differentiate into all three cell types whilst cultured on microcarriers, ADSCs were seeded onto microcarriers with different mechanical properties, allowed to attach and subsequently transferred into the appropriate differentiation media for 14 days (with regular media changes).

Quantitative RT-PCR demonstrated when placed in adipogenic induction medium the expression of FABP4 was upregulated on microcarriers with all three compressive moduli (compared to multipotent ADSCs cultured on tissue culture plastic) (Figure 46). On microcarriers containing compressive moduli of with 8, 155, 273 kPa a fold increase gene expression of 147,463, 135,694 and 106,463 was observed respectively. This was higher than we analysed using monolayer culture. This was corroborated by microscopy (Figure 43), where adipogenesis qualitatively appeared higher on 8kPa microcarriers.

The osteogenic marker RGC32 was upregulated in all differentiation induction conditions, on all microcarrier compositions. When cultured in osteogenic induction media, the highest level of gene expression was observed on 8kPa microcarriers. In addition a very similar level of fold increase in gene expression was observed on 155kPa and 273 kPa microcarriers.

Like the osteogenic marker RGC32, the upregulation of the early chondrogenic marker aggrecan was observed in all conditions. The highest fold increase in aggrecan expression (140 fold increase) was observed on microcarriers with on 273kPa microcarriers. CD73 (NT5E) showed a consistent decrease in gene expression in all conditions.
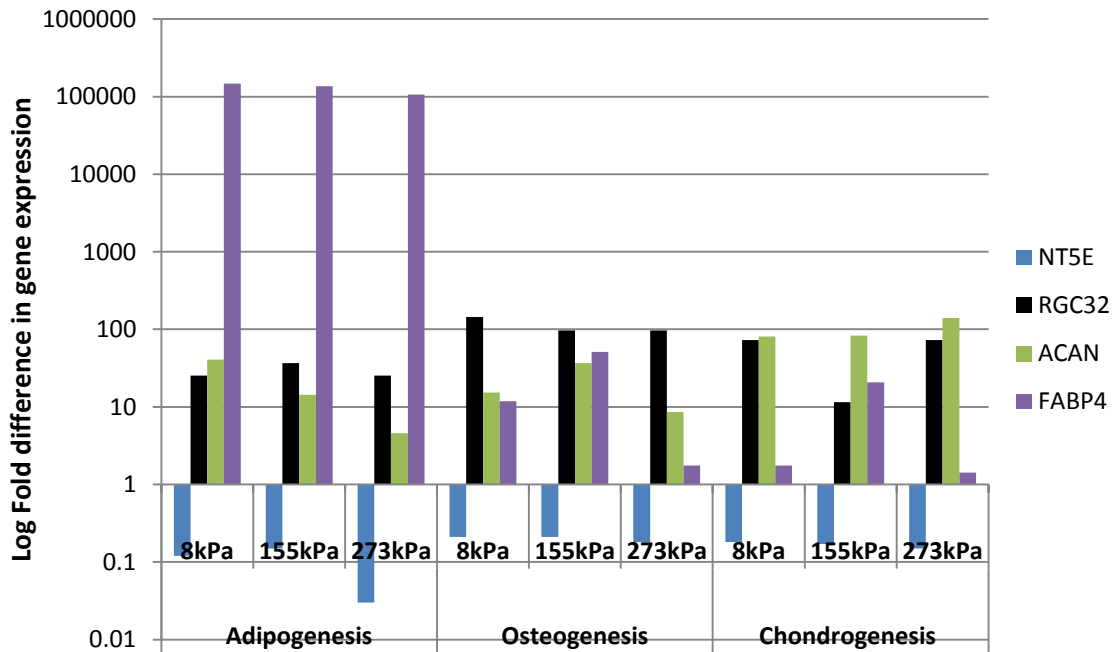
Figure 46 RT PCR analysis of ADSCs grown on microcarriers of different compressive moduli, cultured in differentiation induction medium.

ADSCs cultured on microcarriers with a range of compressive moduli were cultured for 14 days in differentiation induction medium. The levels of lineage specific gene expression was detected using RT-PCR and compared to multipotent ADSCs cultured on tissue culture plastic to determine fold increases in expression.

4.11 Adipogenesis is supported on microcarriers with a variety of compressive moduli.

After 2 days in culture, the microcarriers were transferred to adipogenic differentiation medium in static culture for 14 days. To assess adipogenic differentiation, cells were stained with Lipidtox, a neutral lipid stain which selectively stains lipid droplets, and analysed using confocal microscopy. As demonstrated by whole well imaging (shown in Figure 43), each microcarrier type responded differently to adipogenic differentiation. Soft substrates, i.e. 8kPa microcarriers, aggregated to form large multi-microcarrier units with very few microcarriers remaining as discrete particles (as they were prior to differentiation). As demonstrated by confocal images, (Figure 43), Lipidtox stained adipocytes were observed covering the entire surface of the 8kPa microcarrier. It was further observed that cell density was very high with the interstices (the space between adjoining hexagonally close pack microspheres) between microcarriers in the multi-microcarrier units, wherein Lipidtox staining, and hence adipogenesis appeared highest. This effect appeared to be less pronounced on stiffer 155kPa and 273kPa microcarriers, where the majority of the microcarriers remained

discrete with few microcarrier aggregates of typically 5 microcarriers or less. Differentiated adipocytes appeared to be confined on the whole to the interstices between microcarriers, as indicated by dark masses between microcarriers on the whole well images. Overall all microcarrier types supported adipogenesis.
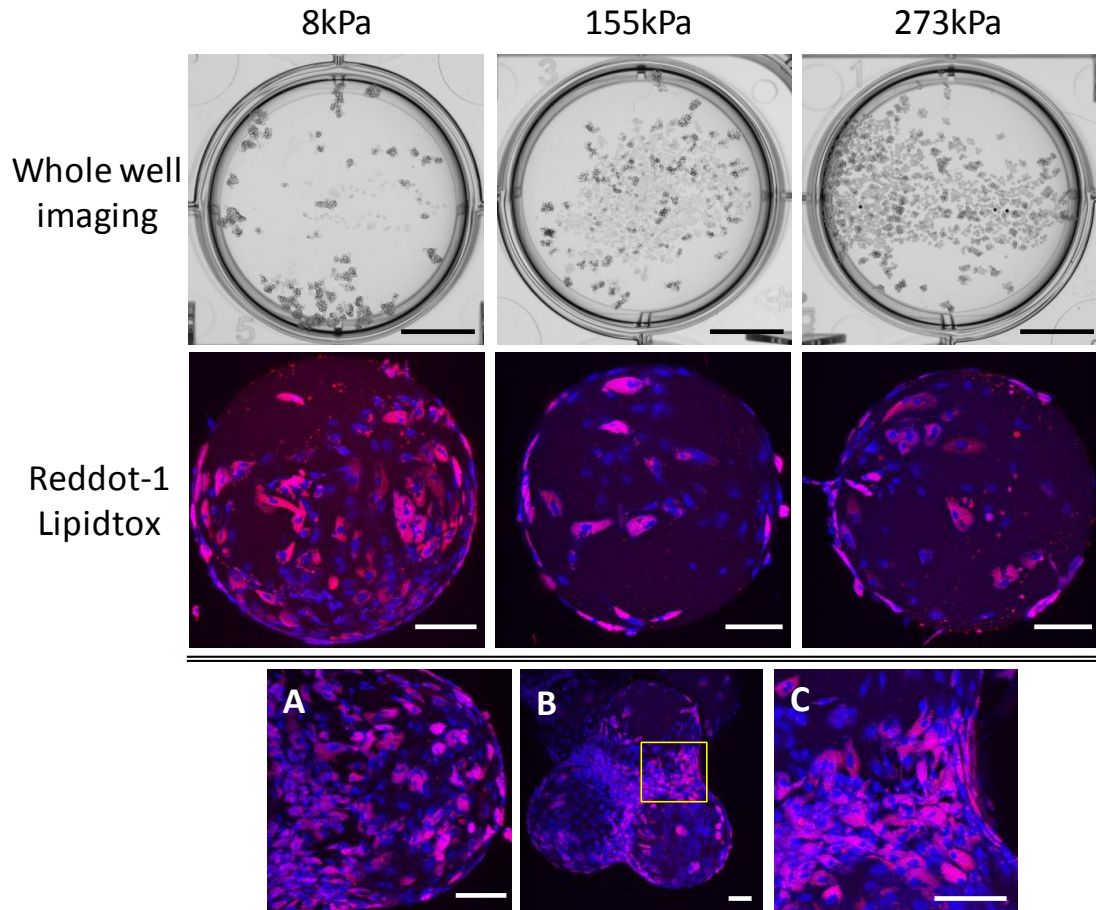
Figure 47 ADSCs cultured in adipogenic induction media on microcarriers containing a range of compressive moduli

ADSCs were cultured in adipogenic induction media for 14 days. Whole well images representing microcarrier aggregation (Scale bar 10mm) Confocal images showing Lipidtox which selectively stains neutral lipids within lipid droplets. Nuclei (shown here in blue) are labelled using Reddot-1. (A) A representative image of 8kPa microcarriers containing differentiated adipocytes covering its surface. (B and C) Concentrated cells found within microcarrier interstices demonstrated a high level of adipogenesis. (Scale bar100μm)

4.12 Osteogenic differentiation of cells on microcarriers as confirmed by Alizarin red S Staining

To assess the osteogenic differentiation potential of ADSCs cultured on microcarriers with a range of compressive moduli, cell-laden microcarriers were transferred to osteogenic induction medium 2 days post seeding where they remained with regular medium changes for 14 days. Cell morphology was observed by phase-contrast microscopy and using the Alizarin Red S histochemical stain which can detect calcium (by forming an alizarin red S-calcium complex in a chelation process), a marker of osteogenic differentiation and extracellular matrix mineralisation.

Whole-well images showed the distribution of microcarriers within 6 well plates. Over 14 days, the medium transitioned from clear to opaque, an indication of matrix deposition. As before, the 8kPa microcarriers were fully aggregated into 3 main islands. As is evident from the whole-well images, (Figure 48) cells were most dense within interstices. The 155kPa microcarriers remained relatively sparse, however similarly to 8kPa microcarriers it was observed that the cells were most dense at interstices between microcarriers. The 273kPa microcarriers, like the 8kPa microcarriers were fully aggregated. Contrastingly, it was difficult to define the 273kPa microcarrier edges as cells covered the microcarrier aggregates forming large sheet-like structures (Figure 48).

After 14 days in osteogenic induction medium, cells on all three types of microcarrier demonstrated the capacity to form Alizarin Red S positive condensed nodules with high calcium content as shown by Figure 48. The nodules became trapped within the cell/matrix surrounding the microcarriers. ADSCs cultured on microcarriers in non-induction medium formed adherent layers without nodule formation and showed no signs of calcium deposition and hence displayed no Alizarin Red S staining.

Alizarin Red staining on 8kPa microcarriers, showed two types of staining. Cells covering the surface of microcarriers, stained bright red, indicating less mineralised areas. In addition, dark red to black mineralised nodules were observed between microcarrier interstices. Like 8kPa microcarriers, staining on 155kPa microcarriers appeared to be focused at interstices between microcarriers where aggregates of cells and dark calcium nodules were found. However, unlike 8kPa microcarriers, nodules were not confined to interstices, and could also observed at other points on the surface of the microcarriers. In addition, a large amount of bright red, less mineralised staining

could be seen over the surface of the carriers, however this was inconsistent. In contrast, dark red Alizarin red staining on 273kPa microcarriers was localised solely to interstices between microcarriers (as shown in Figure 48). Unlike in softer microcarriers, no bright red staining was observed on the surface of the spheres and extended networks of cells can be observed spanning the 273kPa microcarrier aggregates. These observations indicate that ADSCs can differentiate into osteocytes on all three types of microcarrier, resulting in the formation of mineralised matrix when cultured in osteogenic induction conditions.
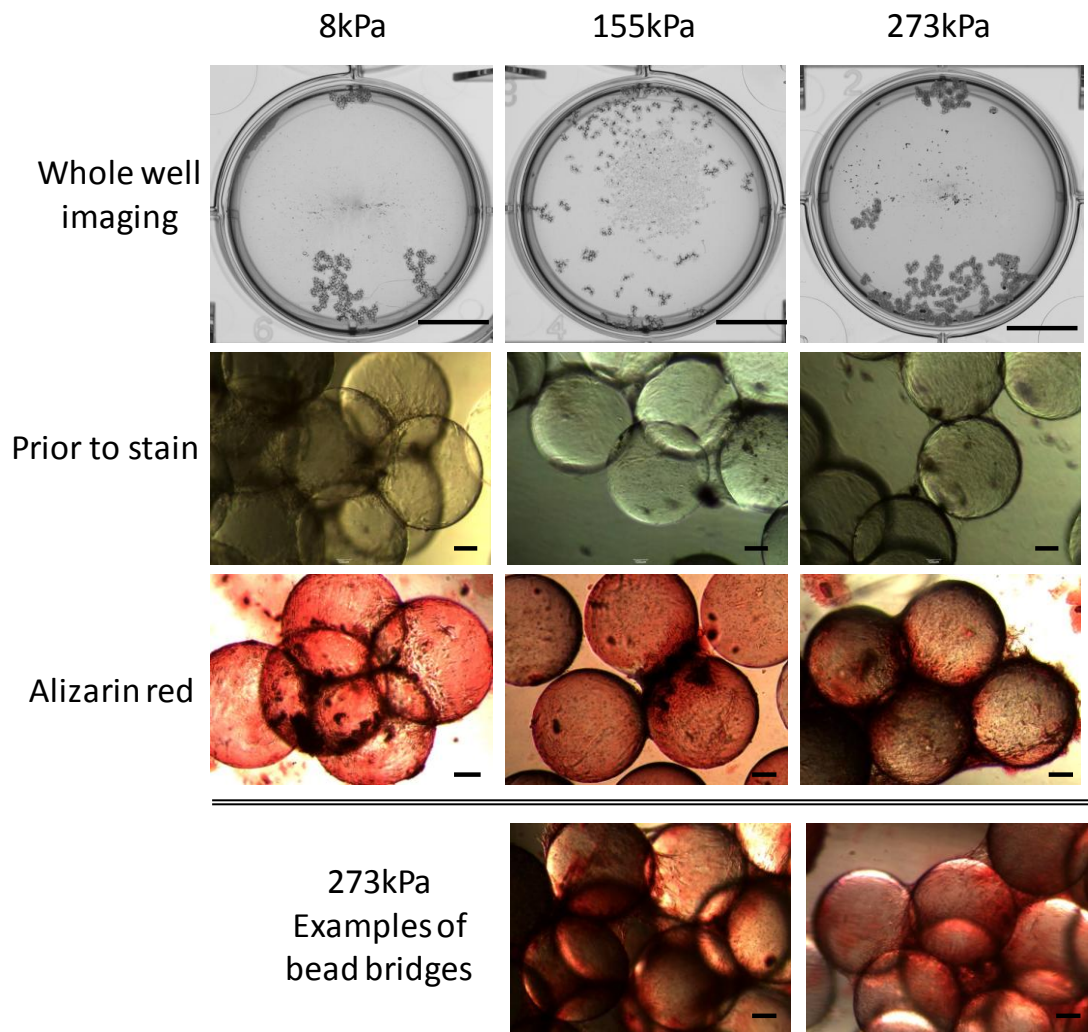
Figure 48 ADSCs cultured in osteogenic induction media on microcarriers containing a range of compressive moduli

ADSCs were cultured in osteogenic induction media for 14 days. Whole well images representing microcarrier aggregation (Scale bar 10mm) Brightfield images showing Alizarin red staining of calcium secreted from the cells. Cells cultured on 273kPa microcarriers formed a layer of cells which spanned multiple microcarriers. (Scale bar100μm)

4.13 Spontaneous cell aggregation in response to chondrogenic differentiation medium

For effective chondrogenic differentiation of MSCs, typically cells are cultured as high density micromass cultures, forming a pellet which facilitates cell-cell interactions reminiscent of the prechondrogenic condensations during embryonic development. When cells are cultured with the combination of 3D culture and supplemented medium with growth factors MSCs lose their characteristic fibroblastic morphology, become rounded and start to express cartilage specific matrix components.

To assess the chondrogenic differentiation potential of ADSCs cultured on microcarriers with a range of compressive moduli, cell-laden microcarriers were transferred to chondrogenic induction medium 2 days post seeding where they remained with regular medium changes for 14 days. Prior to chondrogenic induction, cell laden microcarriers were discrete structures, with the exception of 273kPa microcarriers, which (as described in Section 4.7 contained bridges between microcarriers. After 14 days post chondrogenic differentiation, cells displayed a varied behaviour dependent upon microcarrier composition. 8kPa microcarriers aggregated within the well and cells condensed at interstices between microcarriers. Cells on 155kPa microcarriers combined to form small pellets on the edge of a single microcarrier or a small group of carriers. The contact between microcarriers remained minimal with and all of the microcarriers were dispersed across the majority of the well. The numerous pellets had a rounded morphology and were of varied size. The microcarriers the highest compressive modulus of 273kPa, aggregated within the well. Over 14 days cells from multiple carriers combined to form large rounded pellets. Several pellets contained semi-transparent centres within which dark masses could be observed.
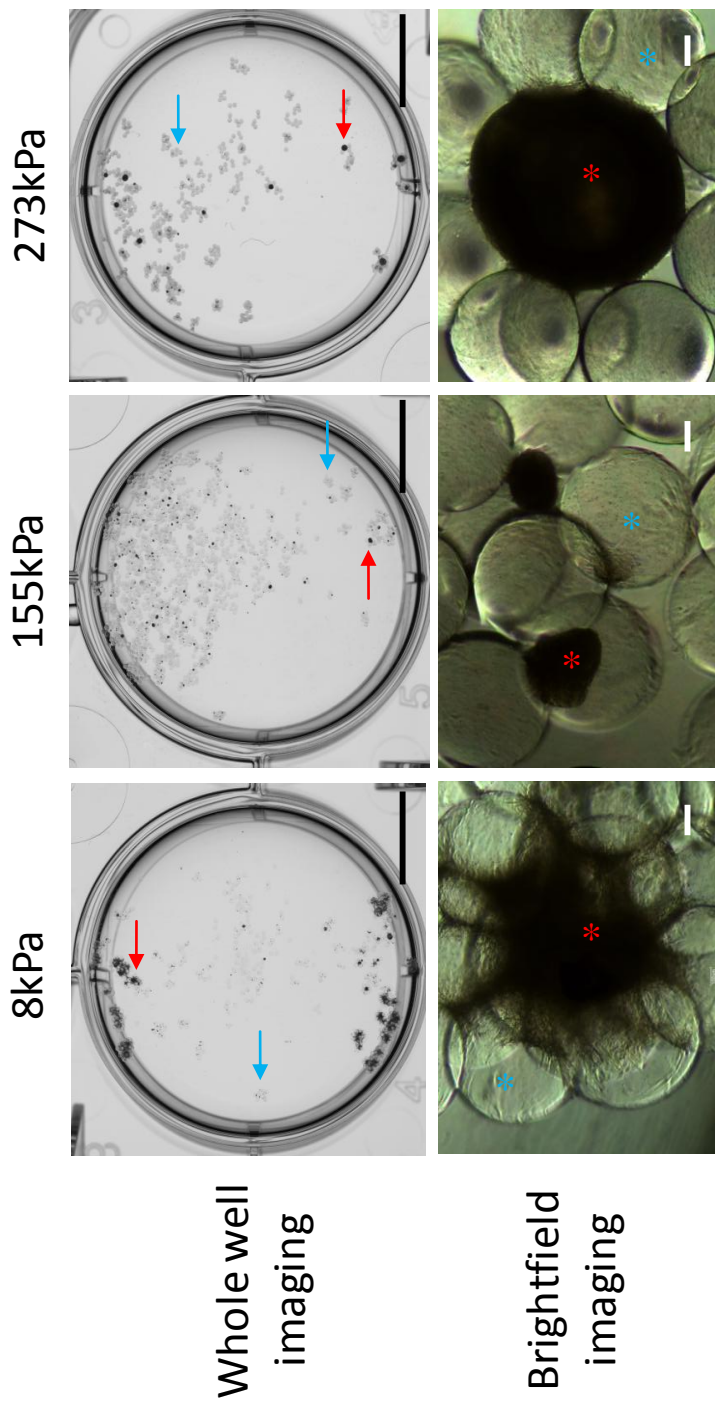
Figure 49 ADSCs cultured in chondrogenic induction media on microcarriers containing a range of compressive moduli

ADSCs were cultured in chondrogenic induction media for 14 days. Whole well images representing microcarrier aggregation (Scale bar 10mm) Representative brightfield images demonstrate compressive moduli spontaneous cell aggregation on microcarriers. Red Asterisk/red arrows indicates condensed cell aggregates. Blue asterisks/blue arrows indicate hydrogel microcarriers. (Scale bar100µm)

4.14   Production of cartilage-specific extracellular matrix

After 14 days in culture cell pellets/microcarrier constructs were embedded in paraffin wax and sectioned for staining. Histological sections were stained using Haematoxylin and Eosin (H&E) to highlight cell nuclei and cytoplasm. H&E staining showed that the structure of the cell pellets on 8kPa and 273kPa comprised three distinct areas resembling the zonal structure of articular cartilage (Figure 51 and Figure 53). A 'superficial-like zone' at the edge of the pellet consisted of spindle cells highly organised and aligned parallel to the surface, a structure resembling the superficial zone of *in vivo* articular cartilage. In a 'deep-like zone', obvious morphological differences were observed in the three populations, with decreasing cell number and increasing ECM content. Decreasing cell number and hence, increasing intercellular space is essential to allow ECM accumulation, giving cartilage its unique properties (353). Cell morphology of MSCs changed during chondrogenesis from spindle fibroblastic shape to more spherical shapes in the centre of the pellet.   In addition H&E staining was partly absorbed by the microcarriers indicating their presence. In the 8kPa microcarriers, the microcarriers were deformed during the embedding process, however densely accumulated cells were observable between microcarriers. A clear superficial zone can be visualised with a layer of flattened cells at the edge of the pellet (Figure 51). Cells became sparser and rounded towards the centre of the pellet and intercellular space increases, which is indicative of a 'deep zone'. On 155kPa microcarriers small pellets had a thin superficial zone, approximately 1 cell layer thick, with small intercellular space. Cells in the core formed a swirl like pattern containing mainly enlarged and rounded cells. On 273kPa microcarriers, spindle shaped cells parallel to the surface of the pellet generated a very prominent edge. In addition a low cell density core with rounded cells and large intercellular space indicating matrix deposition.

In addition, within the 'deep and middles zones' there was evidence of columns of rounded cells within lacunae (cavities within the cartilage matrix, typically containing single cells), were orientated perpendicular to the surface indicative of chondrocyte proliferation. Spindle cells were observed on all edges, including the inner edge of the pellet. The cellular organisation resembled certain characteristic features present in normal articular cartilage (354).

Positive   metachromatic   Toluidine blue   staining   sulphated   proteoglycans of chondrogenic pellets provided information on the extent of matrix formation. The 8kPa and 273kPa microcarriers displayed varying degrees of sulphated proteoglycan

accumulation within the pellets. Within 8kPa microcarriers, staining was strongest at the surface of the pellets. In 155kPa microcarriers, strong staining was observed throughout the pellets indicating the uniform presence of proteoglycans. In all 273kPa pellets, cells within the superficial zone displayed strong staining, representative images are shown in Figure 52. In addition, unlike the 155kPa microcarriers, a middle zone was observed which showed weak toluidine blue staining with large intercellular spaces and few cells. In the deep zone, cell density increased with examples of cells contained in lacunae.

Chondrogenic differentiation of ADSCs in the three conditions was evaluated by assessing by the presence and of cartilage-specific extracellular matrix proteins collagen types I and II. As MSCs express collagen I whereas chondrocytes primarily express collagen II (190, 352). As observed from the 8kPa microcarriers, the cells formed a network which spanned multiple microcarriers as seen in (Figure 47). A more magnified view illustrates defined superficial and deep zones (Figure 51). Within the latter few cells were observed and within the intercellular spaces positive co-localised staining for the presence of collagen types I and II was observed. Smaller rounded pellets present on 155kPa microcarriers did not produce any detectable levels of Collagen types I and II by immunocytochemistry. Type I and II Collagen staining was positive throughout the deep zone of the large pellets found on 273kPa microcarriers and faintly present towards the mid/superficial zone between cells. However, unlike cells around 8kPa microcarriers the deep zone and mid zones of the pellet contained a high density of cells, decreasing the possible space for ECM accumulation.
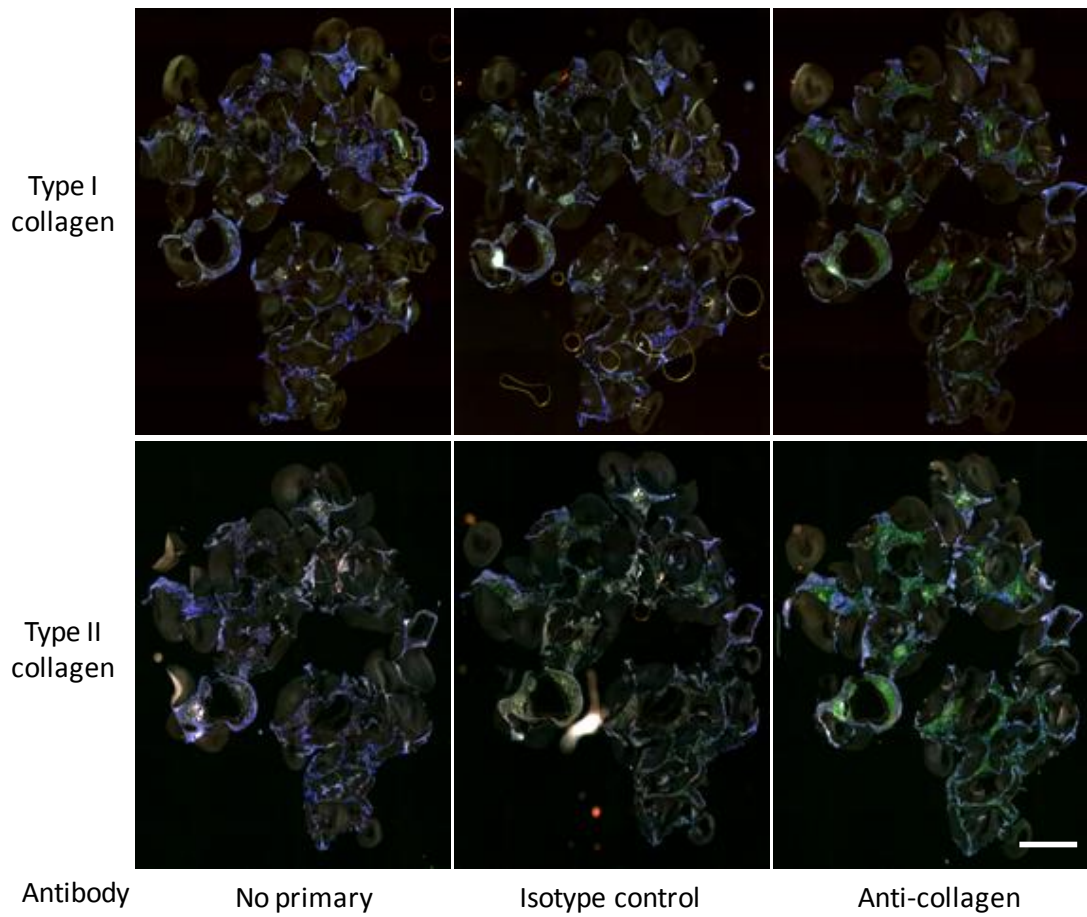
Figure 50 Collagen type 1 and II expression in cell aggregates on 8kPa microcarriers

ADSCs cultured on 8kPa microcarriers were placed in chondrogenic induction medium for 14 days. Immunocytochemistry analysis of microcarriers aggregates detected co-localised Collagen type 1 and II expression within the cell aggregates indicating chondrogenic differentiation. (500μm)
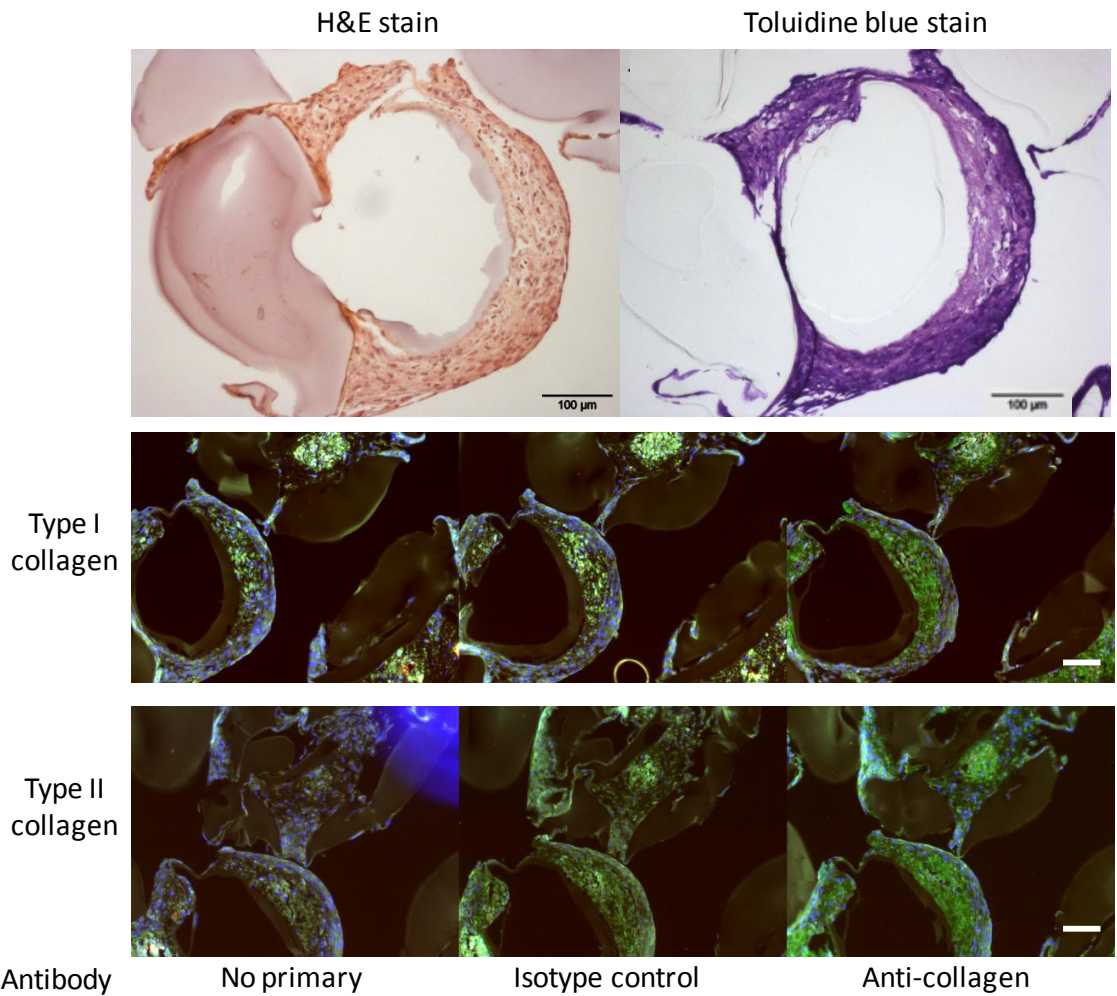
Figure 51 Analysis of ECM production in cell aggregates on 8kPa microcarriers

H&E staining demonstrated an organised cellular struture. Metachromatic toludine blue staining indicated the presence of a sulphated GAG matrix indicating the formation of zonal compartments with different ECM properties. Immunocytochemistry demonstrated collagen type I and II colocalised within the area between the flat cell layer and the microcarrier denoted 'middle/deep zones' (Scale bar 100μm)

| | H&E stain | Toluidine blue stain |
| | | |

Type I collagen

Type II collagen

| Antibody | No primary | Isotype control | Anti-collagen |
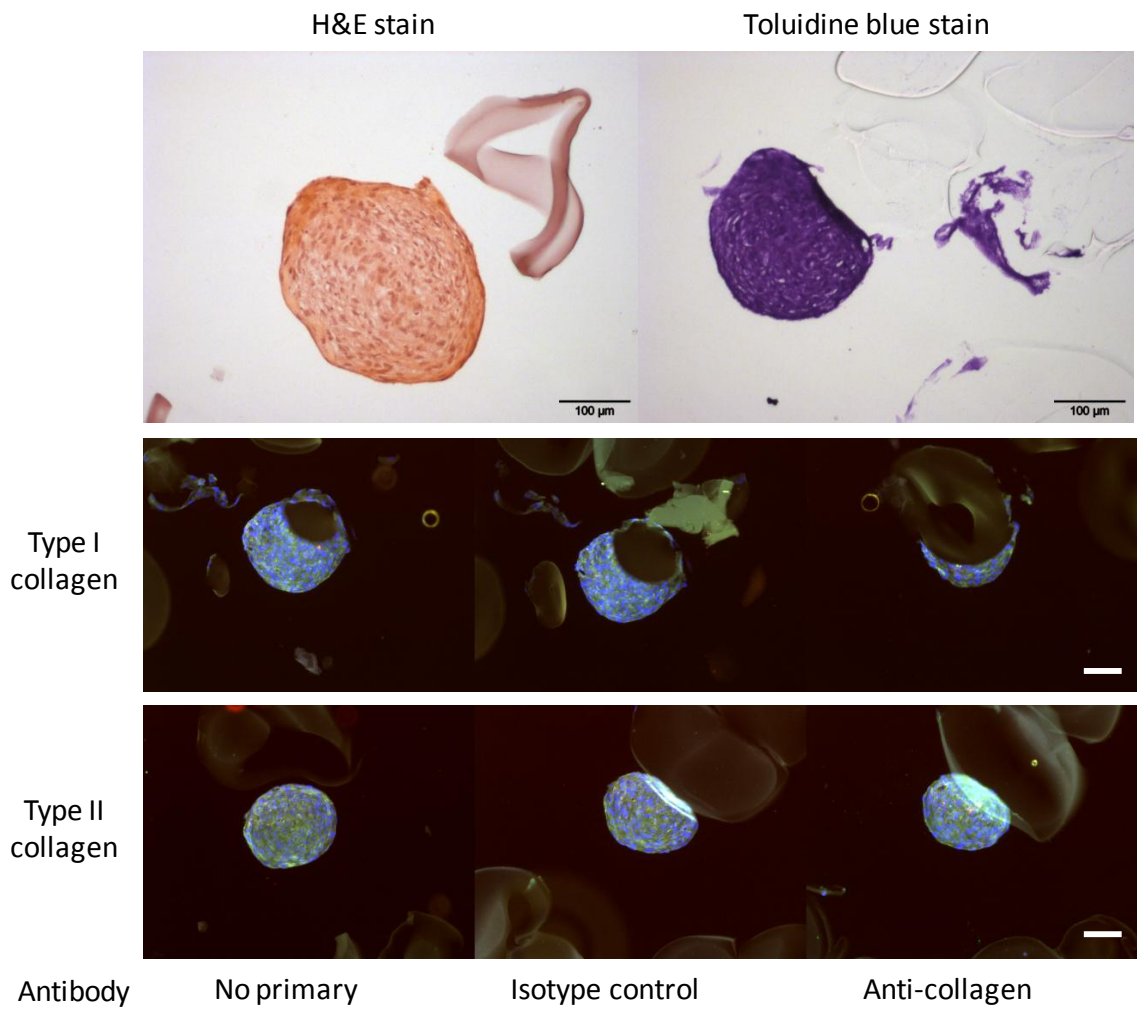
Figure 52 Analysis of ECM production in cell aggregates on 155kPa microcarriers

H&E staining demonstrated condensed cells within a pellet. Toludine blue staining indicated the presence of a sulphated GAG matrix uniformly across the pellet section. Immunocytochemistry demonstrated no collagen type I and II was present within the pellet (Scale bar 100µm)
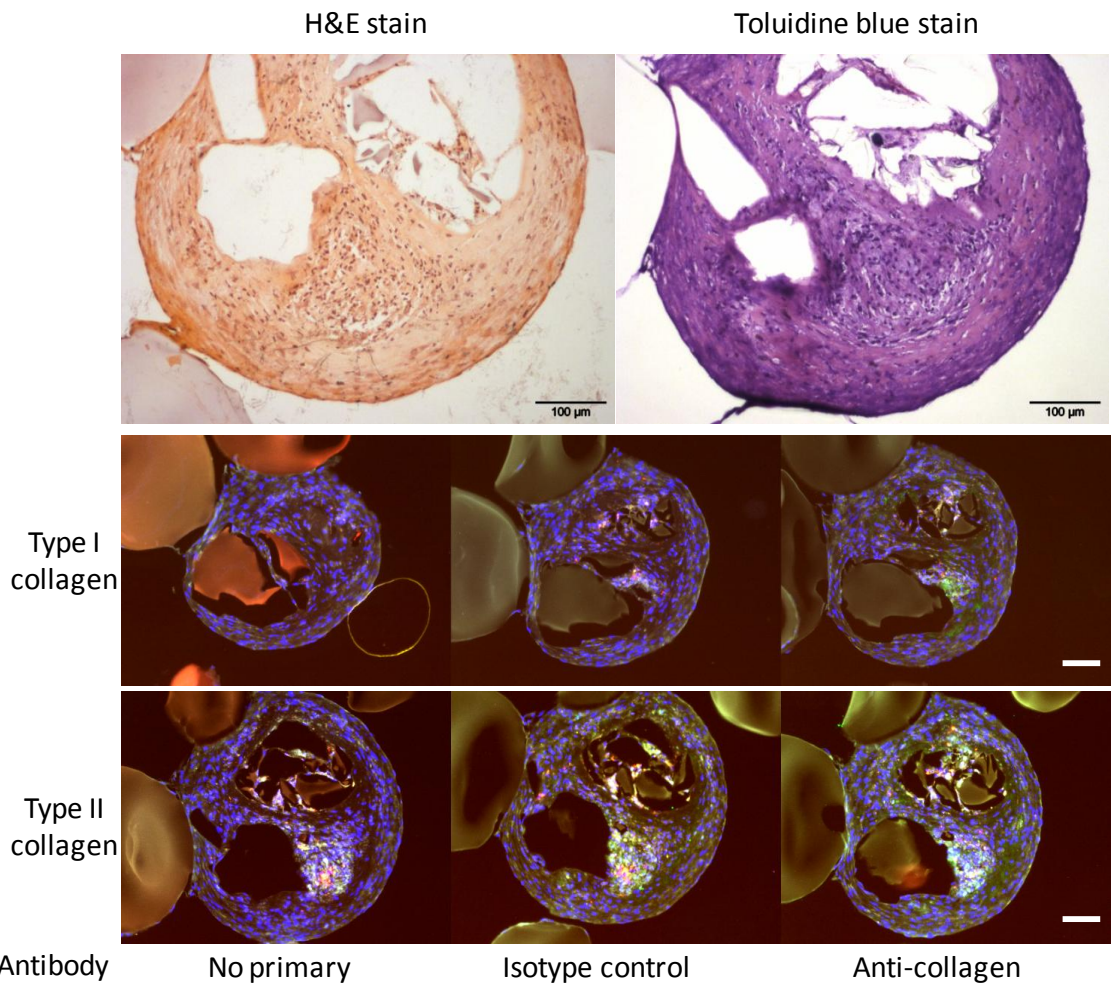
Figure 53 Analysis of ECM production in cell aggregates on 273kPa microcarriers

H&E staining demonstrated an organised cellular struture. Metachromatic toludine blue staining indicated the presence of a sulphated GAG matrix indicating the formation of zonal compartments with different ECM properties. Immunocytochemistry demonstrated collagen type I and II colocalised within the middle/sleep zone (Scale bar 100μm)

4.15 Comparisons with other microcarriers

Traditionally, microcarriers are used for the expression of therapeutic antibodies and proteins. Therefore to assess the ability of the developed microcarriers to sustain cell growth and biological function we compared our newly developed microcarriers alongside four commonly used commercially available equivalents with a range of properties (Appendix 1). Using a CHO cell line expressing a monoclonal antibody, we showed comparable levels of cell attachment and antibody production on our novel microcarriers. However optimisation is required to be competitive with commercially available microcarriers developed for CHO cell culture.

4.16 Discussion

Several synthetic hydrogels have been generated in an attempt to mimic the *in vivo* cell niche. It has been shown that presenting cues derived from the ECM can improve cell growth, intracellular signalling and differentiation (217). To incorporate elements of the ECM hydrogels have been modified to contain chemical, mechanical and topographical cues. PEGDMA hydrogels are bio-inert and lack any cell-adhesive cues (240). Several peptides have been used to functionalise PEG hydrogels and increase MSC attachment (Chapter 1 Figure 3). In addition several key studies have investigated the effect of mechanical compressibility in influencing stem cell differentiation (189, 271, 306). However there is conflicting reports in the literature over the precise factors that influence stem cell growth and behaviour (308, 344, 345). This is most likely due to intrinsic material properties influencing cell behaviour. In addition, studies have often probed the effect of an individual cue (e.g. peptide ligand) on cell attachment.

Previously the literature largely investigated the effects of biomaterial substrates on the culture and differentiation of human BM-MSCs. However, BM-MSCs have been shown to possess a different differentiation potential to ADSCs (355). Using the bioinert microcarriers developed herein, the chemical and mechanical properties can be finely tuned independently of one another to systematically assess the effect of adhesive peptide, peptide concentration on ADCS attachment and the effect of compressibility on differentiation. To develop microcarriers for ADSC expansion it is important that the expanded cells maintain their characteristics including multipotent potential. The effects of microcarrier properties on MSC attachment and differentiation were initially assessed in static culture.

4.16.1 Optimisation of cell attachment to microcarriers in static culture

The initial probability of cell microcarrier binding events is random, and is largely dependent on cell proximity to the microcarrier surface. In optimum conditions, the ratio of cells to microcarriers should be high enough to permit cell adhesion to all microcarriers.

As the microcarriers are neutrally charged, initial attachment to the microcarrier is reliant on cells contacting microcarriers long enough to form an interaction. As microcarriers and cells are both in suspension, any decrease in culture volume should

increase the probability of cell to microcarrier contact. The result of this investigation confirmed this hypothesis, as reducing the culture volume increased cell attachment. Initially cells were inoculated with microcarriers containing 3mls of medium, this showed total cell adhesion to 5-10 cells per microcarrier. A549 cells typically have a 'cobblestone' appearance. In TCP, A549 epithelial cells do not assume this morphology until over 50% confluent, when cell-cell contacts and small colonies are formed. It was observed that after several days in culture, the expansion of A549 cells onto microspheres in 3mL of medium had not occurred. However, cells cultured in 500µL of medium had $1/6^{th}$ less volume for movement, which was reflected in an increase in cell binding, and spreading of cells was observed. There was however a lower limit on this effect. Consequently the same microcarriers and cells density cultured in 150µL of medium resulted in a meniscus forming inside the well. Attachment to microcarriers at the edge of the well was increased. However, several microcarriers remained in the centre of the well and dehydrated preventing any cell attachment. For future experiments the lower threshold was set at 250µL, which is sufficient to cover the base of a well in a 24 well plate, preventing the hydrogel microcarriers drying out.

4.16.2 Comparison of cell seeding densities on the rate of initial cell attachment

After inoculation, cells attach to microcarriers in a random fashion and the number of adhered cells per microcarrier can be predicted using Poisson distribution (356). In optimum conditions, the ratio of cells to microcarriers should be high enough to permit cell adhesion to all microcarriers. It has been suggested that a minimum average of around 5-6 cells per microcarrier is optimum for charged microcarriers (356, 357)and it is predicted that the amount of microcarriers without any cell adhesion would be less than 1%. The rate of cell adhesion to uncharged microcarriers would be predicted to be slower (358), dependent on cell lines, microcarrier size and composition (358), and so the initial seeding densities were determined experimentally for the microcarrier system herein.

From our results it was clear that there is an upper limit to the system. Not all cells adhered to the uncharged microcarriers upon initial seeding into the cell culture vessel, leaving many cells unattached in the medium. This led to the formation of cell aggregates. It is well established that when adherent cells fail to bind to a solid growth support they undergo apoptosis (anoikis) (359). If this occurs in microcarrier culture toxic metabolites can be released into the culture medium, impeding the growth rate of

the culture. Based on our results, an optimum cell seeding density of 2.5 x 10^4 cells per 24 well plate was chosen. This gives an approximate ratio of 69 cells per microcarrier, much higher than any other reported in the literature.

4.16.3 Peptide incorporation effect on cell attachment

Several peptides have previously been used to render hydrogels bio-adhesive for MSC adhesion (chapter 1 Figure 3). However there is some controversy within the literature regarding the optimum adhesive peptide and peptide concentration required for MSC attachment and differentiation. For example, IKVAV and RGD modified surfaces have been shown to promote adhesion and spreading of ADSCs to polycaprolactone surfaces (347). Frith et al. (2012), also showed human MSCs bound to IKVAV and YIGSR functionalised on polystyrene-block-poly(ethylene oxide)-copolymer surfaces, however the cells failed to spread and remained rounded (360). This possibly represents a species specific difference in adhesion, but could also be due to the mechanical or topographical properties of the material which are not detailed in the study.

Adhesive peptide concentration is known to effect cell growth, migration and differentiation (344). Yang *et al.* incorporated RGD at a concentration of 0.025, 1.25 and 2.5mM into PEG hydrogels and showed an increased in human BM-MSC osteogenic differentiation corresponding to increase RGD concentration (308).

Several peptides (namely cRADfC, cRGDfC, IKVAV, and YIGSR) were incorporated into PEGDMA 'flat' hydrogels to assess ADSC attachment. Qualitatively, cell attachment was highest on IKVAV modified hydrogels, however cell distribution was inconsistent across the surface of the hydrogel. PEGDMA, a known non-cell adhesive biomaterial, showed some attachment to a small area of the gel. It was postulated that this was due to a topographical change in the gel surface, which possibly occurred during gel manufacture (handling). The nonsense peptide cRADfC was incorporated to assess whether cell attachment to the hydrogels was peptide specific (as it is not recognised by cell surface integrins). Very little attachment was observed to YIGSR and RADfC gels. This concurred with results by Santiago *et al.* who demonstrated ADSCs could not bind YISGSR functionalised polycaprolactone surfaces. ADSC attachment showed the formation of cell colonies on cRGDfC 0.35mM hydrogels. To isolate MSCs from biological samples, MSCs are routinely seeded at very low cell densities, to produce colonies of highly proliferative cells. Therefore it was

hypothesised that initial cell adhesion was low to 0.35mM RGDfC modified hydrogels due to the concentration of adhesive RGD ligand.

To explore the effect of RGDfC concentration on ADSC attachment several flat hydrogels were produced containing a range of RGDfC concentrations (0.35, 1 and 2mM). Flat PEGMDA hydrogels were generated using an optimised technique to try and standardise cell surface binding area. In addition the size of the gels was increased to make handling easier. This prevented the top of the gel being contacted during handling, which could potentially alter the surface topography. As visualised using immunocytochemistry, PEGDMA gels showed limited attachment cell spreading. ADSC attachment increased as peptide concentration increased from 0.35mM to 2mM. Colony-forming units were still observed on 0.35mM cRGDfC hydrogels. However this was not observed on 1mM or 2mM hydrogels which showed even attachment. This differs from literature reports, for example Liu et al. (2012) generated a PEG hydrogel containing an RGD gradient (0-0.25mM) using microfluidics and observed an RGD concentration of 0.107–0.143 mM showed the maximum rat BM-MSCs attachment (361). This could show specific differences in adhesion to the RGD peptide.

The microcarrier topography can influence cell attachment. Therefore all peptides (cRADfC, cRGDfC, IKVAV, and YIGSR) were incorporated into microcarriers (at three concentrations, 0.1, 0.35 and 1mM). Cell attachment and proliferation was monitored over 7 days using the Prestoblue viability assay. Attachment to microcarriers containing the cRGDfC peptide was consistently high in all three concentrations, with the highest cell attachment and growth was observed on (1mM) microcarriers. Contrary to cRGDfC functionalised flat hydrogels, no cell colonies were observed on microcarriers at any RGD concentration. Despite showing high attachment on flat gels, IKVAV showed a peptide dependent increase in cell attachment, however, when incorporated into microcarriers ADSC attachment and proliferation (at any concentrations) did not match that of RGDfC. Visualisation of cell attachment by SEM and phase contrast microscopy reiterated these This concurs with previous research as RGD modified Polyethersulfone (PES) surfaces have shown to promote adhesion of ADSCs (362).

Microcarriers containing the highest level of attachment after 7 days (cRGDfC 1mM) were analysed further to assess the intracellular cytoskeleton organisation. Organised stress fibers and microtubules were observed. In addition, cell viability was

visualised using a LIVE/DEAD assay, which showed viable cells attached to the microcarrier surface.

The 1mM RGDfC microcarrier was selected to probe the influence of compressive moduli on cell attachment and differentiation. It was hypothesised that peptide concentration and substrate compressibility act synergistically. Ideally, all peptides, in particular the IKVAV peptide would also be taken forward. However due to cost and time restrictions we focussed on the single peptide that showed the highest adhesion and proliferation over seven days in static culture (cRGDfC). Future work would attempt to generate an array microfluidic system to produce microcarriers with a combination of properties (Discussed further Chapter 6).

4.16.4 Substrate compressive moduli effects microcarrier aggregation and differentiation.

Effective MSC differentiation has been extensively studied, and to date has largely focused on developing optimum medium compositions. Previously instructive biomaterials have also been used to direct MSC differentiation, and have found differentiation into lineage specific cell differentiation when cells are cultured on substrates with similar elastic modulus of tissues *in vivo*. Seminal research conducted by Engler *et al.* has shown MSCs demonstrated lineage specific differentiation when cultured on substrates with similar elastic properties to the native counterpart *in vivo*. For example, MSCs differentiated into neurons, myocytes or osteocytes when cultured on neural, (0.1-1kPa), muscle (8-14kPa) and bone (27-40kPa) respectively.

In this study ADSCs were cultured on RGDfC (1mM) microcarriers with a compressive modulus of either 8kPa, 155kPa or 273kPa. After 5 days in culture, ADSCs adhered to all three microcarrier types. As changes in matrix properties are modulated by the actin cytoskeleton, phalloidin staining (which selectively binds F actin) was performed. A pronounced cytoskeleton and cell spreading was observed on all microcarrier types. However, Engler *et al.* demonstrated an elongated MSC phenotype on substrates with a modulus of 11kPa. Differences seen in this study could be due to the influence of RGD peptides and/or surface curvature of the microcarriers.

RT-PCR analysis was performed to demonstrate if the compressive properties of the microcarrier primed ADSCs to differentiate into a specific lineage. An upregulation of aggrecan, an early chondrogenic differentiation marker was observed on all

microcarrier types. The expression increased in concordance with compressive modulus, with a 700 and 1323 fold increase in 8kPa and 273 kPa respectively. It has been shown that cells can differentiate into lineage specific cells as a direct result of changes in matrix elasticity to resemble native counterpart tissues. The compressive modulus for articular cartilage has been reported to be 314kPa (363). This could potentially explain the increase in aggrecan expression.

To assess the effect of substrate compressibility on ADSC differentiation, cell-laden microcarriers were transferred to either adipogenic, osteogenic or chondrogenic induction medium in static culture, i.e. the culture was not stirred or agitated. The microcarriers generated have a low density, they can settle but are easily placed into suspension (a requirement for future bioreactor experiments). Cell-laden microcarriers began differentiation culture as discrete spheres, distributed randomly within a tissue culture well. Interestingly, after 14 days in differentiation media, microcarriers formed large multi-microcarrier aggregates. The extent of aggregation varied between microcarriers with different compressive moduli and differentiation induction media, despite starting from the same population of microcarriers. For example, 273kPa microcarriers remained relatively sparse after adipogenic differentiation and was significantly more aggregated in osteogenic and chondrogenic differentiation conditions. This appeared to be a microcarrier compressive modulus specific response, as opposed to a result of adipogenesis, as 8kPa microcarriers clustered into three islands under identical adipogenic culture conditions. A lack of aggregation was observed on 155kPa microcarriers under any differentiation induction conditions, whereas aggregation occurred in every condition on 8kPa microcarriers. It was postulated that microcarriers within the incubator may have been disturbed, for example during opening and closing of the incubator door, or alternatively during regular medium changes. Cell to cell adhesion may have occurred between adjacent settled microcarriers as a result of microcarrier collisions, and hence resulting in the microcarriers aggregating.

MSCs can be easily differentiated into adipocytes and therefore hold great potential for adipose tissue engineering. However the uses of MSCs are limited due to the reduction in adipogenic potential after conventional *ex vivo* expansion on tissue culture plastic. Adipogenesis of cell laden microcarriers in static culture resulted in aggregates forming in all microcarrier compositions. Typically cell proliferation is restricted after the addition on adipogenic induction media, however high cell densities

were observed at interstices within microcarriers. It was postulated this was a sight for ECM matrix accumulation, resulting in cell migration. Chen *et al.* have demonstrated that effective MSC adipogenesis was influenced by high cell densities (254). RT-PCR demonstrated the expression of the FABP4 gene (a marker for early adipogenic differentiation) was upregulated in the in all cultures. Compared to endogenous controls, a 106,000 (8kPa) to 147,000 (273kPa) fold increase in gene expression of FABP4 was observed. Immunocytochemistry results reiterated RT-PCR data which showed differentiated adipocytes over the entire surface of the 8kPa microcarrier surface, whereas adipogenesis was concentrated to interstices in 155kPa and 273kPa microcarriers. It is currently impossible to quantify the precise number of cells within a population that effectively differentiate from an MSC into an adipocyte. However FABP4 expression showed a higher fold increase in gene expression when compared to cells cultured in monolayer culture on tissue culture plastic.

ADSCs cultured on microcarriers with a range of compressive moduli underwent osteogenesis as observed from calcium staining using alizarin red. As compressive modulus increased, the positive staining was more isolated to interstices and areas concentrated in cells Engler *et al*. showed osteogenic differentiation of MSCs was higher on 25-40kPa hydrogels (compared to 8kPa). Osteogenesis was confirmed by RT-PCR analysis which demonstrated an upregulation of RGC32 gene expression (an osteogenic marker) on cells cultured on all three microcarrier types, the highest fold increase was observed on 8kPa microcarriers. Osteogenic media is supposed to limit cell proliferation, however after differentiation on 273kPa microcarriers, cells covered microcarrier aggregates in a sheet-like appearance, which was not observed on the other microcarrier types. Previous studies have shown BM-MSCs encapsulated within PEGDA hydrogels showed an increase in osteogenic markers in response to increasing RGD concentration from 0 to 2.5mM (308), indicating cRGDfC concentration could influence differentiation. Future work would investigate the effect of RGDfC peptide concentration on osteogenesis.

Chondrogenesis does not occur effectively in monolayer culture, as cells require a 3D environment for efficient differentiation. The standard method to promote MSC chondrogenesis is pellet or micromass culture whereby cells are seeded in droplets containing high cell densities (~8x10^6 cells/mL). Therefore to promote chondrogenesis in biomaterials, MSCs are often encapsulated within a hydrogel matrix (345). In a study by Toh *et al.* an increase in chondrogenesis, measured by ECM secretion, of hyaluronic

acid based hydrogels was higher on decreasing crosslinking density (increasing in mesh size) and decreasing compressive modulus (~6kPa) (364).

Several tissue engineering strategies are currently being developed to replace damaged articular cartilage; as the tissue has limited capacity for self-repair due to avascularity and low cellular mitotic activity. Current methods are unable to restore native structure of cartilage. Chondral lesions can arise from trauma or disease, and often becomes progressively deteriorated leading to osteoarthritis (365).

Several studies have demonstrated the generation of cartilage-like tissue using MSCs and chondrocytes on cells encapsulated within biomaterials, in particular PEG-based hydrogels (190, 245). However, one of the key unresolved challenges in cartilage tissue engineering is the inability to generate tissue that replicates the highly organised zonal structure of articular cartilage, in particular the spatially distinct regions containing varying ECM compositions and mechanical properties. Generating cartilage that mimics the zonal spatial organisation of articular cartilage is essential for generating a clinically effective transplant for tissue engineering treatments (366). Four zones exist, the superficial, transitional (middle), deep, and calcified zones (Figure 54). The ECM contained within these zones is responsible for providing the cartilage with its physical properties. For example, hyaline cartilage contains an ECM rich in type II collagen and proteoglycans, which aids the material elasticity. Directing a single stem cell population to differentiate into different zonal phenotypes within a single 3D structure presents a major challenge in cartilage research. The ability to accomplish this would be advantageous in providing alternative, native-like cartilage replacements, which would eliminate the need for donor tissues.

ADSCs cultured on microcarriers containing a range of compressive moduli could spontaneously migrate to form large multicellular aggregates (or pellets) when placed in chondrogenic differentiation media. This effect was moduli specific, as cell aggregation varied on microcarriers with different properties. For example, 8kPa microcarriers generated large microcarrier aggregates, where cells spontaneously migrated from monolayer culture on the microcarrier surface to form a condensed network of cells between microcarriers. On 155kPa microcarriers, few microcarrier aggregates formed resulting in small cell pellets, as contributing cells were derived from a single microcarrier. 273kPa microcarriers also formed multi-microcarrier aggregates, however unlike on 8kPa microcarriers, cells from multiple microcarriers migrated to

form one large rounded pellet, which was simultaneously anchored to several microcarriers. In every condition very few cells were observed on the microcarrier surface after chondrogenesis, indicating pellets were comprised of migrated cells rather than newly proliferated cells.
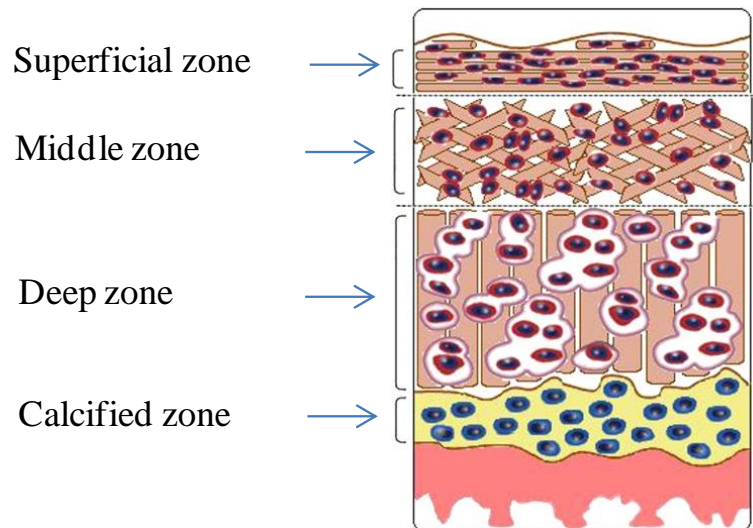
Figure 54 Schematic representation of zonal compartments within Articular cartilage

Articular cartilage is organised into zonal compartments with varying cell architecture and matrix properties. A superficial zone comprising of densely compact cells aligned parallel to the cartilage surface. A middle zone transitioning to a deep zone as intracellular space increase and is filled with ECM matrix. Adapted from (353).

Cells pellets generated on 8kPa and 273kPa microcarriers differentiated into structures resembling the superficial, transitional, or deep zones of articular cartilage, as observed by H&E staining. It was postulated that the highly unusual formation of multi-cellular pellets from monolayer culture was a result of ECM secretion. PEGDMA hydrogels have been shown to be resistant to protein absorption onto its surface. As matrix proteins are unable to bind to the microcarrier, they could be deposited onto cells, in particular on cells within microcarrier interstices, and hence provide a scaffold for cell adhesion. As cells migrate towards the ECM (either by sensing a chemical or mechanical gradient) more matrix proteins are secreted, further supporting the structure, and resulting in the pellets becoming more architecturally organised. As this is the first instance of this being reported in the literature, future work would quantify ECM protein secretion from the medium.

Histology and immunochemistry confirmed the production of cartilage specific proteins in 8kPa and 273kPa hydrogel microcarriers. Zonal regions were highlighted by

toluidine blue staining, which demonstrated spatially distinct areas with varying degrees of sulphated glycosaminoglycans. Collagen type I and II was expressed throughout the 'middle or deep' zone within cell aggregated on 8kPa microcarriers. Collagen type I is constitutively expressed by multipotent MSCs, however only after cells have undergone chondrogenesis do they express Collagen type II (367), indicating pellets formed from 8kPa and 273kPa microcarriers effectively underwent chondrogenesis. This was unexpected as 8kPa microcarriers have a relatively lower compressive modulus than that of articular cartilage. However, Park *et al.* have shown that MSCs had an increased expression of collagen type II after chondrogenesis on substrates with 1kPa than 15kPa (368). In addition, chondrogenesis has been shown to be inhibited by RGD when BM-MSCs were encapsulated with Alginate hydrogels (369).

RT-PCR confirmed the findings from histology and immunohistochemistry analysis and revealed that aggrecan, (an early chondrogenic marker) was upregulated (approximately 100 fold) in all microcarrier types, when normalised to multipotent controls cultured in monolayer on tissue culture plastic. However, prior to the addition of chondrogenic differentiation media, aggrecan expression was upregulated by 1000 fold increase in expression. This indicates aggrecan was actually downregulated after the introduction of chondrogenic differentiation media. This is likely due to aggrecan being transiently expressed in MSCs during chondrogenesis, were expression is upregulated in the first week and decreases significantly in the second and third week of differentiation (370). In addition, Mwale *et al.* found aggrecan was constitutively expressed in human MSCs in monolayer culture prior to chondrogenic differentiation (371). In this study this was not observed in ADSCs cultured in monolayer on tissue culture plastic. However this could provide an explanation for ADSCs cultured on microcarriers.

Directing the differentiation of a single stem population into spatially organized native-like articular cartilage has not yet been reported. Our ability to tailor the culture conditions and environmental signals through biomaterial compositions could allow for directed differentiation of a single stem cell population into the various zonal phenotypes of articular chondrocytes. The resulting chondrocytes should have the capability to produce zone-specific ECM and consequently possess spatially varying mechanical properties that are similar to native articular cartilage.

4.17 Conclusion

In summary, ADSCs bind and proliferate on RGDfC and IKVAV modified microcarriers, and not YIGSR. In addition cells adhered to microcarriers with a range of compressive moduli (8, 155 and 273kPa) and were capable of differentiating into adipocytes, osteocytes and chondrocytes. RT-PCR and immunohistochemistry data showed adipogenesis and osteogenesis was higher on 8kPa microcarriers. Spontaneous cell aggregation was observed on microcarriers which showed moduli specific differences. Immunocytochemistry showed 8 and 273kPa microcarriers induce differentiation of MSCs into chondrocytes that match specific zones of articular cartilage which expressed Collagen types I and II. Overall, the microcarriers developed herein are capable of sustaining cell adhesion and growth whilst remaining multipotent. Further work would attempt to expand ADSCs on RGDfC microcarriers at 155kPa.

5.0 ADSC expansion on novel microcarriers in spinner flask bioreactors

5.1   Introduction

Mesenchymal stem cells are located in several tissues in the body, such as bone marrow, fat and muscle, however the populations are largely dormant and present in small quantities. To use MSCs for clinical purposes, such as tissue engineering or cell-based therapies, large cell quantities are required (372).

Conventionally, MSC expansion is performed in 2D monolayer culture on tissue culture treated plastic flasks. However, this format has limited surface area available for cell expansion, and hence requires extensive handling for numerous cell passages and medium refreshments. This method is both labour intensive and increases susceptibility to contaminations. Furthermore, cultures cannot be monitored or controlled, resulting in suboptimal culturing conditions and low productivity. Therefore, strategies are required to isolate MSCs and expand to (tens of) millions of cells in a controlled, cost-effective, and reproducible way. Currently, extensive research is being performed on the development of bioreactors as they are highly productive, easily scalable and culture conditions can be closely monitored (373). As MSCs are anchorage dependent, to maximise expansion in a bioreactor a large surface area is required (373, 374). Microcarriers provide a large surface area for cell growth and proliferation, and have been extensively studied for the expansion of cells in spinner flasks.

In a typical bioreactor system, microcarriers are placed in growth medium, after which, cells are inoculated and allowed to bind and grow on the surface of the microcarriers. The culture is maintained with moderate stirring to keep the microcarriers in suspension and to increase nutrient and oxygen transfer throughout the medium, providing an easily controllable, homogeneous growth environment (375, 376). Within a given bioreactor, the binding affinity of cells to the microcarrier surface will depend on the cell line, the microcarrier characteristics (including charge, composition and size), the medium composition, and the cell loading per microcarrier (377). The initial rate of cell adsorption onto the microcarrier can also be influenced by bioreactor design, including the bioreactor material, capacity, inoculum density and rate and type of culture agitation. The optimum parameters vary between different cell types and bioreactors used. Consequently, the conditions that effect cell attachment, distribution on the surface of microcarriers (including growth rate) must be identified and optimised for a particular system.

Microcarrier culture within spinner flask bioreactors has previously been used to expand MSCs (113, 378). Most studies have used charge as the primary means of cell attachment to microcarriers. However, charge is undesirable in MSC expansion as cell retrieval can be difficult, reducing the final cell yield. In addition, charged microcarriers rely on animal serum for cell attachment and positive charges have been shown to effect cell spreading and differentiation (379). Few studies have expanded MSCs on charge neutral microcarriers within spinner flask bioreactors (like those developed herein) where attachment is dependent on integrin interaction. At the time of writing, MSCs have not been expanded on a synthetic tunable microcarrier substrate. The aim of this work was to test whether the optimised novel synthetic microcarriers were capable of supporting ADSC attachment and expansion in a stirred culture system while maintaining the characteristic immunophenotype and multipotency differentiation potential. To achieve this, the bioreactor design, cell seeding density and stirring regime were optimised to increase ADSC expansion.

5.2 ADSC expansion on novel microcarriers

To assess the expansion potential of ADSCs on novel microcarriers (155kPa 1mM cRGDfC), ADSCs were seeded directly into three spinner flasks at a density of 5,000 cells/cm^2 (12,667 microcarriers in 30mLs of medium) and cultured for 7 days. The microcarrier culture was stirred intermittently (for 1 minute every 45 minutes) at a low rpm (21rpm) for the life span of the culture. Partial media changes (50%) were performed every three days. During the cultivation of ADSCs on microcarriers, growth was monitored over time in triplicate using a Prestoblue cell viability assay (Figure 55). The microcarriers were agitated to create a homogenous solution and removed using a pipette from at least two different positions and analysed in triplicate daily. As this process potentially yields different quantities of microcarriers cell viability was normalised to microcarrier number assessed *via* microscopy. A cell viability assay was preferred to cell counting as this enabled more samples to be analysed, did not require cells to be removed from the microcarrier (removing error from inefficient or incomplete detachment). In addition, the assay was not affected by any detached dead cells (380).

A general trend of increasing cell proliferation over time was observed in each culture, with a temporary decrease in viable cells at 120 hours (Figure 55). As this reading was taken before a scheduled partial media change (which took place every 3 days), a lack of nutrients or an accumulation of toxic metabolites could have potentially restricted cell growth. As the number of viable cells increased in each condition (normalised to microcarrier number), standard deviation also increased indicating variability within the culture. From bright-field images (Figure 56) it was observed that whilst some microcarriers were fully colonised by cells, others had little to no cell attachment. In addition, after 7 days cell aggregates had formed within microcarrier interstices. A final cell density could not be accurately established as cells contained within interstices could not be fully dissociated from one another.
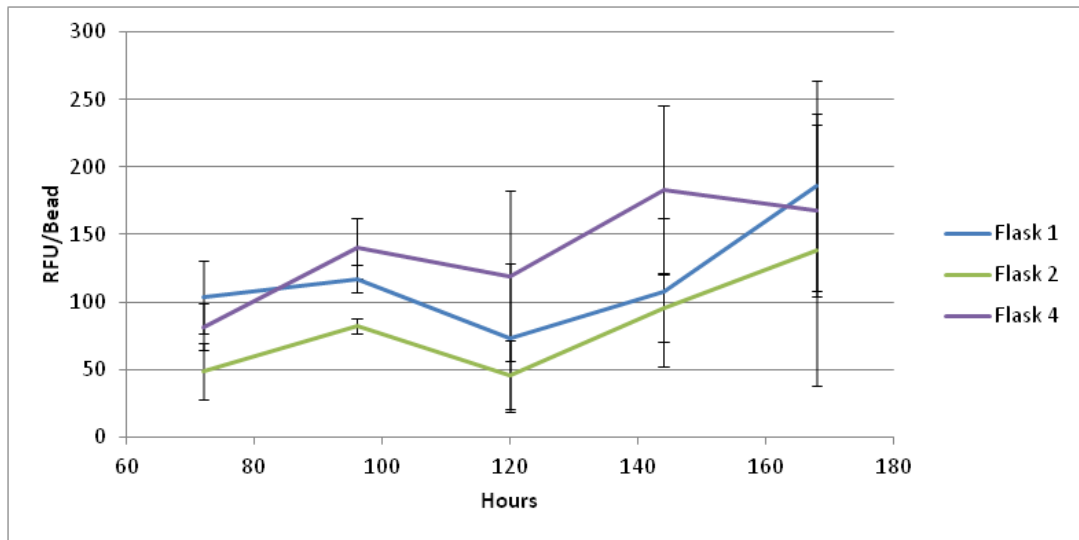
Figure 55 Prestoblue cell viability assay

Growth of ADSCs on microcarriers was monitored over time in triplicate using a Prestoblue cell viability assay. Cell number increase over time was observed in each culture, with a temporary decrease in viable cells at 120 hours.
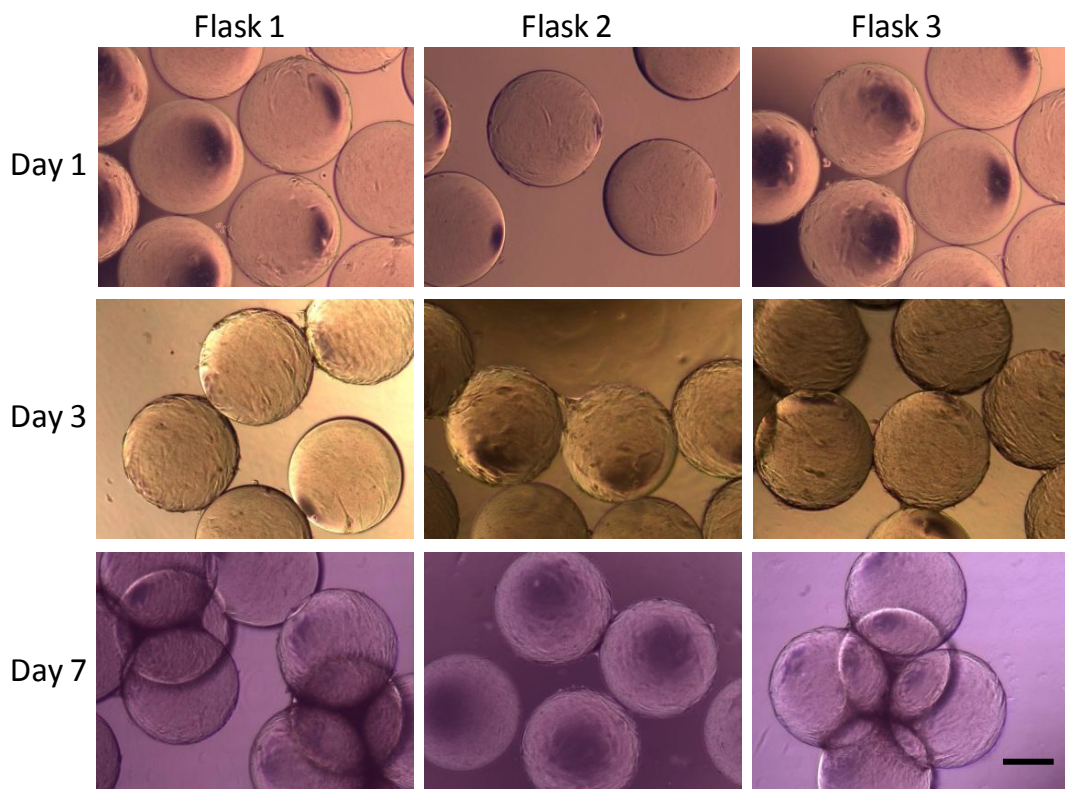
Figure 56 Brightfield microscopy of ADSC bound microcarriers grown in a stirred bioreactor.

Cell attachment to microcarriers was observed after 1,3, and 7 days. Binding and growth appeared inconsistent, with the ADSCs accumulating within microcarriers interstices at day 7 (Scale bar 250μm).

5.3   Morphological analysis

In stirred suspension microcarrier cultures, the distribution and morphology of ADSCs during cell adherence and proliferation was shown by inverted bright field microscopy (representative images are shown in Figure 56). Cell attachment to microcarriers was observed after 24 hours in culture and cells demonstrated a partially rounded morphology. Few unattached cells could be observed in the medium. On day 3, cell colonisation of microcarriers increased, and attached cells appeared to have a flattened morphology. In addition, cell bridges were observed between adjacent microcarriers. After 7 days of cultivation, cells appeared to have reached confluency on many microcarriers. However this was inconsistent, as can be seen Figure 56, some microcarriers have little to no cell attachment. Microcarriers appeared to have aggregated with ADSCs accumulating within microcarriers interstices. The microcarrier culture was stirred intermittently for 7 days. However, the impeller speed was not sufficient to fully suspend the multi cell-laden microcarrier aggregates, which settled at the base of the spinner flask. Following this observation the culture was terminated on Day 7.

To probe the influence of the spinner flask culture upon ADSC attachment and spreading, the cytoskeleton organisation was examined after 7 days. The actin cytoskeleton was visualised using TRITC conjugated phalloidin, which selectively stains F-actin. After 7 days in culture, ADSC spreading was visualised on the microcarriers as shown in Figure 57. Analysis of the phalloidin stained F-actin cytoskeleton displayed well defined parallel stress fibres which were mostly stretched along the long axis of the cells. Phalloidin staining corroborated phase contrast images, showing a heterogeneous distribution of cells over the microcarrier population. For example, highly populated microcarriers were observed, in addition to 'unoccupied' microcarriers with no cell attachment. Contrastingly, many cell bridges connecting microcarriers could be observed, indicating bead to bead transfer.
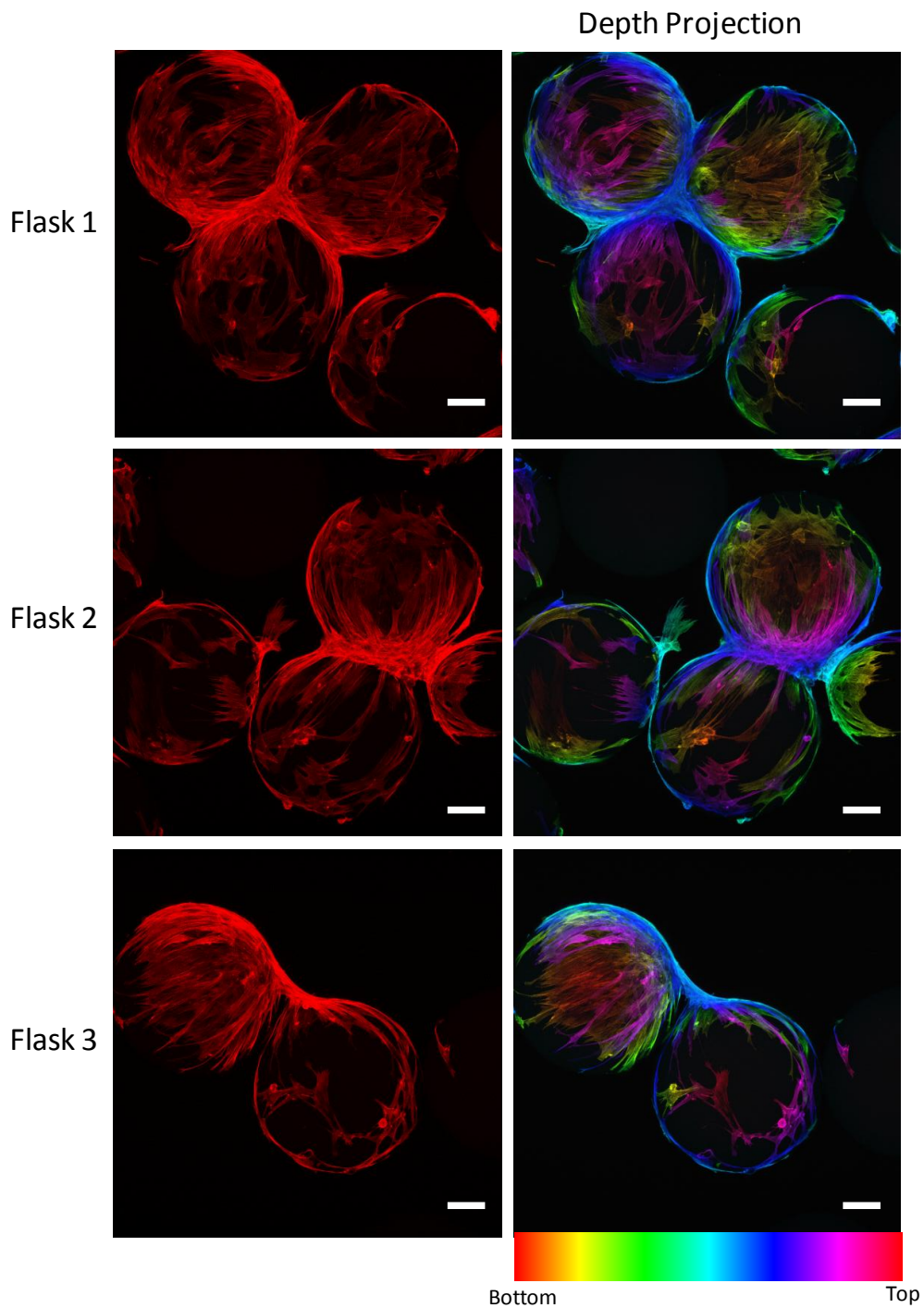
Figure 57 Visualisation of the actin cytoskeleton of ADSC cells grown on microcarriers in spinner flasks

Analysis of the F-actin cytoskeleton stained with phalloidin displayed well defined parallel stress fibers which were mostly stretched along the long axis of the cells. Images have been false coloured to allow depth perception of cells.

5.4   Expression of lineage-specific gene transcripts

Following the bioreactor expansion of ADSCs, quantitative RT-PCR analysis was used to detect the expression of mRNA transcripts associated with lineage specific differentiation. To determine whether microcarrier culture had an effect of priming ADSC differentiation to a particular lineage, RT-PCR analyses were performed for CD73, a marker for multipotency and three early differentiation genes: RGC32, FABP4, and Aggrecan (ACAN), which are early cell markers for osteogenesis, adipogenesis, and chondrogenesis, respectively and normalised to multipotent controls cultured on tissue culture plastic (Figure 58). Cell-laden microcarriers cultured in spinner flasks for 7 days revealed CD73 expression remained largely unchanged in the cultures, indicating multipotency remained. The expression of the chondrogenic-specific gene, aggrecan was upregulated in all three cultures. The upregulation was most pronounced in spinner flask 3 (a 259 fold increase), which also showed the highest total cell growth over 7 days. As discussed in Chapter 4 (Section 4.13), differentiation into chondrocytes was associated with a spontaneous aggregation of cells on the microcarrier surface to form a pellet like structure. As can be seen with phase contrast images (Figure 56), this was not observed on cells cultured on microcarriers after spinner flask expansion, where cells formed a monolayer on the sphere surface (with the exception of cells found in interstices). Low levels of the adipocyte-specific gene, Fatty Acid Binding Protein (FABP4) were detected, with a slight upregulation compared to control. However, this was not significant, as adipogenic induction in ADSC-laden microcarriers in static culture generated a 136,000 fold increase in FABP4 gene expression. Furthermore, phalloidin staining demonstrated spread cells with well-defined actin structures. This is atypical of adipocytes, which generally have a round morphology. In addition, an increase in the osteogenic marker RGC32 showed an upregulation with a maximum 4-fold increase in expression in flask 1. This indicates the cell population was heterogeneous.
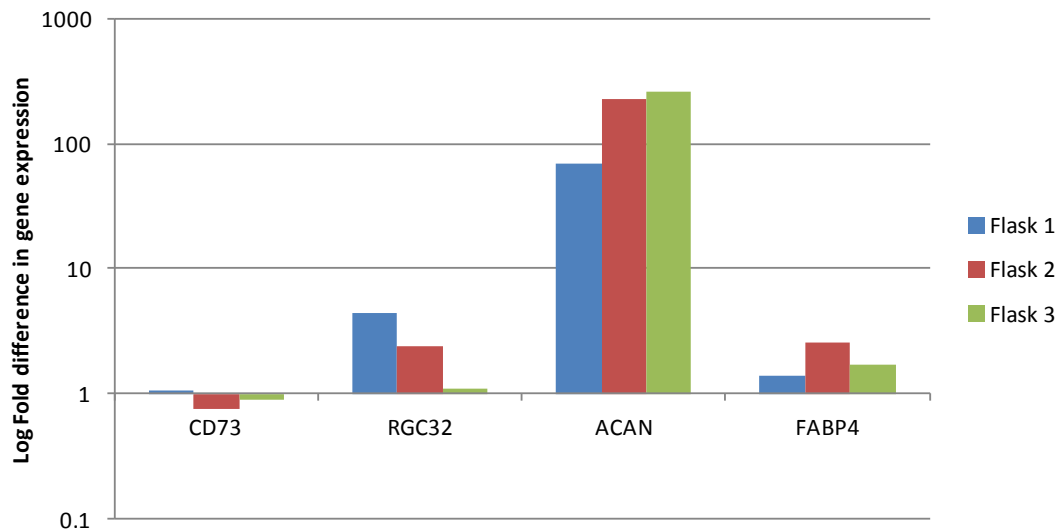
Figure 58 RTPCR analysis of ADSCs grown on microcarriers in spinner flasks.

Cell-laden microcarriers cultured in spinner flasks for 7 days revealed CD73 expression remained largely unchanged in the cultures, indicating multipotency remained. The expression of the chondrogenic-specific gene, aggrecan was upregulated in all three cultures.

5.5   Effect of cell seeding density on ADSC expansion

In order to increase ADSC expansion, the bioreactor conditions were optimised. In the previous experiment, as cell number increased in each culture, the standard deviation also increased. This indicates variability within the culture, in particular inconsistent cell seeding on microcarriers. To ensure a homogenous distribution of microcarriers and cells, and to prevent cells attaching to the top layer of settled microcarriers only, the intermittent stirring speed was increased from 21rpm to 60rpm. In addition, it was hypothesised that cell transfer *via* bead to bead transfer requires the microcarriers to contact for a sufficient amount of time as to allow cells to migrate from one microcarrier to an adjacent microcarrier. To maximise the probability of microcarriers contacting one another, cells and microcarriers were stirred intermittently for the entire lifespan of the culture. In addition, medium changes were increased from every three days to every two days, to replenish nutrients and remove potentially toxic metabolites from the culture.

In the first attempt to expand ADSCs on microcarriers, the cell seeding density was 5,000 cells/cm^2, as recommended by the suppliers of ADSCs (Invitrogen). This equates to approximately 35 cells per microcarrier. To increase the surface area available for expansion, microcarriers were seeded with ADSCs in spinner flasks at four

164

different seeding densities, 2236 cells/cm^2, 1183 cells/cm^2 394 cells/cm^2 and 131 cells/cm^2 (17, 9, 3 and 1 cells/microcarrier respectively) and cultured for 14 days. Cell number was measured on day 14, and cell viability was measured daily using the Prestoblue assay, and normalised to microcarrier number (manually counted by microscopy).

5.6   Analysis of cell proliferation of ADSCs on microcarriers

In stirred suspension microcarrier culture, cells seeded at the lowest density (131 cells/cm^2) demonstrated a small increase in viable cell numbers between 24-120 hours, followed by a phase of cell proliferation (120-366 hours) (Figure 59). ADSCs seeded at 394 cells/cm^2 also showed low amounts of viable cells until 72 hours, before steadily increasing and eventually reaching a maximum value at day 14. Cells seeded at 2236 cells/cm^2 generated slightly lower amounts of viable cells after 24 hours than was observed than cells seeded at 1183 cells/cm^2, however the total viable cells seeded at 2236 cells/cm^2 was higher after 14 days. Cells seeded at 1183 cells/cm^2 demonstrated growth after 24 hours. Overall, cell number was found to be highest on microcarriers seeded with ADSCs at a density of 2236 cells/cm^2. Over the culture period, viable cell numbers per microcarrier increased steadily in all four seeding density conditions. However, as viable cell numbers increased, variation in readings also increased. As multiple samples were analysed, and viable cell number was normalised to microcarrier number this indicated inconsistent colonisation of the microcarriers. The increase in viable cell number in stirred microcarrier cultures was also consistent with findings made using the inverted bright field images data, which showed an increase of colonisation (and inconsistency) of the cells during the cell culture period (Figure 61).
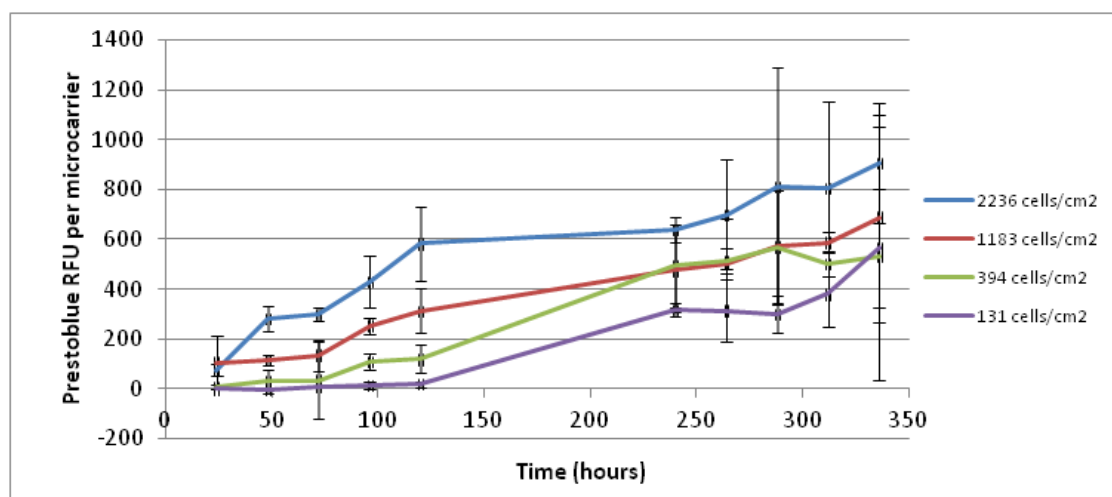
Figure 59 Prestoblue analysis of the affect of seeding density on population growth of ADSCs in stirred bioreactors.

Microcarriers were seeded with ADSCs in spinner flasks at four different seeding densities (2236, 1183, 394 and 131 cells/cm^2) and cultured for 14 days. Cell viability was measured daily using the Prestoblue assay, and normalised to microcarrier number (manually counted by microscopy).

Culture conditions	Initial seeding density (10^5 cells/mL) Based on 30mLs	Cells seeded	Final cell density (10^5 cells/mL)	Final cell number (10^5 cells/mL)	Fold increase	Population doubling	Doubling time
2236 cells/cm^2	7177.97	215339	0.73 ± 0.09	73.35 ± 0.09	34.06±0.44	5.09	50.57 ± 0.14
1183 cells/cm^2	3800	114000	0.7 ±0.009	56.07 ±0.009	49.18±0.89	5.62	46.30 ± 0.22
394 cells/cm^2	1266.67	38000	0.3 ± 0.01	31.21 ± 0.01	82.13±3.03	6.36	42.30 ± 0.29
131 cells/cm^2	422.23	12667	0.26 ± 0.08	26.30 ± 0.08	207.65±6.40	7.70	36.34 ± 0.18

Figure 60 Trypan blue viability assay analysis to determine affect of seeding density on expansion capacity of ADSCs in stirred bioreactors.

Microcarriers were seeded with ADSCs in spinner flasks at four different seeding densities (2236, 1183, 394 and 131 cells/cm^2) and cultured for 14 days. Cell number was measured on day 14 using the Trypan Blue assay. An inverse relationship between initial seeding density and both doubling time and fold increase in expansion is demonstrated.

To determine how many viable cells can be generated through microcarrier culture, cells were removed from microcarriers after 14 days in spinner flask culture and viable cells were counted using a Trypan blue cell viability assay. The increase in viable cells, as shown by the Prestoblue viability assay, was found to correlate to cell number (Figure 56). After 14 days of culture, the highest quantity of ADSCs was observed in

the culture seeded at the highest cell/microcarrier ratio at 2236 cells/cm^2, which reached a cell density of 0.7 ± 0.09 x 10^5 cells/mL, but corresponded to the lowest fold increase in total cell number of 34.06 ± 0.44.

A general trend of decreasing final cell density was observed as cell/microcarrier seeding ratio decreased. Contrastingly, the fold increase in expanded cells increased. For example, cells seeded at a lower seeding density of 131 cells/cm^2 expanded to a density of (0.26 ± 0.08) x 10^5 cells/mL, resulting in a fold increase of 207.65 ± 6.40 (Figure 56).

The doubling time of ADSCs has been shown to vary according to tissue culture media. In MesenPro RS (Invitrogen), a proprietary low FBS media, ADSCs have a doubling time of 36 ± 4hrs. However, ADSCs cultured in 'classical' medium comprised of DMEM and 10% FBS (as used in this study) have a doubling time of 54 ± 4hrs. During this study the doubling time of ADSCs decreased from approximately 50 hours in the highest seeding density to 36 hours in the lowest seeding density.

5.7   Microscopical analysis

The distribution and morphology of ADSCs during cell adherence and proliferation in the four different culture conditions was shown by inverted bright field microscopy (representative images are shown in Figure 61). Cell attachment to microcarriers was observed after 24 hours in culture, an even distribution of cells was observed on each microcarrier, and cells demonstrated flattened cell morphology. On day 7, cell colonisation of microcarriers increased and attached cells continued to have a flattened morphology. However, despite an even distribution of cells being observed after 24 hours, cell confluency on microcarriers appeared to be inconsistent across all conditions. From this two hypotheses were generated i) initial cell attachment was not even, and/or cell survival after initial attachment was inconsistent (possibly due to lack of cell-cell contact on microcarriers where few cells were attached) ii) the migration of cells from one microcarrier to another (bead-to-bead transfer) could only occur if cells were in close enough proximity to an adjacent microcarrier. If cell confluency was reached on a microcarrier, the ability of cells to transfer to a less confluent microcarrier could increase the surface area available for cell expansion. After 14 days of cultivation, visual inspection of the culture indicated many microcarriers appeared to have reached confluency. As initial cell seeding density increased, confluency appeared greater and

more even between the microcarriers. This was more consistent than seen in the previous attempt at 5,000 cells/cm^2, as can be seen Figure 61, where all microcarriers had some cell attachment. In addition, very few multi-microcarriers aggregates were observed.
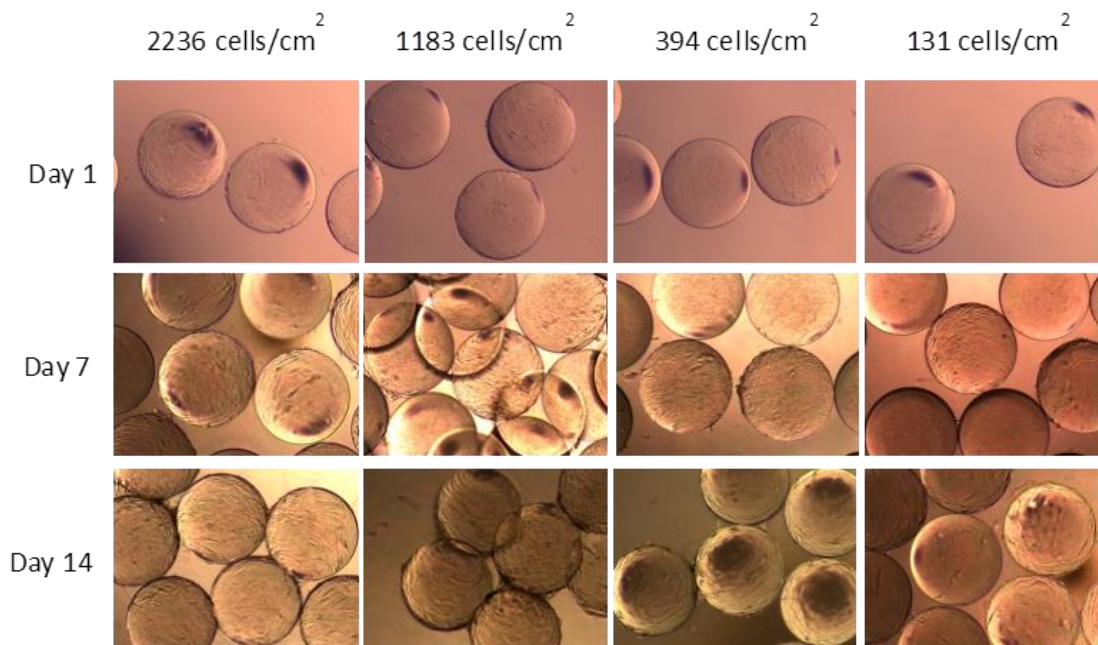
Figure 61 Brightfield microscopy of ADSC bound microcarriers grown in a stirred bioreactor from a range of seeding densities.

Cell attachment to microcarriers was observed after 1,7 and 14 days in culture. At early timepoints cell binding was observed on each microcarrier, and cells demonstrated flattened cell morphology. Despite an even distribution of cells being observed after 24 hours, cell confluency on microcarriers at later timepoints appeared to be inconsistent across all conditions

5.8   The effect of different seeding densities on the expression of lineage-specific gene transcripts.

To determine if differences in initial seeding density had an effect of priming ADSC differentiation, quantitative RT-PCR was performed to analyse gene expression of early differentiation markers (Figure 62). Cell-microcarrier constructs were removed from spinner flasks after 14 days and analysed. CD73, (a multipotency marker) expression was downregulated consistently (on average a 0.48 ± 0.06 fold decrease) in all four conditions compared to multipotent ADSC controls.

RGC32 (an osteogenesis marker) was upregulated in all four conditions, with cells seeded at 394 cells/cm^2 showing the highest increase (6.8 fold). As seen previously, aggrecan gene expression demonstrated a consistent upregulation across all

168

four conditions. Upregulation ranged from 372 to 572 fold, however no apparent relationship between expression and seeding density could be identified. However, this is noteworthy, as chondrogenic induction in ADSC-laden microcarriers in static culture generated a 1052 fold increase in Aggrecan gene expression.
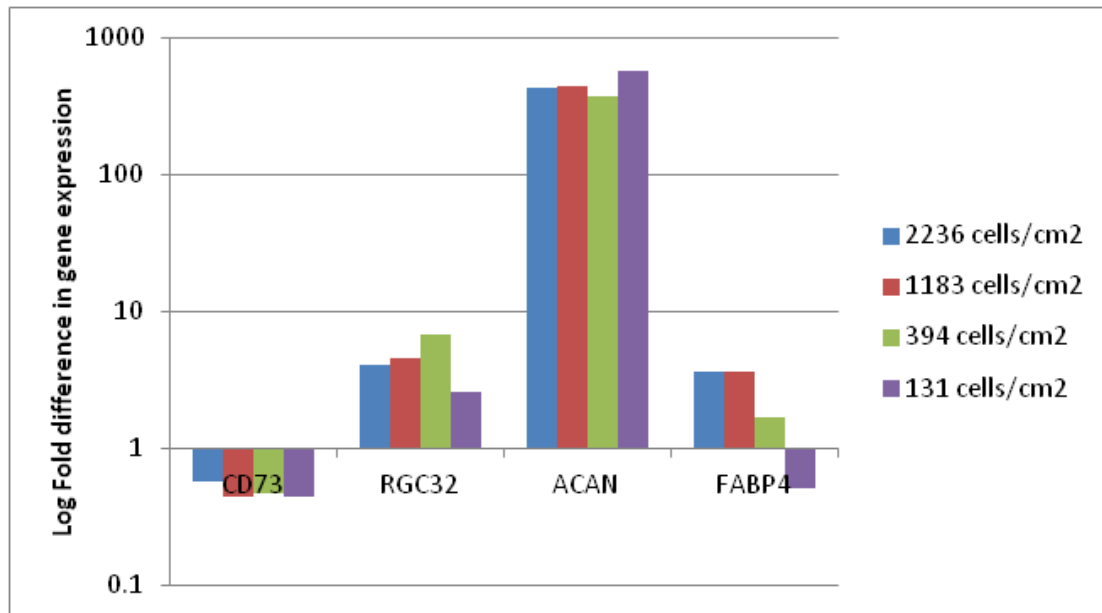
Figure 62 RT-PCR analysis of ADSCs grown on microcarriers within a stirred bioreactor from a range of seeding densities.

Cell-microcarrier constructs were removed from spinner flasks after 14 days and analysed for a range of markers. Although CD73 (multipotency), RGC32 (osteogenesis) and FabP4 (Adipogenesis) remained relatively unchanged, there was a large increase in the expression of ACAN (chondrogenesis).

FABP4 expression, an early marker for adipogenic differentiation was upregulated in the three highest seeding densities. At the two highest seeding densities, FAP4 expression showed an equal fold increase. At a lower initial seeding density of 394 cells/cm^2, expression was still upregulated, but with a reduced fold increase. Furthermore, FABP4 was downregulated in the flask containing the lowest initial seeding density of 131 cells/cm^2. It has previously been observed that adipogenesis is highest on microcarriers where there is a high cell density. As cell density was highest on 2236 cells/cm^2 this could explain the increased expression of early adipogenic genes.

5.9   Histological analysis

To assess the multipotency potential of spinner flask expanded ADSCs, cell-laden microcarriers from both experiments, i.e. after 7 days or after 14 days, were transferred to multi-well plates and maintained in adipogenic, chondrogenic, or

osteogenic medium for a further 14 days and analysed using histochemical analysis. Approximately 30 microcarriers per condition were visualised and approximately 5 images were taken, microcarriers appeared consistent across all conditions (representative images are in Figure 63).

Cell-laden microcarriers maintained in adipogenic induction medium demonstrated adipogenesis as evidenced by positive Oil Red O staining of lipid droplets. Microcarriers cultured in the presence of chondrogenic induction medium showed that cells formed spontaneous aggregates (similar to those observed in Section 4 Figure 52), that stained intensely with alcian blue (indicating a sulfated matrix). Microcarriers cultured in the presence of osteogenic induction media showed matrix mineralization with intense alizarin red staining (Figure 63).
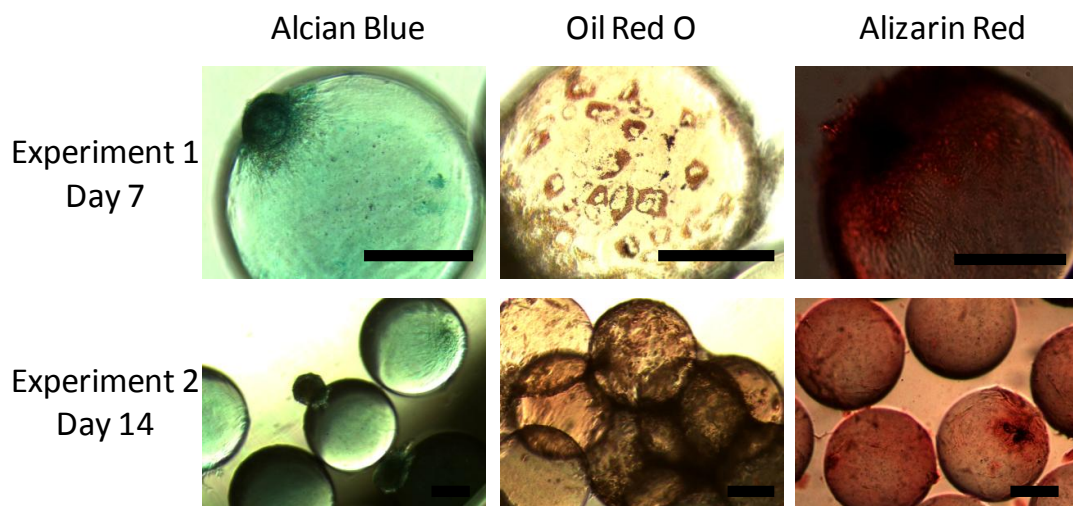
Figure 63 Histological analysis of cells driven into differentiation after 7 or 14 days growth on microcarriers in a bioreactor.

To assess the differentiation potential of ADSCs maintained on microcarriers within a bioreactor for 7 and 14 days, cell-laden microcarriers were placed into chondrogenic, adipogenic or osteogenic differentiation media for a further 14 days and stained for differentiation markers. ADSCs still retained the potential to differentiate into all three cell types.

5.10 Discussion

ADSCs are anchorage dependant, and therefore need to be attached to a surface for cell growth and expansion. Microcarriers are ideal candidates as they provide a large surface area to volume ratio. Several published reports detail the culture and expansion of MSCs on microcarriers and have demonstrated the resulting cell populations are multipotent, however have no increase in expansion compared to cells grown on standard 2D plastic. The published reports vary according to microcarrier composition, MSC type (species, source and method of isolation), bioreactor design and culture duration, making direct comparisons difficult, (Eibes *et al.*, 2010 (381); Frauenschuh *et al.,* 2007 (374); Hewitt *et al.,* 2011 (140); Malda and Frondoza, 2006 (128); Sart *et al.,* 2009 (378); Schop *et al.,* 2008 (113); Yang *et al.,* 2007 (167)).

Few of the reported studies used human MSCs, and the processes described were not suitable for the manufacture of cell therapeutics due to the reliance on animal products, both in the culture medium and microcarrier composition. In the development of GMP-compliant expansion protocols to generate cell therapies, Santos *et al.* (2011) made a significant improvement on previously published studies, reporting the expansion of human BM-MSCs and ADSCs in a xeno-free microcarrier system, with an 18-fold and 16-fold expansion respectively in 14 days (138). The microcarriers employed were plastic coated with CELLstart™ xeno-free substrate (a proprietary formulation, Invitrogen). However, they reported low seeding efficiencies, 23% (BM-MSCs) and 22% (ADSCs) respectively (and therefore low overall process efficiency).

In Chapter 4 it was demonstrated that novel synthetic microcarriers can support ADSC attachment and proliferation. To generate large quantities of cells, microcarriers are cultured within stirred bioreactors, such as spinner flasks, which use an impeller to mechanically agitate the culture volume. This creates a homogenous environment, and facilitates the transfers of nutrients and diffusion of gases throughout the culture volume, ultimately yielding increased cell growth. In addition to increasing cell number, microcarrier systems must generate a homogenous population of ADSCs which all maintain their original characteristics, including differentiation potential. This is important if the expanded cell populations are to be used in clinical therapies. In this study, we demonstrated that isolated ADSCs can be expanded on novel synthetic microcarriers in stirred suspension cultures to yield viable cells with retained multipotent potential.

5.10.1 Effect of initial seeding density on ADSC expansion

Cell seeding density per microcarrier is a critical parameter to optimise cell expansion. If the cell to microcarrier ratio is too low this will lead to an extensive lag phase (356). Alternatively, if the cell microcarrier ratio is too high the available cell surface area is reduced, limiting the amount of expanded cells (382). In optimum conditions, the ratio of cells to microcarriers should be high enough to permit cell adhesion to all microcarriers. It has been suggested that a minimum average of around 5-6 cells per microcarrier is optimum for charged microcarriers (356, 357). Using Poisson distribution, Frauenshuh *et al.* (2007) predicted that the amount of (charged) microcarriers without any cell adhesion using this seeding density is less than 1% (358). This is optimized for charged microcarriers; however, the rate of cell adhesion to uncharged microcarriers is slower. On uncharged microcarriers the initial probability of cell microcarrier binding events is random, and is largely dependent on cell proximity to the microcarrier surface, to form an integrin-peptide ligand attachment.

Cells seeded at 35 cells per microcarrier formed aggregates between interstices after 7 days which were difficult to dissociate, preventing accurate cell counts from being taken. Hence, the expansion in the microcarriers couldn't be quantified. The results would suggest an upper limit on cell seeding density per microcarrier. Therefore, to assess the effects of cell seeding density on cell expansion, several cell seeding densities were tested, 2236 cells/cm^2, 1183 cells/cm^2 394 cells/cm^2 and 131 cells/cm^2 (17, 9, 3 and 1 cells/microcarrier respectively). In this study, a ratio of 17 cells per bead yielded the highest number of cells after 14 days (7.3 million cells) generating a cell doubling time of 51 hours, or 5.09 population doublings over 14 days. This is similar to the reported doubling rate of ADSCs of approximately 54 hours ± 4 hours, when cultured in DMEM and 10% FBS. Alternatively at 1 cell per microcarrier the doubling time was significantly reduced to 36.4 hours, indicating 7.7 population doublings over 14 days. This is similar to the doubling rate reported for ADSCs in a proprietary low serum media (MesenPro RS, Invitrogen) of 36 hours ± 4 hours. This correlated to data from Kehoe *et al.* (2012) who also noted an increase in doubling time on microcarriers seeded with higher cell densities (111). MSCs expanded *ex vivo* for clinical therapies not only require large lot sizes, but also require the cells to be delivered as quickly as possible. The decrease in doubling time observed herein is therefore advantageous for MSC expansion. The results presented here were generated using DMEM and 10%

MSC-qualified FBS, future work would look at the effect of using different medium compositions on cell-doubling rate on microcarriers.

ADSCs seeded at 1 cell per microcarrier generated a 207 fold increase in cell number over 14 days, with fold expansion decreasing as initial seeding density increased. However, even the lowest increase (73-fold), is considerably higher than previously reported in the literature for microcarrier based expansion of ADSCs (16- 26 fold increase in 14 days (138)).

A limiting factor in MSC expansion in monolayer culture is surface area. As shown by Schop *et al.* one method to expand the culture without passaging the adherent cells is the introduction of fresh microcarriers during the culture (378). Cell expansion occurs *via* bead to bead transfer, (the migration of cells from one microcarrier to another) increasing the available surface area for MSC culture. In future experiments the upper limit on cell expansion on the microcarriers would be explored, in particular the time taken in culture for cell proliferation to plateau due to lack of available surface area. In addition the potential to expand the surface area by adding fresh microcarriers throughout the culture time would be investigated.

5.10.2 Effect of stirring regime on initial cell attachment

Cell culture on microcarriers typically utilises stirred suspension bioreactors, such as spinner flasks. Conventionally, cultures are stirred intermittently straight after seeding (for the next 4-18hours) to allow cell adhesion, and then switched to continuous stirring for cell growth. This provides a homogenous culture environment and allows nutrients and oxygen to be transferred throughout the culture. This bioreactor design has previously been optimised for microcarriers which rely largely on inherent charge potential for cell attachment (115), where cells are electrostatically attracted to the microcarrier surface resulting in high initial cell attachment. (121). The primary method of cell attachment to the uncharged microcarriers used in this study is via peptide-integrin interactions. It has been demonstrated that attachment to uncharged microcarriers is slower than to charged microcarriers.

To assess cell morphology and distribution of expanded ADSCs, microcarrier samples were removed from the bioreactors daily. For cultures seeded at 5,000 cells/ cm^2 showed cell attachment to be highly variable after 24 hours. In the event of unevenly distributed cell attachment across the entire microcarrier population, the

cultures were intermittently agitated (1 minute every 45 minutes at 21rpm) for the length of the culture, to allow bead-to-bead transfer. It is hypothesised that the migration of cells from one microcarrier to another is dependant on the proximity of microcarriers. To increase the probability of a cell-laden microcarrier becoming adjacent to another microcarrier with space for a cell to attach and grow, the cultures were stirred intermittently (as opposed to the conventional continuous stirring).

Bead-to-bead transfer was observed between the novel microcarriers in samples seeded at 5,000 cells/cm^2 (Figure 56). After 7 days the attachment appeared to be fully confluent on some microcarriers with cell bridges and cell accumulation at interstices between microcarriers. This resulted in microcarriers forming large aggregates which were too dense to be fully suspended when agitated at 21rpm.

Cells contained within aggregates experience different culture conditions, including oxygen and nutrient transfer. The aim of this study was to generate a homogenous population of expanded ADSCs with multipotent potential. The early chondrogenic marker aggrecan demonstrated a fold increase in expression in all three cultures. Furthermore, the multipotent marker CD73 showed little change in expression in all three cultures. This could indicate cells cultured within interstices experience a pseudo 3D environment, promoting chondrogenic differentiation. The variation between spinner flasks and the remainder of CD73 expression, and increased adipogenic and osteogenic markers indicates a heterogeneous cell population. However, there is a lack of specific cell surface markers to identify MSC populations. Some markers have been proposed to identify MSCs, i.e. STRO-1 and CD105, the most common method is plastic adherence and colony formation (49). This method cannot establish the percentage of differentiated cells in response to culture conditions. Microarray analysis has shown CD73 to be expressed in MSC differentiated chondrocytes (383) casting doubt into the suitability of it as a multipotency marker. To establish the multipotency of expanded cells, microcarriers were placed in differentiation medium and the differentiated cells were analysed with stains to detect expression of lineage specific proteins.

All microcarriers previously reported for MSC expansion are polydisperse with a relatively wide range of diameters. This factor could potentially provide a non-homogenous culture, as confluency can occur at different rates depending on the available surface area of the microcarrier, generating a heterogeneous environment.

174

The microcarriers used in this study were generated using microfluidics and are highly monodisperse and hence cell adhesion should be very similar on all microcarriers. Variations in attachment are most likely due to problems with bioreactor protocols and design, including homogenous distribution of cells and microcarriers during the initial attachment phase. When cells were seeded at 5,000 cells/cm^2, multiple microcarrier aggregates were formed with confluent cells. Simultaneously a population of microcarriers had little to no cell attachment. To ensure a homogenous distribution of microcarriers and cells during the attachment phase of the culture (estimated to be approximately 24 hours), and to prevent cells only attaching to the top layer microcarriers, the intermittent stirring speed was increased from 21rpm to 60rpm to ensure all microcarriers were displaced after agitation. During the culture with different cell to microcarrier ratios cell attachment appeared even after 24 hours, however after 7 days attachment varied between microcarriers. After 14 days the cells appeared to be evenly distributed over the microcarriers with few microcarrier aggregates observed. The increase in agitation speed can also increase the shear force experienced by a cell and increase microcarrier collisions, potentially dislodging newly attached cells if the attachment is weak. Previous studies investigating the effect of impeller speed on cell expansion have involved continuously stirred cultures using a variety of impeller geometries. Hence these data are not directly comparable to the culture system described herein.

The influence of shear effects on MSC differentiation has been linked to microcarrier diameter. By decreasing microcarrier diameter from 3m to 0.5mm, *Kong et al.* (2011) observed an increase in osteogenic differentiation in BM-MSCs cultured in continuously agitated spinner flasks (266). The effect of shear force on cell attachment has not been investigated in this study; however, as the microcarriers are monodisperse the relationship between shear force and microcarrier diameter should be identical in all cultures. This is unlike most previous studies, where commercially available polydisperse microcarriers were used. Future work will optimise the stirring regime to maximise cell expansion, whilst maintaining cell phenotype.

Aggrecan expression is an early chondrogenic differentiation marker and has been shown to be upregulated in the first week of ADSC chondrogenic differentiation, and its expression is reduced in week 2 and week 3 of differentiation (384). Within both 7 and 14 day experiments, aggrecan expression was upregulated with no dependence on initial seeding density. Despite this result the cell morphology appeared spread and did

not form spontaneous aggregates or pellets as shown previously in cell-laden microcarriers undergoing chondrogenic differentiation (Figure 56 and Figure 61). The cells cultured at different cell seeding densities were shown to still be able to differentiate into three lineages by histochemical analysis, demonstrating their multipotency. Further work would analyse the expression of several other genes linked to chondrogenic differentiation.

5.10.3 Effect of nutrient depletion and metabolite accumulation on cell growth

In order to develop a bioreactor system, it is essential to understand the cell requirements for optimal cell growth. Cell growth can be inhibited by a lack of appropriate nutrients or by an excess of metabolites. To achieve optimal culture conditions, the media feeding and refreshing regime is crucial (113). Whilst cells proliferate and grow, cells consume nutrients such as glucose and glutamine (in addition to other amino acids). Simultaneously cells produce and secrete metabolites, such as lactate and ammonia. If the metabolites accumulate in the culture media, at certain concentrations they can inhibit cell growth. Schop *et al.* determined an increase in lactate concentration (24mM), inhibits cell growth in human BM-MSCs, which was shown to vary between donors (113). However, their differentiation potential remained unchanged. To prevent inhibition of cell growth, the replenishing the media should be optimised to prevent depletion of essential nutrients and the accumulation of metabolite production. Increase in cell growth correlates to increased nutrient consumption and metabolite production, therefore quickly proliferating cells will require more frequent media refreshments.

In the first attempt to expand ADSCs on the novel microcarriers, the feeding regime was a partial media change (50%) every three days. ADSCs expanded on microcarriers in spinner flasks for 7 days, at a seeing density of 5,000 cells/cm^2 demonstrated a notable decrease in the number of viable cells (Figure 55) after 120 hours in culture. As the number of viable cells was assessed directly before a scheduled media refreshment, this could be as a result of nutrient depletion or metabolite accumulation in the culture media. Schop *et al.* demonstrated exponential growth BM-MSCs on microcarriers using the same feeding regime (partial media change (50%) every three days) without generating inhibitory levels of the metabolites lactate and ammonia for 9 days. However, after this point the inhibiting concentrations of ammonia (2.4mM) became too high and glucose levels were depleted to near 0mM. Santos *et al.*

(2011) cultured ADSCs cultured on plastic microcarriers in xeno-free media over 14 days and showed that after an optimised daily feeding regime (partial media change (25%)), lactate and glucose levels did not inhibit cell growth (138). Glucose concentration (both high and low) has been shown to have no effect on BM-MSCs grown in tissue culture flasks, including no change in proliferation, differentiation potential or trophic factor secretion. This has been confirmed by Sart *et al.* (2010) and Schop *et al.* (2008) when expanding MSCs on microcarriers (113, 378). This indicates lactate and ammonia are metabolites responsible for effecting cell growth and therefore should be monitored regularly. Due to cost restraints, nutrient depletion and metabolite production was not analysed in our system. Future optimisation of the bioreactor design will address this issue. In the second experiment cells were seeded at a significantly lower density. To reduce the potential effects of metabolite accumulation the media changes were increased to 50% partial media change every two days. From cell viability graphs the cells showed linear growth over 14 days.

5.10.4 Effect of oxygen tension on ADSC growth and differentiation

An additional parameter that can affect cell growth is oxygen concentration throughout the bioreactor. Oxygen tension can affect cell metabolism, for example, an increase in glucose metabolism has been shown in cells cultured in hypoxic conditions. However, reports on the effects of oxygen concentration on MSC growth rates are conflicting. Schop *et al.* (2010) compared oxygen concentration (3% 'hypoxic' and 20% 'normal') on BM-MSCs cultured on microcarriers in spinner flasks and showed oxygen concentration had no effect on the rate of cell growth. Similarly, Wang *et al.* showed hypoxic conditions had no effect on human ADSCs growth when cultured within alginate microcarriers in static culture. Contrastingly, BM-MSCs cultured in monolayer in tissue culture flasks demonstrated faster growth rates in hypoxic conditions (3% O_2) compared to 20% O_2 (138). In addition, Kehoe *et al.* (2012) showed BM-MSCs cultured on collagen microcarriers had faster growth rates under hypoxic conditions (5% O_2 compared to 21% O_2). However as variations in MSC isolation can yield different subpopulations of MSCs with different characteristics, direct comparisons can be difficult.

In addition to cell growth rates, oxygen tension has been shown to affect the differentiation potential of BM-MSCs cultured on microcarriers Schop *et al.* (2008) observed an increase in chondrogenesis in cells expanded under hypoxic (3% O_2)

conditions. This could be due to a recreation of hypoxic conditions experienced in native cartilage stimulating chondrogenic differentiation. Wang *et al*. also reported increased chondrogenesis in ADSCs cultured under hypoxic condition (5% O_2), the typical oxygen concentration in articular cartilage. However, the authors debated whether this was an independent phenomenon or a result of oxygen tension combined with matrix effects. For example, ADSCs grown in alginate or agarose retain a spherical morphology and show little expression of type I collagen, whereas, fibrin or gelatin matrices promote a more fibroblastic morphology and the expression of both type I and type II collagen. However, changes in oxygen conditions were not shown to influence adipogenesis or osteogenesis on BM-MSC s expanded on microcarriers (113).

In our study, the spinner flasks were intermittently stirred, therefore diffusion of oxygen throughout the culture would be reduced compared to continuously stirred cultures described in the literature. An upregulation of the early chondrogenesis marker, aggrecan was observed in all seeding densities using quantitative RT-PCR. However no obvious morphological changes were observed. As cells require a 3D environment to differentiate and express chondrocyte specific genes this was unexpected. In our study cells were cultured on microcarriers in intermittent culture conditions. As the restrictions of equipment available the spinner flasks did not have an online monitoring system to probe the culture and test the oxygen concentration in real time. To increase aeration of cultures oxygen sparging has been previously used to by Sart *et al.* (2010) to increase MSC growth rate.

6.0   Discussion

MSCs are a promising cell source for regenerative medicine to repair or replace damaged tissues (1). MSCs are located in several tissues in the body, such as bone marrow, fat and muscle, however the populations are largely dormant and are present in small quantities (372). To use MSCs for clinical purposes, such as tissue engineering or cell-based therapies, strategies are required to isolate MSCs and expand to (tens of) millions of cells in a controlled, cost-effective, and reproducible way (372). Therefore, methods to rapidly expand MSC populations whilst maintaining cell multipotency and viability are currently being developed. Currently, extensive research is being performed on the development of bioreactors for efficient expansion of MSCs, as these offer several advantages over conventional methods (monolayer culture in tissue culture plastic flasks). They are highly productive, easily scalable and culture conditions can be closely monitored (373). In particular, the key parameters that affect cell growth can be monitored and controlled, such as medium composition and oxygen tension, resulting in reproducible cultures. In addition, as it does not require extensive manual handling, the risk of contamination is reduced; a factor of paramount importance in developing safe, reliable populations of cells for clinical therapies.

As MSCs are anchorage dependent and so large surface area is required to maximise expansion in a bioreactor (373, 374). Microcarriers provide a large surface area for cell growth and proliferation, and have been extensively studied for the expansion of cells in spinner flasks (166, 381). To efficiently expand MSCs for clinical therapies, an animal free expansion culture systemis required. Animal products must be removed from both the culture media and microcarriers. The aim of this thesis was to develop an entirely synthetic microcarrier using microfluidics for MSC expansion, free of animal-derived components.

In this study, a microfluidic platform capable of generating monodisperse synthetic microcarriers with tunable chemical, topographical and mechanical properties has been developed (Chapter 3). Representative PEGDMA microcarriers containing bio-adhesive ECM–derived peptides were produced using two different tethering chemistries. In addition, microcarriers containing three different compressive moduli and diameters were produced. The resulting microcarriers were well characterised. To assess the ability of the microcarriers to support ADSC attachment and growth, several bio-adhesive peptides (at a range of concentrations) were incorporated into PEDGMA microspheres. Over 7 days in static culture, an RGD based peptide cRGDfC at a concentration of 1mM was shown to support stable ADSC adhesion and growth.

Furthermore, microcarriers with a range of compressive moduli were generated (containing the optimised 1mM cRGDfC peptide), to probe the effects of microcarrier compressibility on MSC differentiation. Moduli specific differences were observed in cell phenotype after osteogenic, adipogenic and chondrogenic induction (Chapter 4). Microcarriers with the optimised chemical (1mM cRGDfC) and mechanical (155kPa) properties were selected for ADSC expansion. We demonstrated successful expansion of viable ADSCs within a spinner flask bioreactor system on novel synthetic microcarriers over 14 days (Chapter 5). Cell expansion was optimised by varying the cell seeding density. ADSCs showed a 207 fold expansion over 14 days when seeded at the lowest seeding density, higher than any reported studies of microcarrier based MSC expansion. The study also demonstrated the expanded ADSC population maintained multipotent potential, capable of differentiating into adipocytes, osteocytes and chondrocytes, essential for use in clinical applications.

6.1   Microfluidic synthesis of PEGDMA hydrogel microspheres with tunable chemical, mechanical and topographical characteristics

The overall aim of this project was to develop a synthetic microcarrier capable of providing a solid growth support for MSC expansion within a bioreactor. Recent advances in the field of biomaterials have shown that presenting cues derived from the ECM can affect and improve cell growth, intracellular signalling and differentiation (217). Previously, a wealth of research has eluded to possible biomaterial compositions that could control MSC fate (189, 271, 306). Various parameters have been considered, including chemical compositions, biomechanical properties and surface topographies. However, published reports on the precise cellular responses to various biomaterials, (such as MSC response to bio-adhesive peptides) are often conflicting (308, 344, 345). This is largely due to the subtle differences in scaffold properties used to probe the effects of ECM derived cues on cell growth and behaviour.

In chapter 3, an array system was generated whereby ECM derived cues could be tested systematically to ascertain the factors that can regulate MSC growth and differentiation. The synthetic polymer, PEGDMA, was selected as it is hydrophilic, easy to manipulate (compatible for use with microfluidics), resistant to non-specific protein adsorption, biocompatible and non-immunogenic (210). When crosslinked, the resulting

hydrogel has high water content and possesses mechanical properties similar to that of soft tissue (321). PEGDMA hydrogels are uncharged and lack any cues that allow the directed binding and attachment of cells, providing a "blank" bioinert microcarrier. To add an adhesive element to the microcarrier, commonly-used ECM derived peptides were incorporated to mimic the native microenvironment (241). In addition, the polymer content and microcarrier diameter was altered to generate an array of microcarriers with a wide range of biochemical and biophysical properties.

PEGDMA hydrogels have been widely used to assess the effects of compressibility, bio-adhesive peptide, and topography on MSC fate (241, 261, 308). However, typically the studies were performed on cells encapsulated within the photopolymerisable hydrogel, and focussed on assessing one parameter individually. For example, Jongpaiboonkit *et al.* (2009) developed a hydrogel array system for analysing adhesion and viability of MSC to IKVAV and RGD based peptides encapsulated *within* degradable and non-degradable PEG hydrogels (346). This method generates a 3D culture system, however cell-cell contacts are lost as the cells are entrapped within a hydrogel, and surface topography cannot be assessed (345). Cells cultured on microcarriers in monolayer culture experience a different microenvironment, and therefore it was hypothesised that MSC responses to changes in these parameters could behave differently to those previously reported in the literature. At the time of writing this study, it is the first time compressibility, bio-adhesive peptide, and topography studies have been performed stable in combination, on MSCs grown in monolayer culture.

To generate PEGDMA microcarriers with tunable biochemical and biophysical properties a microfluidic platform capable of generating monodisperse microspheres was developed. In chapter 3, the optimisation and development of a microfluidic method to produce synthetic microcarriers using UV photo-polymerisation is described. To achieve this, a range of microfluidic chips, with varying channel designs were manufactured and assessed. The resulting method was reproducible and generated highly monodisperse microcarriers with uniform characteristics.

The incorporation of adhesive peptides using "click" chemistry was simple and inexpensive. This was a key result as previous methods involved using expensive precursor molecules and lengthy characterisation; and gave non-reproducible product yields. The only requirement is for a thiol group which can be incorporated into the

peptide design *via* cysteine residues. A fibronectin motif, cyclic peptide cRGDfC, and two linear peptides containing the commonly used laminin motifs IKVAV and YIGSR were incorporated this way. The cyclic RGD sequence used in this study binds the integrin αvβ3, and studies have shown that compared to linear analogues, the cyclic form has increased specificity and has up to 240 times enhanced biological activity (385). The linear forms of the laminin based peptide IKVAV and YIGSR were used in this study as no cyclic forms have currently been reported in the literature.

Using the method outlined in Chapter 3, further work would incorporate a wider range of thiol-bearing peptides into microcarriers to optimise cell attachment. In 2010, Corning applied for patent protection for a surface coating for use on tissue culture plastic to support adhesion and expansion of BM-MSCs in serum-free media (Synthemax, Corning). Technical publications demonstrated BM-MSC expansion was ~100 fold higher than on conventional tissue culture treated plastic and after multiple passages retained high levels of multipotent markers (for Synthemax coatings in DMEM and 10% FBS over several passages) (386). The Synthemax surface coating contains an acrylated peptide sequence derived from vitronectin, Ac-KGGPQVTRGDVFTMP, which contains the cell binding motif RGD. By culturing BM-MSCs in serum free media (SFM) on this surface they showed approximately a 4-fold increase in expansion (over 1 passage) compared to normal tissue culture conditions, i.e. tissue culture treated plastic classical media (DMEM containing 10% FBS). However, there is no published literature demonstrating the use of this surface to culture MSCs. In addition, Synthemax has not been shown to be compatible with MSCs isolated from other sources. Future studies would incorporate this peptide sequence, *via* its acrylate functionality and compare it to results obtained from this study. CellStart, a similar propriety attachment factor, designed for the use in SFM culture of MSCs has recently, (2012) been shown to support the adhesion of BM-MSCs and ADSCs, but not placental cord derived MSCs (92). Furthermore, peptide incorporation could be expanded to explore the influence of peptides that target non-integrin receptors, and hence other signalling pathways, i.e. active fragments of growth factors such as TGF beta (known to mediate chondrogenesis in MSCs) (340).

By altering the PEGDMA (wt %) concentration an array of microcarriers were produced with a range of compressive moduli between 8kPa to 231kPa. A linear relationship exists between PEGDMA content (wt %) and compressive moduli, however there was a limit on the range of compressive moduli that could be produced.

For example, hydrogels with a compressive modulus less than 8 kPa were very weak and not manipulable. Few studies have analysed the effect of compressive modulus on MSCs grown in 2D, however, Engler *et al.* have previously shown a compressible modulus of between 0.1-1kPa is required to drive neurogenesis in MSCs (255). To improve the range of compressive moduli generated within the microcarrier, different molecular weight PEDGMA could be used altering the final cross-linking density of the hdyrogel (210, 387).

6.2   Cyclic RGDfC supports MSC attachment and proliferation on 1mM microcarriers

To assess the ability of the microcarriers developed in chapter 3 to sustain ADSC adhesion and growth, the effect of incorporating several peptides covalently linked into the hydrogel was investigated. Peptide modified flat hydrogels were produced and showed that ADSCs bound preferentially to cRGDfC hydrogels compared to the laminin based sequences. This was unexpected as it had previously been reported that ADSCs adhered and spread more extensively on IKVAV modified polycaprolactone surfaces, as compared to RGD or YIGSR modified surfaces (347). ADSC attachment to RGDfC modified hydrogels at a concentration of 0.35mM resulted in the formation of cell colonies, indicating that the cell attachment was low. As the cell seeding density per cm^2 hydrogel surface was relatively high, the effect of increasing cRGDfC peptide concentration upon cell attachment was explored, and showed an increase in cell attachment coinciding with an increase in peptide concentration. At a concentration of 1mM, cells attached uniformly to the surface of the hydrogel. It was hypothesised that factors such as topography and peptide ligand density could act synergistically to affect MSC fate. Therefore it was decided to test the range of peptides and peptide concentrations on microcarriers. From the data gathered it was concluded that 1mM RGDfC showed qualitatively the highest level of cell attachment and proliferation over 7 days, as seen using a viability assay. Live/dead assays and cytoskeleton staining confirmed cell viability data.

6.3   Compressive moduli influences MSC differentiation

To assess the effect of compressibility on cell attachment ADSCs were cultured on microcarriers with different mechanical properties for 5 days. To assess the multipotency of the attached cells, ADSC-laden microcarriers were transferred directly into differentiation induction medium. This result was significant as it demonstrated the adhered cells were still multipotent and could undergo osteogenic, chondrogenic and adipogenic differentiation on the surface of the microcarriers. This was confirmed using RT-PCR analysis and the upregulation of lineage specific gene expression. At the time of writing, direct differentiation on microcarrier surfaces has not been shown in the literature before. The original aim of this thesis was to generate microcarriers for stem cell expansion. However, this result generates an interesting potential function for the microcarriers as tissue engineering scaffolds. As the PEGDMA microcarriers are irreversibly covalently crosslinked, modifications to the polymer backbone to include a biodegradable element would be required. Several research groups have modified PEGDMA hydrogels to include a biodegradable element, such as incorporating hydrolytically degradable poly(lactic acid) PLA linkages (236) or enzymatically-sensitive sites which are cleavable by matrix metalloproteinases (MMP) secreted by cells (234). These constructs could be placed directly into the tissue requiring repair, which offers several advantages over MSC infusion (discussed in Chapter 1).

An interesting result was observed when stimulating chondrogenesis in ADSCs cultured on microcarriers with varying compressive moduli. Cells migrated from monolayer culture on the surface of the microcarrier spontaneously to form pellet. In addition, it was shown that the pellets had an organised structure which contained distinct regions resembling that of articular cartilage. At the time of writing, this is the first time this has been reported with on tissue culture plastic or on biomaterials. MSC differentiation into chondrocytes, is of particular interest in tissue engineering as it is a prerequisite for cartilage regeneration.

It was originally thought that the only the hardest substrate would be able to support chondrogenesis. However, herein the presence of collagen type II in cell pellets was demonstrated (using immunocytochemistry) on both the softest 8kPa and the hardest 232kPa substrates. Chondrogenesis can be monitored by assessing the expression and secretion of collagen isoforms, as MSCs express collagen I whereas chondrocytes primarily express collagen II (190, 352). Both isoforms were expressed in the hard and soft microcarrier substrates, indicating the presence of MSCs and

chondrocytes. The expression of collagen type II is an important result because it is one of the major components of the hyaline cartilage and plays a key role in maintaining chondrocyte function. This is essential when assessing scaffolds for tissue engineering and repair of cartilage defects (352).

As microcarrier aggregation was higher in the softest and hardest microcarrier tested, cell density within the pellets was higher. In 2010, Tang *et al.* demonstrated that cell-cell contacts influenced differentiation of MSCs into adipocytes and osteocytes (261). Herein, it is hypothesised the spontaneous migration of cells from monolayers to form multi-cellular pellets occurs due to a lack of RGD peptide dependency after chondrogenesis. In addition, the secretion of ECM proteins, which are not able to bind to the non-protein adhesive PEGDMA microcarrier, could potentially provide a scaffold for cells. To assess this further the expression of other genes and collagen isoforms could be analysed.

In chapter 3, the microfluidic production of microcarriers with a range of diameters was accomplished. Due to time constraints it was not possible to assess the effect of substrate curvature on MSC attachment and differentiation. As spontaneous aggregation of MSCs has never been reported during chondrogenesis (in tissue culture plastic, in monolayer culture), it was hypothesised that surface curvature, in addition to substrate compressibility, influenced pellet formation. Future work would attempt to establish the effect of surface curvature on this phenomenon.

6.4   ADSC expansion on novel microcarriers

The aim of this study was to assess the feasibility of expanding ADSCs on the novel microcarriers developed in Chapter 3. By evaluating the data obtained from culturing ADSCs on various microcarriers in static culture (chapter 4), microcarriers containing 1mM RGDfC with a compressive modulus of 155kPa were selected as a model to test ADSC expansion within spinner flasks. Initial studies demonstrated that ADSCs can attach and proliferate on novel microcarriers within spinner flask culture for 14 days. Importantly, after 14 days of expansion on the novel microcarriers, the adhered cells were shown to be multipotent.

6.5   Effect of initial seeding density on ADSC expansion

Cell seeding density (relative to microcarrier concentration) is a critical parameter to optimise cell expansion. If the initial cell to microcarrier ratio is too low this will lead to an extensive lag phase (356). Alternatively, if the cell to microcarrier ratio is too high, the available surface area for cell expansion is reduced, limiting the potential for cell expansion (382). To maximise the available surface area for cell expansion, and hence cell yield, it is important to generate homogenous culture conditions, with an even distribution in cells over the microcarrier population. In chapter 5, the effect of cell seeding density on ADSC expansion was assessed. Initially, a seeding density of 35 cells per microcarrier (equating to 5,000 cells/cm^2, the recommended seeding density in flasks (Invitrogen)) was trialled. However, due to inefficient agitation a non-homogenous culture was generated. This led to the formation of aggregates of cell laden microcarriers, and hence the culture was terminated after 7. In addition, it was difficult to retrieve cells from the culture and determine an accurate level of cell expansion. However, the cells remained multipotent, and when placed in differentiation induction media showed positive staining for the relevant lineage specific histological stains.

To maximise expansion, several cell seeding densities were tested. An initial seeding ratio of 17 cells per bead (cultured in DMEM and 10% MSC qualified FBS) yielded the highest number of cells after 14 days (7.3 million cells). This indicated a doubling time of 51 hours, or 5.09 population doublings. This is similar to the reported doubling rate of ADSCs cultured in DMEM and 10% FBS of approximately 54 hours ± 4 hours. Alternatively at 1 cell per microcarrier the doubling time was significantly reduced to 36.4 hours, indicating 7.7 population doublings over 14 days. This is similar to the doubling rate reported for ADSCs in a propriety low serum media (MesenPro RS, Invitrogen) of 36 hours ± 4 hours. This correlated to data from Kehoe *et al.* (2012) who also noted an increase in doubling time on microcarriers seeded with higher cell densities (111). This is an important result as technologies developed for autologous cell therapies need to expand populations of *ex vivo* MSCs as rapidly as possible.

The data presented in this study was generated from the microcarrier system developed herein, showed the generated fold increase in ADSCs was higher than any value reported in the literature for human MSCs expanded on microcarriers. Microcarriers cultured at a ratio of 1 cell per bead had a 207 fold increase in ADSC number after 14 days. This was over 14 times higher than a similar study conducted in

xeno-free medium by Santos *et al.* (2011), who expanded ADSC on similarly uncharged microcarriers. Furthermore, the expanded ADSC population was capable of differentiating into lineage specific progeny when stimulated by induction medium, indicating the cells remained multipotent after expansion. It is important that the cells remain phenotypically and characteristically unaltered after expansion if they are to be utilised in clinical therapies. Despite an upregulation in the early chondrogenesis marker aggrecan, cells demonstrated a tri-lineage differentiation potential in line with ISCT guidelines to define a multipotent MSC.

To improve upon the expansion protocol developed herein, the bioreactor design would need to be optimised to assess the effects of parameters known to influence cell expansion in spinner flasks, for example, shear stress, metabolism, stirring regime and cell seeding density. Furthermore, within this project the phenomenon of bead to bead transfer was repeatedly observed. This is important in microcarrier based expansion systems, as it offers the opportunity to increase cell surface area in a closed system without the need for manually passaging cell populations, reducing the risk of contamination. In addition, the influence of microcarrier properties, in particular the compressibility of the microcarrier, and diameter should be assessed when analysing the effects of shear stress on cell viability and growth. During agitation, shear stress on cells is not the only factor which effects cell viability, microcarrier collisions also can affect cell health. The effects of microcarrier stiffness on these collisions could be assessed further.

6.6   Future Work

6.6.1   Developing the microfluidic platform to generate a microcarrier array to systematically assess MSC function

It is hypothesised that biochemical and biophysical cues act synergistically to control MSC fate. To generate microcarriers with different chemical compositions (using the microfluidic platform developed in chapter 3), the MicroPlant has to be dissembled, cleaned, the fluidic inputs changed and then reassembled. This is time consuming and restricted the combination of microcarrier compositions that could be analysed in this project. Ideally, a microfluidic system that could generate microcarriers with a range of chemical compositions by fluid mixing on chip, by altering the fluid inputs would be desirable. Theoretically by varying the relative quantities of PEGDMA

and synthetic peptides, the mechanical and bio-adhesive properties of the microcarrier would be controlled and finely tuned.

To address this, a microfluidic system with the capacity to vary polymer concentration was designed, and both peptide composition and concentration simultaneously tuned using on-chip gradient formation within our prototype chip designs. Computer controlled syringe drivers can be paired to produce reciprocal flow rates ensuring a smooth linear gradient of polymer input on chip. This second generation MicroPlant will allow the regulation of compressibility (through polymer gradient), peptide display (through peptide gradient), and peptide composition (by ratiometrically mixing multiple peptides) within the same production run. In order to distinguish between microcarriers of different compositions, the use of fluorescent tags was investigated. These would ideally be passively but permanently incorporated into the polymer matrix. Preliminary experiments involving fluorescently tagged proteins and Q-dots enabled facile distinction between three populations of microcarrier mixed in culture (Figure 64). Photostable fluorescent Q-dots, (which have been shown to be stably incorporated into microcarriers during manufacture will be used to ascertain a ratiometric fluorescent readout indicative of the biomechanical properties within the microcarrier. For example Red 625nm Q-dots will be incorporated within 10% polymer, green 515nm Q-dots within 20% polymer. Ratiometric fluorescence from both the microscope, and from a plate reader assay would allow us to identify beads against known controls to give a direct readout of the variable biomechanical properties in the sample, whilst also giving an immediate readout that on-chip mixing has been successful. Due to the broad excitation and narrow emission spectra of Q-dots, more than 6 different solutions could theoretically be mixed, and ratiometrically calculated (388).
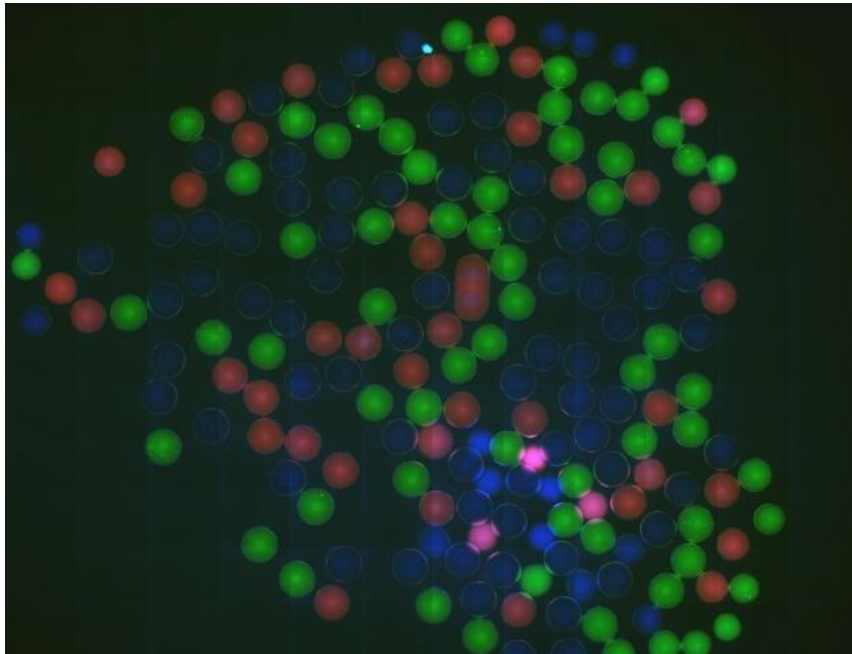
Figure 64 Incorporation of fluorescent antibodies into microcarriers

To generate microcarriers containing fluorescent tags, fluorescently conjugated antibodies (goat anti-mouse Alexa 405,488,568 (Invitrogen,UK)) were incorporated into PEGDMA solutions prior to microfluidic generation of cross-linked microspheres.

By manipulating the microfluidic channel size within the MicroPlant, it was possible to produce microcarriers of defined sizes whilst maintaining their monodispersity. An initial proof of principle study has produced beads of 261, 460 and 950 micron diameter. Smaller microcarriers carry a greater surface area:volume ratio, and so would provide a greater surface area for cell attachment for an equivalent amount of starting material (thus reducing material costs). However with a decrease in microcarrier size comes a change in surface curvature which could affect cell binding efficiency, maintenance of multipotency, and a decrease in cell survivability within a stirred bioreactor. Advances in the development of the microfluidic process will produce a library of microcarriers that can then be assessed for their effects on stem cell biology.

Microcarriers containing a wide range of topographical, chemical, and mechanical properties have been generated. In future applications, (for example when generating an array with combinations of all three parameters), it could prove useful to track or identify microcarriers by including a unique fluorescent tag. Further work would investigate this more thoroughly and determine the effects (if any) on cytocompatibility.

6.6.2 Generating therapeutically relevant lot sizes of MSCs using the novel synthetic microcarrier based expansion

Typically, MSC infusion therapies require approximately 150-300 million cells per treatment. In this study, the highest yield of ADSCs after 14 day expansion was 7.3 million cells. This experiment was performed in a 250mL spinner flask containing approximately 12,500 microcarriers. To generate the microcarriers used in this experiment, the current MicroPlant was run for 1 hour. To generate 150 million cells using the current protocol in 14 days, 21 batches of microcarriers (based on 12,667 microcarriers/hour) would be required. For this technology to be used routinely to generate therapeutically relevant quantities of MSCs, it must be scaled up to generate more microcarriers per hour. To achieve this, a single chip could be produced containing several independent channels running in parallel on the same MicroPlant. The manifold would not require extensive changes as the steel base already contains several fluid entry points. In addition to scaling up manufacture, downstream processing of the microcarriers also needs to be optimised. Currently the microspheres are produced in a continuous phase of cytocompatible oil. Subsequently the oil is removed by washing using a water and surfactant approach (Chapter 2), which is time consuming and impractical at larger scales. As the microcarriers contain peptides which are expensive and possibly sensitive to harsh solvents, a careful approach has to be taken when removing the oil. In future, a column based approach could be explored, whereby the microcarriers are placed within a column containing a porous frit, and are washed using a continuous flow of water and surfactant, potentially reducing the handling time required to remove the oil and lowers risk of contamination.

To successfully implement the novel microcarriers produced herein to expand MSCs commercially, the cost of developing and producing the bioreactor culture system is crucial. Although bioreactor expansion of MSCs is significantly cheaper than conventional tissue culture based practices, specialised media and the microcarrier chemical costs are large. To generate the bio-adhesive microcarriers, peptides are bulk modified into the hydrogel microcarrier. As the cells are cultured on the microsphere surface only these results in large quantities of peptides being wasted. A limiting factor in this project was the cost of peptide, at approximately £70 per 1 hour batch of microcarriers. To produce the quantity of microcarriers estimated to yield 150 million MSCs using the current method and at the current price of peptide would cost £1,450. This futher highlights the need for optimisation in all parts of the project.

6.6.3   Developing a xeno-free culture system for the expansion of MSCs

MSCs expanded for clinical therapies must follow rigorous and ever-evolving GMP guidelines. As discussed in Chapter 1, this will require the removal of animal components from both the culture medium and the microcarrier to prevent potential contamination. Charged microcarriers require serum proteins to facilitate cell adhesion to their surface. To circumvent this issue Santos *et al.* (2011) coated uncharged plastic microcarriers with CELLstart™, a xeno-free cell attachment substrate (a proprietary formulation, Invitrogen). Using the first fully demonstrated ADSC compatible xeno-free medium developed during the experimental period of this thesis in 2009 (StemPro MSC SFM, Invitrogen), the group demonstrated the feasibility of expanding ADSCs in xeno-free conditions (389). However, ~75% of the initial seeded cells were lost and cell growth experienced an extensive lag phase. In addition, Santos *et al.* showed a 14-fold increase in ADSC expansion over 14 days. This is significantly higher than MSC fold increases previously reported for microcarrier culture. In this study, typical fold increases in ADSC number (also over 14 days) ranged from 33 to 207, depending on initial cell seeding density. However, direct comparisons are difficult, as cell doubling time varies greatly according to medium composition. According to the manufacturers of StemPro MSC SFM (Invitrogen), SFM media decreases doubling rates and 'hMSCs grown in classical medium, have a flattened cell morphology and reach confluency between 1.0–3.0 x 10^4 cells/cm^2, hMSCs grown in STEMPRO® MSC SFM have a much smaller, spindle-shaped morphology and can reach densities >1.0 x 10^5 cells/cm^2' when compared to classical medium, DMEM and 10% MSC-qualified FBS, (as used in this study) (389). This is important as a decrease in cell area increases the surface area available for expansion, and therefore has a direct influence on the potential cell yield generated from a microcarrier culture. However, it is not evident from the publish reports, whether the effect on cell morphology is solely attributable to the media composition or the use of CellStart attachment factor. In addition, Timmins *et al.* (2012) could not reproduce the results found by Santos *et al.* when using human MSCs from a different source (92).

The expansion of ADSCs on microcarriers described in this study is in the presence of 'classical medium' DMEM containing 10% MSC-qualified FBS. However, PEGDMA is resistant to non-specific protein adsorption onto the microcarrier surface Therefore, proteins such as vitronectin and fibronectin are not able to bind to the microcarrier surface and influence cell attachment. It is hypothesised that the removal of

serum will not dramatically affect ADSC attachment or expansion on novel microcarriers, as seen in the study by Santos *et al*.

6.6.4 Microcarrier cryobanking

In both chapters 4 and 5 the attachment and growth of ADSCs have been demonstrated on a range on novel microcarriers both in static and stirred cultures. In addition, 'on microcarrier' differentiation into adipocytes, osteocytes and chondrocytes has also been demonstrated. A potential application of the technology described in this work is drug discovery. The development of biomaterials for stem cell culture is a rapidly increasing area of research. A challenge however, is analysing the constructs in a high throughput manner. The generation of highly reproducible monodisperse synthetic microcarriers using microfluidics, with precise control and uniformity of size and chemical composition, which can be transferred using standard pipetting techniques could create a homogenous population of cell laden microspheres for testing different compounds. In addition to having a library of microcarriers containing different characteristics, we have shown a range of microcarriers containing fluorescently labelled dyes which can be potentially used to track microcarriers.

In developing MSCs for autologous and allogeneic therapies, cryobanking important area of MSC research, as patients' cells can be isolated and expanded *ex vivo*, before being stored long term until required. Future work will attempt to cryopreserve both expanded ADSCs and lineage specific progeny on microcarriers and characterise the effect of cryopreservation on cells to determine both viability and 'stemness', i.e. where applicable, their multipotent potential.

Final conclusion

The study has fulfilled its original aims. A robust, repeatable microfluidic system capable of generating synthetic PEGDMA hydrogel microcarriers containing a range of chemical, mechanical and topographical cues was established. Furthermore, proof of principal compositions were generated, however the method developed herein can be used to create microcarriers containing a variety of properties. Microcarriers modified to contain fibronectin derived cRGDfC peptide and the laminin based IKVAV peptide supported ADSC attachment and growth in a concentration dependent manner in static culture. Aggrecan expression, an early chondrogenic differentiation marker was upregulated in all conditions tested, which could indicate a heterogeneous culture

containing some differentiated cells. However aggrecan has been questioned as a marker for chondrogenesis, and so future work should examine a range of chondrogenic markers to investigate this further. Our data would also question the validity of this marker as ADSCs cultured on cRGDfC modified microcarriers were capable of differentiating into osteocytes, chondrocytes and adipocytes on the microcarrier surface, indicating culture on microcarriers maintained multipotent potential. Substrate compressibility was found to effect ADSC differentiation, corroborating previous literature reports. ADSCs cultured on microcarriers formed spontaneous multicellular aggregates containing spatially distinct regions resembling native articular cartilage and expressing collagen type II. Bioreactor culture demonstrated successful ADSC expansion with fold increases in cell number far higher than have previously been reported in the literature. High cell seeding densities produced large quantities of viable cells. However, decreasing initial cell seeding density, increased the total fold expansion and reduced cell doubling rates. Further optimisation of the system is required, especially when switching the system into serum-free medium, however the microcarriers developed herein hold great potential for the expansion of ADSCs for regenerative medicine and tissue engineering.

7.0 Appendix 1

Comparable effects of CHO cell culture on both commercially available and novel microcarriers

Traditionally, microcarriers are used for the expression of therapeutic antibodies and proteins. Therefore to assess the ability of the developed microcarriers to sustain cell growth and biological function we compared the previously developed microcarriers alongside four commonly used commercially available equivalents with a range of properties.

CHO DP12 cells (a CHO K1 (DHFR-) clone #1934) capable of producing humanized monoclonal anti-IL8 antibody *(purchased from ATCC)* was seeded on different microcarrier types and cell viability was monitored over 7 days. In addition antibody production was also monitored over 7 days. Results were compared to a non-transfected CHO K1 cell line. The microcarriers tested comprised of 3 positively charged microcarriers Cytodex (1), Cytodex (3), Cytopore (1) and 1 charge-neutral microcarrier type, Pronectin F. More information regarding the above microcarrier properties can be found in Figure 2.
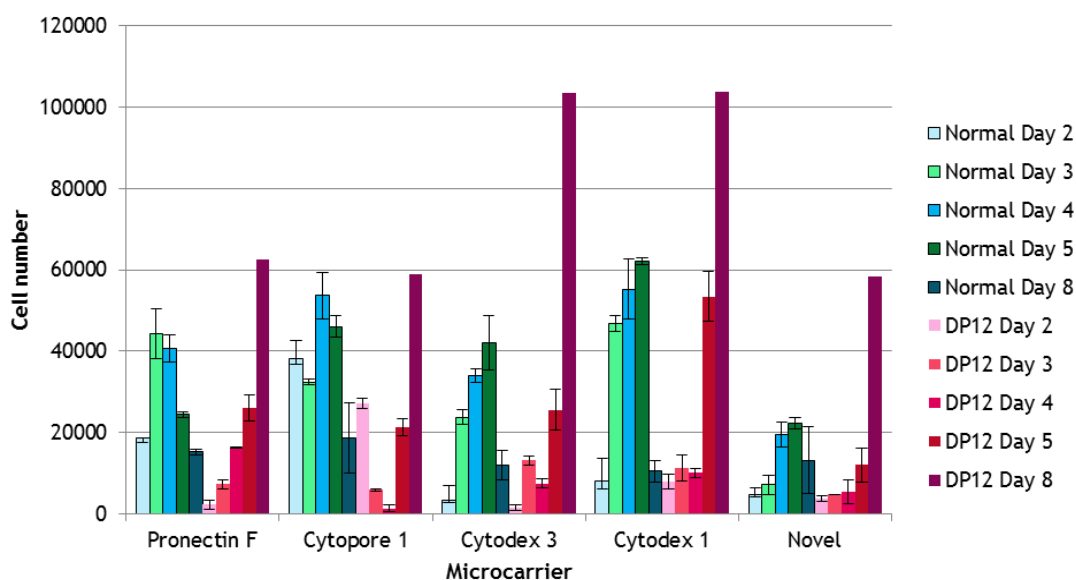
To measure attachment and viability, CHO K1 and DP12 cells were seeded onto various microcarrier types in ultra-low attachment tissue culture plates under static culture conditions and their viability was measured using a Prestoblue assay. The highest initial attachment was seen on Cytopore microcarriers. Cytopore microcarriers are macroporous and provide a large surface area for attachment and have been

developed specifically for CHO cell culture. CHO K1 cells showed a general trend of growth peaking at day 3-5 but rapidly declining by Day 8. This could be potentially due to over confluency. CHO DP12 cell demonstrated a low level of initial attachment, but grew steadily over 8 days on all microcarrier types reaching a very high level of confluency on both Cytodex 1 and 3 microcarriers. The novel microcarriers developed in Chapter 3 demonstrated a comparable level of attachment for both cell types over 8 days. Pronectin F microcarriers contain a poly-RGD synthetic protein conjugated to its surface.
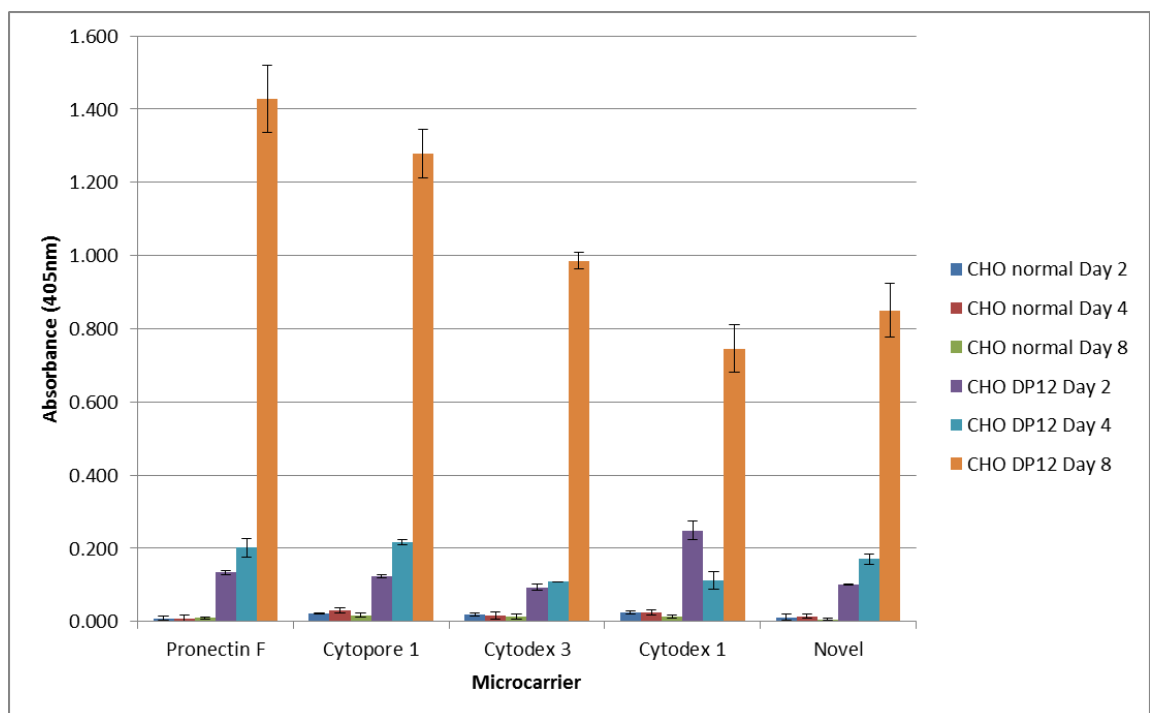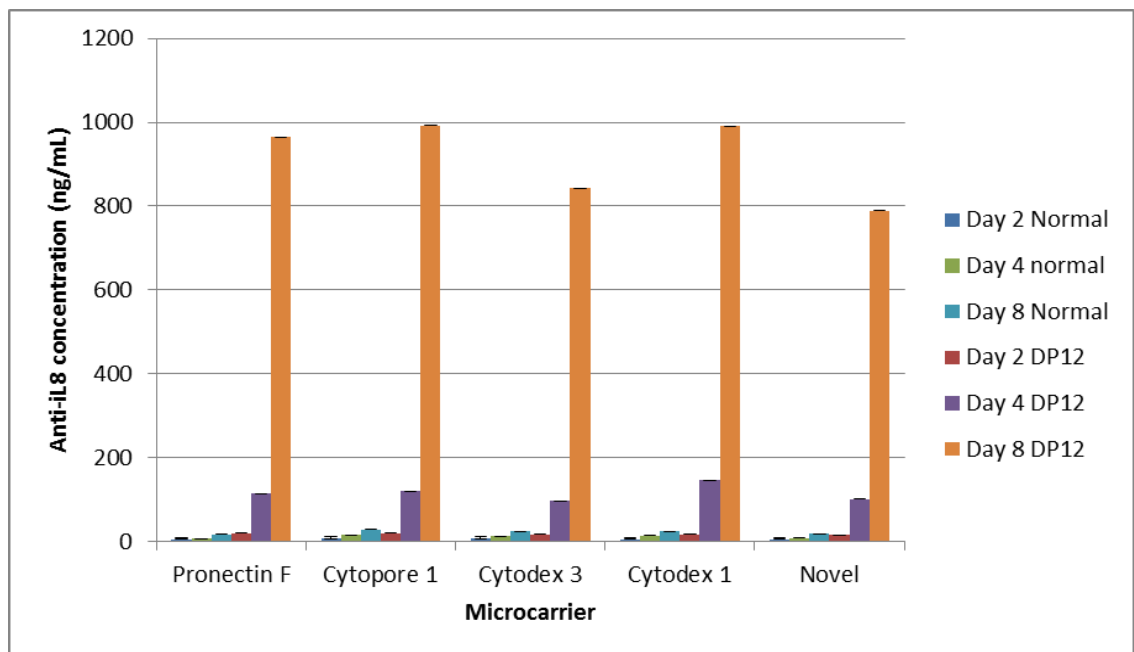
The total level of anti-IL-8 produced by CHO DP12 cells on various microcarriers was monitored by ELISA over 7 days. As expected CHO K1 cells produced no antibody as they are not transfected with the appropriate vector to express the anti-iL8 antibody. All microcarrier types supported antibody production, with Cytopore and Cytodex 1 microcarriers yielding the highest concentration of antibody, despite viability data suggesting the Cytopore microcarriers after 8 days cell attachment was approximately half that of Cytodex 1 microcarriers. The hydrogel microcarriers developed in herein produced the lowest quantity of antibody; however this experiment demonstrates the ability of hydrogel microcarriers produced to support cell expansion and the production of therapeutic proteins.

Appendix 2

The efficiency of the Taqman assay dues (FAM) to amplify a particular locus was determined by perfoming RT-PCR on a serial dilution of RNA concentrations (Starting concentration 1 µg). The efficiency was calculated automatically using RealPlex software.

Locus position	Efficiency	R squared value
AGCN (NM_001135.3)	1.10	0.966
CD73 (NM_002526.3)	1.11	0.996
B2M (NM_004048.2)	0.93	0.998
FABP4 (NM_001442.2)	0.94	0.998
RGCC (NM_014059.2)	0.91	0.997

8.0 References

1.   Polak J, Mantalaris, S., Harding, S.E.,. Advances in Tissue Engineering. 2008;Imperial College Press:1-903.
2.   Daar AS, Greenwood HL. A proposed definition of regenerative medicine. Journal of Tissue Engineering and Regenerative Medicine. 2007;1(3):179-84.
3.   V. Ramakrishna PBJaLS. Stem Cells and Regenerative Medicine –A Review. Annual Review & Research in Biology. 2011;1(4):79-110.
4.   Evans MJ, Kaufman MH. Establishment in culture of pluripotential cells from mouse embryos. Nature. 1981;292(5819):154-6.
5.   Amit M, Carpenter MK, Inokuma MS, Chiu C-P, Harris CP, Waknitz MA, et al. Clonally Derived Human Embryonic Stem Cell Lines Maintain Pluripotency and Proliferative Potential for Prolonged Periods of Culture. Developmental Biology. 2000;227(2):271-8.
6.   Xu C, Inokuma MS, Denham J, Golds K, Kundu P, Gold JD, et al. Feeder-free growth of undifferentiated human embryonic stem cells. Nat Biotech. 2001;19(10):971-4.
7.   Kriks S, Shim J-W, Piao J, Ganat YM, Wakeman DR, Xie Z, et al. Dopamine neurons derived from human ES cells efficiently engraft in animal models of Parkinson/'s disease. Nature.480(7378):547-51.
8.   Germano IM, Emdad L, Qadeer ZA, Binello E, Uzzaman M. Embryonic stem cell (ESC)-mediated transgene delivery induces growth suppression, apoptosis and radiosensitization, and overcomes temozolomide resistance in malignant gliomas. Cancer Gene Therapy. 2010;17(9):664-74.
9.   Jones S. ES cell therapy in two patients with eye disease. Nat Biotech. 2012;30(3):251-.
10.   Aboody K, Capela A, Niazi N, Stern Jeffrey H, Temple S. Translating Stem Cell Studies to the Clinic for CNS Repair: Current State of the Art and the Need for a Rosetta Stone. Neuron.70(4):597-613.
11.   Deshmukh RS. Drug Discovery Models and Toxicity Testing Using Embryonic and Induced Pluripotent Stem-Cell-Derived Cardiac and Neuronal Cells. Stem Cells International. 2012;2012:9.
12.   Robertson JA. Human embryonic stem cell research: ethical and legal issues. Nat Rev Genet. 2001;2(1):74-8.
13.   Burt RK, Verda L, Kim D-A, Oyama Y, Luo K, Link C. Embryonic Stem Cells As an Alternate Marrow Donor Source. The Journal of Experimental Medicine. 2004 April 5, 2004;199(7):895-904.
14.   Tomokazu Amano TP, Li-Ying Sung, Jessica Lennington, Joanne Conover, and Xiangzhong Yang. Nuclear Transfer Embryonic Stem Cells Provide an In Vitro Culture Model for Parkinson's Disease. Cloning and Stem Cells. 2009;11(1):77-88.
15.   Arora N, Daley GQ. Pluripotent Stem Cells in Research and Treatment of Hemoglobinopathies. Cold Spring Harbor Perspectives in Medicine. April 1, 2012;2(4).
16.   K. Takahashi SY. Induction of pluripotent stemcells from mouse embryonic and adult fibroblast cultures by defined factors. Cell. 2006;126 (663-676).
17.   Chin MH, Mason MJ, Xie W, Volinia S, Singer M, Peterson C, et al. Induced Pluripotent Stem Cells and Embryonic Stem Cells Are Distinguished by Gene Expression Signatures. Cell stem cell. 2009;5(1):111-23.
18.   Josowitz R, Carvajal-Vergara X, Lemischka IR, Gelb BD. Induced pluripotent stem cell-derived cardiomyocytes as models for genetic cardiovascular disorders. Current Opinion in Cardiology. 2011;26(3):223-9

19.   Wernig M, Zhao J-P, Pruszak J, Hedlund E, Fu D, Soldner F, et al. Neurons derived from reprogrammed fibroblasts functionally integrate into the fetal brain and improve symptoms of rats with Parkinson's disease. Proceedings of the National Academy of Sciences. 2008 April 15, 2008;105(15):5856-61.

20.   Choi K-D, Yu J, Smuga-Otto K, Salvagiotto G, Rehrauer W, Vodyanik M, et al. Hematopoietic and Endothelial Differentiation of Human Induced Pluripotent Stem Cells. STEM CELLS. 2009;27(3):559-67.

21.   Lowry WE, Quan WL. Roadblocks en route to the clinical application of induced pluripotent stem cells. Journal of Cell Science. 2010 March 1, 2010;123(5):643-51.

22.   Hongyan Zhou SW, Jin Young Joo, Saiyong Zhu, Dong Wook Han, Tongxiang Lin, Sunia Trauger,, Geoffery Bien SY, Yong Zhu, Gary Siuzdak, Hans R. Schler, Lingxun Duan, and Sheng Ding. Generation of Induced Pluripotent Stem Cells Using Recombinant Proteins. Cell stem cell. 2009;4(6):581.

23.   Wu SM, Hochedlinger K. Harnessing the potential of induced pluripotent stem cells for regenerative medicine. Nat Cell Biol. 2011;13(5):497-505.

24.   Zhao T, Zhang Z-N, Rong Z, Xu Y. Immunogenicity of induced pluripotent stem cells. Nature. 2011;474(7350):212-5.

25.   Mizuno H, Tobita M, Uysal AC. Concise review: adipose-derived stem cells as a novel tool for future regenerative medicine. Stem cells. 2012 May;30(5):804-10.

26.   Friedenstein AJ, Piatetzky-Shapiro II, Petrakova KV. Osteogenesis in transplants of bone marrow cells. Journal of Embryology and Experimental Morphology. 1966 December 1966;16(3):381-90.

27.   Woodbury D, Reynolds K, Black IB. Adult bone marrow stromal stem cells express germline, ectodermal, endodermal, and mesodermal genes prior to neurogenesis. Journal of Neuroscience Research. 2002;69(6):908-17.

28.   Deans RJ, Moseley AB. Mesenchymal stem cells: Biology and potential clinical uses. Experimental hematology. 2000;28(8):875-84.

29.   Gussoni E, Soneoka Y, Strickland CD, Buzney EA, Khan MK, Flint AF, et al. Dystrophin expression in the mdx mouse restored by stem cell transplantation. Nature. 1999;401(6751):390-4.

30.   Petersen BE, Bowen WC, Patrene KD, Mars WM, Sullivan AK, Murase N, et al. Bone Marrow as a Potential Source of Hepatic Oval Cells. Science. 1999 May 14, 1999;284(5417):1168-70.

31.   Rojas M, Xu J, Woods CR, Mora AL, Spears W, Roman J, et al. Bone Marrowâ€"Derived Mesenchymal Stem Cells in Repair of the Injured Lung. American Journal of Respiratory Cell and Molecular Biology. 2005 August 1, 2005;33(2):145-52.

32.   Pittenger MF, Mackay AM, Beck SC, Jaiswal RK, Douglas R, Mosca JD, et al. Multilineage Potential of Adult Human Mesenchymal Stem Cells. Science. 1999 April 2, 1999;284(5411):143-7.

33.   Ferrand J, Lehours P, Prochazkova-Carlotti M, Chambonnier L, Varon C. Human Bone Marrow-Derived Stem Cells Acquire Epithelial Characteristics through Fusion with Gastrointestinal Epithelial Cells. PLoS ONE. 2011;6(5):e19569.

34.   Wagner W, Feldmann RE, Seckinger A, Maurer MH, Wein F, Blake J, et al. The heterogeneity of human mesenchymal stem cell preparationsâ€"Evidence from simultaneous analysis of proteomes and transcriptomes. Experimental hematology. 2006;34(4):536-48.

35.   Horwitz EM, Le Blanc K, Dominici M, Mueller I, Slaper-Cortenbach I, Marini FC, et al. Clarification of the nomenclature for MSC: The International Society for Cellular Therapy position statement. Cytotherapy. 2005;7(5):393-5.

36.   Meirelles LdS, Chagastelles PC, Nardi NB. Mesenchymal stem cells reside in virtually all post-natal organs and tissues. Journal of Cell Science. 2006 June 1, 2006;119(11):2204-13.

37.   Aust L, Devlin B, Foster SJ, Halvorsen YDC, Hicok K, Laney Td, et al. Yield of human adipose-derived adult stem cells from liposuction aspirates. Cytotherapy. 2004;6(1):7-14.

38.   Bray GA. Medical Consequences of Obesity. Journal of Clinical Endocrinology & Metabolism. 2004 June 1, 2004;89(6):2583-9.

39.   Katz AJ LR, Hedrick MH, Futrell JW. Emerging approaches to the tissue engineering of fat. Clinical Plastic Surgery. 1999;26(4):587-603.

40.   Geiger PCBaH. Adipose-Derived Mesenchymal Stromal/Stem Cells: Tissue Localization, Characterization, and Heterogeneity. Stem Cells International. 2012;11.

41.   Zuk PA ZM, Mizuno H, Huang J, Futrell JW, Katz AJ, Benhaim P, Lorenz HP, Hedrick MH. Multilineage Cells from Human Adipose Tissue: Implications for Cell-Based Therapies. Tissue engineering. 2001;7(2):211-28.

42.   John K. Fraser MZ, Isabella Wulur and Zeni Alfonso. Adipose-Derived Stem Cells. Methods in Molecular Biology. 2008;449(1):59-67.

43.   De Ugarte DA, Morizono K, Elbarbary A, Alfonso Z, Zuk PA, Zhu M, et al. Comparison of Multi-Lineage Cells from Human Adipose Tissue and Bone Marrow. Cells Tissues Organs. 2003;174(3):101-9.

44.   Oedayrajsingh-Varma M, van Ham S, Knippenberg M, Helder M, Klein-Nulend J, Schouten T, et al. Adipose tissue-derived mesenchymal stem cell yield and growth characteristics are affected by the tissue-harvesting procedure. Cytotherapy. 2006;8(2):166-77.

45.   Strem BM, Hicok KC, Zhu M, Wulur I, Alfonso Z, Schreiber RE, et al. Multipotential differentiation of adipose tissue-derived stem cells. The Keio Journal of Medicine. 2005;54(3):132-41.

46.   Gimble JM, Katz AJ, Bunnell BA. Adipose-Derived Stem Cells for Regenerative Medicine. Circ Res. 2007 May 11, 2007;100(9):1249-60.

47.   Mitchell JB, McIntosh K, Zvonic S, Garrett S, Floyd ZE, Kloster A, et al. Immunophenotype of Human Adipose-Derived Cells: Temporal Changes in Stromal-Associated and Stem Cell–Associated Markers. STEM CELLS. 2006;24(2):376-85.

48.   McIntosh K, Zvonic S, Garrett S, Mitchell JB, Floyd ZE, Hammill L, et al. The Immunogenicity of Human Adipose-Derived Cells: Temporal Changes In Vitro. STEM CELLS. 2006;24(5):1246-53.

49.   Simmons PJ, Torok-Storb B. Identification of stromal cell precursors in human bone marrow by a novel monoclonal antibody, STRO-1. Blood. 1991 July 1, 1991;78(1):55-62.

50.   Gronthos S, Franklin DM, Leddy HA, Robey PG, Storms RW, Gimble JM. Surface protein characterization of human adipose tissue-derived stromal cells. Journal of Cellular Physiology. 2001;189(1):54-63.

51.   Krampera M, Pasini A, Pizzolo G, Cosmi L, Romagnani S, Annunziato F. Regenerative and immunomodulatory potential of mesenchymal stem cells. Current Opinion in Pharmacology. 2006;6(4):435-41.

52.   Uccelli A, Moretta L, Pistoia V. Mesenchymal stem cells in health and disease. Nat Rev Immunol. 2008;8(9):726-36.

53.   Bunnell BA, Flaat M, Gagliardi C, Patel B, Ripoll C. Adipose-derived stem cells: Isolation, expansion and differentiation. Methods. 2008;45(2):115-20.

54.   Ankrum J, Karp JM. Mesenchymal stem cell therapy: Two steps forward, one step back. Trends in molecular medicine. 2010;16(5):203-9.

55.   Phinney DG, Prockop DJ. Concise Review: Mesenchymal Stem/Multipotent Stromal Cells: The State of Transdifferentiation and Modes of Tissue Repair—Current Views. STEM CELLS. 2007;25(11):2896-902.
56.   Iso Y, Spees JL, Serrano C, Bakondi B, Pochampally R, Song Y-H, et al. Multipotent human stromal cells improve cardiac function after myocardial infarction in mice without long-term engraftment. Biochemical and Biophysical Research Communications. 2007;354(3):700-6.
57.   Ortiz LA, DuTreil M, Fattman C, Pandey AC, Torres G, Go K, et al. Interleukin 1 receptor antagonist mediates the antiinflammatory and antifibrotic effect of mesenchymal stem cells during lung injury. Proceedings of the National Academy of Sciences. 2007 June 26, 2007;104(26):11002-7.
58.   Lee RH, Pulin AA, Seo MJ, Kota DJ, Ylostalo J, Larson BL, et al. Intravenous hMSCs Improve Myocardial Infarction in Mice because Cells Embolized in Lung Are Activated to Secrete the Anti-inflammatory Protein TSG-6. Cell stem cell. 2009;5(1):54-63.
59.   Togel F, Weiss K, Yang Y, Hu Z, Zhang P, Westenfelder C. Vasculotropic, paracrine actions of infused mesenchymal stem cells are important to the recovery from acute kidney injury. American Journal of Physiology - Renal Physiology. 2007 May 2007;292(5):F1626-F35.
60.   van Poll D, Parekkadan B, Borel Rinkes I, Tilles A, Yarmush M. Mesenchymal Stem Cell Therapy for Protection and Repair of Injured Vital Organs. Cellular and Molecular Bioengineering. 2008;1(1):42-50.
61.   Rehman J, Traktuev D, Li J, Merfeld-Clauss S, Temm-Grove CJ, Bovenkerk JE, et al. Secretion of Angiogenic and Antiapoptotic Factors by Human Adipose Stromal Cells. Circulation. 2004 March 16, 2004;109(10):1292-8.
62.   da Silva Meirelles L, Fontes AM, Covas DT, Caplan AI. Mechanisms involved in the therapeutic properties of mesenchymal stem cells. Cytokine & Growth Factor Reviews. 2009 2009/12//;20(5â€"6):419-27.
63.   Bernardo ME, Locatelli F, Fibbe WE. Mesenchymal Stromal Cells. Annals of the New York Academy of Sciences. 2009;1176(1):101-17.
64.   Barbash IM, Chouraqui P, Baron J, Feinberg MS, Etzion S, Tessone A, et al. Systemic Delivery of Bone Marrowâ€"Derived Mesenchymal Stem Cells to the Infarcted Myocardium. Circulation. 2003 August 19, 2003;108(7):863-8.
65.   Gao J DJ, Muzic RF, Lundberg M, Caplan AI. The Dynamic in vivo Distribution of Bone Marrow-Derived Mesenchymal Stem Cells after Infusion. Cells Tissues Organs. 2001;169:12-20.
66.   Sackstein R, Merzaban JS, Cain DW, Dagia NM, Spencer JA, Lin CP, et al. Ex vivo glycan engineering of CD44 programs human multipotent mesenchymal stromal cell trafficking to bone. Nat Med. 2008;14(2):181-7.
67.   Schrepfer S, Deuse T, Reichenspurner H, Fischbein MP, Robbins RC, Pelletier MP. Stem Cell Transplantation: The Lung Barrier. Transplantation Proceedings. 2007;39(2):573-6.
68.   Salem HK, Thiemermann C. Mesenchymal Stromal Cells: Current Understanding and Clinical Status. STEM CELLS.28(3):585-96.
69.   Kode JA, Mukherjee S, Joglekar MV, Hardikar AA. Mesenchymal stem cells: immunobiology and role in immunomodulation and tissue regeneration. Cytotherapy. 2009;11(4):377-91.
70.   Patel ANaG, J. Potential clinical applications of adult human mesenchymal stem cell (Prochymal®) therapy. Stem Cells and Cloning: Advances and Applications. 2011 4:61-72.
71.   CR. M. Osiris Therapeutics Reports Interim Data for COPD Stem Cell Study. Press Release. 2009.

72.   Laflamme MA, Murry CE. Regenerating the heart. Nat Biotech. 2005;23(7):845-56.

73.   Schuleri KH, Feigenbaum GS, Centola M, Weiss ES, Zimmet JM, Turney J, et al. Autologous mesenchymal stem cells produce reverse remodelling in chronic ischaemic cardiomyopathy. European Heart Journal. 2009 November 1, 2009;30(22):2722-32.

74.   Hare JM, Traverse JH, Henry TD, Dib N, Strumpf RK, Schulman SP, et al. A Randomized, Double-Blind, Placebo-Controlled, Dose-Escalation Study of Intravenous Adult Human Mesenchymal Stem Cells (Prochymal) After Acute Myocardial Infarction. Journal of the American College of Cardiology. 2009;54(24):2277-86.

75.   Toma C, Pittenger MF, Cahill KS, Byrne BJ, Kessler PD. Human Mesenchymal Stem Cells Differentiate to a Cardiomyocyte Phenotype in the Adult Murine Heart. Circulation. 2002 January 1, 2002;105(1):93-8.

76.   Le Blanc K, Frassoni F, Ball L, Locatelli F, Roelofs H, Lewis I, et al. Mesenchymal stem cells for treatment of steroid-resistant, severe, acute graft-versus-host disease: a phase II study. The Lancet. 2008/5/16/;371(9624):1579-86.

77.   Jakub Tolar PV, and Armand Keating. Mesenchymal Stromal Cells for Graft-Versus-Host Disease. Human Gene Therapy. 2011;22(3):257-62.

78.   Nombela-Arrieta Cs, Ritz J, Silberstein LE. The elusive nature and function of mesenchymal stem cells. Nat Rev Mol Cell Biol.12(2):126-31.

79.   Yoo KH, Jang IK, Lee MW, Kim HE, Yang MS, Eom Y, et al. Comparison of immunomodulatory properties of mesenchymal stem cells derived from adult human tissues. Cellular Immunology. 2009;259(2):150-6.

80.   Alhadlaq A MJ. Mesenchymal stem cells: isolation and therapeutics. Stem Cells Dev. 2004;13(4):436-48.

81.   Lutolf MP, Gilbert PM, Blau HM. Designing materials to direct stem-cell fate. Nature. 2009;462(7272):433-41.

82.   Weir C, Morel-Kopp M-C, Gill A, Tinworth K, Ladd L, Hunyor SN, et al. Mesenchymal Stem Cells: Isolation, Characterisation and In Vivo Fluorescent Dye Tracking. Heart, Lung and Circulation. 2008;17(5):395-403.

83.   Liu SQ, Tay R, Khan M, Rachel Ee PL, Hedrick JL, Yang YY. Synthetic hydrogels for controlled stem cell differentiation. Soft Matter.6(1):67-81.

84.   Li W-J, Tuli R, Okafor C, Derfoul A, Danielson KG, Hall DJ, et al. A three-dimensional nanofibrous scaffold for cartilage tissue engineering using human mesenchymal stem cells. Biomaterials. 2005;26(6):599-609.

85.   Na SSaK. Mesenchymal Stem Cell-Based Tissue Engineering for Chondrogenesis. Journal of Biomedicine and Biotechnology. 2011.

86.   Caplan AI. Adult mesenchymal stem cells for tissue engineering versus regenerative medicine. Journal of Cellular Physiology. 2007;213(2):341-7.

87.   Barry FP, Murphy JM. Mesenchymal stem cells: clinical applications and biological characterization. The International Journal of Biochemistry & Cell Biology. 2004;36(4):568-84.

88.   Jon Rowley EA, Andrew Campbell, Harvey Brandwein, Steve Oh. Meeting Lot-Size Challenges of Manufacturing Adherent Cells for Therapy. BioProcess International. 2012;10(3):16-22.

89.   Fekete N, Rojewski MT, FÃ¼rst D, Kreja L, Ignatius A, Dausend J, et al. GMP-Compliant Isolation and Large-Scale Expansion of Bone Marrow-Derived MSC. PLoS ONE.7(8):e43255.

90.   Kirouac DC, Zandstra PW. The Systematic Production of Cells for Cell Therapies. Cell stem cell. 2008;3(4):369-81.

91.   Rubio D, Garcia-Castro J, MartÃ-n MaC, de la Fuente R, Cigudosa JC, Lloyd AC, et al. Spontaneous Human Adult Stem Cell Transformation. Cancer Research. 2005 April 15, 2005;65(8):3035-9.

92.   Timmins NE, Kiel M, Günther M, Heazlewood C, Doran MR, Brooke G, et al. Closed system isolation and scalable expansion of human placental mesenchymal stem cells. Biotechnology and Bioengineering.109(7):1817-26.

93.   Colter DC, Class R, DiGirolamo CM, Prockop DJ. Rapid expansion of recycling stem cells in cultures of plastic-adherent cells from human bone marrow. Proceedings of the National Academy of Sciences. 2000 March 28, 2000;97(7):3213-8.

94.   Dahl JA, Duggal S, Coulston N, Millar D, Melki J, Shahdadfar A, et al. Genetic and epigenetic instability of human bone marrow mesenchymal stem cells expanded in autologous serum or fetal bovine serum. The International journal of developmental biology. 2008;52(8):1033-42.

95.   Chabannon C BJ, Sielleur I, Douville J, Faucher C, Gravis G, Arnoulet C, Oziel-Taieb S, Blaise D, Novakovitch G, Camerlo J, Chabbert I, Genre D, Appel M, Armstrong D, Maraninchi D, Viens P. Production of ex vivo expanded hematopoietic cells and progenitors in a closed bioreactor, starting with a small volume marrow collection: A feasibility study in patients with poor-risk breast cancer and receiving high-doses of cyclophosphamide. Int J Oncol. 1999 15(3):511-8.

96.   Wang G, Zhang W, Jacklin C, Freedman D, Eppstein L, Kadouri A. Modified CelliGen-packed bed bioreactors for hybridoma cell cultures. Cytotechnology. 1992;9(1):41-9.

97.   Park S, Stephanopoulos G. Packed bed bioreactor with porous ceramic beads for animal cell culture. Biotechnology and Bioengineering. 1993;41(1):25-34.

98.   Meuwly F, Ruffieux PA, Kadouri A, von Stockar U. Packed-bed bioreactors for mammalian cell culture: Bioprocess and biomedical applications. Biotechnology Advances. 2007 2007/2//;25(1):45-56.

99.   Aung T, Miyoshi H, Tun T, Ohshima N. Chondroinduction of mouse mesenchymal stem cells in three-dimensional highly porous matrix scaffolds. Journal of Biomedical Materials Research. 2002;61(1):75-82.

100.   Tun T, Miyoshi H, Ema H, Nakauchi H, Ohshima N. New Type of Matrix Support for Bone Marrow Cell Cultures:In Vitro Culture and In Vivo Transplantation Experiments. ASAIO Journal. 2000;46(5):522-6.

101.   Ouyang A, Yang S-T. A two-stage perfusion fibrous bed bioreactor system for mass production of embryonic stem cells. Expert Opinion on Biological Therapy. 2008;8(7):895-909.

102.   Amanda W. Lund BY, Jan P. Stegemann, and George E. Plopper. . The Natural and Engineered 3D Microenvironment as a Regulatory Cue During Stem Cell Fate Determination. Tissue Engineering Part B: Reviews. 2009;15(3):371-80.

103.   Rodrigues CAV, Fernandes TG, Diogo MM, da Silva CuL, Cabral JMS. Stem cell cultivation in bioreactors. Biotechnology Advances. 2011/12//;29(6):815-29.

104.   Mitchell DA, Pandey A, Sangsurasak P, Krieger N. Scale-up strategies for packed-bed bioreactors for solid-state fermentation. Process Biochemistry. 1999;35(1â€"2):167-78.

105.   Baraniak P, McDevitt T. Scaffold-free culture of mesenchymal stem cell spheroids in suspension preserves multilineage potential. Cell and Tissue Research.347(3):701-11.

106.   Watanabe K, Ueno M, Kamiya D, Nishiyama A, Matsumura M, Wataya T, et al. A ROCK inhibitor permits survival of dissociated human embryonic stem cells. Nat Biotech. 2007;25(6):681-6.

107.   Mohamet L, Lea ML, Ward CM. Abrogation of E-Cadherin-Mediated Cellular Aggregation Allows Proliferation of Pluripotent Mouse Embryonic Stem Cells in Shake Flask Bioreactors. PLoS ONE.5(9):e12921.

108.   Dang SM, Gerecht-Nir S, Chen J, Itskovitz-Eldor J, Zandstra PW. Controlled, Scalable Embryonic Stem Cell Differentiation Culture. STEM CELLS. 2004;22(3):275-82.

109.   Larijani MR SA, Pournasr B, Hajihoseini V, Hassani SN, Totonchi M, Yousefi M, Shamsi F, Salekdeh GH, Baharvand H. Long-term maintenance of undifferentiated human embryonic and induced pluripotent stem cells in suspension. Stem Cells Dev. 2011;20(11):1911-23.

110.   Bartosh TJ, Ylöstalo JH, Mohammadipoor A, Bazhanov N, Coble K, Claypool K, et al. Aggregation of human mesenchymal stromal cells (MSCs) into 3D spheroids enhances their antiinflammatory properties. Proceedings of the National Academy of Sciences. August 3, 2010;107(31):13724-9.

111.   Daniel E. Kehoe DJ, Lye T. Lock, and Emmanuel S. Tzanakakis. . Scalable Stirred-Suspension Bioreactor Culture of Human Pluripotent Stem Cells. Tissue Engineering Part A. 2010;16(2):405-21.

112.   Van Wezel AL. Growth of Cell-strains and Primary Cells on Micro-carriers in Homogeneous Culture. Nature. 1967;216(5110):64-5.

113.   Schop D, Janssen FW, Borgart E, de Bruijn JD, van Dijkhuizen-Radersma R. Expansion of mesenchymal stem cells using a microcarrier-based cultivation system: growth and metabolism. Journal of Tissue Engineering and Regenerative Medicine. 2008;2(2-3):126-35.

114.   Phillips BW, Horne R, Lay TS, Rust WL, Teck TT, Crook JM. Attachment and growth of human embryonic stem cells on microcarriers. Journal of Biotechnology. 2008;138(1–2):24-32.

115.   Levine D. D, W., Wang, I., William, C. and Thilly, G. . Optimization of growth surface parameters in microcarrier cell culture. Biotechnology and Bioengineering. 1979;21(5):821-45.

116.   Kuo MJ, Lewis, C. Jr., Martin, R. A., Miller, R. E., Schoenfeld, R. A., Schuck, J. M., and Wildi, B. S. Growth of Anchorage Dependent Mammalian Cells on Glycine-Derivatized Polystyrene in Suspension Culture. In Vitro. 1981;17(10):901-6

117.   Hong Y, Gao, C., Xie, Y., Gong, Y., and Shen, J. Collagen-coated polylactide microspheres as chondrocyte microcarriers. Biomaterials. 2005;26(32): 6305-13.

118.   Wissemann KW, and Jacobson, B. S. . Pure gelatin microcarriers: Synthesis and use in cell attachment and growth of fibroblast and endothelial cells. In Vitro Cellular & Developmental Biology - Plant. 1985;21(7).

119.   Tielens S, Declercq, H., Gorski, T., Lippens, E., Schacht, E., and Cornelissen, M. Gelatin-Based Microcarriers as Embryonic Stem Cell Delivery System in Bone Tissue Engineering: An in-Vitro Study. Biomacromolecules. 2007;8(3):825-32.

120.   Nie Y, Bergendahl V, Hei DJ, Jones JM, Palecek SP. Scalable culture and cryopreservation of human embryonic stem cells on microcarriers. Biotechnology Progress. 2009;25(1):20-31.

121.   Mukhopadhyay A, Mukhopadhyay, S. N., and Talwar, G. P. Influence of serum proteins on the kinetics of attachment of vero cells to cytodex microcarriers. Journal of Chemical Technology & Biotechnology. 1993;56(4):369-74.

122.   Carani J, Dame, M., Beals, T. F., and Wass, J. A. Growth of three established cell lines on glass microcarriers. Biotechnology and Bioengineering. 1983;25(5):1359-72.

123.   Kobayashi N, Okitsu, T. Maruyama, M., Totsugawa, T., Kosaka, Y., Hayashi, N., Nakaji, S., and Tanaka, N. Development of a cellulose-based microcarrier

containing cellular adhesive peptides for a bioartificial liver. Transplantation Proceedings. 2003;35(1):443-4.

124.   Kasai S, Sawa, M., Nishida, Y., Onodera, K., Hirai, S., Yamamoto, T., and Mito, M. Cellulose microcarrier for high-density culture of hepatocytes. Transplant Procedings. 1992 24(6):2933-4.

125.   Tao X, Shaolin, L., and Yaoting, Y. Preparation and culture of hepatocyte on gelatin microcarriers. Journal of Biomedical Materials Research Part A. 2003;65A(2):306-10.

126.   Reuveny S, Mizrahi, A., Kotler, M., and Freeman, A. Mammalian cell propagation on derivatized polyacrylamide microcarriers. Developmetnal Biology Standard. 1983;55:11-23.

127.   Lovati AB VE, Talò G, Recordati C, Bonizzi L, Galliera E, Broggini M, Moretti M. Biodegradable microcarriers as cell delivery vehicle for in vivo transplantation and magnetic resonance monitoring. J Biol Regul Homeost Agents. 2011 25(2):63-74.

128.   Malda J, Frondoza CG. Microcarriers in the engineering of cartilage and bone. Trends in Biotechnology. 2006;24(7):299-304.

129.   Nienow A. Reactor Engineering in Large Scale Animal Cell Culture. Cytotechnology. 2006;50(1):9-33.

130.   Miller JAKaWM. Bioreactor Development for Stem Cell Expansion and Controlled Differentiation. Curr Opin Chem Biol. 2007;11(4):394-8.

131.   Lakhotia S, Papoutsakis ET. Agitation induced cell injury in microcarrier cultures. Protective effect of viscosity is agitation intensity dependent: Experiments and modeling. Biotechnology and Bioengineering. 1992;39(1):95-107.

132.   King JA, Miller WM. Bioreactor development for stem cell expansion and controlled differentiation. Current Opinion in Chemical Biology. 2007;11(4):394-8.

133.   Papoutsakis ET. Fluid-mechanical damage of animal cells in bioreactors. Trends in Biotechnology. 1991;9(1):427-37.

134.   Potier E, Noailly J, Ito K. Directing bone marrow-derived stromal cell function with mechanics. Journal of Biomechanics.43(5):807-17.

135.   Yourek G, McCormick SM, Mao JJ, Reilly GC. Shear stress induces osteogenic differentiation of human mesenchymal stem cells. Regenerative Medicine. 2012/08/13;5(5):713-24.

136.   Yi W, Sun Y, Wei X, Gu C, Dong X, Kang X, et al. Proteomic profiling of human bone marrow mesenchymal stem cells under shear stress. Molecular and Cellular Biochemistry.341(1):9-16.

137.   Marlene Knippenberg MNH, Behrouz Zandieh Doulabi, Cornelis M. Semeins, Paul I.J.M. Wuisman, and Jenneke Klein-Nulend. Adipose Tissue-Derived Mesenchymal Stem Cells Acquire Bone Cell-Like Responsiveness to Fluid Shear Stress on Osteogenic Stimulation. Tissue engineering. 2005;11:11-2.

138.   Francisco dos Santos PZA, Manuel M. Abecasis, Jeffrey M. Gimble, Lucas G. Chase, Andrew M. Campbell, Shayne Boucher, Mohan C. Vemuri, Cláudia Lobato da Silva, and Joaquim M.S. Cabral. . Toward a Clinical-Grade Expansion of Mesenchymal Stem Cells from Human Sources: A Microcarrier-Based Culture System Under Xeno-Free Conditions. Tissue Engineering Part C: Methods. 2011;17(12):1201-121.

139.   Singh V. Disposable bioreactor for cell culture using wave-induced agitation. Cytotechnology. 1999;30(1):149-58.

140.   Hewitt C, Lee K, Nienow A, Thomas R, Smith M, Thomas C. Expansion of human mesenchymal stem cells on microcarriers. Biotechnology Letters.33(11):2325-35.

141.   Weber C, Pohl S, Pã¶rtner R, Wallrapp C, Kassem M, Geigle P, et al. Expansion and Harvesting of hMSC-TERT. The open biomedical engineering journal. 2007;1:38-46.

142.   Yang HS, Jeon O, Bhang SH, Lee S-H, Kim B-S. Suspension Culture of Mammalian Cells Using Thermosensitive Microcarrier That Allows Cell Detachment Without Proteolytic Enzyme Treatment. Cell Transplantation.19(9):1123-32.

143.   Sun LY LS, Li YS, Harn HJ, Chiou TW. Functional cells cultured on microcarriers for use in regenerative medicine research. Cell Transplant 2011;20(1):49-62.

144.   Wang C, Gong Y, Lin Y, Shen J, Wang D-A. A novel gellan gel-based microcarrier for anchorage-dependent cell delivery. Acta Biomaterialia. 2008;4(5):1226-34.

145.   Wang C, Gong Y, Zhong Y, Yao Y, Su K, Wang D-A. The control of anchorage-dependent cell behavior within a hydrogel/microcarrier system in an osteogenic model. Biomaterials. 2009;30(12):2259-69.

146.   Malda J, Kreijveld E, Temenoff JS, Blitterswijk CAv, Riesle J. Expansion of human nasal chondrocytes on macroporous microcarriers enhances redifferentiation. Biomaterials. 2003;24(28):5153-61.

147.   Frondoza C, Sohrabi A, Hungerford D. Human chondrocytes proliferate and produce matrix components in microcarrier suspension culture. Biomaterials. 1996;17(9):879-88.

148.   Thissen H, Chang KY, Tebb TA, Tsai WB, Glattauer V, Ramshaw JAM, et al. Synthetic biodegradable microparticles for articular cartilage tissue engineering. Journal of Biomedical Materials Research Part A. 2006;77A(3):590-8.

149.   Curran SJ CR, Curran JM, Hunt JA. Expansion of human chondrocytes in an intermittent stirred flow bioreactor, using modified biodegradable microspheres. Tissue Eng. 2005;11(9-10):1312-22.

150.   Fischer EM LP, Van Blitterswijk CA, De Bruijn JD. Bone formation by mesenchymal progenitor cells cultured on dense and microporous hydroxyapatite particles. Tissue Eng. 2003 9(6):1179-88.

151.   A A Demetriou SML, P M Novikoff, A B Novikoff, N R Chowdhury, J Whiting, A Reisner, and J R Chowdhury. Survival, organization, and function of microcarrier-attached hepatocytes transplanted in rats. Proc Natl Acad Sci U S A. 1986;83(19):7475-9.

152.   Sun-Woong Kang OJ, and Byung-Soo Kim. . Poly(lactic-co-glycolic acid) Microspheres as an Injectable Scaffold for Cartilage Tissue Engineering. Tissue engineering. 2005;11(3-4):438-47.

153.   Voigt M SM, Schaefer DJ, Andree C, Horch R, Stark GB. Cultured epidermal keratinocytes on a microspherical transport system are feasible to reconstitute the epidermis in full-thickness wounds. Tissue Eng. 1999 5(6):563-72.

154.   Cepeda ILF, J.; Cornfeldt, M. L.; O'Kusky, J. R.; Doudet, D. J.. J. . Human retinal pigment epithelial cell implants ameliorate motor deficits in two rat models of Parkinson disease. Neuropathol Exp Neurol. 2007;66:576-84.

155.   Stover Np BREST, et al. INtrastriatal implantation of human retinal pigment epithelial cells attached to microcarriers in advanced parkinson disease. Archives of Neurology. 2005;62(12):1833-7.

156.   Nagaki M, Kano T, Muto Y, Yamada T, Ohnishi H, Moriwaki H. Effects of intraperitoneal transplantation of microcarrier-attached hepatocytes on D-galactosamine-induced acute liver failure in rats. Journal of Gastroenterology. 1990;25(1):78-87.

157.   Suh KS, Lilja H, Kamohara Y, Eguchi S, Arkadopoulos N, Neuman T, et al. Bioartificial Liver Treatment in Rats with Fulminant Hepatic Failure: Effect on DNA-Binding Activity of Liver-Enriched and Growth-Associated Transcription Factors. Journal of Surgical Research. 1999;85(2):243-50.

158. Xu Q, Yu D, Qiu Y, Zhang H, Ding Y. Function of a New Internal Bioartificial Liver: An In Vitro Study. Annals of Clinical & Laboratory Science. 2003 Summer 2003;33(3):306-12.

159. Voigt MA, C.; Kalt, T.; Dormann, S.; Schaefer, D. J.; Walgenbach, K. J.; Stark, G. B. Human recombinant EGF protein delivered by a biodegradable cell transplantation system. Tissue Eng. 2002;8:263-72.

160. Kang SWJ, O.; Kim, B. S. Poly(lactic-co-glycolic acid) microspheres as an injectable scaffold for cartilage tissue engineering. Tissue Eng. 2005;11(438-447).

161. Huss FR, Junker, J. P., Johnson, H., and Kratz, G. Macroporous gelatine spheres as culture substrate, transplantation vehicle, and biodegradable scaffold for guided regeneration of soft tissues. In vivo study in nude mice. Journal of plastic, reconstructive & aesthetic surgery : JPRAS. 2007;60(5):543-55.

162. Tatard VM, Venier-Julienne, M. C., Saulnier, P., Prechter, E., Benoit, J. P., Menei, P., and Montero-Menei, C. N. Pharmacologically active microcarriers: a tool for cell therapy. Biomaterials. 2005;26(17):3727-37.

163. Maldaa J, and Frondoza, C. G. . Microcarriers in the engineering of cartilage and bone. Trends in Biotechnology. 2006;24(7):299-304.

164. Phillips BW, Horne, R., Lay, T. S., Rust, W.L., Teck, T. T. and Crook, J. M. Attachment and growth of human embryonic stem cells on microcarriers. Journal of Biotechnology. 2008;138(1-2):24-32

165. Wu QF WC, Dong B, Wang LS. Cultivation of human mesenchymal stem cells on macroporous CultiSpher G microcarriers. Zhongguo Shi Yan Xue Ye Xue Za Zhi. 2003;11(1):15-21.

166. Caroline Ferrari FB, 1 Emmanuel Guedon,1 Eric Olmos,1 Nguyen Tran,2 Isabelle Chevalot,1 and Annie Marc1. Study of expansion of porcine bone marrow mesenchymal stem cells on microcarriers using various operating conditions. BMC Proc. 2011;5:100.

167. Yang Y, Rossi FMV, Putnins EE. Ex vivo expansion of rat bone marrow mesenchymal stromal cells on microcarrier beads in spin culture. Biomaterials. 2007;28(20):3110-20.

168. Chai C, Leong KW. Biomaterials Approach to Expand and Direct Differentiation of Stem Cells. Mol Ther. 2007;15(3):467-80.

169. Dima Sheyn GP, Dvir Netanely, Eytan Domany, and Dan Gazit. The Effect of Simulated Microgravity on Human Mesenchymal Stem Cells Cultured in an Osteogenic Differentiation System: A Bioinformatics Study. Tissue Engineering Part A. 2010;16(11):3403-12.

170. Meyers VE, Zayzafoon M, Douglas JT, McDonald JM. RhoA and Cytoskeletal Disruption Mediate Reduced Osteoblastogenesis and Enhanced Adipogenesis of Human Mesenchymal Stem Cells in Modeled Microgravity. Journal of Bone and Mineral Research. 2005;20(10):1858-66.

171. Schulte VA, Diìez M, Moìller M, Lensen MC. Surface Topography Induces Fibroblast Adhesion on Intrinsically Nonadhesive Poly(ethylene glycol) Substrates. Biomacromolecules. 2009;10(10):2795-801.

172. Chun KW, Yoo, H. S., Yoon, J. J., and Park, T. G. Biodegradable PLGA Microcarriers for Injectable Delivery of Chondrocytes: Effect of Surface Modification on Cell Attachment and Function. Biotechnology Progress. 2004;20(6):1797-801.

173. Varania J, Bendelowa, M. J., Chunb, J. H., and Hillegas, W. A. . Cell growth on microcarriers: comparison of proliferation on and recovery from various substrates Journal of Biological Standardization. 1986;14(4):331-6.

174. Varani J, Dame, M., Rediske, J., Beals, T. F., and Hillegas, W. Substrate-dependent differences in growth and biological properties of fibroblasts and epithelial

cells grown in microcarrier next term culture. Journal of Biological Standardization. 1985;13(1):67-76

175. Mukhopadhyay A, Mukhopadhyay, S. N., and Talwar, G. P. Cellular affinity is the only deciding factor for microcarrier selection for the cultivation of anchorage dependent cells. Biotechnology Techniques. 1993;7(3):   173-6.

176. Crawford A, and Hatton, P. V. Cell-Biomaterial Interactions in Skeletal Tissue Engineering. Biomedicine & Pharmacotherapy. 2008;62(8):493-4.

177. Shimazu K, Toda S, Miyazono M, Sakemi T, Sugihara H. Morphogenesis of MDCK cells in a collagen gel matrix culture under stromal adipocyte-epithelial cell interaction. Kidney Int. 2001;60(2):568-78.

178. Wiegandt K, Goepfert, C., Richter, T., Fritsch, D., Janßen, R., and Pörtner, R. In Vitro Generation of Cartilage-Carrier-Constructs on Hydroxylapatite Ceramics with Different Surface Structures. Open Biomed Eng J. 2008;2:64-70.

179. Wang C, Gong, Y., Lin, Y., Shen, J., and Wang, D. A. A novel gellan gel-based microcarrier for anchorage-dependent cell delivery. Acta Biomaterialia. 2008;4(5):1226-34.

180. Singh A, Elisseeff J. Biomaterials for stem cell differentiation. Journal of Materials Chemistry.20(40):8832-47.

181. Wichterle O, Lim D. Hydrophilic Gels for Biological Use. Nature. 1960;185(4706):117-8.

182. Liu Y, Goldberg AJ, Dennis JE, Gronowicz GA, Kuhn LT. One-Step Derivation of Mesenchymal Stem Cell (MSC)-Like Cells from Human Pluripotent Stem Cells on a Fibrillar Collagen Coating. PLoS ONE.7(3):e33225.

183. Salasznyk RM, Williams WA, Boskey A, Batorsky A, Plopper GE. Adhesion to Vitronectin and Collagen I Promotes Osteogenic Differentiation of Human Mesenchymal Stem Cells. Journal of Biomedicine and Biotechnology. 2004;2004(1):24-34.

184. Overstreet M, Sohrabi A, Polotsky A, Hungerford DS, Frondoza CG. COLLAGEN MICROCARRIER SPINNER CULTURE PROMOTES OSTEOBLAST PROLIFERATION AND SYNTHESIS OF MATRIX PROTEINS. In Vitro Cellular & Developmental Biology - Animal. 2003 2012/08/06;39(5 & 6):228-34.

185. Marklein RA, Burdick JA. Controlling Stem Cell Fate with Material Design. Advanced Materials.22(2):175-89.

186. Chan BP, So KF. Photochemical crosslinking improves the physicochemical properties of collagen scaffolds. Journal of Biomedical Materials Research Part A. 2005;75A(3):689-701.

187. Lee CH, Singla A, Lee Y. Biomedical applications of collagen. International Journal of Pharmaceutics. 2001;221(1â€"2):1-22.

188. Im G, II, Shin Y-W, Lee K-B. Do adipose tissue-derived mesenchymal stem cells have the same osteogenic and chondrogenic potential as bone marrow-derived cells? Osteoarthritis and cartilage / OARS, Osteoarthritis Research Society. 2005;13(10):845-53.

189. Park S-H, Gil ES, Shi H, Kim HJ, Lee K, Kaplan DL. Relationships between degradability of silk scaffolds and osteogenesis. Biomaterials.31(24):6162-72.

190. Wang Y, Blasioli DJ, Kim H-J, Kim HS, Kaplan DL. Cartilage tissue engineering with silk scaffolds and human articular chondrocytes. Biomaterials. 2006;27(25):4434-42.

191. Kleinman HK, Martin GR. Matrigel: Basement membrane matrix with biological activity. Seminars in Cancer Biology. 2005;15(5):378-86.

192. Sato T, Vries RG, Snippert HJ, van de Wetering M, Barker N, Stange DE, et al. Single Lgr5 stem cells build cryptÂ–villus structures in vitro without a mesenchymal niche. Nature. 2009;459(7244):262-5.

193.   Amit M, Itskovitzâ€Eldor J, Irina K, Robert L. Feederâ€Free Culture of Human Embryonic Stem Cells. Methods in Enzymology: Academic Press; 2006. p. 37-49.

194.   Uemura M, Refaat MM, Shinoyama M, Hayashi H, Hashimoto N, Takahashi J. Matrigel supports survival and neuronal differentiation of grafted embryonic stem cell-derived neural precursor cells. Journal of Neuroscience Research.88(3):542-51.

195.   Serban MA, Liu Y, Prestwich GD. Effects of extracellular matrix analogues on primary human fibroblast behavior. Acta Biomaterialia. 2008;4(1):67-75.

196.   Campbell JJ LD, Bader DL. Dynamic compressive strain influences chondrogenic gene expression in human mesenchymal stem cells. Biorheology. 2006;43(3-4):455-70.

197.   Malafaya PcB, Silva GA, Reis RL. Naturalâ€"origin polymers as carriers and scaffolds for biomolecules and cell delivery in tissue engineering applications. Advanced Drug Delivery Reviews. 2007;59(4â€"5):207-33.

198.   Bian L, Zhai DY, Tous E, Rai R, Mauck RL, Burdick JA. Enhanced MSC chondrogenesis following delivery of TGF-Î²3 from alginate microspheres within hyaluronic acid hydrogels in vitro and in vivo. Biomaterials.32(27):6425-34.

199.   V. L. Workman SBDPKDDP. Microfluidic chip-based synthesis of alginate microspheres for encapsulation of immortalized human cell. Biomicrofluidics. 2007;1(1).

200.   Justice BA, Badr NA, Felder RA. 3D cell culture opens new dimensions in cell-based assays. Drug Discovery Today. 2009;14(1â€"2):102-7.

201.   Chen X-G, Liu C-S, Liu C-G, Meng X-H, Lee CM, Park H-J. Preparation and biocompatibility of chitosan microcarriers as biomaterial. Biochemical Engineering Journal. 2006;27(3):269-74.

202.   Costa-Pinto AR, Correlo VM, Sol PC, Bhattacharya M, Srouji S, Livne E, et al. Chitosan–poly(butylene succinate) scaffolds and human bone marrow stromal cells induce bone repair in a mouse calvaria model. Journal of Tissue Engineering and Regenerative Medicine.6(1):21-8.

203.   Lao L, Tan H, Wang Y, Gao C. Chitosan modified poly(l-lactide) microspheres as cell microcarriers for cartilage tissue engineering. Colloids and Surfaces B: Biointerfaces. 2008;66(2):218-25.

204.   Maeng Y-J, Choi S-W, Kim HO, Kim J-H. Culture of human mesenchymal stem cells using electrosprayed porous chitosan microbeads. Journal of Biomedical Materials Research Part A.92A(3):869-76.

205.   West JL. Biofunctional Polymers In: Wnek GLBG, editor. Encyclopedia of Biomaterials and Biomedical Engineering: Informa Healthcare 2004.

206.   Tibbitt MW, and Anseth, K. S. . Hydrogels as extracellular matrix mimics for 3D cell culture. Biotechnology and Bioengineering. 2009;103(4):655-63.

207.   Lee KY, Mooney DJ. Hydrogels for Tissue Engineering. Chemical Reviews. 2001;101(7):1869-80.

208.   Hoffman A, S,. Hydrogels for Biomedical Applications. Annals of the New York Academy of Sciences. 2001;944(BIOARTIFICIAL ORGANS III: TISSUE SOURCING, IMMUNOISOLATION, AND CLINICAL TRIALS):62-73.

209.   Drury JL, Mooney DJ. Hydrogels for tissue engineering: scaffold design variables and applications. Biomaterials. 2003;24(24):4337-51.

210.   Pfister PM, Wendlandt M, Neuenschwander P, Suter UW. Surface-textured PEG-based hydrogels with adjustable elasticity: Synthesis and characterization. Biomaterials. 2007;28(4):567-75.

211.   Hahn MS, Taite, L. J., Moon, J. J., Rowland, M. C., Ruffino, K. A., and West, J. L. Photolithographic patterning of polyethylene glycol hydrogels. Biomaterials. 2006;27(12):2519-24.

212.	Mann BK, Gobin, A. S., Tsai, A. T., Schmedlen, R. H. and West, J. L. Smooth muscle cell growth in photopolymerized hydrogels with cell adhesive and proteolytically degradable domains: synthetic ECM analogsnext term for tissue engineering. Biomaterials. 2001;22(22):3045-51.

213.	Merrill EWSad, Salzman, E.W. Polyethylene oxide as a biomaterial. ASAIO Journal. 1983;6(2):60-4.

214.	Gombotz WR, Guanghui, W., Horbett,T. A., and Hoffman, A. S. . Protein adsorption to poly(ethylene oxide) surfaces. Journal of Biomedical Materials Research. 2004;25(12):1547 - 62.

215.	Lin-Gibson S, Bencherif S, Cooper JA, Wetzel SJ, Antonucci JM, Vogel BM, et al. Synthesis and Characterization of PEG Dimethacrylates and Their Hydrogels. Biomacromolecules. 2004;5(4):1280-7.

216.	Bryant SJ, and Anseth, KS Hydrogel properties influence ECM production by chondrocytes photoencapsulated in poly(ethylene glycol) hydrogels. Journal of Biomedical Materials Research. 2002;59(1):63-72.

217.	Nuttelman CR, Tripodi MC, Anseth KS. Synthetic hydrogel niches that promote hMSC viability. Matrix Biology. 2005;24(3):208-18.

218.	Chelsea N. Salinas BBC, Andrea M. Kasko, Kristi S. Anseth. Chondrogenic Differentiation Potential of Human Mesenchymal Stem Cells Photoencapsulated within Poly(Ethylene Glycol)–Arginine-Glycine-Aspartic Acid-Serine Thiol-Methacrylate Mixed-Mode Networks. Tissue Engineering. 2007;13(5):1025-34.

219.	Hlady V, Buijs J. Protein adsorption on solid surfaces. Current Opinion in Biotechnology. 1996;7(1):72-7.

220.	Davis GE. Affinity of integrins for damaged extracellular matrix: [alpha]v[beta]3 binds to denatured collagen type I through RGD sites. Biochemical and Biophysical Research Communications. 1992;182(3):1025-31.

221.	Bhadriraju K, Hansen LK. Hepatocyte adhesion, growth and differentiated function on RGD-containing proteins. Biomaterials. 2000;21(3):267-72.

222.	Altankov G, Grinnell, F., and Groth, T. Studies on the biocompatibility of materials: Fibroblast reorganization of substratum-bound fibronectin on surfaces varying in wettability. Journal of Biomedical Materials Research. 1996;30(3):385-91.

223.	Underwood PA, Steele JG, Dalton BA. Effects of polystyrene surface chemistry on the biological activity of solid phase fibronectin and vitronectin, analysed with monoclonal antibodies. J Cell Sci. 1993 March 1, 1993;104(3):793-803.

224.	Denise JI, Steven SS, George AT. Effect of the conformation and orientation of adsorbed fibronectin on endothelial cell spreading and the strength of adhesion. Journal of Biomedical Materials Research. 1993;27(8):1103-13.

225.	Elbert DL, and Hubbell, J. A. Surface treatments of polymers for biocompatibility. Annual Review of Materials Science. 1996;26(1):365-94

226.	Hern DL, and Hubbell, J. A. Incorporation of adhesion peptides into nonadhesive hydrogels useful for tissue resurfacing. Journal of Biomedical Materials Research. 1998;39(2):266-76.

227.	Maheshwari G, Brown G, Lauffenburger DA, Wells A, Griffith LG. Cell adhesion and motility depend on nanoscale RGD clustering. J Cell Sci. 2000 May 15, 2000;113(10):1677-86.

228.	Huang G, Zhou Z, Srinivasan R, Penn MS, Kottke-Marchant K, Marchant RE, et al. Affinity manipulation of surface-conjugated RGD peptide to modulate binding of liposomes to activated platelets. Biomaterials. 2008;29(11):1676-85.

229.	Hersel U, Dahmen, C., and Kessler, H. RGD modified polymers: biomaterials for stimulated cell adhesion and beyond. Biomaterials. 2003;24(24):4385-415.

230.	Ruoslahti E. RGD AND OTHER RECOGNITION SEQUENCES FOR INTEGRINS. Annual Review of Cell and Developmental Biology. 1996;12(1):697-715.

231. Albelda SM, Buck CA. Integrins and other cell adhesion molecules. FASEB J. 1990 August 1, 1990;4(11):2868-80.
232. Mann BK, Schmedlen RH, West JL. Tethered-TGF-[beta] increases extracellular matrix production of vascular smooth muscle cells. Biomaterials. 2001;22(5):439-44.
233. West JL. Bioactive Hydrogels: mimicking the ECM with synthetic materials. CRC Press. 2005:275 - 9.
234. Lin C-C, Anseth K. PEG Hydrogels for the Controlled Release of Biomolecules in Regenerative Medicine. Pharmaceutical Research. 2009;26(3):631-43.
235. Tan H, Marra KG. Injectable, Biodegradable Hydrogels for Tissue Engineering Applications. Materials.3(3):1746-67.
236. Nicodemus GD, Bryant SJ. Cell encapsulation in biodegradable hydrogels for tissue engineering applications. Tissue engineering Part B, Reviews. 2008;14(2):149-65.
237. Choi C-H, Jung J-H, Hwang T-S, Lee C-S. <i>In situ</i> microfluidic synthesis of monodisperse PEG microspheres. Macromolecular Research. 2009;17(3):163-7.
238. Burdick. JLIaJA. Photopolymerizable and Degradable Biomaterials for Tissue Engineering Applications. Tissue engineering. 2007;13(10):2369-85.
239. Nuttelman CR, Tripodi MC, Anseth KS. In vitro osteogenic differentiation of human mesenchymal stem cells photoencapsulated in PEG hydrogels. Journal of Biomedical Materials Research Part A. 2004;68A(4):773-82.
240. Salinas CN, Anseth KS. Mixed Mode Thiolâ^'Acrylate Photopolymerizations for the Synthesis of PEGâ^'Peptide Hydrogels. Macromolecules. 2008;41(16):6019-26.
241. Salinas CN, Cole BB, Kasko AM, Anseth KS. Chondrogenic differentiation potential of human mesenchymal stem cells photoencapsulated within poly(ethylene glycol)-arginine-glycine-aspartic acid-serine thiol-methacrylate mixed-mode networks. Tissue engineering. 2007;13(5):1025-34.
242. Lecamp L, Houllier F, Youssef B, Bunel C. Photoinitiated cross-linking of a thiol-methacrylate system. Polymer. 2001;42(7):2727-36.
243. Neil BC, Christopher NB. Kinetics of thiol-ene and thiol-acrylate photopolymerizations with real-time fourier transform infrared. Journal of Polymer Science Part A: Polymer Chemistry. 2001;39(19):3311-9.
244. Polizzotti BD, Fairbanks BD, Anseth KS. Three-Dimensional Biochemical Patterning of Click-Based Composite Hydrogels via Thiolene Photopolymerization. Biomacromolecules. 2008;9(4):1084-7.
245. Salinas CN, Anseth KS. The enhancement of chondrogenic differentiation of human mesenchymal stem cells by enzymatically regulated RGD functionalities. Biomaterials. 2008;29(15):2370-7.
246. Zhu J. Bioactive modification of poly(ethylene glycol) hydrogels for tissue engineering. Biomaterials.31(17):4639-56.
247. Katayama Y, Battista M, Kao W-M, Hidalgo A, Peired AJ, Thomas SA, et al. Signals from the Sympathetic Nervous System Regulate Hematopoietic Stem Cell Egress from Bone Marrow. Cell. 2006;124(2):407-21.
248. Pelham RJ, Wang Y-l. Cell locomotion and focal adhesions are regulated by substrateâ€‰flexibility. Proceedings of the National Academy of Sciences. 1997 December 9, 1997;94(25):13661-5.
249. Discher DE, Janmey P, Wang Y-l. Tissue Cells Feel and Respond to the Stiffness of Their Substrate. Science. 2005 November 18, 2005;310(5751):1139-43.
250. Dokukina IV, Gracheva ME. A Model of Fibroblast Motility on Substrates with Different Rigidities. Biophysical Journal.98(12):2794-803.

251. Shih Y-RV, Tseng K-F, Lai H-Y, Lin C-H, Lee OK. Matrix stiffness regulation of integrin-mediated mechanotransduction during osteogenic differentiation of human mesenchymal stem cells. Journal of Bone and Mineral Research.26(4):730-8.
252. Dong Li JZ, Farhan Chowdhury, Jianjun Cheng, Ning Wang, and Fei Wang. Role of mechanical factors in fate decisions of stem cells. Regen Med. 2011;6(2):229-40.
253. Betapudi V. Myosin II Motor Proteins with Different Functions Determine the Fate of Lamellipodia Extension during Cell Spreading. PLoS ONE.5(1):e8560.
254. McBeath R, Pirone DM, Nelson CM, Bhadriraju K, Chen CS. Cell Shape, Cytoskeletal Tension, and RhoA Regulate Stem Cell Lineage Commitment. Developmental Cell. 2004;6(4):483-95.
255. Engler AJ, Sen S, Sweeney HL, Discher DE. Matrix Elasticity Directs Stem Cell Lineage Specification. Cell. 2006;126(4):677-89.
256. Saha K, Pollock JF, Schaffer DV, Healy KE. Designing synthetic materials to control stem cell phenotype. Current Opinion in Chemical Biology. 2007;11(4):381-7.
257. Evans ND MC, Gentleman E, LaPointe V, Patankar SN, Kallivretaki M, Chen X, Roberts CJ, Stevens MM. Substrate stiffness affects early differentiation events in embryonic stem cells. Eur Cell Mater. 2009;21(18):1-13.
258. Fisher OZ, Khademhosseini A, Langer R, Peppas NA. Bioinspired Materials for Controlling Stem Cell Fate. Accounts of Chemical Research. 2009 2012/08/06;43(3):419-28.
259. van der Flier LG, Clevers H. Stem Cells, Self-Renewal, and Differentiation in the Intestinal Epithelium. Annual Review of Physiology. 2009;71(1):241-60.
260. Kilian KA, Bugarija B, Lahn BT, Mrksich M. Geometric cues for directing the differentiation of mesenchymal stem cells. Proceedings of the National Academy of Sciences. March 16, 2010;107(11):4872-7.
261. Tang J, Peng R, Ding J. The regulation of stem cell differentiation by cell-cell contact on micropatterned material surfaces. Biomaterials.31(9):2470-6.
262. Dike LE CC, Mrksich M, Tien J, Whitesides GM, Ingber DE. Geometric control of switching between growth, apoptosis, and differentiation during angiogenesis using micropatterned substrates. In Vitro Cell Dev Biol Anim. 1999;35(8):441-8.
263. Ruiz SA, Chen CS. Emergence of Patterned Stem Cell Differentiation Within Multicellular Structures. STEM CELLS. 2008;26(11):2921-7.
264. Bari Murtuza JWN, and Ali Khademhosseini. Micro- and Nanoscale Control of the Cardiac Stem Cell Niche for Tissue Fabrication. Tissue Engineering Part B: Reviews. 2009;15(4):443-54.
265. Sanz-Herrera JA, Moreo P, GarcÃa-Aznar JM, DoblarÃ© M. On the effect of substrate curvature on cell mechanics. Biomaterials. 2009;30(34):6674-86.
266. John J. Schmidt JJ, and Hyunjoon Kong. . The Interplay Between Cell Adhesion Cues and Curvature of Cell Adherent Alginate Microgels in Multipotent Stem Cell Culture. Tissue Engineering Part A. 2011;17(21-22):2687-94.
267. Jane H. Maduram EG, 2 Huang Hu,3 Chang Liu,3 and Milan Mrksich4,*. Subcellular curvature at the perimeter of micropatterned cells influences lamellipodial distribution and cell polarity. Cell Motil Cytoskeleton. 2008 65(11):841-52.
268. Dunn GA, Heath JP. A new hypothesis of contact guidance in tissue cells. Experimental Cell Research. 1976;101(1):1-14.
269. Smeal R, Rabbitt R, Biran R, Tresco P. Substrate Curvature Influences the Direction of Nerve Outgrowth. Annals of Biomedical Engineering. 2005;33(3):376-82.
270. Rumpler M, Woesz A, Dunlop JWC, van Dongen JT, Fratzl P. The effect of geometry on three-dimensional tissue growth. Journal of The Royal Society Interface. 2008 October 6, 2008;5(27):1173-80.

271.   Berry CC, Campbell G, Spadiccino A, Robertson M, Curtis ASG. The influence of microscale topography on fibroblast attachment and motility. Biomaterials. 2004;25(26):5781-8.

272.   Tan G, Liao J, Ning C, Zhang L. Preparation, characterization, and drug-release properties of PEG-DA-based copolymer hydrogel microspheres. Journal of Applied Polymer Science.125(5):3509-16.

273.   Salvador A, Igartua M, HernÃ¡ndez RM, Pedraz JL. Combination of immune stimulating adjuvants with poly(lactide-co-glycolide) microspheres enhances the immune response of vaccines. Vaccine.30(3):589-96.

274.   Amit Chaudhary*1 UN, Parul Patel2. Hydrogels: Recent Advanced Drug Delivery: A Review. Asian Journal of Pharmacy and Life Science. 2012;2(2).

275.   Cohen S, Bano MC, Visscher KB, Chow M, Allcock HR, Langer R. Ionically crosslinkable polyphosphazene: a novel polymer for microencapsulation. Journal of the American Chemical Society. 1990 2012/08/07;112(21):7832-3.

276.   Mann BK, Gobin AS, Tsai AT, Schmedlen RH, West JL. Smooth muscle cell growth in photopolymerized hydrogels with cell adhesive and proteolytically degradable domains: synthetic ECM analogs for tissue engineering. Biomaterials. 2001;22(22):3045-51.

277.   Young CJ, Poole-Warren LA, Martens PJ. Combining submerged electrospray and UV photopolymerization for production of synthetic hydrogel microspheres for cell encapsulation. Biotechnology and Bioengineering.109(6):1561-70.

278.   Lacík I, Briššová M, Anilkumar AV, Powers AC, Wang T. New capsule with tailored properties for the encapsulation of living cells. Journal of Biomedical Materials Research. 1998;39(1):52-60.

279.   Prüße U, Dalluhn J, Breford J, Vorlop KD. Production of Spherical Beads by JetCutting. Chemical Engineering & Technology. 2000;23(12):1105-10.

280.   Brandenberger HR, Widmer F. Immobilization of Highly Concentrated Cell Suspensions Using the Laminar Jet Breakup Technique. Biotechnology Progress. 1999;15(3):366-72.

281.   Franco CL, Price J, West JL. Development and optimization of a dual-photoinitiator, emulsion-based technique for rapid generation of cell-laden hydrogel microspheres. Acta Biomaterialia.7(9):3267-76.

282.   Gu H, Duits MHG, Mugele F. Droplets Formation and Merging in Two-Phase Flow Microfluidics. International Journal of Molecular Sciences.12(4):2572-97.

283.   Oh JK, Drumright R, Siegwart DJ, Matyjaszewski K. The development of microgels/nanogels for drug delivery applications. Progress in Polymer Science. 2008;33(4):448-77.

284.   Olabisi RM, Lazard ZW, Franco CL, Hall MA, Kwon SK, Sevick-Muraca EM, et al. Hydrogel microsphere encapsulation of a cell-based gene therapy system increases cell survival of injected cells, transgene expression, and bone volume in a model of heterotopic ossification. Tissue engineering Part A.16(12):3727-36.

285.   van Dijke KC, Veldhuis G, Schroën K, Boom RM. Simultaneous formation of many droplets in a single microfluidic droplet formation unit. AIChE Journal.56(3):833-6.

286.   A. J. Electrostatic micro- and nanoencapsulation and electroemulsification: a brief review. J Microencapsul. 2008;25(7):443-68.

287.   Watanabe H, Matsuyama T, Yamamoto H. Preparation of immobilized enzyme gel particles using an electrostatic atomization technique. Biochemical Engineering Journal. 2001;8(2):171-4.

288.   Whitesides GM. The origins and the future of microfluidics. Nature. 2006;442(7101):368-73.

289.   Workman VL, Dunnett, S. B., Kille. P., and Palmer, D. D. . On-Chip Alginate Microencapsulation of Functional Cells. Macromolecular Rapid Communications. 2008;29(2):165-70.

290.   Joanicot M, and Armand, A. . Applied Physics: Droplet Control for Microfluidics. Science. 2005 August 5, 2005;309(5736):887-8.

291.   Link DR, Anna SL, Weitz DA, Stone HA. Geometrically Mediated Breakup of Drops in Microfluidic Devices. Physical Review Letters. 2004;92(5):054503.

292.   Nisisako T, Torii T, Higuchi T. Droplet formation in a microchannel network. Lab on a chip. 2002;2(1):24-6.

293.   van der Graaf S, Nisisako T, SchroÃ«n CGPH, van der Sman RGM, Boom RM. Lattice Boltzmann Simulations of Droplet Formation in a T-Shaped Microchannel. Langmuir. 2006 2012/08/13;22(9):4144-52.

294.   Wan J. Microfluidic-Based Synthesis of Hydrogel Particles for Cell Microencapsulation and Cell-Based Drug Delivery. Polymers.4(2):1084-108.

295.   Sugiura S, Nakajima M, Kumazawa N, Iwamoto S, Seki M. Characterization of Spontaneous Transformation-Based Droplet Formation during Microchannel Emulsification. The Journal of Physical Chemistry B. 2002 2012/08/13;106(36):9405-9.

296.   Nisisako T, Torii T, Higuchi T. Novel microreactors for functional polymer beads. Chem Eng J. [Article]. 2004;101(1-3):23-9.

297.   Cohen I, Li H, Hougland JL, Mrksich M, Nagel SR. Using Selective Withdrawal to Coat Microparticles. Science. 2001 April 13, 2001;292(5515):265-7.

298.   Huang KS, Lai TH, Lin YC. Manipulating the generation of Ca-alginate microspheres using microfluidic channels as a carrier of gold nanoparticles. Lab on a chip. 2006;6(7):954-7.

299.   Choi C, Jung, J., Hwang, T., and Lee, C. In Situ Microfluidic Synthesis of Monodisperse PEG Microspheres. Macromolecular Research. 2009;17(3):163-7.

300.   Hern DLaH, J. A. Incorporation of adhesion peptides into nonadhesive hydrogels useful for tissue resurfacing. Journal of Biomedical Materials Research. 1998;39(2):266-76.

301.   Bencherif SA, Srinivasan A, Sheehan JA, Walker LM, Gayathri C, Gil R, et al. End-group effects on the properties of PEG-co-PGA hydrogels. Acta Biomaterialia. 2009;5(6):1872-83.

302.   Franz N, Timm U, Hohenberg H. Monitoring and Analysis of the Environment for Biomaterials in the ESEM Under "Wet Mode" Conditions. Microscopy and Microanalysis. 2003;9(SupplementS03):482-3.

303.   Freshney R. Culture of Animal Cells: A Manual of Basic Technique. New York: Alan R. Liss, Inc.; 1987.

304.   Livak KJ, Schmittgen TD. Analysis of Relative Gene Expression Data Using Real-Time Quantitative PCR and the 2â^'Î"Î"CT Method. Methods. 2001;25(4):402-8.

305.   Lin C-C, Anseth KS. Controlling Affinity Binding with Peptide-Functionalized Poly(ethylene glycol) Hydrogels. Advanced Functional Materials. 2009;19(14):2325-31.

306.   Peyton SR, Raub CB, Keschrumrus VP, Putnam AJ. The use of poly(ethylene glycol) hydrogels to investigate the impact of ECM chemistry and mechanics on smooth muscle cells. Biomaterials. 2006;27(28):4881-93.

307.   Zhu JM, Roger E. Design properties of hydrogel tissue-engineering scaffolds. Expert Review of Medical Devices. 2011;8(5):607-26.

308.   Yang F, Williams CG, Wang D-a, Lee H, Manson PN, Elisseeff J. The effect of incorporating RGD adhesive peptide in polyethylene glycol diacrylate hydrogel on osteogenesis of bone marrow stromal cells. Biomaterials. 2005;26(30):5991-8.

309.   Hern DL, Hubbell JA. Incorporation of adhesion peptides into nonadhesive hydrogels useful for tissue resurfacing. Journal of Biomedical Materials Research. 1998;39(2):266-76.

310.   Schmedlen RH, Masters KS, West JL. Photocrosslinkable polyvinyl alcohol hydrogels that can be modified with cell adhesion peptides for use in tissue engineering. Biomaterials. 2002;23(22):4325-32.

311.   Zhao DS, Roy B, McCormick MT, Kuhr WG, Brazill SA. Rapid fabrication of a poly(dimethylsiloxane) microfluidic capillary gel electrophoresis system utilizing high precision machining. Lab on a chip. 2003;3(2):93-9.

312.   Thorsen T, Roberts RW, Arnold FH, Quake SR. Dynamic Pattern Formation in a Vesicle-Generating Microfluidic Device. Physical Review Letters. 2001;86(18):4163-6.

313.   Tan J, Xu JH, Li SW, Luo GS. Drop dispenser in a cross-junction microfluidic device: Scaling and mechanism of break-up. Chem Eng J. 2008;136(2â€"3):306-11.

314.   Christopher GF, Anna SL. Microfluidic methods for generating continuous droplet streams. Journal of Physics D: Applied Physics. 2007;40(19):R319.

315.   Cramer C, Fischer P, Windhab EJ. Drop formation in a co-flowing ambient fluid. Chemical Engineering Science. 2004;59(15):3045-58.

316.   Silva NA, Cooke MJ, Tam RY, Sousa N, Salgado AJ, Reis RL, et al. The effects of peptide modified gellan gum and olfactory ensheathing glia cells on neural stem/progenitor cell fate. Biomaterials. 2012;33(27):6345-54.

317.   Joy A, Cohen DM, Luk A, Anim-Danso E, Chen C, Kohn J. Control of Surface Chemistry, Substrate Stiffness, and Cell Function in a Novel Terpolymer Methacrylate Library. Langmuir. 2011 2012/09/07;27(5):1891-9.

318.   Stephanie JB, Kristi SA. Controlling the spatial distribution of ECM components in degradable PEG hydrogels for tissue engineering cartilage. Journal of Biomedical Materials Research Part A. 2003;64A(1):70-9.

319.   Nguyen KT, West JL. Photopolymerizable hydrogels for tissue engineering applications. Biomaterials. 2002;23(22):4307-14.

320.   Almany L, Seliktar D. Biosynthetic hydrogel scaffolds made from fibrinogen and polyethylene glycol for 3D cell cultures. Biomaterials. 2005;26(15):2467-77.

321.   Lutolf MP, Hubbell JA. Synthetic biomaterials as instructive extracellular microenvironments for morphogenesis in tissue engineering. Nat Biotech. 2005;23(1):47-55.

322.   Raeber GP, Lutolf, M. P.and Hubbell, J. A. Molecularly Engineered PEG Hydrogels: A Novel Model System for Proteolytically Mediated Cell Migration. Biophysical Journal. 2005;89(2):1374-88.

323.   Brenda K. Mann ASG, Annabel T. Tsai, Rachael H. Schmedlen and Jennifer L. West. Smooth muscle cell growth in photopolymerized hydrogels with cell adhesive and proteolytically degradable domains: synthetic ECM analogsnext term for tissue engineering. Biomaterials. 2001;22(22):3045-51.

324.   Mariah S. Hahn HL, Dany Munoz-Pinto, Xin Qu, Yaping Hou, and Melissa A. Grunlan. Influence of hydrogel mechanical properties and mesh size on vocal fold fibroblast extracellular matrix production and phenotype. Acta Biomaterlia. 2008;4(5):1161-71.

325.   Andrea SG, Jennifer LW. Val-ala-pro-gly, an elastin-derived non-integrin ligand: Smooth muscle cell adhesion and specificity. Journal of Biomedical Materials Research Part A. 2003;67A(1):255-9.

326.   Hubbell JA. Bioactive biomaterials. Current Opinion in Biotechnology. 1999;10(2):123-9.

327. Brenda KM, Jennifer LW. Cell adhesion peptides alter smooth muscle cell adhesion, proliferation, migration, and matrix protein synthesis on modified surfaces and in polymer scaffolds. Journal of Biomedical Materials Research. 2002;60(1):86-93.

328. Jonathan WG, Suzanne DT, Brenda KM. Adhesive and mechanical properties of hydrogels influence neurite extension. Journal of Biomedical Materials Research. 2005;72A(1):91-7.

329. Esfandiar B, Kyriacos Z, Antonios GM. Adhesion and migration of marrow-derived osteoblasts on injectable in situ crosslinkable poly(propylene fumarate-co-ethylene glycol)-based hydrogels with a covalently linked RGDS peptide. Journal of Biomedical Materials Research Part A. 2003;65A(2):260-70.

330. Agnihotri SA, Mallikarjuna NN, Aminabhavi TM. Recent advances on chitosan-based micro- and nanoparticles in drug delivery. Journal of Controlled Release. 2004;100(1):5-28.

331. Qiu Q-Q, Ducheyne P, Ayyaswamy PS. Fabrication, characterization and evaluation of bioceramic hollow microspheres used as microcarriers for 3-D bone tissue formation in rotating bioreactors. Biomaterials. 1999;20(11):989-1001.

332. Cristina CB, Cristina CR, Meriem L, Clara Sá M, Mário AB. Proliferation, activity, and osteogenic differentiation of bone marrow stromal cells cultured on calcium titanium phosphate microspheres. Journal of Biomedical Materials Research. 2005;72A(1):57-66.

333. Borden M, El-Amin SF, Attawia M, Laurencin CT. Structural and human cellular assessment of a novel microsphere-based tissue engineered scaffold for bone repair. Biomaterials. 2003;24(4):597-609.

334. Zan Q. WC, Dong L., Liu R., Tian J. Preparation and characterization of biodegradable β-TCP-based composite microspheres as bone tissue engineering scaffolds. Key Engineering Materials. 2007;336-338:1646-9. .

335. Palmer VLWSBDPKDD. Microfluidic chip-based synthesis of alginate microspheres for encapsulation of immortalized human cells. Biomicrofluidics. 2007 1(1).

336. C. H. Choi JHJ, Y. W. Rhee, D. P. Kim, S. E. Shim, and, Lee CS. Generation of monodisperse alginate microbeads and in situ encapsulation of cell in microfluidic device. Biomed Microdevices. 2007;9(6):855

337. S. Xu ZN, M. Seo, P.C. Lewis, E. Kumacheva, P. Garstecki, D.B. Weibel, I. Gitlin, G.M. Whitesides, H.A. Stone. Generation of monodisperse particles using microfluidics: control over size, shape and composition. Angew Chem Int Ed. 2005;44:724.

338. Lin C-HYaY-C. Using a cross-flow microfluidic chip for monodisperse UV-photopolymerized microparticles. Microfluidics and Nanofluidics. 2009;6(2):277-83.

339. Gobin AS, West JL. Cell migration through defined, synthetic ECM analogs. FASEB Journal. 2002 May 1, 2002;16(7):751-3.

340. DeLong SA, Moon JJ, West JL. Covalently immobilized gradients of bFGF on hydrogel scaffolds for directed cell migration. Biomaterials. 2005;26(16):3227-34.

341. Shin H, Zygourakis K, Farach-Carson MC, Yaszemski MJ, Mikos AG. Attachment, proliferation, and migration of marrow stromal osteoblasts cultured on biomimetic hydrogels modified with an osteopontin-derived peptide. Biomaterials. 2004;25(5):895-906.

342. Salinas CN, Anseth KS. The influence of the RGD peptide motif and its contextual presentation in PEG gels on human mesenchymal stem cell viability. Journal of Tissue Engineering and Regenerative Medicine. 2008;2(5):296-304.

343. Mazzoccoli JP, Feke DL, Baskaran H, Pintauro PN. Mechanical and cell viability properties of crosslinked low- and high-molecular weight poly(ethylene glycol) diacrylate blends. Journal of biomedical materials research Part A. 2010;93(2):558-66.

344. Hersel U, Dahmen C, Kessler H. RGD modified polymers: biomaterials for stimulated cell adhesion and beyond. Biomaterials. 2003;24(24):4385-415.

345. Jongpaiboonkit L, King WJ, Murphy WL. Screening for 3D environments that support human mesenchymal stem cell viability using hydrogel arrays. Tissue engineering Part A. 2009;15(2):343-53.

346. Jongpaiboonkit L KW, Murphy WL. Screening for 3D environments that support human mesenchymal stem cell viability using hydrogel arrays. Tissue Eng Part A. 2009;15(2):343-53.

347. Santiago LY, Nowak RW, Peter Rubin J, Marra KG. Peptide-surface modification of poly(caprolactone) with laminin-derived sequences for adipose-derived stem cell applications. Biomaterials. 2006;27(15):2962-9.

348. Williams CG, Malik AN, Kim TK, Manson PN, Elisseeff JH. Variable cytocompatibility of six cell lines with photoinitiators used for polymerizing hydrogels and cell encapsulation. Biomaterials. 2005;26(11):1211-8.

349. Liu Z XL, Xu B, Zhang Y, Mak AF, Li Y, Man WY, Yang M. Covalently immobilized biomolecule gradient on hydrogel surface using a gradient generating microfluidic device for a quantitative mesenchymal stem cell study. Biomicrofluidics. 2012;6(2).

350. Yourek G, Hussain MA, Mao JJ. Cytoskeletal Changes of Mesenchymal Stem Cells During Differentiation. ASAIO Journal. 2007;53(2):219-28 10.1097/MAT.0b013e31802deb2d.

351. Kristopher A. Kilian and Milan Mrksich. Directing Stem Cell Fate by Controlling the Affinity and Density of Ligand-Receptor Interactions at the Biomaterials Interface. Angewandte Chemie Int Ed. 2012;51(20):4891-5.

352. Bosnakovski D, Mizuno M, Kim G, Takagi S, Okumura M, Fujinaga T. Chondrogenic differentiation of bovine bone marrow mesenchymal stem cells (MSCs) in different hydrogels: Influence of collagen type II extracellular matrix on MSC chondrogenesis. Biotechnology and Bioengineering. 2006;93(6):1152-63.

353. Nguyen LH, Kudva AK, Guckert NL, Linse KD, Roy K. Unique biomaterial compositions direct bone marrow stem cells into specific chondrocytic phenotypes corresponding to the various zones of articular cartilage. Biomaterials. 2011;32(5):1327-38.

354. Christoffer K. Abrahamsson FY, Hyoungshin Park, Jonathan M. Brunger, Piia K. Valonen, Robert Langer, Jean F. Welter, Arnold I. Caplan, Farshid Guilak, and Lisa E. Freed, . Chondrogenesis and Mineralization During In Vitro Culture of Human Mesenchymal Stem Cells on Three-Dimensional Woven Scaffolds. Tissue Eng Part A. 2010;16(12):3709-18.

355. Rebelatto CK, Aguiar AM, Moretão MP, Senegaglia AC, Hansen P, Barchiki F, et al. Dissimilar Differentiation of Mesenchymal Stem Cells from Bone Marrow, Umbilical Cord Blood, and Adipose Tissue. Experimental Biology and Medicine. 2008 July 1, 2008;233(7):901-13.

356. Hu WS, Meier J, Wang DIC. A mechanistic analysis of the inoculum requirement for the cultivation of mammalian cells on microcarriers. Biotechnology and Bioengineering. 1985;27(5):585-95.

357. Wei-Shou H, Donald JG, Daniel ICW. Serial propagation of mammalian cells on microcarriers. Biotechnology and Bioengineering. 1985;27(10):1466-76.

358. Kamilla Swiech GMCdS, Teresa C. Zangirolami, Mônica R.C. Iemma, Heloísa S. Selistre-de-Araújo, Cláudio A.T. Suazo. Evaluating kinetic and physiological features of rCHO-K1 cells cultured on microcarriers for production of a recombinant metalloprotease/disintegrin. Electronic Journal of Biotechnology. 2007;10(2).

359. Frisch SM, Ruoslahti E. Integrins and anoikis. Current Opinion in Cell Biology. 1997;9(5):701-6.

360. Frith JE MR, Hudson JE, Cooper-White JJ. Tailored integrin-extracellular matrix interactions to direct human mesenchymal stem cell differentiation. Stem Cells Dev. 2012;1(13):2442-56.

361. Liu Z, Xiao L, Xu B, Zhang Y, Mak AFT, Li Y, et al. Covalently immobilized biomolecule gradient on hydrogel surface using a gradient generating microfluidic device for a quantitative mesenchymal stem cell study. Biomicrofluidics. 2012;6(2):024111-12.

362. Lin YC, Brayfield CA, Gerlach JC, Rubin JP, Marra KG. Peptide modification of polyethersulfone surfaces to improve adipose-derived stem cell adhesion. Acta Biomaterialia. 2009;5(5):1416-24.

363. Pfeiffer E, Vickers SM, Frank E, Grodzinsky AJ, Spector M. The effects of glycosaminoglycan content on the compressive modulus of cartilage engineered in type II collagen scaffolds. Osteoarthritis and Cartilage. 2008;16(10):1237-44.

364. Toh WS, Lim TC, Kurisawa M, Spector M. Modulation of mesenchymal stem cell chondrogenesis in a tunable hyaluronic acid hydrogel microenvironment. Biomaterials. 2012;33(15):3835-45.

365. Hunziker EB. Articular cartilage repair: basic science and clinical progress. A review of the current status and prospects. Osteoarthritis and Cartilage. 2002;10(6):432-63.

366. Klein TJ, Rizzi SC, Reichert JC, Georgi N, Malda J, Schuurman W, et al. Strategies for Zonal Cartilage Repair using Hydrogels. Macromolecular Bioscience. 2009;9(11):1049-58.

367. Adelola OO, Claire C, Maria ZB, Peter EB, Alexander MS. Cartilage Tissue Engineering: the Application of Nanomaterials and Stem Cell Technology.

368. Park JS, Chu JS, Tsou AD, Diop R, Tang Z, Wang A, et al. The effect of matrix stiffness on the differentiation of mesenchymal stem cells in response to TGF. Biomaterials. 2011;32(16):3921-30.

369. Connelly JT, Levenston ME. Inhibition of in vitro chondrogenesis in RGD-modified three-dimensional alginate gels. Biomaterials. 2007;28(6):1071-83.

370. Hamid AA, Idrus RB, Saim AB, Sathappan S, Chua KH. Characterization of human adipose-derived stem cells and expression of chondrogenic genes during induction of cartilage differentiation. Clinics (Sao Paulo, Brazil). 2012;67(2):99-106.

371. Mwale F, Stachura D, Roughley P, Antoniou J. Limitations of using aggrecan and type X collagen as markers of chondrogenesis in mesenchymal stem cell differentiation. Journal of Orthopaedic Research. 2006;24(8):1791-8.

372. Sensebe L, Bourin P. Mesenchymal Stem Cells for Therapeutic Purposes. Transplantation. 2009;87(9S):S49-S53 10.1097/TP.0b013e3181a28635.

373. Martin I, Wendt D, Heberer M. The role of bioreactors in tissue engineering. Trends in Biotechnology. 2004;22(2):80-6.

374. Frauenschuh S, Reichmann E, Ibold Y, Goetz PM, Sittinger M, Ringe J. A Microcarrier-Based Cultivation System for Expansion of Primary Mesenchymal Stem Cells. Biotechnology Progress. 2007;23(1):187-93.

375. Matthew Shane C, Jean-Francois H, Daniel ICW. Hydrodynamic effects on animal cells grown in microcarrier cultures. Biotechnology and Bioengineering. 1987;29(1):130-41.

376. Zandstra PW, Nagy A. STEM CELL BIOENGINEERING. Annual Review of Biomedical Engineering. 2001;3(1):275-305.

377. Cahn F. Biomaterials aspects of porous microcarriers for animal cell culture. Trends in Biotechnology. 1990;8:131-6.

378. Sart S, Schneider Y-J, Agathos SN. Ear mesenchymal stem cells: An efficient adult multipotent cell population fit for rapid and scalable expansion. Journal of Biotechnology. 2009;139(4):291-9.

379. Qiu Q, Sayer M, Kawaja M, Shen X, Davies JE. Attachment, morphology, and protein expression of rat marrow stromal cells cultured on charged substrate surfaces. Journal of Biomedical Materials Research. 1998;42(1):117-27.

380. Baradez M-O, Marshall D. The Use of Multidimensional Image-Based Analysis to Accurately Monitor Cell Growth in 3D Bioreactor Culture. PLoS ONE. 2011;6(10):e26104.

381. Eibes G, dos Santos F, Andrade PZ, Boura JS, Abecasis MMA, da Silva CL, et al. Maximizing the ex vivo expansion of human mesenchymal stem cells using a microcarrier-based stirred culture system. Journal of Biotechnology. 2010;146(4):194-7.

382. Ng YC, Berry JM, Butler M. Optimization of physical parameters for cell attachment and growth on macroporous microcarriers. Biotechnology and Bioengineering. 1996;50(6):627-35.

383. Huang AH, Farrell MJ, Mauck RL. Mechanics and mechanobiology of mesenchymal stem cell-based engineered cartilage. Journal of Biomechanics. 2009;43(1):128-36.

384. Hamid AA, Idrus RBH, Saim AB, Sathappan S, Chua K-H. Characterization of human adipose-derived stem cells and expression of chondrogenic genes during induction of cartilage differentiation. Clinics. 2012;67:099-106.

385. Haubner R, Gratias R, Diefenbach B, Goodman SL, Jonczyk A, Kessler H. Structural and Functional Aspects of RGD-Containing Cyclic Pentapeptides as Highly Potent and Selective Integrin αVβ3 Antagonists. Journal of the American Chemical Society. 1996 2012/09/18;118(32):7461-72.

386. Jennifer L Weber1 PD-S, David M Weber1, Andrei G Fadeev1, Yue Zhou1, Jiwei Yang2, Catherine A Priest2, Ralph Brandenberger2 & Zara Melkoumian1. Corning® Synthemax™ Surface: a tool for feeder-free, xeno-free culture of human embryonic stem cells. Nature Methods. 2010.

387. Sannino A, Netti PA, Madaghiele M, Coccoli V, Luciani A, Maffezzoli A, et al. Synthesis and characterization of macroporous poly(ethylene glycol)-based hydrogels for tissue engineering application. Journal of Biomedical Materials Research Part A. 2006;79A(2):229-36.

388. Braeckmans K, De Smedt SC, Leblans M, Pauwels R, Demeester J. Encoding microcarriers: present and future technologies. Nat Rev Drug Discov. [Review]. 2002 Jun;1(6):447-56.

389. Agata H, Watanabe N, Ishii Y, Kubo N, Ohshima S, Yamazaki M, et al. Feasibility and efficacy of bone tissue engineering using human bone marrow stromal cells cultivated in serum-free conditions. Biochemical and Biophysical Research Communications. 2009;382(2):353-8.